Order Number 9325065

A study of turbulent wakes with and without the presence of free stream turbulence

Ardebili, Mahmoud Khosro, Ph.D.

City University of New York, 1993

U·M·I
300 N. Zeeb Rd.
Ann Arbor, MI 48106

A STUDY OF TURBULENT WAKES WITH AND WITHOUT THE PRESENCE OF FREE STREAM TURBULENCE

BY:

MAHMOUD K. ARDEBILI

A dissertation submitted to Graduate Faculty in Engineering in partial fulfillment of requirement for degree of Doctor of Philosophy, The City University of New York

1993

This manuscript has been read and accepted for the Graduate Faculty in Engineering in satisfaction of the dissertation requirement for the degree of Doctor of Philosophy.

April 29, 1993
Date

Chair of Examining Committee

4/30/93
Date

Executive Officer

Professor Yannis Andreopoulos

Professor Peter Ganatos

Professor Reza Khanbilvardi

Professor Charles Watkins

Supervisory Committee

THE CITY UNIVERSITY OF NEW YORK

Abstract

A STUDY OF TURBULENT WAKES WITH AND WITHOUT THE PRESENCE OF FREE STREAM TURBULENCE

BY

Mahmoud K. Ardebili

Adviser: Professor Rishi Raj

The objective was to investigate symmetric and asymmetric turbulent wakes subjected to free stream turbulence. The wake environment was generated experimentally by using a modified airfoil. Symmetric wake was simulated by merging of two similar boundary layers on two sides of the model into wake. Asymmetric wake was simulated by merging of dissimilar boundary layers on the two sides of the model. Free stream turbulence was generated by placing grids upstream of the model. The mean velocity was obtained with the aid of pressure measurement, and the turbulence quantities were obtained by using hot-wire anemometry.

In order to assess the ability of K-ε and Reynolds stress models to predict turbulent wake under varying free stream conditions, the wake governing equations for the closure models were numerically solved by a second order accurate, parabolic, forward marching finite difference method.

The mean velocity and its flow properties of symmetric and asymmetric wakes were affected by the presence of free stream turbulence. The recovery rate increased while shape factor decreased with higher level and

larger length scale of the free stream turbulence. The displacement thickness and half-wake width became larger under moderate free stream turbulence, and decreased with higher free stream turbulence.

The free stream turbulence affected the turbulence structure of the wake. Increase in the level and length scale of the free stream turbulence increased the level of turbulence quantities in the wake. It affected outer layer of wake, while the inner core of the wake essentially remained unaffected.

The K-ε model and Reynolds stress model of turbulence closure resulted in acceptable prediction of mean velocity throughout the wake. However in far wake the turbulence quantities predicted with the K-ε model are closer to the experimental data than predictions with Reynolds Stress model. The turbulence quantities of wake were predicted with maximum average deviation of 23% in asymmetric wake, and 24% in symmetric wake from the experimental data.

The mean velocity of asymmetric wake under free stream turbulence was predicted successfully with Reynolds stress model, with maximum average deviation of 2% from the experimental data. The maximum average deviation of turbulence quantities from the experimental data was 23%. These deviations increased with increases in the free stream turbulence.

There was too much uncertainty in the estimate of dissipation rate used as initial condition in the wakes for the closure models to be tested with certainty.

ACKNOWLEDGMENT

The author would like to thank his mentor Prof. Rishi Raj for his support and guidance.

The author would like to thanks his father, mother, brothers, and sister for their support and encouragement.

Last but not least, the author would like to thank his wife, Ms. Shahla Nabavi for unending love and devotion she has given him throughout the years.

TABLE OF CONTENT

LIST OF TABLES

LIST OF FIGURES

LIST OF SYMBOLS

A_j, B_j, C_j D_j, R_j	Submatrices used in matrix solution of governing equations.
b	Effective viscosity in K-ε model,
b_{up}, b_{lw}	Half-wake width.
b_i	Coefficient used in King's law.
C	Chord length of wake generating object.
C_1, C_2	Constants used in modeling.
C_d	Drag coefficient.
C_s	Constant used in turbulence closure equations.
$C_{\phi 1}, C_{\phi 2}, C_{\phi 3}$	Constants used in turbulence closure equations.
$C_{\varepsilon 1}, C_{\varepsilon 2}$	Constants used in turbulence closure equations.
C_μ	Constant used in calculation of eddy viscosity.
d	Diameter used in cylinder wake.
D_{ij}	Function pertaining in Reynolds stress model.
E_i	Voltage output of hot wire anemometer.
f	Frequency (Hz).
f_s	Sampling frequency.
$F(\kappa)$	Power specteral function in wave domain.
G	Normal gradient of mean velocity.
H	Shape factor.
h_j	Grid spacing of normal direction in the computational domain.
K	Turbulent kinetic energy $1/2\ \overline{u_i u_i}$.

KBAR	$(K/U_e^2)x\ 100.$
K_o	Constant used in equation (2.4).
K_i	Grid spacing of axial direction in the computational domain.
K_1,K_2	Correction factor of cosine law for each sensor of the cross-wire probe.
L_d	Dissipative length scale of free stream turbulence.
L_{ot}	Half wake width at trailing edge.
m	Parameter pertaining to pressure gradient of wake used in Eqn. 2.4.
N	Function used in Eqn. 2.1.
n_i	Exponent of king's law.
P	Static pressure. Also function pertaining to Reynolds stress model.
PSD	Power spectral density function.
P_{ij}	Function pertaining to Reynolds stress model
$S_{1j}....S_{6j}$	Parameters used in numerical representation of equations.
s'_{ij}	Fluctuating strain rate.
Tu	Free stream turbulence level.
Ta	Taylor number, $(\sqrt{u^2}/U_e)(d/L_X)^{1/5}$.
U	Mean velocity in the axial direction.
$\underline{U}$	Instantaneous velocity vector.
U_c	Centerline velocity.
U_e	Free stream velocity.
$\underline{U}_x$	Instantaneous velocity in the x direction.

U_τ	Friction velocity.
$\overline{u_i u_j}$	Reynolds stress tensor.
$\overline{u^2}$	Fluctuation in the axial direction.
u2bar	$(\overline{u^2}/U_e^2)$x100.
urms	$(\sqrt{\overline{u^2}}/U_e)$x100.
$-\rho\overline{uv}$	Turbulent shear stress.
uvbar	$(\overline{uv}/U_e^2)$x 10^3.
u3bar	$(\overline{u^3}/U_e^3)$x 10^3.
u2vbar	$(\overline{u^2 v}/U_e^3)$x 10^3.
uv2bar	$(\overline{uv^2}/U_e^3)$x 10^3.
$\overline{v^2}$	Fluctuation in the normal direction.
v2bar	$(\overline{v^2}/U_e^2)$x 10^2.
v3bar	$(\overline{v^3}/U_e^3)$x 10^3.
V	Mean velocity in the normal direction.
$\underline{V}_y$	Instantaneous velocity in the y direction.
$\overline{w^2}$	Fluctuation in the binormal direction.
X_i	Cartesian coordinate in tensorial form.
X,Y,Z	Cartesian coordinate.

Greek Symbols

α,β	Angels used in cross wire equations.
α',β'	Parameters pertaining to free stream turbulence used in Eqn. 2.4.
$\delta(\ )$	Residual of quantities being solved in numerical scheme.

δ_{ij}	Kronekor's delta.
ε	Dissipation rate of turbulent kinetic energy.
κ	Constant of log law of boundary layers.
μ	Dynamic viscosity.
ν	Kinematic viscosity.
ξ	Normal gradient of independent quantities of closure equations.
κ	Wave number.
$\sigma_0,\sigma_1,\sigma_2,$	Parameter used in expressing source terms.
σ_k	Apparent Prandtl number for K.
Σ_u	Source term in mean momentum equation.
Σ_ϕ	Source term in closure equations.
τ_1,τ_2	Parameter used in expressing diffusion coefficient.
Γ_ϕ	Diffusion coefficient.
Γ_k	Diffusively of K
ϕ	Independent quantities in closure equation.
ϕ_{ij}	Redistribution term in Reynold stress equation.
$X_{\underline{Ux}}(f,T)$	Fourier transform of $\underline{U_x}$

Subscript

G	Free stream values.
W	Pertaining to wall condition.

Superscript

n	Iteration index.
	Time averaged value.

CHAPTER 1

INTRODUCTION

1.1 Statement of the Problem

Flow past an object has long been of interest in terms of practical as well as theoretical fluid mechanics. Pressure recovery at the end of the object and evolution of the boundary layer on the surface of an object into fully developed wake constitute one of the oldest and most challenging problems in engineering science. The flow field downstream of a streamlined body is also dependent on the preceding boundary layer and its initial conditions.

It is well known that the boundary layer transition from laminar to turbulent one, upstream of trailing edge of a streamlined body will cause the wake to be turbulent in the beginning itself. The turbulent flow in the near wake of a streamlined body is quite complex even in the absence of flow separation on the body. The complexity arises from sudden termination of shear stress on the surface, and the transition of wall bounded turbulent structures to free shear flows. The abrupt removal of shear stress, and the consequent change of no-slip condition on the surface to a finite velocity in the centerline will create a decaying anisotropic turbulent flow field which poses a difficult task to turbulence modelers.

If the wake generating object is asymmetric, the boundary layer on the surfaces of the body will have distinctive characteristics. Merging of

these layers will pose even more difficulties. The wake flow field will have different length and velocity scales on both sides of the wake centerline. In general the wake flow field has been classified into three distinctive regions [1].

i) Inner Wake: This region is dominated by the viscous sublayer of the preceding boundary layer as the core of the wake. However, outside the central core, the flow retains essentially the same characteristics as the original boundary layer. Observation of this region is possible if the boundary layer is not separated at the trailing edge. This region extends to about $X^+=10^2$,where $X^+=XU_\tau/\nu$ in which U_τ is the fricition velocity of the upstream boundary layer.

ii) Near Wake: This region is strongly dependent upon the characteristics of the wake generating object. In this region the inner wake begins to interact with the outer wake. Aerodynamic loading and the shape of the object contribute a great deal of influence on the behavior of this region. The dominating means of transport is turbulence diffusion. This region is documented to be self-preserving, and eventually reaches an asymptotic behavior of the far wake.

iii)Far Wake: This portion of the wake has very small velocity defect. The mean velocity and the turbulence quantities attain a universal distribution independent of the trailing edge conditions. Similarity of velocity profile and the turbulence quantities could be expressed by means of local velocity scale and local length scale.

It is well known that any external factors affecting boundary layer will

also affect the wake following it. One such factor is free stream turbulence. In many practical situations, wake evolves in the presence of free stream turbulence. One such situation exists in multi-stage turbomachinery. In a multi-stage turbomachine, the wake of the blade following first row of blades always evolves under the influence of the turbulence present in the wake of the previous row of blades. The structure of this free stream turbulence depends upon the spacing between stator-rotor and rotor-stator, stage loading and rotation. Increase in the free stream turbulence is known to increase noise level, heat transfer rate, skin friction, hence drag and also enhances transition from laminar to turbulent flow in turbomachines. The last of the foregoing considerations are of special interest in heat transfer related to turbine blade at elevated gas temperatures. The additional turbulence generated in the wake due to the free stream turbulence is also a cause of excessive vibrations in rotor assembly. The free stream turbulence is also known to delay separation by altering the boundary layer profile and, therefore, decreasing the shape factor. This effect is of special significance to hull/propeller flow and stern flow field.

Literature search presented in chapter II indicates that very little is known analytically or experimentally about the parameters affecting the structure of wake turbulence in the presence of free stream turbulence. Some of these parameters are related to the structure of free stream turbulence itself such as the magnitude of its length scale, turbulence kinetic energy, and the degree of isotropy of the external stream. The other parameters are related to the physical shape of the body[2]. The introduc-

tion of asymmetry, as mentioned earlier, not only changes mean velocity distribution, but also causes changes in the turbulence structure as explained in reference [3]. Unavailability of fundamental experimental data of the effect of free stream turbulence on the wake of streamlined bodies has hindered the development of any calculation procedures for the proposed flow field. It is therefore, imperative that a firm data-base be established to obtain the relevant information of fundamental interest on basic and simple structures such as flat plate and then the work be extended to more specific configurations. The experimental data obtained will provide insight into the turbulent flow mechanism to generate appropriate modeling technique for the present complex flow situation.

1.2 Objectives of the Investigation

The experimental and theoretical investigation was undertaken to understand the mechanism of turbulent transport of energy from free stream turbulence to wake and how the wake structure under the new environment dissipates. However, the proposed investigation was performed with the following specific objectives:

•Experimentally determine the effect of free stream turbulence on the wake of a modified isolated airfoil with elliptical leading edge. Carry out measurements on the decay of turbulence intensity and dissipation rate downstream of two turbulence generating grids. The isolated airfoil wake properties; the mean velocity profile, turbulence intensity, Reynolds stress

and frequency spectra are to be measured with and without the pressence of the grids.

•A numerical study on effect of free stream turbulence on symmetric wakes is to be carried out using the K-ε and the higher order Reynolds stress models.

•Carry out a numerical analysis of the effects of free stream turbulence on asymmetric wakes of the proposed isolated airfoil with different boundary layer characteristic on its both sides.

1.3 Methods and Means

The stated problem with specific objectives is investigated with the following means and methods.

•Free stream turbulence was generated with aid of grids. Hot wire anemometry was used to establish the level and dissipation rate of free stream turbulence at different axial locations downstream of the grids.

•Measurement of wake of a modified airfoil with and without the presence of the grids was also carried out with the aid of hot wire anemometry.

•The continuity, mean momentum and other equations as required by closure problem were solved by a forward marching finite difference technique.

CHAPTER 2

LITERATURE SURVEY

2.1 Near and Far Wakes

The flow field downstream of streamlined objects are generally known as wakes. At very low Reynolds number, when the flow field is laminar, the wake has been studied extensively. Extensive solution of laminar wakes are presented in references [4] and [5]. In recent years, with evolution of hot wire anemometry and computational methods, more attention has been focused on turbulent wakes, where due to the statistical nature of turbulence, the closure problem is associated with great deal of empiricism.

The turbulent far wake region, where the flow evolution is relatively slow and viscous stresses are insignificant, has been widely investigated theoretically and experimentally. The theoretical analysis can be found in many texts (Schlichting [6], Tennekes and Lumley [7]). Schlichting solved the turbulent far wake problem for the mean velocity profile using a mixing length concept. The influence of the wake generating object is contained in drag coefficient. The shortcoming of this analysis is the concept of a constant mixing length over the transverse direction of the flow. In latter work, Tennekes and Lumley [7] analyzed the far wake using the self preservation hypothesis, employing again a constant eddy viscosity in the wake, which leads to erroneous results near the edge of the wake. An extensive survey of wake literature is presented in reference [8].

The near wake, where the influence of the wake generating object is

significant, has been studied quite thoroughly. It has been observed, to be affected by its initial conditions specifically the flow field at the trailing edge. Robinson [9] solved the near wake of a flat plate by using similarity. His solution for the centerline mean velocity is:

$$U_c/U_\tau=(1/K)(\ln N-\gamma_r)+B_r \qquad ..(2.1)$$

where the nondimensional parameter N is the solution of the following equation:

$$N(\ln N- 1)=K^2(X\, U_\tau/\nu) \qquad ..(2.2)$$

where U_τ is the friction velocity of the preceding boundary layer at trailing edge, γ_r, Br and K are constants and ν is coefficient of kinematic viscosity.

In later works, Alber [10] worked out the very near wake of a flat plate by using an inner and outer layer coordinate expansion method. He extended the Goldstein [4] solution of laminar wake to turbulent wake, by dividing the near wake into three regions. In region I: a laminar inner layer grows into the trailing edge viscous sublayer. The wake centerline velocity and wake thickness grow as $X^{1/3}$. In region II: a turbulent inner layer grows into the trailing edge wall layer. The subsequent growth of centerline velocity is exactly the same as given in Eqn. 2.1.

Bogucz and Walker [11] using an expansion in the limit of infinite Reynolds number show that the turbulent near wake has a well defined structure. The effect of change in boundary condition at the trailing edge are contained in a thin inner wake region whose thickness grows linearly with distance. In the outer layer, the upstream boundary layer evolves downstream of trailing edge relatively unaffected by the inner core. They

also indicate that to obtain solution for mean velocity and Reynolds stress profiles, a turbulent model has to be assumed. However, the two-layer structure of near wake is independent of the turbulence model.

Page and Ostowari[12] using law of maximum entropy in an isolated system, concluded that there exists a unique value of the time averaged centerline velocity in the near wake of a symmetrical body as a limiting case for turbulent high Reynolds number flow.

Based on their experimental data, Andreopoulos and Bradshaw [13] suggested the following empirical relation:

$$U_c/U_\tau=4.65 \log_{10}(U_\tau X/\nu) +0.7 \qquad ..(2.3)$$

for growth of centerline velocity in the inner region. They also reported that the finite thickness of the trailing edge causes a distributed layer which grows into the inner layer of the original boundary layer.

Ramaprian et al. [14] by studying the wake of a flat plate experimentally, observed the evolution of upstream boundary layer, to asymptotic wake to occur in three distinct stages that takes about 350 wake momentum thickness. They observed that the geometry of trailing edge influences the wake development, and this influence seems to be present over a distance of 200 trailing edge thickness.

Nakayama and Liu [15] studied near wake of a flat plate at various Reynolds numbers. Their results indicate that low-Reynolds number effects are significant and could partially explain the discrepancies in the existing mean velocity data. They also point out that the sudden changes in turbulence quantity downstream of trailing edge are independent of

Reynolds number.

Hah and Lakshminarayana [1] have studied the near wake of an airfoil. They point out that the asymmetry in the wake is maintained up to 1.5 chords length downstream of the airfoil, and the wake recovers slower than a symmetrical wake. The streamline curvature has a substantial effect on velocity profile, and the outer scales of wake do not correlate with wake data in near wake.

Sastry [16] studied the near wake of an airfoil experimentally, and found that due to the curvature of the flow, static pressure at the edges of the wake are different from each other. It attains a maximum value within the wake, the peak occurs near about the point of minimum velocity. This indicates that a viscous-invicid calculation model should be employed in order to predict the complete features of this flow.

Nakayama [17] studied the effect of curvature and pressure gradient on a small-defect wake. He found that curvature and pressure gradient change the mean strain rate so that $\partial U/\partial Y$ is no longer the dominant term. Therefore some consequences of thin shear layer approximation are not valid and turbulence quantities are effected by the extra strain rate due to additional curvature. Most turbulence-model quantities are influenced, however some pure turbulence parameters like Taylor microscale are uninfluenced.

Ramjee, Tulapurkara and Rajasekar [18] carried out measurements of a symmetric airfoil wake in straight and curved ducts. They found out the wakes in curved ducts are asymmetric and the half width of the wake

is larger on the inner side of the flow than on the outer side. The inner side is the portion of the flow between the centerline of the curved duct and the wall nearer to the center of curvature. They also found the intensity of longitudinal turbulence fluctuation to be enhanced on the inner side of the flow and not changed significantly on the outer side.

In a related investigation Browne, Antonia and Shah [19] studied turbulent energy dissipation rate in wake. They measured the nine major terms that make up the total dissipation rate, in a self preserving region of cylinder wake. Their results show that local isotropy assumption is not satisfied. The dissipation rate computed by using the isotropic relation i.e. $\varepsilon=15\nu\overline{(\partial u/\partial X)^2}$, is underestimated by 40% at centerline and by 80% near the edge of the wake.

Park, Kim and Lee [20] studied near wake of an oscillating airfoil experimentally. They varied the mean angle of incidence of the airfoil. They found that at large angle of incidence the airfoil undergoes unsteady separation and the characteristic time scale of the unsteady boundary layer separation is the flow time scale, which is the ratio of chord length to free stream velocity. They also found that the phase lag of wake velocity profile relative to the motion of trailing edge increases linearly with downstream distance.

2.2 Effect of Free stream Turbulence on Wakes

Some scattered information is available on the effect of free stream turbulence on flat plate [21] and cylinder [22] wakes. Symes and Fink [23] point out that the effectiveness of a grid-generated external turbulence in

influencing the development of wake past cylinders depends to a large extent upon the ratio of the length scale of the external turbulence with respect to that of the wake. This ratio must be substantially greater than unity for, when the length scales differ only slightly no influence could be observed.

Pal [24] has done a thorough literature search on the effect of free stream turbulence on boundary layer flow and heat transfer.

Effect of free stream turbulence on large structure in turbulent mixing layer is examined by Chandrsuda et al. [25], and was found to be large. They indicate that if the free stream turbulence is large, Brown-Roshko structure will not form and three-dimensionality develops at an early stage in transition.

Cimbala and Kerin [26] studied effects of free stream condition on far wake of a circular cylinder at relatively low Reynolds number, by measuring frequency spectra . They found that free stream noise plays an important role in development of vortical structures in far wake. They, further, concluded that their results supports the hypothesis that hydrodynamic instability is responsible for the growth of far wake structures rather than the Karman vortex street behind the circular cylinder.

Pal and Raj [27], [28] reported extensive study of effect of free stream turbulence on the wake of a flat plate. They reported that an increase in the free stream turbulence level sharply increases the wake thickness but the effect on the wake recovery rate is very mild. These studies indicate that the level of turbulence intensity $\overline{u^2}$ and $\overline{v^2}$ and Reynolds stress $-\overline{uv}$ in the two

dimensional wake of flat plate increases with the level of free stream turbulence. The same authors derived semiempirical relations to predict the effect of free stream turbulence on velocity and length scale of the wake of a flat plate. By using self-preservation and eddy viscosity models for the closure, the authors arrived at the correlations for the velocity and length scale as:

$$1-U_c/U_e=k\ C_d^{1/2}(X/C+X_0/C)^{-(1+\alpha' Tu-m)/2} \qquad ..(2.4)$$

and,

$$(L-L_{0t})/C=k\ C_d^{1/2}(X/C)^{(1+\beta' Tu-m)/2} \qquad ..(2.5)$$

where α' and β' are free stream turbulence parameters. L_{0t} is the wake's length scale at the trailing edge.

Ardebili et al. [29] experimentally studied the wake of an airfoil when a separation bubble is present on the airfoil's suction surface. These results were compared with the wake obtained after removing the separation bubble with the increase in the free stream turbulence. The different behavior of wakes under the foregoing conditions was noteworthy.

A closely related study indicating the effect on uniformly sheared turbulent flow on a cylinder wake is reported by Ahmed et al.[30]. This study indicates the tendency of the wake to grow faster on the higher free stream velocity side than on the lower free stream velocity side and the turbulence structures on the two sides of the wake appear to behave independently of each other.

Kiya et al.[31] also investigated the effect of free stream turbulence on flow past a cylinder. They found that Taylor number based on longitudi-

nal integral scale, (Ta) and the critical Reynolds number (Re), forming a parameter ($Re^{1.34}Ta$), is well correlated to the following flow properties: the time-mean drag coefficient, base pressure coefficient, and the spanwise correlation length of the surface-pressure fluctuations in the vicinity of the separation point.

Gorla [32] presented an analysis to investigate the combined effect of transient free-stream velocity and free stream turbulence at a stagnation point on a cylinder situated in a cross flow. An extension of this analysis may be applicable to wake flows developing in free stream turbulence environment.

Hah and Lakshminarayana [33] have studied the effect of free stream turbulence on the wake of a compressor rotor, using an elliptic method and simplified Reynolds stress equations. Their numerical scheme requires experimental data on the entire boundary of the calculation domain, which in practice is an extended interpolation, rather than a predicting scheme. However, their experimental results tend to agree qualitatively with those of References [27] and [28].

Evans [34] investigated unsteady laminar boundary layer subject to traveling pressure wave in free stream, computationaly. His results point out that laminar boundary layer exhibits different behavior, depending whether the free stream disturbances consist of standing or traveling waves. His analysis could be extended to turbulent boundary layer and turbulent wake by incorporating an eddy viscosity model.

Liu and Rodi [35] carried out measurements of boundary layer

developing along a flat plate over which wake passed periodically. The wakes were generated by cylinders moving on a squirrel cage in front of the flat plate. They found that plate's boundary layer was turbulent, quite early, underneath the free stream disturbances due to the wakes; while it, initially, remained laminar underneath the undisturbed free stream regions between wakes. The turbulent boundary layer strips underneath the disturbed free stream travel downstream and grow together, so that, the embedded laminar regions disappear, and boundary layer becomes fully turbulent. The location, where this happens, moves upstream with increasing wake passing frequency.

Bandyopadhyay [36] analyzed existing experimental data on boundary layers influences by free stream turbulence. He developed a new correlation of fractional increases in skin friction due to the free stream turbulence. He also studied the effect of low Reynolds number on the outer layer.

2.3 Numerical Analysis of Wakes

Pope and Whitelaw [37] have done numerical studies on turbulent wake generated by flat plate and streamlined bodies. Their results tend to point out that for wakes with no external disturbance, the most accurate turbulent closure model is Reynolds stress equations along with the equation for turbulence dissipation provided there is no recirculation at the trailing edge. However, their calculation procedure, which solves the equations in an elliptical form requires boundary conditions on perimeter of the calculation domain and is dependent on the experimental data.

Patel and Scheuerer [38] also examined asymmetric wake of a flat plate numerically using modeled transport equation for turbulent kinetic energy and its rate of dissipation. Their calculation procedure was an extension of an already developed boundary layer calculation by taking into account the intermittency at outer edges. Their scheme seems to overestimate the shear stress and underestimate the turbulent kinetic energy in the wake.

Recklefs et al. [39] considered far wake of a circular cylinder under the influence of external turbulent stream numerically using the k-ε model and a k-kl model proposed by Launder et al. [40]. Their boundary conditions were those of reference [23]. They showed that the empirical constants in these models are altered due to the presence of free stream turbulence. They did not use the more elaborate Reynolds stress equations. It is yet to be observed how well this model would predict the asymmetric near and far wake under the influence of external disturbance.

Gorla [41] presented a numerical analysis on the effects of free stream turbulence on separation in the case of crossflow over a circular cylinder, using an eddy viscosity model. His results suggest that separation may be delayed by increasing the free stream turbulence. The eddy viscosity model used fails to account for the length scale of free stream turbulence.

Rodi and Scheuerer [42] presented their calculation of boundary layer in the presence of free stream turbulence, by employing the k-ε model and the Reynolds stress equations. The results obtained point out that the

models predict the effect of free stream turbulence qualitatively well. However, all the models fail to predict the additional effects of free stream turbulence length scale on the boundary layer or the wake parameters as observed in the experimental results.

A simple calculation method using boundary layer equations with an algebraic eddy-viscosity formula has been used by Chang et al. [43] for the calculation of mean velocity and Reynolds stress distribution in an asymmetric wake. The model, however, needs to be tested for free stream turbulence effects.

Lakshminarayana and Zhang [44] developed a momentum integral technique for prediction of two- and three-dimensional turbulent wakes by assuming similarity in velocity profiles. They used the same entrainment function for two-dimensional and three-dimensional wake flows. Their method predicts decay properties and essential physics of wake. Their use of the same similarity function in near wake and far wake is questionable.

Horstman [45] analyzed numerically trailing edge flow. He states that the k-ε model works adequately for trailing edge flows with little or no separation. He also points out that the algebraic eddy viscosity model is not appropriate for these kinds of flows.

In a related study, Chen and Patel [46] show that numerical solution of laminar flow around the trailing edge of a flat plate is dependent on the size of the solution domain. They concluded that their large-domain solution is in better agreement with: boundary layer upstream of trailing edge, intermediate wake, and the asymptotic wake than calculation which use

small domain for their calculation.

Agoropoulos and Squire [47] studied, experimentally and numerically, the two-dimensional turbulent wakes mixing with boundary layers. They performed their numerical computation with aid of modified K-ε model and an algebraic stress turbulence model. Their results point out that the algebraic stress turbulence model outperforms the K-ε model. However, both models fail to predict the edge of wake accurately. They attributed this failure to the intermittent nature.

Khodadadi and Vlachos [48] studied effects of turbulence K-ε model constants on computation of confined swirling flow. Their model is the standard K-ε model, and they changed three of the five empirical constants. They computed decaying swirl in developing turbulent pipe flow, and compared the outcome obtained using K-ε model with standard constants and those with the new constants. Their results suggest that the standard constant predicts the decay of tangential velocity in turbulent pipe flow well, as compared to experimental data. Modified constants result in a slower decay rate.

The literature survey clearly establishes the need for advancing the calculation procedure, and the need for accurate data for the proposed investigation.

CHAPTER 3

THEORETICAL FORMULATION

The time averaged continuity and Navier-Stokes equations for an incompressible fluid in Cartesian coordinates is given as:

$$\frac{\partial U_i}{\partial X_i}=0 \qquad ..(3.1)$$

$$\frac{\partial U_i}{\partial t}+U_j\frac{\partial U_i}{\partial X_j}=\frac{1}{\rho}\left[-\frac{\partial P}{\partial X_j}+\frac{\partial}{\partial X_j}\left(\mu\frac{\partial U_i}{\partial X_j}-\rho\overline{u_iu_j}\right)\right] \qquad ..(3.2)$$

For a steady two dimensional thin shear layer flow the above equations after simplification become:

$$\frac{\partial U}{\partial X}+\frac{\partial V}{\partial Y}=0 \qquad ..(3.3)$$

and

$$U\frac{\partial U}{\partial X}+V\frac{\partial U}{\partial Y}=\frac{1}{\rho}\left[-\frac{\partial P}{\partial X}+\frac{\partial}{\partial Y}\left(\mu\frac{\partial U}{\partial Y}-\rho\overline{uv}\right)\right] \qquad ..(3.4)$$

$$\frac{\partial P}{\partial Y}=0 \qquad ..(3.5)$$

For symmetrical as well as asymmetrical wake of a flat plate or uncambered airfoil with moderate curvature,

$$\frac{\partial P}{\partial X}=0 \qquad ..(3.6)$$

The presence of $-\rho\overline{uv}$ in the mean momentum equation requires solving additional equation which constitutes the so called "closure problem". In the present investigation the presence of free stream turbulence and its effect on the closure problem has to be studied.

Free stream turbulence is experimentally observed to increase the levels of turbulence intensity, shear stress, and break up the larger eddies of a simple wake into smaller eddies which enhances the mixing processes associated with turbulence. These effects of free stream turbulence indicate an increase in the turbulent diffusion relative to that of simple wakes. The turbulent diffusional fluxes are generally modeled as proportional to the gradient of the turbulence quantity. Thus, the existence of free stream turbulence does not, therefore, alter the modeling scheme except the constant of proportionality used in the modeling diffusion terms.

3.1 k-ε Model

3.1.1 Energy Equation (k)

The Reynolds stress equation with the aid of Cartesian tensor is given as [49]:

$$\frac{D\overline{u_iu_j}}{Dt} = -(\overline{u_iu_k}U_{j,k} + \overline{u_ju_k}U_{i,k}) - 2\nu\overline{u_{i,k}u_{j,k}} + \overline{\frac{p}{\rho}(u_{i,j}+u_{j,i})} - \overline{(u_iu_ju_k}$$
$$+\delta_{jk}\frac{\overline{u_ip}}{\rho} + \delta_{ik}\frac{\overline{u_jp}}{\rho} - \nu\overline{(u_iu_j)_{,k}})_{,k} \qquad ..(3.7)$$

The equation for transport of turbulent kinetic energy (T.K.E.) is obtained by contracting the indices in Eqn. 3.7 and summing the equations for normal stresses over i. Also, letting K, denote T.K.E.=$(1/2)\overline{u_i u_i}$ and $\varepsilon=\nu\overline{(\partial u_i/\partial X_k)(\partial u_i/\partial X_k)}$ be the dissipation rate of turbulent kinetic energy, Eqn. 3.7 becomes:

$$\frac{DK}{Dt}=-\overline{u_i u_j}\frac{\partial U_i}{\partial X_j}-\frac{\partial}{\partial X_j}(\overline{K' u_j}-\nu\frac{\partial K}{\partial X_j}+\frac{\overline{p u_j}}{\rho})-\varepsilon \qquad ..(3.8)$$

In Eqn. 3.8 the first two terms on the right hand side contain unknown terms which have to be modeled, and ε is obtained by solving the appropriately modeled transport equation for the dissipation rate.

The term $-\overline{u_i u_j}\partial U_i/\partial X_j$ represents the production of T.K.E. and is modeled by assuming an eddy viscosity model which relates the Reynolds stress tensor to the mean velocity gradients and T.K.E. as [50]:

$$-\overline{u_i u_j}=\nu_t(\frac{\partial U_i}{\partial X_j}+\frac{\partial U_j}{\partial X_i})-\frac{2}{3}\delta_{ij}K$$

where ν_t is the eddy viscosity -based upon dimensional analysis- is given as:

$$\nu_t=C_\mu\frac{K^2}{\varepsilon}$$

δ_{ij} is the kroneckers delta, and C_μ is a constant to be determined experimentally.

The second term on the right hand side of Eqn. 3.8 represents the diffusion of the T.K.E. by fluctuation. This term merely acts to re-distribute

the energy in space and does not add any contribution to overall energy level. For high Reynolds number flow, the diffusion due to molecular motion is an order of magnitude smaller than diffusion due to turbulence and can be neglected.

Therefore, the diffusion term is modeled as a gradient of turbulent kinetic energy [50]:

$$-(\overline{K' u_j'} + \frac{\overline{p u_j}}{\rho}) = \tau_k \frac{\partial K}{\partial X_j}$$

where τ_k is an apparent diffusion coefficient for T.K.E. and could be written as $\tau_k = \nu_k/\sigma_k$, where σ_k is an apparent Prandtl number and assumed to be constant. Therefore, Eqn. 3.8 could be written as:

$$\frac{DK}{Dt} = [\nu_t(\frac{\partial U_i}{\partial X_j} + \frac{\partial U_j}{\partial X_i}) - \frac{2}{3}\delta_{ij}K](\frac{\partial U_i}{\partial X_j}) + \frac{\partial}{\partial X_j}[(\frac{\nu_t}{\sigma_k})(\frac{\partial K}{\partial X_j})] - \varepsilon \qquad ..(3.9)$$

3.1.2 Dissipation Rate Equation (ε)

The dissipation rate of turbulence kinetic energy per unit mass is defined as:

$$\varepsilon = 2\nu \overline{s_{ij}' s_{ij}'} \qquad ..(3.10)$$

where s_{ij}' is the fluctuating strain rate and is defined as:

$$s'_{ij}=\frac{1}{2}\left(\frac{\partial u_i}{\partial X_j}+\frac{\partial u_j}{\partial X_j}\right)$$

For high turbulent Reynolds number, Eqn. 3.10 reduces to [49]:

$$\varepsilon=\nu\overline{\left(\frac{\partial u_i}{\partial X_j}\right)\left(\frac{\partial u_i}{\partial X_j}\right)} \qquad ..(3.11)$$

An equation for transport of ε is obtained by differentiating the instantaneous Navier-Stokes equations, multiplying it by $2\nu\partial U_i/\partial X_l$, then ensemble averaging it and using the high Reynolds number simplification, one obtains [51]:

$$\frac{D\varepsilon}{D_t}=-2\nu\overline{\frac{\partial u_i}{\partial X_k}\frac{\partial u_i}{\partial X_l}\frac{\partial u_k}{\partial X_l}}-2\overline{\left(\nu\frac{\partial^2 u_i}{\partial X_k \partial X_l}\right)^2}-\frac{\partial}{\partial X_k}\left[\overline{u_k\varepsilon'}+2\frac{\nu}{\rho}\overline{\frac{\partial u_k}{\partial X_l}\frac{\partial p}{\partial X_k}}\right.$$
$$\left.-\nu\frac{\partial \varepsilon}{\partial X_k}\right]-2\nu\left[\overline{\frac{\partial u_l}{\partial X_l}\frac{\partial u_k}{\partial X_l}}+\overline{\frac{\partial u_l}{\partial X_l}\frac{\partial u_l}{\partial u_k}}\right]\frac{\partial U_l}{\partial X_k}-2\nu\overline{u_k\frac{\partial u_l}{\partial X_l}\frac{\partial^2 U_l}{\partial X_k \partial X_l}} \qquad ..(3.12)$$

In the above equation the sum of the first two terms on the right hand side represents the transfer of energy from large energy containing eddies to small energy dissipating eddies, are thus independent of viscosity as the dissipating parameter. Therefore, one can model these two terms as:

$$2\nu\left[\overline{\frac{\partial u_i}{\partial X_k}\frac{\partial u_i}{\partial X_l}\frac{\partial u_k}{\partial X_l}}-\overline{\left(\frac{\partial^2 u_j}{\partial X_k \partial X_l}\right)^2}\right]=C_{\varepsilon 2}\frac{\varepsilon^2}{K}$$

where $C_{\varepsilon 2}$ is a constant.

The third term on the right hand side of Eqn. 3.12 expresses the

diffusional transport of ε by velocity fluctuation, pressure fluctuation and molecular motion. The diffusion of ε due to molecular motion for high Reynolds number is neglected. Also, the diffusion of ε due to the pressure fluctuation is of lesser importance. Then, the diffusional transport of ε is modeled as [51]:

$$\frac{\partial}{\partial X_j}[C_\varepsilon \frac{K}{\varepsilon}\overline{u_i u_j}\frac{\partial \varepsilon}{\partial X_j}]$$

The generation rate of ε is the fourth term on the right hand side of Eqn. 3.12 is modeled as:

$$2\nu\frac{\partial U_i}{\partial X_k}[\overline{\frac{\partial u_i}{\partial X_l}\frac{\partial u_k}{\partial X_l}}+\overline{\frac{\partial u_l}{\partial X_i}\frac{\partial u_l}{\partial X_k}}]-\frac{\partial U_l}{\partial X_k}[C_{\varepsilon 1}\frac{\varepsilon}{K}\overline{u_i u_j}+c'_{\varepsilon 1}\delta_{ij}]$$

where $C_{\varepsilon 1}$ is a constant and $C'_{\varepsilon 1}$ vanishes when $C'_{\varepsilon 1}\delta_{ij}$ is multiplied by $\partial U_i/\partial X_k$.

Finally the last term on right hand side of Eqn. 3.12 is neglected because it involves higher order derivative [52]. The modeled form of Eqn. 3.12 becomes:

$$\frac{D\varepsilon}{Dt}=-C_{\varepsilon 2}\frac{\varepsilon^2}{K}+C_\varepsilon\frac{\partial}{\partial X_l}[\frac{K}{\varepsilon}\overline{u_i u_j}\frac{\partial \varepsilon}{\partial X_j}]-C_{\varepsilon 1}\frac{\varepsilon}{K}\overline{u_i u_j}\frac{\partial U_i}{\partial X_k} \qquad ..(3.13)$$

Using the eddy viscosity model, Eqn. 3.13 becomes:

$$\frac{D\varepsilon}{Dt}=-C_{\varepsilon 2}\frac{\varepsilon^2}{K}+C_\varepsilon\frac{\partial}{\partial X_l}\{\frac{K}{\varepsilon}[\nu_t(\frac{\partial U_i}{\partial X_j}+\frac{\partial U_j}{\partial X_i})-\frac{2}{3}\delta_{ij}K]\frac{\partial \varepsilon}{\partial X_j}\}$$
$$-C_{\varepsilon 1}\frac{\varepsilon}{K}[\nu_t(\frac{\partial U_i}{\partial X_j}+\frac{\partial U_j}{\partial X_i})-\frac{2}{3}\delta_{ij}K]\frac{\partial U_i}{\partial X_k} \qquad ..(3.14)$$

3.1.3 Free Stream Turbulence

In laboratory, the free stream turbulence is generally produced by placing grids in test section of wind tunnels. The grid generated turbulence is nearly a homogeneous decaying process in the streamwise direction of flow. The level of kinetic energy and dissipation rate of free stream turbulence is governed by Eqn. 3.9 and Eqn. 3.14 in which production and diffusion is negligible. Then Eqn. 3.9 and Eqn. 3.14 reduce to:

$$U_G \frac{\partial K_G}{\partial X} = -\varepsilon_G \qquad ..(3.15)$$

and,

$$U_G \frac{\partial \varepsilon_G}{\partial X} = -C_{\varepsilon 2} \frac{\varepsilon^2{}_G}{K_G} \qquad ..(3.16)$$

where subscript G denotes the free stream flow.

The solution to Eqns. 3.15 and Eqn. 3.16 subject to an initial condition constitutes the boundary conditions for the edge of the wake, and also imposes the effect of free stream turbulence on the wake.

3.2 Reynolds Stress Model

The k-ε model is not capable of predicting the components of Reynolds stress tensor. Moreover, using the eddy viscosity model implies the turbulence to be homogeneous. However, these shortcomings are overcome by solving the equation for transport of components of Reynolds

stress tensor. The Reynolds stress model of closure - hereafter referred to RS- consists of modeling the higher order correlation in Reynolds stress Eqn. 3.7 and an appropriately modeled transport equation for dissipation rate of turbulent kinetic energy (ε), which also appears in Eqn. 3.7.

3.2.1 Reynolds Stress Equation ($\overline{u_i u_j}$)

In this investigation, the modeled form of Eqn. 3.7, is obtained by following the modeling technique of Hanjalic and Launder [53], Launder et al. [54], Shir [55], and Rodi and Scheuerer [42]. The essence of this modeling technique is to represent the last two terms on the right hand side of Eqn. 3.7 in terms of Reynolds stress and mean velocities. In Eqn. 3.7 the right hand side represents production of Reynolds stress, destruction, redistribution (pressure-strain correlation) and diffusion, respectively. The assumptions made in order to simplify Eqn. 3.7 are:

i) High local turbulence Reynolds number.

ii) Isotropy of the smallest scale of motion which are predominantly responsible for dissipation.

Under these assumptions, the second term is modeled as:

$$2\nu\overline{\frac{\partial u_i}{\partial X_k}\frac{\partial u_j}{\partial X_k}} = \frac{2}{3}\delta_{ij}\varepsilon \qquad ..(3.17)$$

The triple correlation in the diffusion term is modeled as:

$$\overline{u_i u_j u_k} = C_s \frac{K}{\varepsilon}\left\{\overline{u_i u_l}\frac{\partial \overline{u_j u_k}}{\partial X_l} + \overline{u_j u_l}\frac{\partial \overline{u_k u_i}}{\partial X_l} + \overline{u_k u_l}\frac{\partial \overline{u_i u_j}}{\partial X_l}\right\}$$

where C_s is a constant, and K represents the turbulent kinetic energy. The molecular diffusion and pressure diffusion are neglected, since they are orders of magnitude smaller than diffusion due to fluctuating motion. A simpler version of this term is given by Daly and Harlow [52], i.e.,

$$\overline{u_i u_j u_k} = C_s \frac{K}{\varepsilon}\overline{u_k u_l}\frac{\partial \overline{u_i u_j}}{\partial X_l} \qquad ..(3.18)$$

which is employed in this formulation.

The pressure-strain correlation term is commonly referred to as "redistribution" term. This term acts to diminish the differences between the normal stresses in their transport equation. Chou [56] proposed that:

$$\overline{\frac{p}{\rho}\frac{\partial u_i}{\partial X_j}} = \phi_{ij,1} + \phi'_{ij,2} \qquad ..(3.19)$$

where, these two terms signify two types of processes; the first one is mutual interaction between turbulence components, while the second term is the interaction between the mean rate of strain and the turbulence. According to [51], Rotta proposed for the first term:

$$(\phi_{ij} + \phi_{ji})_1 = -C_{\phi 1}\frac{\varepsilon}{K}\left(\overline{u_i u_j} - \frac{1}{3}\delta_{ij} 2K\right) \qquad ..(3.20)$$

Many different models have been proposed for the second part of pressure-strain term. For this investigation, the model proposed by Launder, Reece and Rodi [54] which also considers the effect of presence of a solid wall in flow is empolyed. They proposed that the $(\phi_{ij})'_2$ mainly consists of two parts i.e.

$$(\phi_{ij}+\phi_{ji})'_2=(\phi_{ij}+\phi_{ji})_2+(\phi_{ij}=\phi_{ji})_w$$

where, according to their argument; $(\phi_{ij}+\phi_{ji})$ is the second term of redistribution proposed by Hanjalic and Launder [53] and $(\phi_{ij}+\phi_{ji})$w accounts for near-wall turbulence. Then

$$(\phi_{ij}+\phi_{ji})_2=-\frac{C_2+8}{11}(P_{ij}-\frac{2}{3}P\delta_{ij})-\frac{30C_2-2}{55}K(\frac{\partial U_i}{\partial X_j}+\frac{\partial U_j}{\partial X_i}) -\frac{8C_2-2}{11}(D_{ij}-\frac{2}{3}P\delta_{ij}) \quad ..(3.21)$$

and,

$$(\phi_{ij}+\phi_{ji})_w=[0.125\frac{\varepsilon}{K}(\overline{u_iu_j}-\frac{2}{3}\delta_{ij}K)+0.015(P_{ij}-D_{ij})](\frac{K^{\frac{3}{2}}}{\varepsilon}X_2) \quad ..(3.22)$$

Where:

$$P_{ij}=-[\overline{u_iu_k}\frac{\partial U_j}{\partial X_k}+\overline{u_ju_k}\frac{\partial U_i}{\partial X_K}]$$

$$D_{ij}=-[\overline{u_iu_k}\frac{\partial U_k}{\partial X_i}+\overline{u_ju_k}\frac{\partial U_k}{\partial X_i}]$$

$$P=-\overline{u_iu_j}\frac{\partial U_i}{\partial X_j}$$

and x_2 denotes the normal direction to the wall.

Since the three terms in Eqn. 3.21 vanish under contracting of the indices, one could simplify the expression without removing the essential redistributive property of this expression [54]. The first term in Eqn. 3.21 is the dominant term of the three, then Eqn. 3.21 is written as:

$$(\phi_{ij}+\phi_{ji})_2 = -C_{\phi 2}(P_{ij}-\frac{2}{3}P\delta_{ij}) \qquad ..(3.23)$$

The value of $C_{\phi 2}$ differs from that of Eqn. 3.21 to compensate for the simplification.

Therefore, the modeled version of Eqn. 3.7 is given as:

$$\frac{D\overline{u_iu_j}}{Dt} = \frac{\partial}{\partial X_k}(C_s\frac{K}{\varepsilon}\overline{u_ku_l}\frac{\partial\overline{u_iu_j}}{\partial X_l}) - (\overline{u_iu_k}\frac{\partial U_j}{\partial X_k}+\overline{u_ju_k}\frac{\partial U_i}{\partial X_k}) - \frac{2}{3}\delta_{ij}\varepsilon \qquad ..(3.24)$$
$$-C_{\phi 1}\frac{\varepsilon}{K}(\overline{u_iu_j}-\frac{2}{3}\delta_{ij}K) - C_{\phi 2}(P_{ij}-\frac{2}{3}P\delta_{ij}) + (\phi_{ij}+\phi_{ji})_w$$

3.2.2 Dissipation Rate Equation (ε)

One still needs to specify ε, for the present high local turbulent Reynolds number flow, Eqn. 3.13 is adopted as the transport equation for rate of dissipation of turbulent kinetic energy.

3.2.3 Free Stream Turbulence

The effect of free stream turbulence is incorporated into the boundary

conditions associated with the Reynolds stress equation. In the free stream there is no production and the normal as well as transverse components of mean velocity are zero. Therefore, the equation for transport of Reynolds stresses can be simplified to:

$$U_G \frac{\partial \overline{u^2}_G}{\partial X} = -\frac{2}{3}\varepsilon_G - C_{\phi 1}\frac{\varepsilon_G}{K_G}\left(\overline{u^2}_G - \frac{2}{3}K_G\right) \qquad ..(3.25a)$$

$$U_G \frac{\partial \overline{v^2}_G}{\partial X} = -\frac{2}{3}\varepsilon_G - C_{\phi 1}\frac{\varepsilon_G}{K_G}\left(\overline{v^2}_G - \frac{2}{3}K_G\right) \qquad ..(3.25b)$$

$$U_G \frac{\partial \overline{w^2}_G}{\partial X} = -\frac{2}{3}\varepsilon_G - C_{\phi 1}\frac{\varepsilon_G}{K_G}\left(\overline{w^2}_G - \frac{2}{3}K_G\right) \qquad ..(3.25c)$$

The shear stress in the free stream ($\overline{uv}_G$) is set to zero, based on experimental results of grid generated turbulence.

Finally, the equation for decay of dissipation rate for the free stream turbulence with the above mentioned simplification is:

$$U_G \frac{\partial \varepsilon_G}{\partial X} = -C_{\varepsilon 2}\frac{\varepsilon^2{}_G}{K_G} \qquad ..(3.26)$$

Equations 3.24 and 3.13 subject to solution of Eqns. 3.25 and 3.26 constitute the Reynolds stress model.

CHAPTER 4

NUMERICAL ANALYSIS

In the previous chapter, the governing equations in a closed form for the calculation of wake were presented. In the present chapter, the numerical solution of the equation by a second order implicit finite difference schemes are discussed. The governing equations can be numerically represented with finite element or finite difference technique, and the finite element technique has some merit. However, the excessive computer storage and difficulties in the finite element algorithm outweighs the limited increase in the accuracy of the solution over the finite difference method.

The governing equations as presented in the previous chapter are elliptic and can be numerically solved in their present form, with an elliptic method such that of Patankar [57] . However, the elliptic method requires prescribing the boundary conditions on entire calculation domain boundary with experimental information, and also require a great deal of computer storage. The elliptic method is mainly used in flows where a large recirculation zone exists. [58].

In the present case, the numerical solution technique adopted is that of Keller and Cebeci [59]. The governing equations are simplified for a thin shear layer. This simplification reduces the governing equations to

parabolic form. The simplification, used can be represented as follows:

$$\frac{\partial}{\partial X_1} < \frac{\partial}{\partial X_2}$$

$$\frac{\partial^2}{\partial X^2_1} < \frac{\partial^2}{\partial X^2_2}$$

$$\frac{\partial}{\partial X_3} = 0$$

where, X_1 is the streamwise direction of the flow, and X_2 is the normal to the streamwise direction.

In this investigation, two different closure models were used. The first one is k-ε model. In this model one solves the mean momentum equation along with the transport equations for the turbulent kinetic energy (K), and the dissipation rate of turbulent kinetic energy (ε). The term $-\overline{uv}$ in the mean momentum equation is replaced by using eddy viscosity model.

The second model is the Reynolds stress model. In this model one solves the mean momentum equation along with the transport equations for the Reynolds stress, and dissipation rate (ε). The term $(-\overline{uv})$ is not modeled. The variation of this term is predicted from appropriate transport equation for it.

Tables 4.1 and 4.2 present the momentum and the expanded closure equation of the two different models in X,Y coordinates. In the present investigation the governing equations are presented in two different coordinates system.

i) In the case of symmetric wakes, the equations are numerically solved in their present form as given in the Tables 4.1 and 4.2.

ii) In the case of asyimmetric wakes, the equations are transformed from (X,Y) space to (X,Ψ) space, where Ψ is the streamline function (von Mises transformation [6]). The equations are transformed and solved in (X,Ψ) space in order to shorten the computation time, and to ensure convergence since the equations in this form are inherntly more stable.

4.1 Computation of Symmetric Wakes

4.1.1 Momentum Equation

The finite difference solution scheme for the mean momentum equation is independent of the closure model except, the way $-\overline{uv}$ is treated. In the forecoming analysis, the finite difference solution scheme of mean equations are presented for k-ε model. However, in the Reynolds stress model, the equations are the same except; the kinematic viscosity is that of the fluid and there is an additional source term due to $-\overline{uv}$. The resulting equation with the above mentioned notation can be written as follows:

$$U\frac{\partial U}{\partial X}+V\frac{\partial U}{\partial Y}=\frac{\partial}{\partial Y}b\frac{\partial U}{\partial Y} \qquad ..(4.1)$$

where,

$$b=\nu+\nu_{turb}$$

and

$$-\overline{uv}=\nu_{turb}\frac{\partial U}{\partial Y}$$

The continuity and momentum equations are combined by using

streamline function Ψ (where $U=\partial\Psi/\partial Y$ and $V=-\partial\Psi/\partial X$) and a function G representing the normal gradient of mean streamwise velocity U, i.e. $G=\partial U/\partial Y$. Rewriting the momentum equation as a set of first order differential equations, we obtain

$$\frac{\partial \psi}{\partial Y}=U \qquad ..(4.2a)$$

$$\frac{\partial U}{\partial Y}=G \qquad ..(4.2b)$$

$$\frac{1}{2}\frac{\partial U^2}{\partial X}-G\frac{\partial \psi}{\partial X}=\frac{\partial}{\partial Y}(bG) \qquad ..(4.2c)$$

In Eqn. 4.2c the transverse velocity V has been replaced by $\partial\Psi/\partial X$. Equations 4.2 are approximated according to typical grid cell shown in Fig. 4.1. Equations 4.2a and 4.2b are centered on point (i,j-1/2) and Eqn. 4.2c is centered at (i-1/2,j-1/2). The finite difference approximation for a dependent variable ϕ, in a grid cell shown in Fig 4.1 are:

$$\phi_{i,j-\frac{1}{2}}=[\phi_{i,j}+\phi_{i-1,j}]/2$$

$$\phi_{i-\frac{1}{2},j-\frac{1}{2}}=[\phi_{i,j}+\phi_{i,j-1}+\phi_{i-1,j}+\phi_{i-1,j-1}]/4$$

$$\left(\frac{\partial \phi}{\partial Y}\right)_{i,j-\frac{1}{2}}=[\phi_{i,j}-\phi_{i,j-1}]/h_j$$

$$\left(\frac{\partial \phi}{\partial X}\right)_{i-\frac{1}{2},j-\frac{1}{2}}=[\phi_{i,j}+\phi_{i,j-1}]/2K_i-[\phi_{i-1,j}+\phi_{i-1,j-1}]/2K_i$$

The approximation of Eqns. 4.2 (a,b,c) are as follows, respectivly:

$$\frac{1}{h_j}(\psi_{i,j}-\psi_{i,j-1})=\frac{1}{2}(U_{i,j}+U_{i,j-1}) \qquad ..(4.3a)$$

$$\frac{1}{h_j}(U_{i,j}-U_{i,j-1})=\frac{1}{2}(G_{i,j}+G_{i,j-1}) \qquad ..(4.3b)$$

$$\frac{1}{2}\left[\frac{U^2_{i,j}+U^2_{i,j-1}}{2K_i}-\frac{U^2_{i-1,j}+U^2_{i-1,j-1}}{2K_i}\right]-\left[\frac{\psi_{i,j}+\psi_{i,j-1}}{2K_i}\right.$$
$$\left.-\frac{\psi_{i-1,j}+\psi_{i-1,j-1}}{2K_i}\right]\left[\frac{G_{i,j}+G_{i,j-1}}{4}+\frac{G_{i-1,j}+G_{i-1,j-1}}{4}\right] \qquad ..(4.3c)$$
$$=\frac{bG_{i,j}+bG_{i-1,j}}{2h_j}-\frac{bG_{i,j-1}-bG_{i-1,j-1}}{2h_j}$$

Rearranging Eqns. 4.3 and omitting the subscript i yields:

$$h_iU_j+h_jU_{j-1}-2\psi_j+2\psi_{j-1}=0 \qquad ..(4.4a)$$

$$h_jG_j+h_jG_{j-1}-2U_j+2U_{j-1}=0 \qquad ..(4.4b)$$

$$(U^2_j+U^2_{j-1}-2U^2_{i-1,j-\frac{1}{2}})\frac{1}{2K_i}-(\psi_j+\psi_{j-1}-2\psi_{i-1,j-\frac{1}{2}})(G_j+G_{j-1}$$
$$+2G_{i-1,j-\frac{1}{2}})\frac{1}{4K_i}-(bG_j-bG_{j-1}+bG_{i-1,j}-bG_{i-1,j-1})\frac{1}{h_j}=0 \qquad ..(4.4c)$$

In the Reynolds stress model -where no eddy viscosity is assumed- Eqn. 4.4c becomes:

$$(U^2_j+U^2_{j-1}-2U^2_{i-1,j-\frac{1}{2}})/(2K_i)-(\psi_j+\psi_{j-1}-2\psi_{i-1,j-\frac{1}{2}})(G_j$$
$$+G_{j-1}+2G_{i-1,j-\frac{1}{2}})/(4K_i)-\nu(G_j-G_{j-1}+G_{i-1,j}-G_{i-1,j-1})/(h_j)$$
$$-\left[\left(\frac{\partial\overline{uv}}{\partial y}\right)_j+\left(\frac{\partial\overline{uv}}{\partial y}\right)_{j-1}+\left(\frac{\partial\overline{uv}}{\partial y}\right)_{i-1,j}+\left(\frac{\partial\overline{uv}}{\partial y}\right)_{i-1,j-1}\right]/4=0 \qquad ..(4.5)$$

The set of Eqns. 4.4 (a,b,c) or Eqns. 4.4 (a,b) and 4.5 involve only the mean properties of the flow, except the effective viscosity b for the K-ε model and the turbulent shear stress for the Reynols stress model, which

are determined from the closure equations. The finite difference approximation of mean momentum equations are non-linear, and in order to solve them, they are linearized by Newton method [60]. Iterates of the unknowns i.e. Ψ^n_j, G^n_j and U^n_j are introduced as:

$$\psi^n{}_j = \psi^{n-1}{}_j + \delta\psi^{n-1}{}_j \qquad ..(4.6a)$$

$$G^n{}_j = G^{n-1}{}_j + \delta G^{n-1}{}_j \qquad ..(4.6b)$$

$$U^n{}_j = U^{n-1}{}_j + \delta U^{n-1}{}_J \qquad ..(4.6c)$$

The right hand side of Eqns. 4.6 is substituted into Eqns. 4.4. The quadratic and higher order terms of the residuals ($\delta\Psi^n_j$, δG^n_j and δU^n_j) are then neglected. Omitting the superscript n for simplicity, one obtains:

$$h_j\delta U_j + h_j\delta U_{j-1} - 2\delta\psi_j + 2\delta\psi_{j-1} = R_{1j} \qquad ..(4.7a)$$

$$h_j\delta G_j + h_j\delta G_{j-1} - 2\delta U_j + 2\delta U_{j-1} = R_{2j} \qquad ..(4.7b)$$

$$S_{1j}\delta U_{j-1} + S_{2j}\delta\psi_{j-1} + S_{3j}\delta G_{j-1} + S_{4j}\delta U_j + S_{5j}\delta\psi_j + S_{6j}\delta G_j = R_{3j} \qquad ..(4.7c)$$

where,

$$R_{1j} = -h_jU_j - h_jU_{j-1} + 2\psi_j - 2\psi_{j-1}$$
$$R_{2j} = -h_jG_j - h_jG_{j-1} + 2U_j - 2U_{j-1}$$
$$R_{3j} = -[U^2{}_j + U^2{}_{j-1} - 2U^2{}_{i-1,j-\frac{1}{2}}]/2K_i + [\psi_j + \psi_{j-1} - 2\psi_{i-1,j-\frac{1}{2}}][G_j + G_{j-1} + 2G_{i-1,j-\frac{1}{2}}]/4K_i + [(bG)_j - (bG)_{j-1} + (bG)_{i-1,j} - (bG)_{i-1,j-1}]/h_j$$

The coefficients on the left hand side of Eqn. 4.7c are:

$S_{1j}=U_{j-1}/K_t$
$S_{2j}=-[G_j+G_{j-1}+G_{i-1,j}+G_{i-1,j-1}]/4K_t$
$S_{3j}=b_{j-1}/h_j-[\psi_j+\psi_{j-1}-\psi_{i-1,j}-\psi_{i-1,j-1}]/4K_t$
$S_{4j}=U_j/K_t$
$S_{5j}=-[G_j+G_{j-1}+G_{i-1,j}+G_{i-1,j-1}]/4K_t$
$S_{6j}=-b_j/h_j-[\psi_j+\psi_{j-1}-\psi_{i-1,j}-\psi_{i-1,j-1}]/4K_t$

The resulting linear system is written in a matrix form as follows:

$$\underline{\alpha}_j\underline{\delta}_j=\underline{\Gamma}_j \qquad ..(4.8)$$

The expanded version of this system of Eqn. 4.8 is:

$$\begin{vmatrix} A_0 & C_0 & & & \\ B_1 & A_1 & C_1 & & \\ & \cdots & & & \\ & & B_j & A_j & C_j \\ & & & \cdots & \\ & & & B_{L-1} & A_{L-1} & C_{L-1} \\ & & & & B_L & A_L \end{vmatrix} \times \begin{vmatrix} D_0 \\ D_1 \\ \\ D_j \\ \\ D_{L-1} \\ D_L \end{vmatrix} = \begin{vmatrix} R_0 \\ R_1 \\ \\ R_j \\ \\ R_{L-1} \\ R_L \end{vmatrix}$$

Aj, Bj and C_j are 3X3 matrix and D_j, R_j are 1X3 vectors.

The system of Eqn. 4.8 is solved for D_j, by a block elimination method and the solution for U, G and Ψ are updated via Eqns. 4.6. The procedure is repeated until

$$|D_j|<\pi \qquad j=0,1,2,3..$$

where π is an arbitrary small value.

The coefficient matrices A_0 and A_L are greatly dependent upon the boundary conditions of the wake. For case of symmetric wake, where boundary conditions are : $U|_{Y=\infty}=U_e$, $\partial U/\partial Y|_{Y=0}=0$ and $\Psi|_{Y=0}=0$.
This implies that:

$$\delta\psi_0=0,\delta G_0=0,\delta U_L=0 \qquad ..(4.9)$$

4.1.2 Solution of Closure Equations

The closure equations (K and ε equations, in K-ε model and $\overline{u_i u_j}$ in Reynolds stress model) are approximated in the same manner as in the previous section. They can all be written in a general form as:

$$U\frac{\partial\phi}{\partial X}+V\frac{\partial\phi}{\partial Y}=\frac{\partial}{\partial Y}\Gamma\frac{\partial\phi}{\partial Y}+\Sigma_\phi \qquad ..(4.10a)$$

where Γ is an apparent diffusion coefficient, and Σ_ϕ is a source term.

$$\Gamma=\tau_0+\tau_1\phi \qquad ..(4.10b)$$

$$\Sigma_\phi=\sigma_0+\sigma_1\phi+\sigma_2\phi^2 \qquad ..(4.10c)$$

In the k-ε model:

$$\phi=\begin{vmatrix} K \\ \\ \varepsilon \end{vmatrix} \qquad ..(4.11a)$$

and in the Reynolds stress model, ϕ represents:

$$\phi = \begin{vmatrix} \overline{uv} \\ \overline{u^2} \\ \overline{v^2} \\ \overline{w^2} \\ \varepsilon \end{vmatrix} \qquad ..(4.11b)$$

Tables 4.3 and 4.4 give these terms for k-ε and the Reynolds stress model.

Transport equation, Eqn. 4.10 is rewritten as set of first order differential equations.

$$\frac{\partial \phi}{\partial Y} = \xi \qquad ..(4.12a)$$

$$U\frac{\partial \phi}{\partial X} + V\xi = \frac{\partial}{\partial Y}\Gamma\xi + \Sigma_\phi \qquad ..(4.12b)$$

Again the finite difference approximations are obtained by centering Eqn. 4.12a on (i,j-1/2) in the grid cell shown in Fig. 4.1, and Eqn. 4.12b is centered on (i-1/2,j-1/2) . The resulting equations are:

$$(\phi_{i,j} - \phi_{i,j-1})\frac{1}{h_j} = (\xi_{i,j} + \xi_{i,j-1})\frac{1}{2} \qquad ..(4.13a)$$

$$\frac{U}{2K_i}(\phi_{i,j} + \phi_{i,j-1} - 2\phi_{i,j-\frac{1}{2}}) + \frac{V}{4}(\xi_{i,j} + \xi_{i,j-1} + 2\xi_{i,j-\frac{1}{2}}) =$$
$$\frac{1}{4}[(\Gamma\xi)_{i,j} - (\Gamma\xi)_{i,j-1} + (\Gamma\xi)_{i-1,j} - (\Gamma\xi)_{i,j-1}] + \Sigma_\phi \qquad ..(4.13b)$$

Equations 4.13 are linearized by using the Newton method.

$$-\frac{h_J}{2}\delta\xi_{j-1} + \delta\phi_{j-1} - \frac{h_j}{2}\delta\xi_j + \delta\phi_j = R_{1j} \qquad ..(4.14a)$$

$$S_{1j}\delta\xi_{j-1} + S_{2j}\delta\phi_{j-1} + S_{3j}\delta\xi_j + S_{4j}\delta\phi_j = R_{2j} \qquad ..(4.14b)$$

where,

$$R_{1j}=-\phi_{i,j}+\phi_{i,j-1}-\frac{h_j}{2}(\xi_{i,j}+\xi_{i,j-1})$$

$$R_{2j}=-\frac{U}{2K_i}(\phi_j+\phi_{j-1}-2\phi_{i-1,j-\frac{1}{2}})-\frac{V}{4}(\xi_j+\xi_{j-1}+2\xi_{i-1,j-\frac{1}{2}})$$

$$+\frac{1}{2h_j}[(\Gamma\xi)_j-(\Gamma\xi)_{j-1}+(\Gamma\xi)_{i-1,j}-(\Gamma\xi)_{i-1,j-1}]+\Sigma_\phi$$

and

$$S_{1j}=-\frac{V}{4}+\frac{1}{2h_J}\Gamma_{j-1}$$

$$S_{2j}=-\frac{U}{2K_i}-\frac{1}{4}(\sigma_1+2\sigma_2\phi)_{j-1}+\frac{1}{2h_j}(\tau_1\xi)_{j-1}$$

$$S_{3j}=-\frac{V}{4}+\frac{1}{2h_j}\Gamma_j$$

$$S_{4j}=-\frac{U}{2K_i}-\frac{1}{4}(\sigma_1+2\sigma_2\phi)_j-\frac{1}{2h_j}(\tau_1\xi)_j$$

In the above formulation, U, V and Σ_ϕ are approximated at point (i-1/2,j-1/2) of grid cell shown in Fig. 4.1. The boundary conditions for the closure equations are $\phi|_{Y=\infty}=\phi_e$ and $\partial\phi/\partial Y|_{Y=0}=0$. This implies that:

$$\delta\xi_0=0,\ \ \delta\phi_l=0 \qquad ..(4.15)$$

The linearized finite difference equations are then written in the matrix form of Eqn. 4.8. However, when ϕ represents $\overline{uv}$ the boundary conditions are $\delta\phi_0=0$ and $\delta\phi_L=0$; the matrix is ajdusted for that. The diagonal and the off diagonals submatrices are 2X2 in this case. The matrices are then solved by the same block elimination method of Eqn. 4.8.

4.2 Computation of Asymmetric Wakes

4.2.1 von Mises Transformation.

Under this transformation instead of the Cartesian coordinates (X,Y), von Mises[6] introduced streamline function ψ along with streamwise coordinate X as independent variables. By employing the streamline function continuity is automatically satisfied, and therefore, one has to solve one less equation. In the case of asymmetric wakes, where many more grid points have to be used relative to the case of symmetric wakes, this transformation saves a great deal of computation time. In this context the transformation is given as:

$$\frac{\partial}{\partial X}=\frac{\partial}{\partial X}-V\frac{\partial}{\partial \psi} \qquad ..(4.16a)$$

$$\frac{\partial}{\partial Y}=U\frac{\partial}{\partial \psi} \qquad ..(4.16b)$$

Then the momentum equation becomes:

$$U\frac{\partial U}{\partial X}=U\frac{\partial}{\partial \psi}bU\frac{\partial U}{\partial \psi}+\Sigma_u \qquad ..(4.17)$$

and the common form of the closure equation becomes:

$$U\frac{\partial \phi}{\partial X}=U\frac{\partial}{\partial \psi}(\Gamma_\phi U\frac{\partial \phi}{\partial \psi})+\Sigma_\phi \qquad ..(4.18)$$

The transverse direction Y is calculated via:

$$Y=\int\frac{1}{U}d\psi \qquad ..(4.19)$$

Tables 4.5 and 4.6 give the equivalent terms for K-ε and Reynolds stress models. Equations 4.17 and 4.18 have a common form, the solution

technique for one is presented in the following section.

4.2.2 Solution of Governing Equation in (X,Ψ) Space

As explained earlier, the system of governing equations are written as set of first order partial differential equations.

$$\frac{\partial \phi}{\partial \psi} = \xi \qquad ..(4.20a)$$

$$U\frac{\partial \phi}{\partial X} = U\frac{\partial}{\partial \psi}(U\Gamma\xi) + \Sigma_\phi \qquad ..(4.20b)$$

The finite difference approximations are obtained by centering Eqn. 4.19a on (i,j-1/2) in the grid cell shown in Fig. 4.1, and Eqn. 4.19b is centered on (i-1/2,j-1/2) . The resulting system of equations are linearized by using the newton method,

$$-h_j\frac{\delta\xi_{j-1}}{2} + \delta\phi_{j-1} - h_j\frac{\delta\xi_j}{2} + \delta\phi_j = R_{1j} \qquad ..(4.21a)$$

$$S_{1j}\delta\xi_{j-1} + S_{2j}\delta\phi_{j-1} + S_{3j}\delta\xi_j + S_{4j}\delta\phi_j = R_{2j} \qquad ..(4.21b)$$

where

$$R_{1j} = -\phi_i + \phi_i - h_j\frac{\xi_i - \xi_i}{2}$$

$$R_{2j} = -\frac{U}{2K_i}(\phi_j + \phi_{j-1} - 2\phi_{i-1,j-\frac{1}{2}}) + \frac{U^2}{2h_j}[(\Gamma\xi)_j - (\Gamma\xi)_{j-1}]$$
$$+\frac{1}{2h_j}[(\Gamma\xi)_{i-1,j} - (\Gamma\xi)_{i-1,j-1}] + UG(\Gamma\xi)_{i-\frac{1}{2},j-\frac{1}{2}} + \Sigma_\phi$$

and

$$S_{1j}=(U^2/h_j-UG/2)\Gamma_{j-1}/2$$

$$S_{2j}=U/(2K_i)+(U^2/h_j-UG/2)(\tau_1\phi)_{j-1}/2-(\sigma_1+2\sigma_2\phi)_{j-i}/4$$

$$S_{3j}=(U^2/h_j-UG/2)\Gamma_j/2$$

$$S_{4j}=U/2K_i-(U^2/h_j-UG/2)(\tau_1\phi)_j/2-(\sigma_1+2\sigma_2\phi)_j/4$$

In the present formulation G represents the gradient of mean velocity with respect to streamline function i.e., $G=\partial U/\partial\Psi$. The system of Eqns. 4.21, subject to the boundary conditions, $\delta\phi_0=0$ and $\delta\phi_L=0$, are written in form of matrix Eqn. 4.8, and are solved by the same block elimination method.

In Reynolds stress model, if the mean momentum equation is written in the form of Eqn. 4.18 the coefficient of diffusion would be kinematic viscosity ν. Due to small magnitude of ν the diffusion term would have an order of magnitude smaller than the source term, and the equation becomes essentially first order. This causes inaccuracy in the solution. To avoid this the source term in the mean momentum equation is combined with the diffusion term, and the equation written in the following form:

$$U\frac{\partial U}{\partial X}=U\frac{\partial}{\partial\psi}[U(\nu\frac{\partial U}{\partial\psi}-\frac{\overline{uv}}{U})]$$

The above version of mean momentum equation is approximated in the same manner as the other equations and is solved with the same block elimination technique.

	D /Dt	Dif.	Prod.	Diss.
K	$U\frac{\partial K}{\partial X}+V\frac{\partial K}{\partial Y}$	$\frac{1}{\rho\sigma_K}\frac{\partial}{\partial Y}[\mu_T\frac{\partial K}{\partial Y}]$	$\frac{\mu_T}{\rho}(\frac{\partial U}{\partial Y})^2$	$-\varepsilon$
ε	$U\frac{\partial \varepsilon}{\partial X}+V\frac{\partial \varepsilon}{\partial Y}$	$\frac{1}{\rho\sigma_\varepsilon}\frac{\partial}{\partial Y}[\mu_T\frac{\partial \varepsilon}{\partial Y}]$	$\frac{C_{\varepsilon 1}}{\rho}\mu_T\frac{\varepsilon}{K}(\frac{\partial U}{\partial Y})$	$-C_{\varepsilon 2}(\frac{\varepsilon^2}{K})$

$$\mu_T=C_\mu\rho\frac{K^2}{\varepsilon}$$

Table 4.1 K-ε Model

	D /Dt	Dif.	Prod.	Diss.	Φ_{ij}
$\overline{u^2}$	$U\frac{\partial \overline{u^2}}{\partial X}+V\frac{\partial \overline{u^2}}{\partial Y}$	$C_S\frac{\partial}{\partial Y}[\frac{K}{\varepsilon}\overline{v^2}\frac{\partial \overline{u^2}}{\partial Y}]$	$-2\overline{uv}\frac{\partial U}{\partial Y}$	$-\frac{2}{3}\varepsilon$	$-C_{\phi 1}\frac{\varepsilon}{K}[\overline{u^2}-\frac{2}{3}K]+\frac{4}{3}C_{\phi 2}\overline{uv}\frac{\partial U}{\partial Y}$
$\overline{v^2}$	$U\frac{\partial \overline{v^2}}{\partial X}+V\frac{\partial \overline{v^2}}{\partial Y}$	$C_S\frac{\partial}{\partial Y}[\frac{K}{\varepsilon}\overline{v^2}\frac{\partial \overline{v^2}}{\partial Y}]$	0	$-\frac{2}{3}\varepsilon$	$-C_{\phi 1}\frac{\varepsilon}{K}[\overline{v^2}-\frac{2}{3}K]-\frac{2}{3}C_{\phi 2}\overline{uv}\frac{\partial U}{\partial Y}$
$\overline{w^2}$	$U\frac{\partial \overline{w^2}}{\partial X}+V\frac{\partial \overline{w^2}}{\partial Y}$	$C_S\frac{\partial}{\partial Y}[\frac{K}{\varepsilon}\overline{v^2}\frac{\partial \overline{w^2}}{\partial Y}]$	0	$-\frac{2}{3}\varepsilon$	$-C_{\phi 1}\frac{\varepsilon}{K}[\overline{w^2}-\frac{2}{3}K]-\frac{2}{3}C_{\phi 2}\overline{uv}\frac{\partial U}{\partial Y}$
$\overline{uv}$	$U\frac{\partial \overline{uv}}{\partial X}+V\frac{\partial \overline{uv}}{\partial Y}$	$C_S\frac{\partial}{\partial Y}[\frac{K}{\varepsilon}\overline{v^2}\frac{\partial \overline{uv}}{\partial Y}]$	$-\overline{v^2}\frac{\partial U}{\partial Y}$	0	$-C_{\phi 1}\frac{\varepsilon}{K}\overline{uv}+C_{\phi 2}\overline{v^2}\frac{\partial U}{\partial Y}$
ε	$U\frac{\partial \varepsilon}{\partial X}+V\frac{\partial \varepsilon}{\partial Y}$	$C_\varepsilon\frac{\partial}{\partial Y}[\frac{K}{\varepsilon}\overline{v^2}\frac{\partial \varepsilon}{\partial Y}]$	$-C_{\varepsilon 1}\frac{\varepsilon}{K}\overline{uv}(\frac{\partial U}{\partial Y})$	$-C_{\varepsilon 2}\frac{\varepsilon^2}{K}$	0

Table 4.2 Reynolds Stress Model

ϕ	τ_0	τ_0	σ_0	σ_1	σ_2
K	$\frac{1}{\rho\sigma_K}\mu_T$	0	$\frac{\mu_T}{\rho}(\frac{\partial U}{\partial Y})^2-\varepsilon$	0	0
ε	$\frac{1}{\rho\sigma_\varepsilon}\mu_T$	0	0	$\frac{C_{\varepsilon 1}}{\rho}\frac{\mu_T}{K}(\frac{\partial U}{\partial Y})^2$	$-\frac{C_{\varepsilon 2}}{K}$

Table 4.3 Various Terms in Common Form of K-ε Model

ϕ	τ_0	τ_0	σ_0	σ_1	σ_2
$\overline{u^2}$	$c_s\frac{K}{\varepsilon}\overline{v^2}$	0	$\frac{2}{3}(C_{\phi 1}-1)\varepsilon+(\frac{4}{3}C_{\phi 2}-2)\overline{uv}\frac{\partial U}{\partial Y}$	$-C_{\phi 1}\frac{\varepsilon}{K}$	0
$\overline{v^2}$	0	$C_s\frac{K}{\varepsilon}$	$\frac{2}{3}(C_{\phi 1}-1)\varepsilon-\frac{2}{3}C_{\phi 2}\overline{uv}\frac{\partial U}{\partial Y}$	$-C_{\phi 1}\frac{\varepsilon}{K}$	0
$\overline{w^2}$	$C_s\frac{K}{\varepsilon}\overline{v^2}$	0	$\frac{2}{3}(C_{\phi 1}-1)\varepsilon-\frac{2}{3}C_{\phi 2}\overline{uv}\frac{\partial U}{\partial Y}$	$-C_{\phi 1}\frac{\varepsilon}{K}$	0
$\overline{uv}$	$C_s\frac{K}{\varepsilon}\overline{v^2}$	0	$(C_{\phi 1}-1)\overline{v^2}\frac{\partial U}{\partial Y}$	$-C_{\phi 1}\frac{\varepsilon}{K}$	0
ε	$C_s\frac{K}{\varepsilon}\overline{v^2}$	0	0	$-C_{\varepsilon 1}\frac{\overline{uv}}{K}\frac{\partial U}{\partial Y}$	$-\frac{C_{\varepsilon 1}}{K}$

Table 4.4 Various Terms in Common Form of Reynolds Stress Model

ϕ	τ_0	τ_0	σ_0	σ_1	σ_2
K	$\frac{1}{\rho\sigma_K}\mu_T$	0	$\frac{\mu_T}{\rho}U^2(\frac{\partial U}{\partial \Psi})^2-\varepsilon$	0	0
ε	$\frac{1}{\rho\sigma_\varepsilon}\mu_T$	0	0	$\frac{C_{\varepsilon 1}}{\rho}\frac{\mu_T}{K}U^2(\frac{\partial U}{\partial \Psi})^2$	$-\frac{C_{\varepsilon 2}}{K}$

Table 4.5 Various Terms in Common Form of K-ε Model in (X,Ψ) Space

ϕ	τ_0	τ_0	σ_0	σ_1	σ_2
$\overline{u^2}$	$c_s\frac{K}{\varepsilon}\overline{v^2}$	0	$\frac{2}{3}(C_{\phi 1}-1)\varepsilon+(\frac{4}{3}C_{\phi 2}-2)\overline{uv}U\frac{\partial U}{\partial \Psi}$	$-C_{\phi 1}\frac{\varepsilon}{K}$	0
$\overline{v^2}$	0	$C_s\frac{K}{\varepsilon}$	$\frac{2}{3}(C_{\phi 1}-1)\varepsilon-\frac{2}{3}C_{\phi 2}\overline{uv}U\frac{\partial U}{\partial \Psi}$	$-C_{\phi 1}\frac{\varepsilon}{K}$	0
$\overline{w^2}$	$C_s\frac{K}{\varepsilon}\overline{v^2}$	0	$\frac{2}{3}(C_{\phi 1}-1)\varepsilon-\frac{2}{3}C_{\phi 2}\overline{uv}U\frac{\partial U}{\partial \Psi}$	$-C_{\phi 1}\frac{\varepsilon}{K}$	0
$\overline{uv}$	$C_s\frac{K}{\varepsilon}\overline{v^2}$	0	$(C_{\phi 1}-1)\overline{v^2}U\frac{\partial U}{\partial \Psi}$	$-C_{\phi 1}\frac{\varepsilon}{K}$	0
ε	$C_s\frac{K}{\varepsilon}\overline{v^2}$	0	0	$-C_{\varepsilon 1}\frac{\overline{uv}}{K}U\frac{\partial U}{\partial \Psi}$	$-\frac{C_{\varepsilon 1}}{K}$

Table 4.6 Various Terms in Common Form of Reynolds Stress Model in (x,Ψ) Space

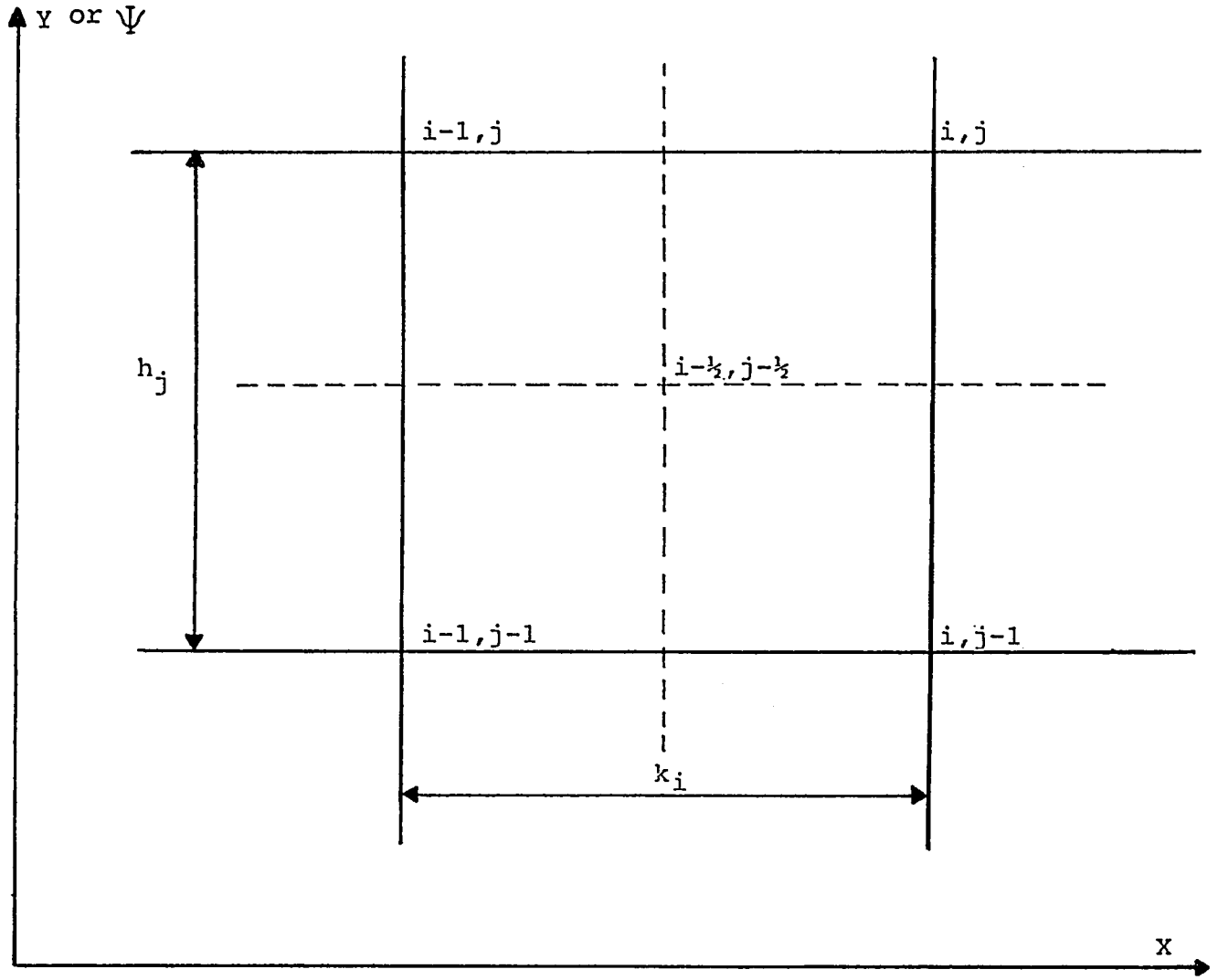

Fig. 4.1 A Typical Grid Cell in Computational Domain

CHAPTER 5

EXPERIMENTAL EQUIPMENT, METHOD, INSTRUMENTATION AND DATA PROCESSING

The objective of this experimental program was to study the effect of different length scales and levels of free stream turbulence on the development and characteristics of symmetric as well as asymmetric wakes. The study includes measurement of decay of grid generated turbulence intensity and integral length scale. The wake properties, mean velocity profile, turbulence intensity, Reynolds stress and frequency spectra were measured with the same inlet free stream velocity but different turbulence levels and integral length scales in the free stream.

5.1 Model

The model used was 704.7 mm (long) by 457.2 mm (wide) and is made of 9.5 mm thick aluminum plate, as shown in Fig. 5.1. The leading edge of the model is rounded to a 1:2 elliptical shape. The last 228.5 mm is tapered at an inclined angle of 1.15 degree along its width, terminating in a nominal trailing edge thickness of 0.5 mm. A 2.5 mm diameter steel trip wire was used. It was glued at a distance of 80 mm from the leading edge on either side of the model to promote early boundary layer transition. The thickness of the boundary layer at the trailing edge was about 14 mm

with the presence of the trip wires. The half wake width very close to the trailing edge of the plate was 12.5 mm. However, in the case of asymmetric wake the trip wire on the upper surface of model was removed and the first 457.2 mm of upper side of the model was covered by 20 grate sand paper. The model was bolted horizontally in the test section. A description of the wind tunnel is given by Hazarika [61]. The free stream velocity was maintained as close as possible to 22.5 m/s.

5.2 Turbulence Generating Grid

Free stream turbulence was generated with the aid of grids. Two sets of grids were employed in the experimentation. Grid one was a biplane grid made of cylindrical plexiglass rods, having diameter of 3.18 mm. The distance between the centerlines of the rods was 25.4 mm giving a mesh size (m/d) of 8. The solidity ratio was 0.18 which was well below the maximum allowable ratio of 0.5.

Grid two was also a biplane grid made of rectangular plexiglass square rods of 6.36 by 3.18 mm, with the larger dimension facing the flow. The distance between the centerline of each rod was 50.8 mm resulting in a mesh size of 8. the solidity ratio was 0.18, well below the maximum allowable ratio of 0.5.

The grids were placed a distance of 83.2 mm ahead of the leading edge of the model. Grid one produced relatively more isotropic turbulence than grid two. However, grid two produced higher level and larger length

scale free stream turbulence than grid one. The ratio of normal turbulent stress produced by both grids varied between 0.92 to 0.95.

5.3 Mean Velocity and Turbulence Quantities Measurement

5.3.1 Mean Velocity

Profiles of mean velocity in the wake were measured with the aid of a 1.6 mm pitot-static probe. The mean free stream velocity was measured with aid of a 1.6 mm pitot-static probe positioned in the free stream. This velocity was used as a reference velocity for non-dimensionalizing the local velocities.

Profiles of mean velocity in the boundary layer upstream of the trailing edge were measured by using a pitot tube to measure the total pressure at a station and then a static probe to measure the static pressure at the same location. The difference between the two measurements was used to calculate the mean velocity.

The pressure probes were connected to precalibrated Validyne pressure transducers and demodulators. The output of the transducers and demodulator were digitized with aid of Metrabyte SSH4 sample and hold unit in combination with DASH-20 A/D board. The digitized data were processed in real time to obtain the mean pressure.

5.3.2 Turbulence Quantities

A single sensor hot-wire probe was used for establishment of free

stream turbulence and uniformity of the grid generated free stream turbulence.

A cross hot-wire probe was used for measurement of mean velocity as well as the turbulence quantities in the wake and the grid generated turbulent free stream. A schematic of the cross wire and its position relative to the model coordinate frame is given in Fig. 5.2.

The output voltage of each hot-wire anemometer is related to the effective velocity according to King's law. i.e.

$$E_i^2 = E_{0,i}^2 + b_i U_{eff,i}^{n_i}; \text{ for } i=1,2 \qquad ..(5.1)$$

where $E_{0,i}$, b_i, and n_i are obtained from calibration of each wire, E_i is output voltage of the i^{th} anemometer, and $U_{eff,i}$ is the effective velocity related to wire i.

The effective velocity is related to the velocity vector through the cosine law which makes the assumption that the component of velocity vector normal to the plane of the cross wire does not contribute to the effective velocity. Under this condition, one can resolve the instantaneous velocity vector $\underline{U}$ as:

$$U_{eff,1}^2 = \underline{U}^2(\cos^2\beta + K_1^2 \sin^2\beta) \qquad ..(5.2)$$

and

$$U_{eff,2}^2 = \underline{U}^2(\cos^2\alpha + K_2^2 \sin^2\alpha) \qquad ..(5.3)$$

where K_1 and K_2 are correction factor of the cosine law and depend on the diameter to length ratio and the material of the hot-wire. They are obtained

by calibration. Due to the orthogonal construction of the cross-wire; one can say:

$$\alpha+\beta=\frac{\pi}{2} \qquad ..(5.4)$$

Equations 5.2 and 5.3 were simplified using Eqn. 5.4 to obtain the instantaneous velocity vector, as well as angle β, resulting in the following equations:

$$\underline{U}=\left[\frac{2U_{eff,1}^{2}}{1+K_1^2+(1-K_1^2)\cos 2\beta}\right]^{\frac{1}{2}} \qquad ..(5.5)$$

$$\beta=\frac{1}{2}\cos^{-1}\left[\frac{U_{eff,1}^{2}(1+K_2^2)-U_{eff,2}^{2}(1+K_1^2)}{U_{eff,1}^{2}(1-K_2^2)+U_{eff,2}^{2}(1-K_1^2)}\right] \qquad ..(5.6)$$

The instantaneous velocities in (X,Y) direction can, therefore, be computed as:

$$\underline{U}_x=\underline{U}(\cos\gamma\cos\beta+\sin\gamma\sin\beta) \qquad ..(5.7)$$

$$\underline{U}_y=\underline{U}(\sin\gamma\cos\beta-\cos\gamma\sin\beta) \qquad ..(5.8)$$

Where γ is the angle between the x-axis and sensor number 2.

5.3.3 Data Processing

The voltage output of the anemometers connected to each sensor of the cross-wire probe were low-pass filtered and then digitized and stored. During the data processing the effective velocity on each wire is computed by using digitized voltages for each sensor and employing Eqn. 5.1 and the calibration curve for each wire. The magnitude of the instantaneous velocity and the angles it makes with the sensors are then calculated by employing

Eqns. 5.5 and 5.6. Thereafter, the instantaneous velocities in X and Y coordinates are determined by applying Eqns. 5.7 and 5.8. The mean velocity, the turbulence intensities as well as shear stress are thus found by statistical averaging of these instantaneous velocities.

5.3.4 Power Spectra

The power spectral density of the fluctuating streamwise velocity is obtained by using the data collected with cross wire measurements. The instantaneous values of steamwise velocity $\underline{U}_x$ computed from Eqn. 5.7 is Fourier transformed. The power spectral density (PSD) is then computed from the Fourier components of the transformed velocities.

The power spectral density function is related to Fourier transform of $\underline{U}_x$, $X_{\underline{Ux}}(f,T)$, by relation [62],

$$PSD = \frac{2}{T} |X_{\underline{Ux}}(f,T)|^2 \qquad ..(5.9)$$

where T represents the finite time interval of sample record, and is equal to the number of samples in the record (N) divided by the sampling frequency (f_s), $X_{\underline{Ux}}(f,T)$ is given by

$$X_{\underline{Ux}}(f,T) = \frac{1}{f_s} \sum_{n=0}^{N-1} \underline{U}_X(n) e^{-i2\pi fn/f_s} \qquad ..(5.10)$$

The Fourier components at discrete frequencies, f_m are computed and related to $X_{\underline{Ux}}(f,T)$ as follows:

$$X_{\underline{Ux}}(m)=X_{\underline{Ux}}(f_m,T)f_s=\sum_{n=0}^{N-1}\underline{U}_x(n)e^{-i2\pi mn/N} \quad m=0,1,..,N-1 \qquad ..(5.11)$$

where $f_m=mf_s/N$. The values of Fourier components are computed by a radix 2 FFT (Fast Fourier Transform) technique [63]. This algorithm was employed to reduce the computation time.

5.4 Measurement of Dissipation Rate of Energy in Free Stream

The dissipation rate of turbulence kinetic energy ε is given as:

$$\varepsilon=\nu\overline{\left(\frac{\partial u_i}{\partial X_j}\right)\left(\frac{\partial u_i}{\partial X_j}\right)} \qquad ..(5.12)$$

In the dissipation scale of turbulence, due to its very small length scale, the turbulence structure tends to be isotropic. In isotropic turbulence, the most important term in Eqn. 5.12 is $(\partial u/\partial X)^2$ and hence Eqn. 5.12 reduces to (Hinze [64]):

$$\varepsilon=15\nu\overline{\left(\frac{\partial u}{\partial X}\right)^2} \qquad ..(5.13)$$

The term $\overline{(\partial u/\partial X)^2}$ will be measured by implementing the Taylor's frozen turbulence hypothesis.

The Taylor approximation states that:

$$u_i(\underline{X},t)=u_i(\underline{X}-U\tau,\ t+\tau) \qquad ..(5.14)$$

This approximation is valid if:

$$\frac{1}{\overline{(u^2)}^2}/\ U \ll 1 \qquad ..(5.15)$$

A consequence of Eqn. 5.15 is the determination of mean values of turbulence velocity gradients from single anemometer by performing time differentiation i.e.:

$$\overline{\left(\frac{\partial u}{\partial X}\right)^2} = \frac{1}{U^2}\overline{\left(\frac{\partial u}{\partial t}\right)^2} \qquad ..(5.16)$$

Therefore, Eqn. 5.16 could be rewritten as:

$$\varepsilon = 15\frac{\nu}{U^2}\overline{\left(\frac{\partial u}{\partial t}\right)^2} \qquad ..(5.17)$$

The dissipation rate of turbulence kinetic energy in the free stream was determined by using the cross-wire probe data. The cross wire has sensing elements smaller than Taylor microscale in the free stream. The stored data was processed to determine $\overline{(\partial u/\partial X)^2}$, by performing time differentiation of instantaneous axial velocity and ensemble averaging of the square of derivatives.

A summary of the quantities measured is given in Table 5.1.

FREE STREAM FLOW PROPERTIES MEASURED

Test Model	Turbulence Quantities	Mean Velocity	Dissipation Rate
GRID 1	$\overline{u^2}$, $\overline{v^2}$	U	ε
GRID 2	$\overline{u^2}$, $\overline{v^2}$	U	ε

WAKE FLOW PROPERTIES MEASURED

SYMMETRIC WAKE

Test Model	Turbulence Quantities	Mean Velocity
Airfoil	$\overline{u^2}$, $\overline{v^2}$, $\overline{uv}$	U
Grid 1+ Airfoil	$\overline{u^2}$, $\overline{v^2}$, $\overline{uv}$	U
Grid 2+ Airfoil	$\overline{u^2}$, $\overline{v^2}$, $\overline{uv}$	U

ASYMMETRIC WAKE

Test Model	Turbulence Quantities	Mean Velocity	Spectra
Airfoil	$\overline{u^2}$, $\overline{v^2}$, $\overline{uv}$	U	F(κ)
	$\overline{u^3}$, $\overline{u^2v}$, $\overline{uv^2}$, $\overline{v^3}$		
Grid 1+ Airfoil	$\overline{u^2}$, $\overline{v^2}$, $\overline{uv}$	U	F(κ)
	$\overline{u^3}$, $\overline{u^2v}$, $\overline{uv^2}$, $\overline{v^3}$		
Grid 2+ Airfoil	$\overline{u^2}$, $\overline{v^2}$, $\overline{uv}$	U	F(κ)
	$\overline{u^3}$, $\overline{u^2v}$, $\overline{uv^2}$, $\overline{v^3}$		

Table 5.1 Summary of Measured Quantities

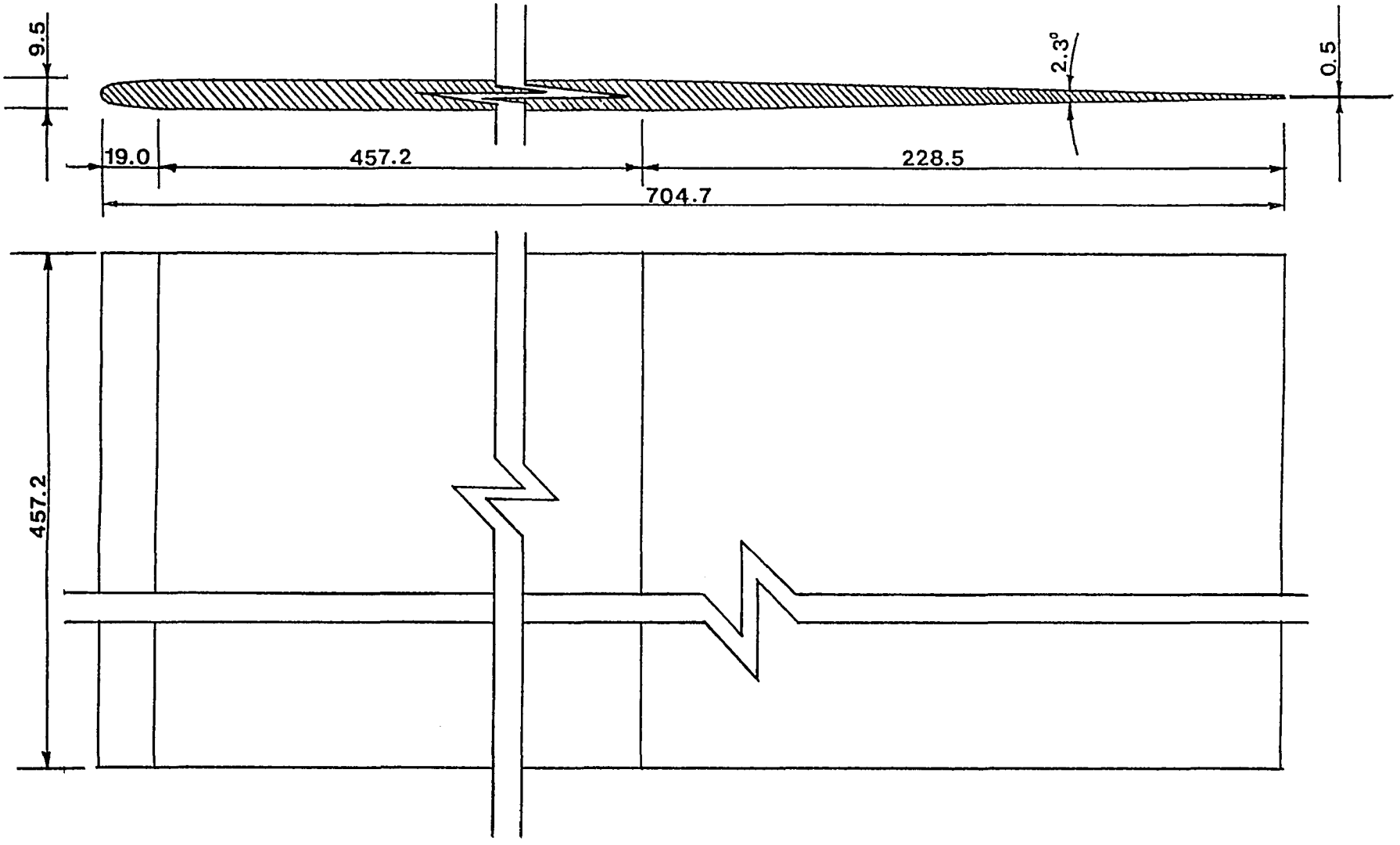

Fig. 5.1 Schematic of Wake Generating Model

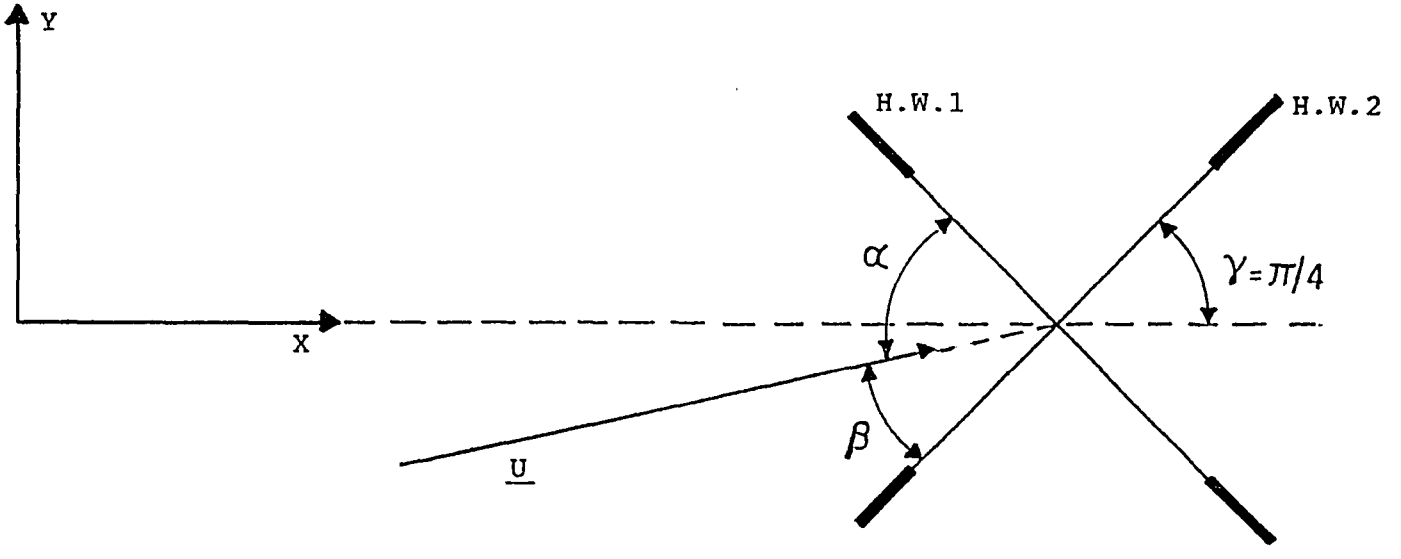

Fig. 5.2 Schematic of Cross–Wire Probe Position Relative to Model Coordinate Frame

CHAPTER 6

EXPERIMENTAL RESULTS

6.1 Grid Generated Free Stream Turbulence

Free stream turbulence was generated by the aid of two sets of grids. The grids are described in the pervious chapter, and the details of free steam turbulence generated by these two grids are presented here.

The turbulence level, dissipation rate and the turbulence length scale for the first grid -here on referred to as grid 1- are presented in Fig. 6.1. In these and all the data presented in this investigation, the origin of the axial position i.e. X=0 is at the trailing edge of the wake generating plate. The grids were positioned 788 mm upstream of the trailing edge. The dissipation rate is nondimensionalized by the free stream velocity and the momentum thickness of the wake at the trailing edge in the presence of this grid (θ_0).

Over the axial distance of measurement, the turbulence level decreases by about 10%, the length scale remains essentially constant and the dissipation rate decays by about 20%. The small changes in these quantities is due to the fact that measurement was done about 31 mesh length downstream of the grid. The turbulence was essentially isotropic. The ratio ($\overline{u^2}/\overline{v^2}$) of the grid generated turbulence was found equal to about

0.94. It varied from 0.92 at one station to 0.95 at another station.

Fig. 6.2 presents the turbulence quantities associated with the second grid- here on referred to grid 2. The turbulence level decreases by about 12%, the length scale remains essentially constant except at station X=12.7 mm where it peaks. This is attributed to experimental error. The dissipation rate decays by about 35%. These measurements were taken about 16 mesh length downstream of the grid. The turbulence was less isotropic than grid 1. The ratio $(\overline{u^2}/\overline{v^2})$ of turbulence generated by grid 2 was found equal to about 0.92. It varied from 0.89 at one station to 0.95 at another station.

The level of free stream turbulence generated by grid 2 is about twice as much as generated by grid 1. The dissipation rate of energy due to turbulence of grid 2 is three times that of grid 1. The length scale of turbulence due to grid 2 is about 3 times that of grid 1. From results presented above, one can conclude that the free stream turbulence generated by grid 2 should have much more effect on the wake development than that generated by grid 1 and when no free stream turbulence is present.

6.2 Symmetric Wake

The symmetric wake was generated with trip wire on the plate 80 mm downstream of leading edge on both sides of the plate. Three different kinds of wakes were measured for this case. First wake measured was without

any grid generated free stream turbulence. The second kind of wake was the wake with grid 1 in place, and the third wake was with grid 2 in place.

6.2.1 Mean Velocity

Figure 6.3 presents the mean velocity profile of the wake developed without free stream turbulence at four axial stations ranging from X=0 to X=152.4 mm, X=0 corresponds to the trailing edge of the plate. The profiles of mean velocity of the wake developed under free stream turbulence generated by grid 1 are given in Fig. 6.4 and the ones for grid 2 are presented in Fig. 6.5. It can be seen that these profiles are quite symmetrical. The wake recovery, and important integral properties for the three different wakes are given in Table 6.1 and shown in Figs. 6.6, 6.7 and 6.8.

It can be seen from these figures that grid 2, which generated the highest level of turbulence intensity and largest length scale, affects the wake development the most. The centerline velocity of wake is smallest with no free stream turbulence present. The shape factor is lowest with highest free stream turbulence. The displacement thickness of the wake with gird 1 turbulence is larger than no grid, while the displacement thickness of the wake with grid 2 turbulence is smaller than no grid. Similar to the displacement thickness results, the value of half wake width is larger under grid 1 turbulence and smaller under grid 2 turbulence as compared to no free stream turbulence case. Figure 6.9 presents the development of half

wake width, nondimensionalized with local momentum thickness, under varied free stream turbulence levels.

This variation in profiles of various properties is attributed to the preceding boundary layer on the plate generating the wake. In grid 2 the free stream turbulence level is high, and it affects the originating boundary layer the most. It makes the boundary layer profile fuller -lower shape factor - and, therefore, the half wake width is smaller. The higher level of free stream turbulence level, however, increases the recovery rate of wake as shown in Fig. 6.10. In Figs. 6.9 and 6.10 appropriate data of Andreopoulos et al.[13] has been presented for comparison purposes.

6.2.2 Turbulence Quantities

Figures 6.11, 6.12 and 6.13 show the distribution of turbulent intensities and shear stress across the wake under the influence of the three different free stream turbulence levels. Due to symmetry of the wake only the lower half of the wake was measured. At station I, (X=0 mm) the maximum values of $\overline{u^2}$, $\overline{v^2}$ and $\overline{uv}$ overshoot the maximum values of corresponding quantities at upstream boundary layer. This is attributed to a small separation region at the trailing edge of plate. It can be seen that these turbulent quantities become larger with larger free stream turbulence level and length scale.

Figure 6.14 presents a comparison of the turbulence axial and lateral intensities, and shear stress at two different axial stations. These quantities

are presented in local similarity variables. The turbulence quantities are normalized with respect to the local maximum value of the quantity in that profile. The normal distance Y is normalized with the half wake width.

It seems that the higher free stream turbulence increases the wake thickness and the level of turbulence quantities. As observed from Fig. 6.14 the edge values of turbulence intensities increase significantly with increases in free stream turbulence. These values also approach a finite value at the edge of the wake, which is essentially the same value as in the free stream. This indicates that the presence of disturbance in the free stream affects the outer layer of the wake and the inner core of the wake remains relatively unaffected by the disturbance in the free stream.

6.3 Asymmetric Wake

The asymmetric wake was generated by installing sand paper on the upper side of wake generating plate. The wake is then formed by the merger of two different boundary layers emanating from the upper and lower sides of the plate. There were three different free stream turbulence conditions imposed on the wake: grid 0 corresponds to no free stream turbulence, grid 1 corresponds to free stream turbulence generated by the presence of grid 1, and grid 2 corresponds to free stream turbulence generated by the pressence of grid 2.

6.3.1 Mean Velocity

Figures 6.15, 6.16 and 6.17 present the mean velocity profiles of the asymmetric wake measured at 4 axial stations ranging from X=0, at trailing edge to far wake at X=152.4 mm. The profiles of the initial boundary layer upstream of the trailing edge are also presented along with these profiles.

It is observed from these figures that boundary layers on the upper and lower surface of the plate are quite asymmetrical, and the subsequent wake is asymmetrical as well. The degree of asymmetry reduces with increasing axial distance, and the profiles become essentially symmetrical about the point of minimum velocity at the last axial station. It is noteworthy to see that the tendency toward symmetry is enhanced with increased level of free stream turbulence.

The lateral location of centerline velocity (the minimum velocity) does not vary and is essentially constat at Y=0 mm- the geometrical center of the trailing edge of the plate. This indicates that there was not a significant pressure gradient imposed on the wake due to substantially higher thickness of the boundary layer on the upper surface.

The important integral properties of the wake under varied free stream turbulence conditions are presented in Table 6.2 and are plotted in Figs. 6.18, 6.19 and 6.20. The data presented in the table and shown in the figures illustrate that at any measuring station the centerline velocity is largest and shape factor is smallest with grid 2, while the displacement thickness is largest with grid 1.

Comparison of wake centerline recovery rate and half wake width

under the varying conditions in the free stream is presented in Figs. 6.21 and 6.22. In Fig. 6.21, the half wake width of the upper layer and the lower layer of the wake has been presented along with the sum of the two. In Fig. 6.22, centerline recovery rate [Ue/(Ue-Uc)] of the symmetric wakes are also plotted along with those of the asymmetric wake. It can be observed from these figures, that higher level and larger length scale of free steam turbulence influences the wake recovery most strongly. However, the growth of the half wake width seems to be slowed by presence of free stream disturbance in the near wake, and is accelerated in far wake as indicated in Fig. 6.21. This behavior was also observed in the symmetric wake. At this stage it is not quite certain that this phenomenon is due to experimental scatter or some other phenomenon that has to be investigated further.

6.3.2 Turbulence Quantities

Variation of turbulence quantities $\overline{u^2}$, $\overline{v^2}$ and the Reynold stress $\overline{uv}$ across the wake at four axial stations and the initial boundary layer under three distinct free stream conditions are presented in Figs. 6.23, 6.24 and 6.25.

There are several noteworthy observations about these figures. One is the overshoot of the maximum value of these quantities in first (X=0) and the second (X=12.7 mm) axial stations, from their maximum value at initial boundary layer. This overshoot -as was the case in symmetric wake- is

attributed to increased mixing caused by presence of a recirculation region at the trailing edge of the plate. The overshoot subsides by axial station X=50.8 mm, and it seems to be most pronounced in $\overline{u^2}$ and to some extent in $\overline{uv}$. There also seems to be some irregularity in profile of $\overline{v^2}$ at the trailing edge (X=0) in all the cases of free stream turbulence levels. It has too many peaks and minima. This could be due to the recirculation region at the trailing edge, although no evidence of it is present in the $\overline{u^2}$ profile. It could also be attributed to the close proximity of the cross-wire to the trailing edge which interferes with the heat transfer of the sensor and may result in $\overline{v^2}$ being irregular at that location.

The turbulence quantities retain asymmetry up to the last station. The values of the turbulence quantities are higher on the upper layer of the wake, emanating from the rough side of the plate, than the lower layer of the wake. Higher level of free stream turbulence increases the peak values of these quantities. The effective thickness of these quantities across the wake becomes wider with high free stream turbulence conditions.

Figure 6.26 presents comparison of the turbulence quantities at two streamwise stations. They are plotted in local similarity variable. To obtain the plot, the turbulent quantities on the upper side of the wake is normalized with the local peak value on the upper side of the profile and the normal distance Y is normalized with local half wake width on the upper layer. The lower layer of the profiles is normalized in the same manner but with the local values of the lower wake. The geometrical center

Y=0 is used as the border between the upper and lower wake. These figures illustrate that free stream turbulence affects the outer layer of the wake and the inner core of the wake is essentially unchanged with higher free stream turbulence. It is interesting to note that as expected the quantities u2bar, v2bar tend to a finite value at the edge of the wake. The edge value of u2bar and v2bar are essentially that of the turbulence present in the free stream.

6.3.3 Triple Correlation

Figures 6.26, 6.27 and 6.27 present the triple correlations $\overline{u^3}$, $\overline{u^2v}$, $\overline{uv^2}$ and $\overline{v^3}$ across the wake, under varying free stream conditions. The correlations $\overline{u^3}$ and $\overline{uv^2}$ play a role in modeling of diffusion terms. $\overline{u^2v}$ and $\overline{v^3}$ represent the lateral diffusion flux of $\overline{u^2}$ and $\overline{v^2}$ in Y-direction. These quantities usually have the same sign as Y, but in a small region near the centerline they have opposite sign to Y. The changed sign stems from the boundary layer upstream of the trailing edge. Close to surface, $\overline{u^2v}$ and $\overline{v^3}$ also change sign. The thin layer grows into the wake as it develops.

It is interesting to note that the maximum values of $\overline{u^2v}$ and $\overline{v^3}$ overshoot the upstream boundary layer and then decays. This decay is amplified in the presence of free stream turbulence. The overshoot is largest with higher free stream disturbance level, and is also present in the minima of $\overline{u^2v}$ in the lower layer of the wake, but is not as prominent as in the upper layer.

The distribution of $\overline{u^2v}$ and $\overline{v^3}$ under no free stream truculence at

downstream stations show the same qualitative trends as those reported by references [13] and [16]. However, the maxima and minima of these profiles as reported by present investigation and references [13] and [16] differ. Table 6.3 gives the maxima and minima of these profiles. The differences in these values are attributed to the experimental set ups. It can be seen from Table 6.3 that the present measurements are within acceptable range of the same quantities measured by other investigations.

6.4 Power Spectra

The power spectral density function, PSD of u' the streamwise intensity of turbulence in the upper layer of the wake and location where u' is maximum at three axial station, namely X=-31.75 mm, X=12.7 mm and X=152.4 mm, subjected to the varying level and length scale of free stream turbulence are presented in Figs. 6.29, 6.30 and 6.31. Each PSD plot is compilation of 2048 discrete frequencies, and the fluctuation in the spectrum are due to this large number of components, and are basically a numerical phenomenon aroused in the computation of the spectra. However, there are some peaks at frequency of 3500 Hz and above. These peaks are attributed to the ambient noise present during the experimentation. The signal from the hot wires was low-pass filtered at a frequency of 15 KHz, but noise of lower frequency did get recorded along with the hot wire signal. The magnitude of these peaks in comparison to energy carrying content of spectra is small and it seems that they do not

contribute substantial error in the measurement.

It can be seen that at low frequency PSD is relatively higher with larger free stream disturbance. This indicates that u' becomes larger with higher free stream turbulence.

Due to large number of discrete frequency at which power spectrum density was available and the fluctuation of the spectral content, the spectral function in wave domain was obtained by first smoothing the power spectra density in frequency domain. This procedure involved, (i) keep the first 6 values of power spectra density unchanged, (ii) obtain an average value for every twenty values of power spectra density. Thereafter, the power spectra density in wave number domain was obtained by using the procedure suggested by Hazarika[61].

Comparison of spectral function in wave domain of maximum u' at upper boundary layer, upper layer of the wake at X=12.7 mm, and lower layer of the wake at X=50.8 mm subjected to varying free stream turbulence are presented in Fig. 6.31. It is seen from these figures that the free stream turbulence does not affect the spectra significantly, which indicates that the mechanism of energy transfer from the larger eddies to the smaller energy dissipating eddies are not greatly affected by presence of free stream turbulence, except larger eddies contain higher level of energy.

X mm	δ^* mm	θ mm	H	U_c/U_e	b/θ	Tu%	Ld/θ_0	grid
0	5.70	4.11	1.39	0.23	0.62	0	0	0
12.7	5.24	3.99	1.31	0.56	2.18	0	0	0
50.8	4.60	3.63	1.27	0.67	3.37	0	0	0
152.4	4.11	3.39	1.21	0.75	4.65	0	0	0
0	6.29	4.69	1.34	0.22	0.54	2.27	4.44	1
12.7	5.70	4.49	1.27	0.57	2.03	2.27	4.53	1
50.8	5.15	4.19	1.23	0.68	3.07	2.20	4.49	1
152.4	4.72	4.02	1.17	0.77	4.37	2.08	4.53	1
0	4.64	3.64	1.27	0.27	0.44	4.68	12.41	2
12.7	4.11	3.44	1.20	0.63	1.82	4.65	12.67	2
50.8	3.72	3.23	1.15	0.75	3.03	4.49	12.40	2
152.4	3.23	2.92	1.11	0.84	5.40	4.16	12.69	2

Table 6.1 Integral Properties of Symmetric Wake

X mm	δ^* mm	θ mm	H	U_c/U_e	b_{up}/θ_0	b_{lw}/θ_0	Tu%	Ld/θ_0	GRID
-31.7 upper	4.71	2.82	1.67	--	--	--	--	--	0
-31.7 lower	2.69	1.63	1.65	--	--	--	--	--	0
0	7.58	5.35	1.42	0.18	0.30	0.26	0	0	0
12.7	6.95	5.15	1.35	0.54	1.50	0.83	0	0	0
50.8	6.24	4.78	1.30	0.64	1.91	1.08	0	0	0
152.4	5.62	4.54	1.24	0.73	2.22	1.48	0	0	0
-31.7 upper	5.12	3.35	1.53	--	--	--	--	--	1
-31.7 lower	3.01	1.95	1.55	--	--	--	--	--	1
0	7.99	5.79	1.38	0.22	0.29	0.27	2.27	4.44	1
12.7	7.47	5.67	1.32	0.55	1.48	0.75	2.27	4.53	1
50.8	6.90	5.43	1.27	0.65	1.92	1.01	2.20	4.49	1
152.4	6.35	5.24	1.21	0.74	2.33	1.46	2.08	4.53	1
-31.7 upper	4.16	2.87	1.45	--	--	--	--	--	2
-31.7 lower	2.06	1.25	1.65	--	--	--	--	--	2
0	6.95	5.40	1.29	0.23	0.11	0.22	4.68	12.41	2
12.7	6.45	5.32	1.22	0.60	1.07	0.66	4.65	12.67	2
50.8	5.85	4.97	1.18	0.72	1.67	1.02	4.49	12.40	2
152.4	5.10	4.52	1.13	0.81	2.20	1.75	4.16	12.69	2

Table 6.2 Integral Properties of Asymmetric Wake

NEAR WAKE

u2vbar

Min:	Y (mm)	Max:	Y (mm)	X (mm)	Ref.
-0.06	0.6	0.09	15.2	12.7	[present]
-0.13	2.5	0.045	48.0	25.0	[13]
-0.18	2.0	0.11	21.1	12.7	[16]

v3bar

Min:	Y (mm)	Max:	Y (mm)	X (mm)	Ref.
-0.03	-2.5	0.065	15.2	12.7	[present]
-0.04	-2.0	0.045	1.5	25.0	[13]
-0.19	-1.8	0.11	31.1	12.7	[16]

FAR WAKE

u2vbar

Min:	Y (mm)	Max:	Y (mm)	X (mm)	Ref.
-0.04	3.8	0.07	15.2	152.4	[present]
-0.035	-21.5	0.05	50.6	400	[13]
-0.09	10.9	0.12	36.3	381	[16]

v3bar

Min:	Y (mm)	Max:	Y (mm)	X (mm)	Ref.
-0.035	-10.2	0.05	15.2	152.4	[present]
-0.03	-25.8	0.025	50.6	400	[13]
-0.07	-19.6	0.12	36.3	381	[16]

Table 6.3 Maxima and Minima of u2vbar and v3bar Profile, Asymmetric Wake, Under No Free Stream Turbulence

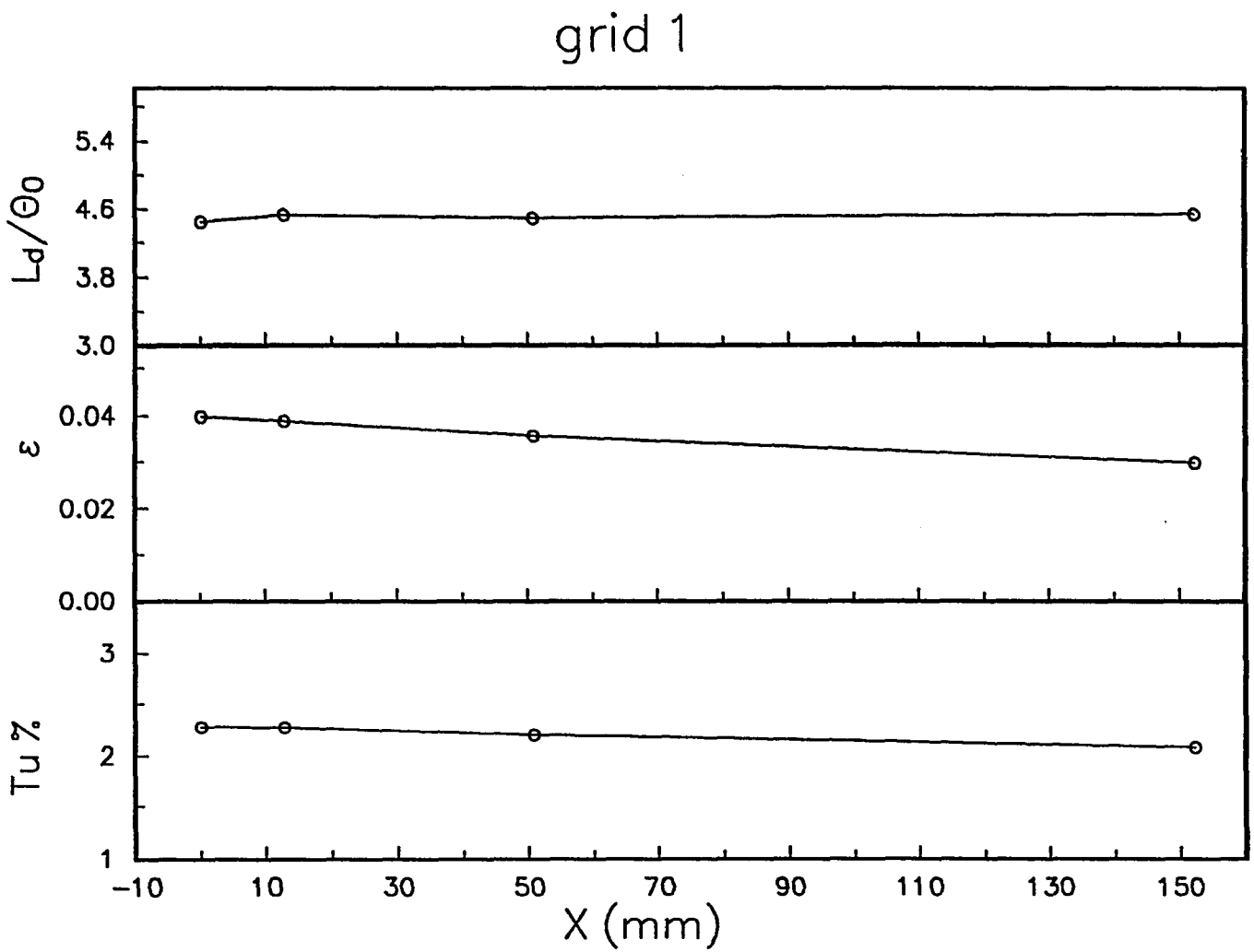

Fig. 6.1 Free Stream Turbulence Generated by Grid 1

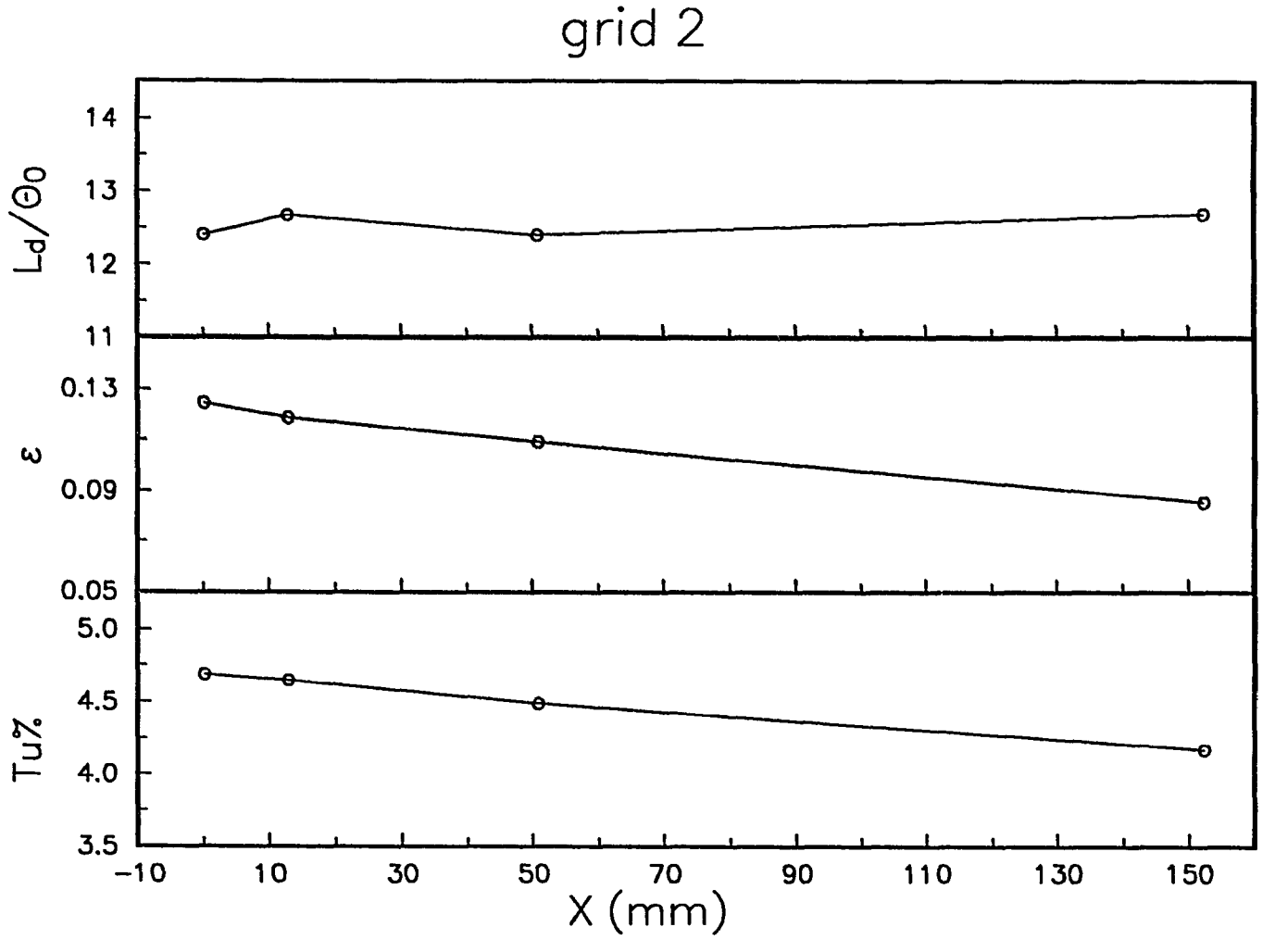

Fig. 6.2 Free Stream Turbulence Generated by Grid 2

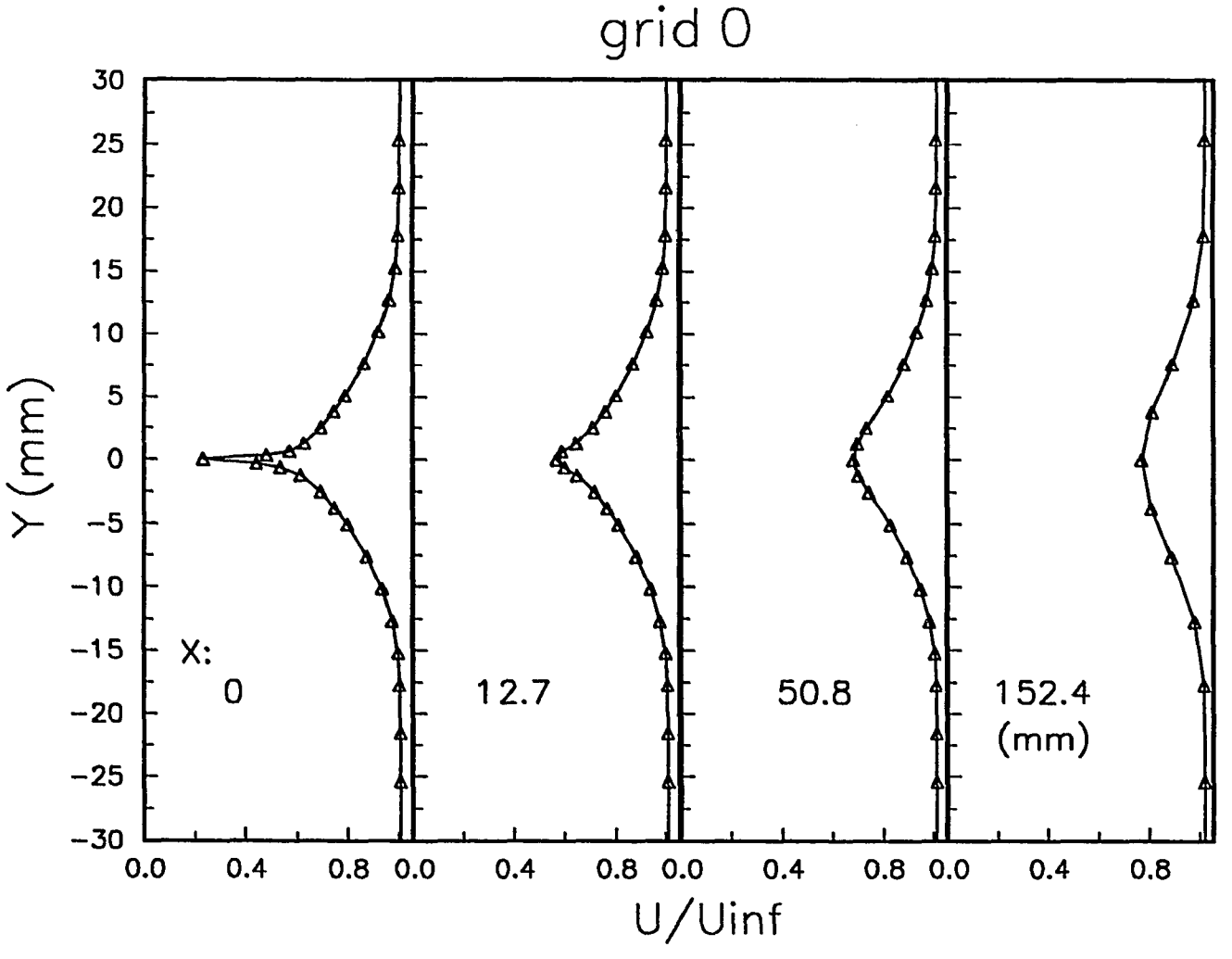

Fig. 6.3 Mean Velocity, Symmetric Wake Under No Free Stream Turbulence

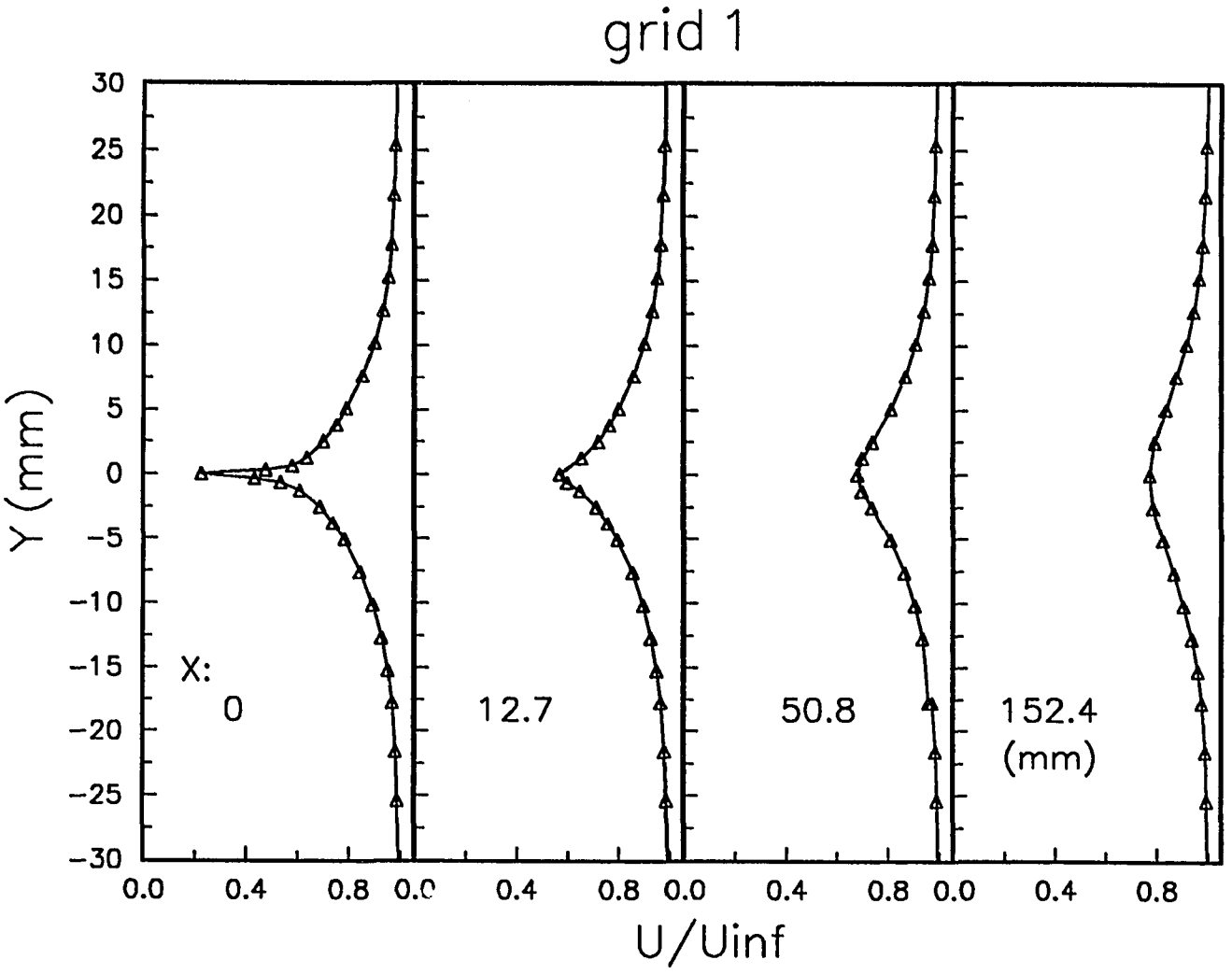

Fig. 6.4 Mean Velocity, Symmetric Wake Under Free Stream Turbulence Generated by Grid 1

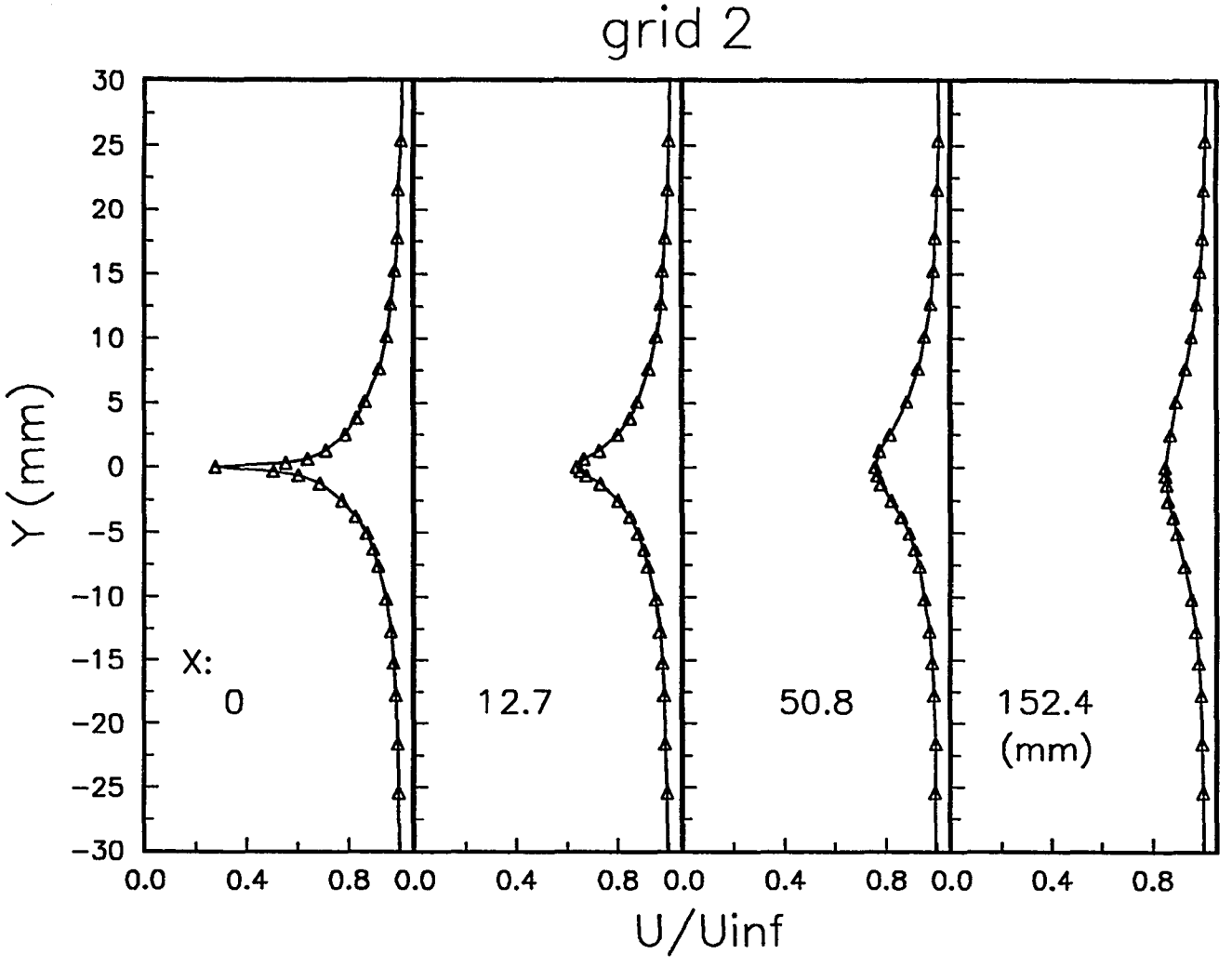

Fig. 6.5 Mean Velocity, Symmetric Wake Under Free Stream Turbulence Generated by Grid 2

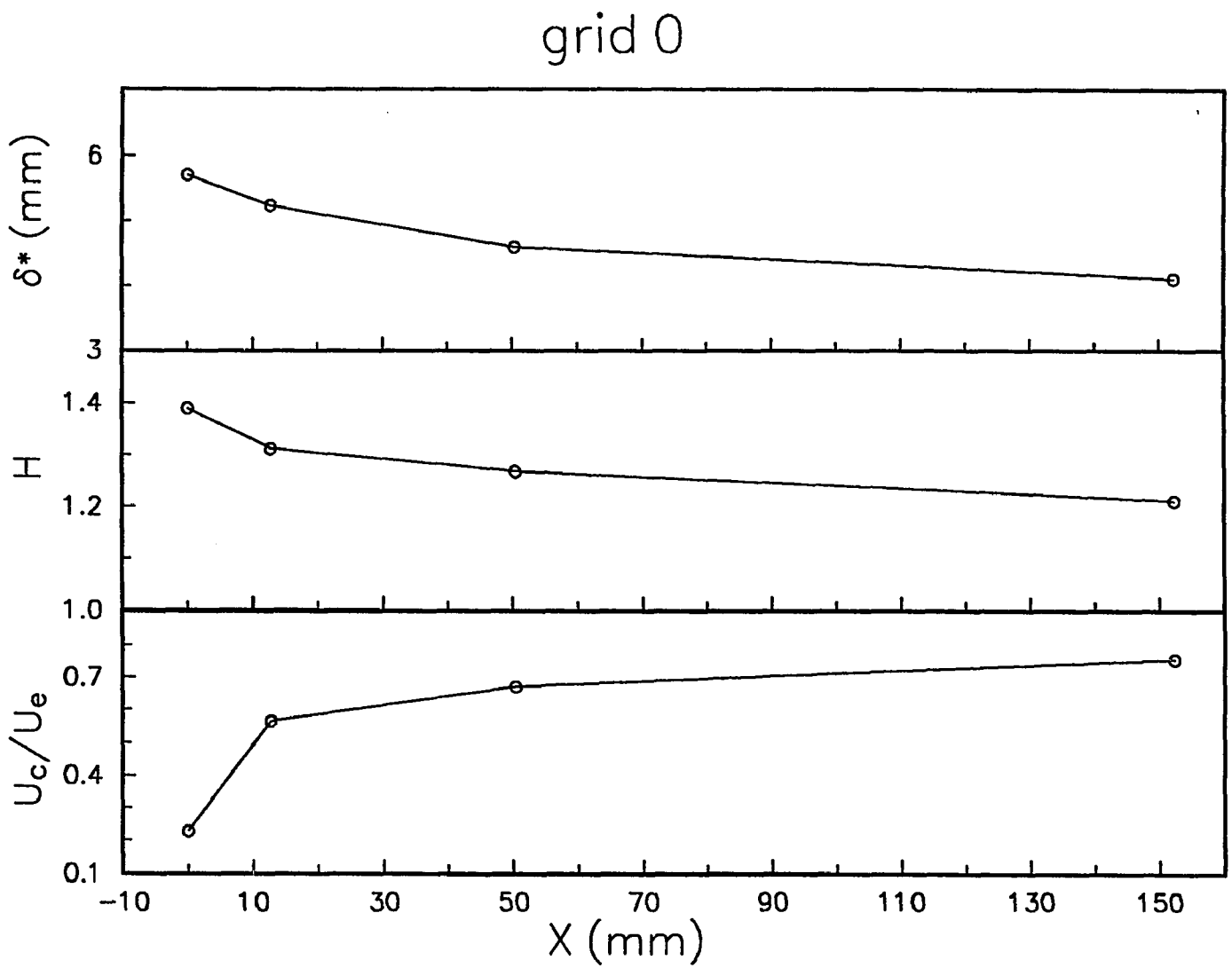

Fig. 6.6 Wake Recovery and Inetgral Properties of Symmetric Wake Under No Free Stream Turbulence

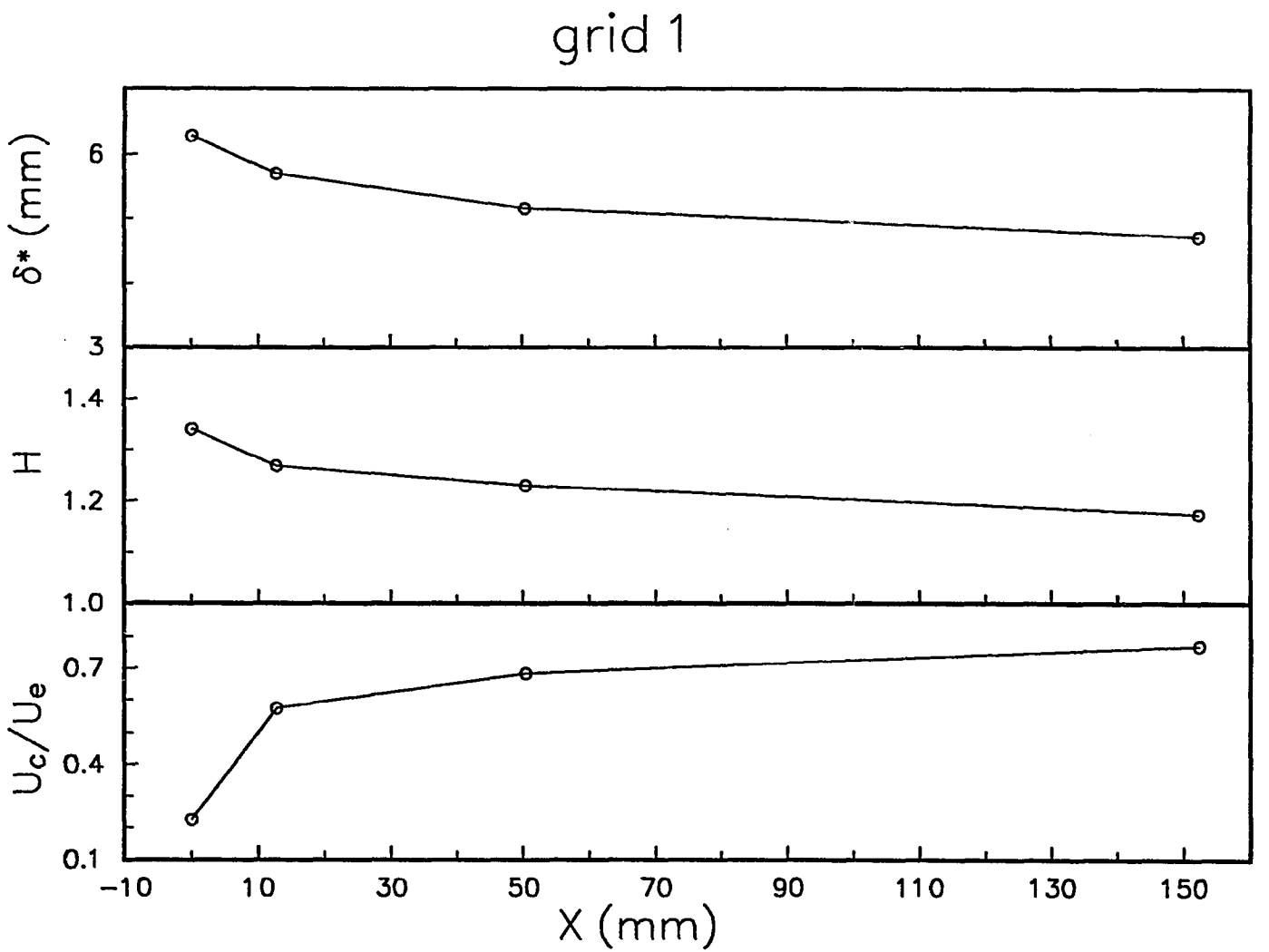

Fig. 6.7 Wake Recovery and Inetgral Properties of Symmetric Wake Under Free Stream Turbulence Generated by Grid 1

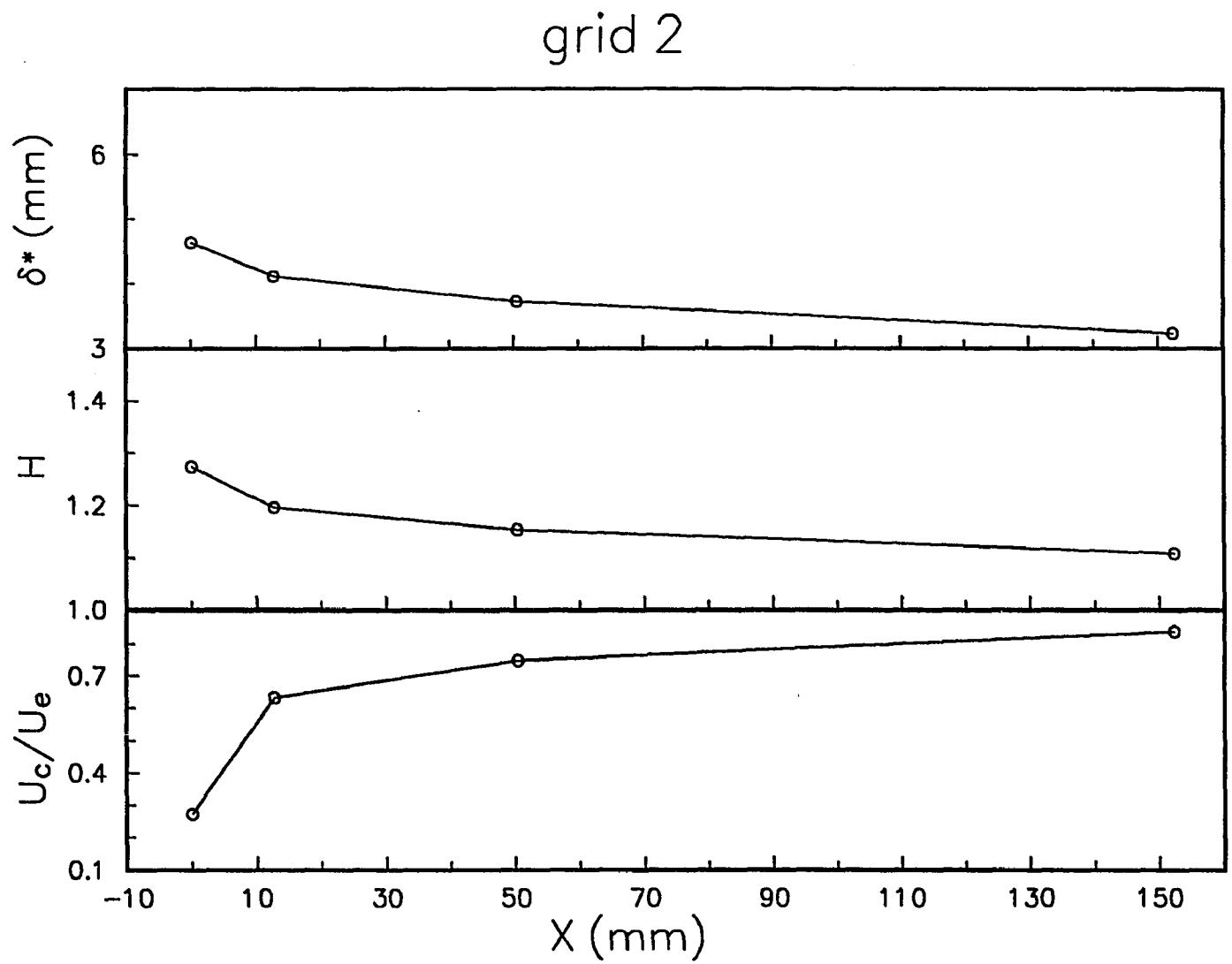

Fig. 6.8 Wake Recovery and Inetgral Properties of Symmetric Wake Under Free Stream Turbulence Generated by Grid 2

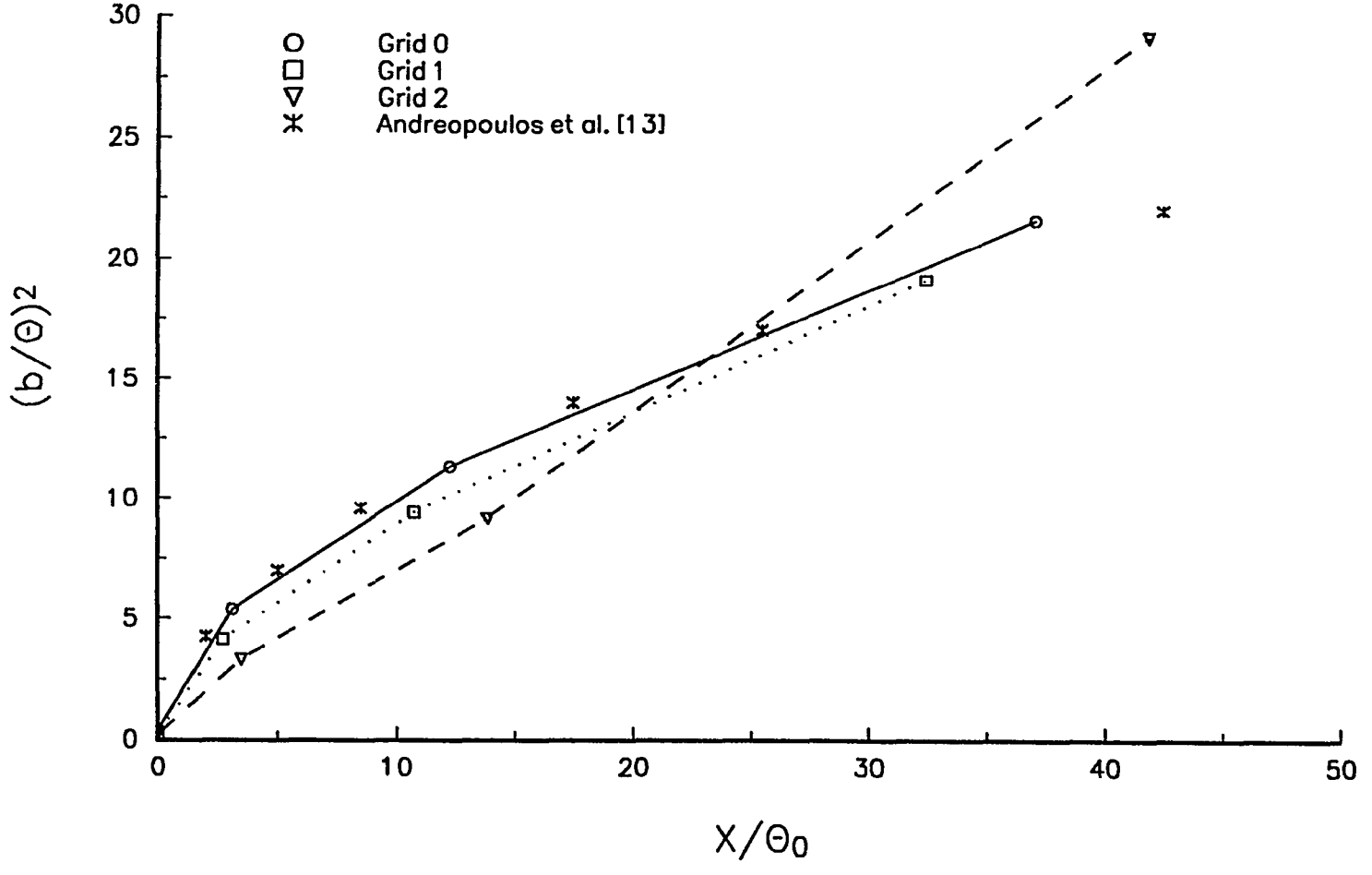

Fig. 6.9 Variation of Half Wake Width With Axial Distance Symmetric Wake

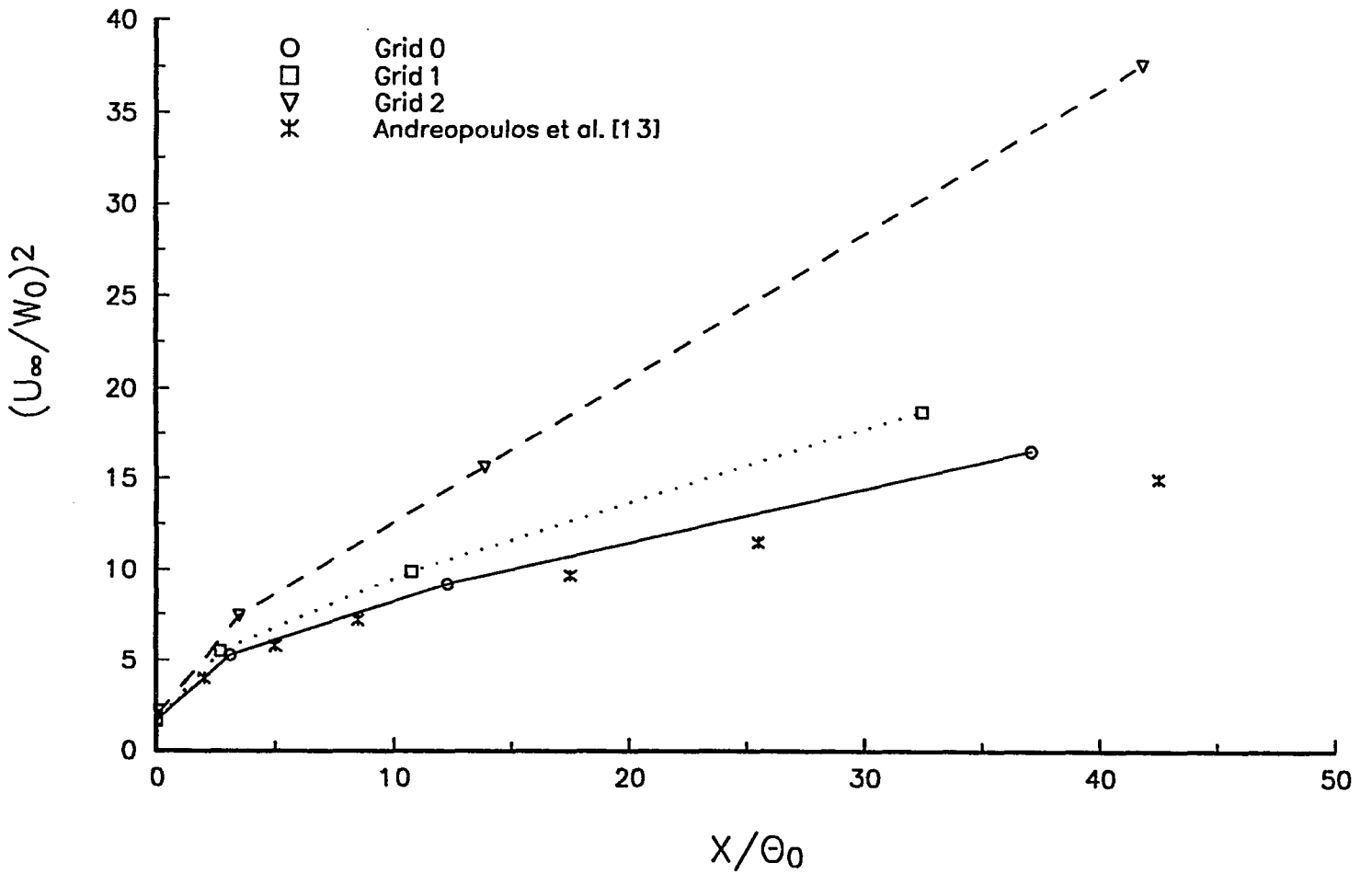

Fig. 6.10 Variation of Centerline Recovery Rate With Axial Distance, Symmetric Wake

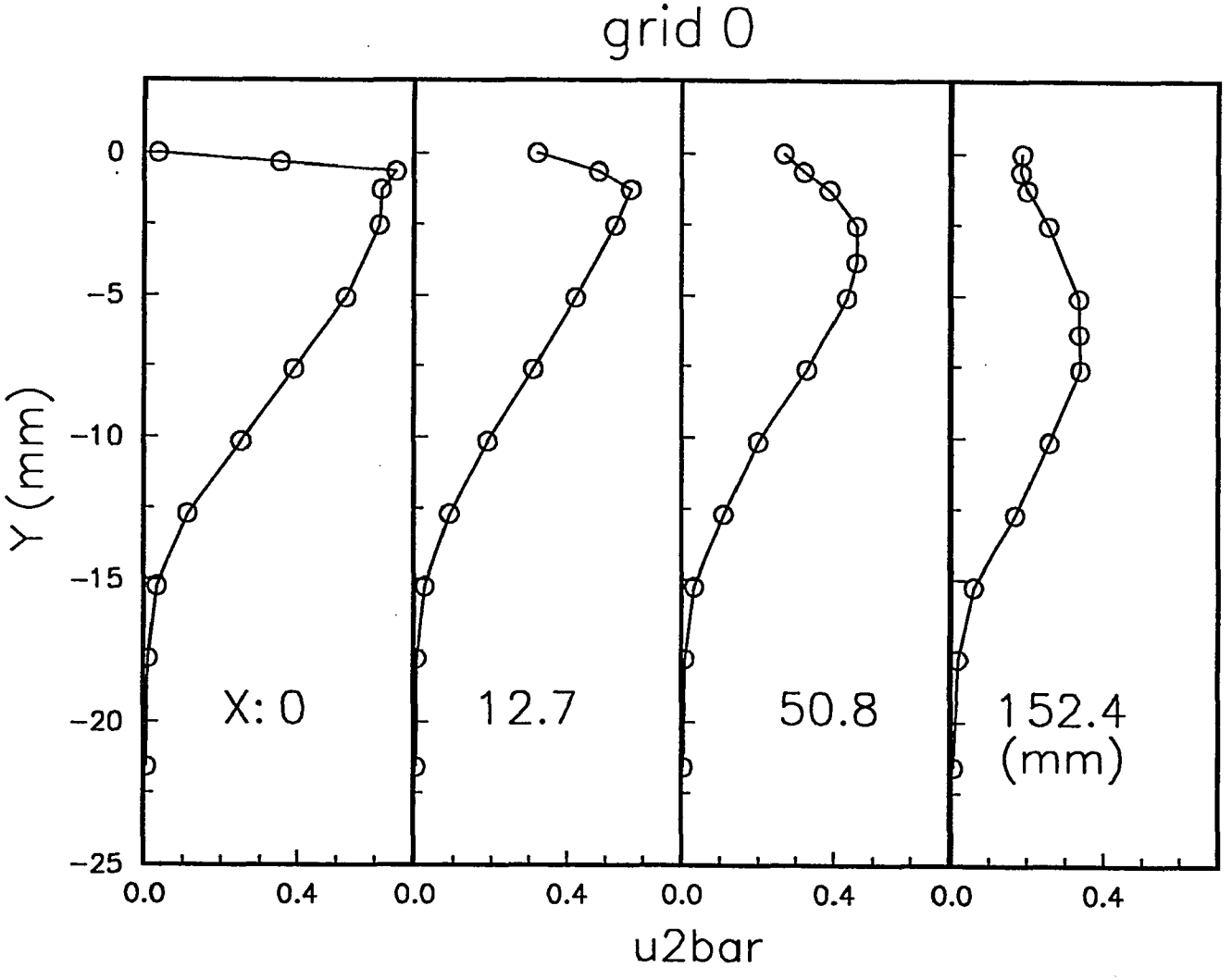

Fig. 6.11a Distribution of $(\overline{u^2}/U_\infty{}^2)*10^2$, Symmetric Wake, Under No Free Stream Turbulence

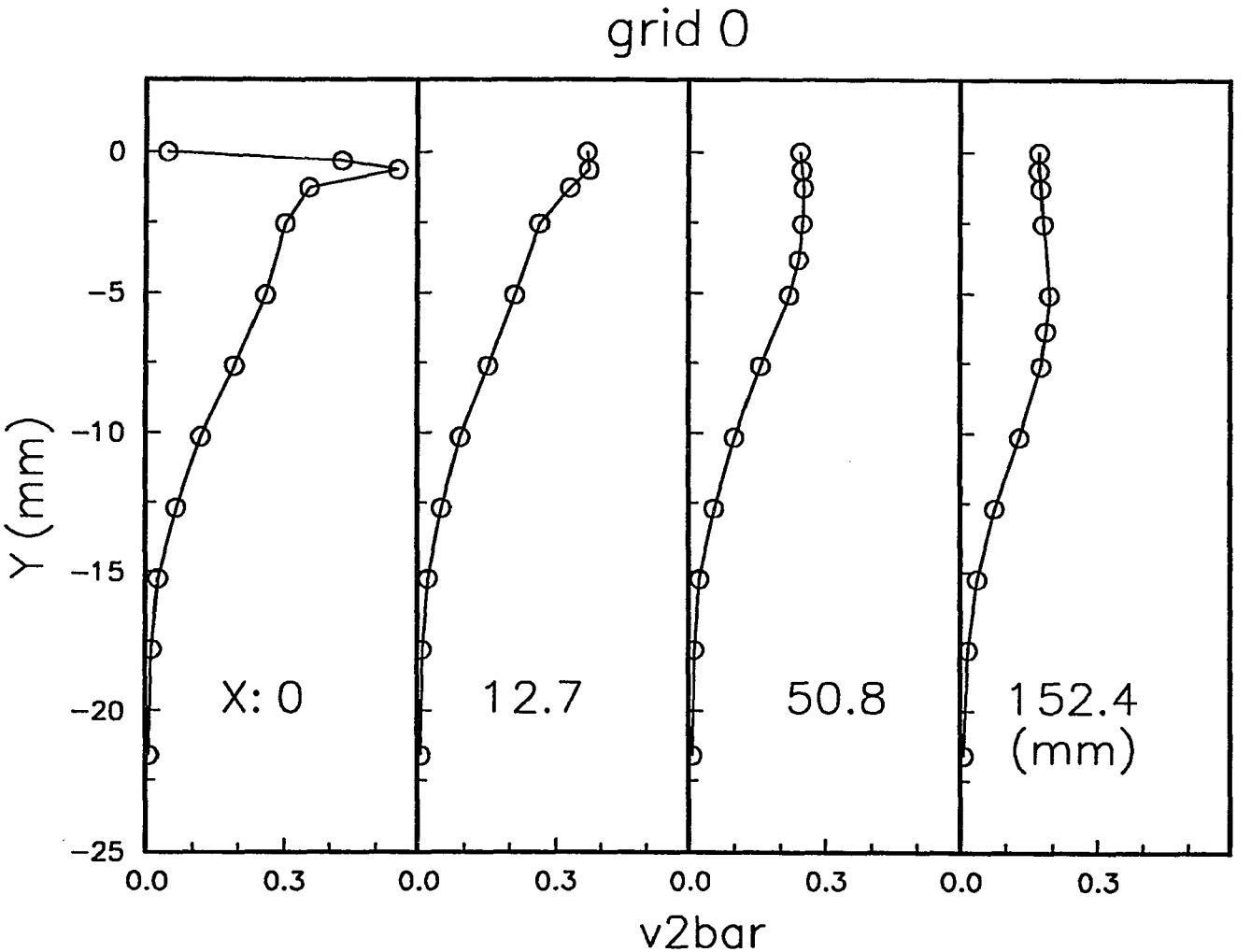

Fig. 6.11b Distribution of $(\overline{v^2}/U_\infty{}^2)*10^2$, Symmetric Wake, Under No Free Stream Turbulence

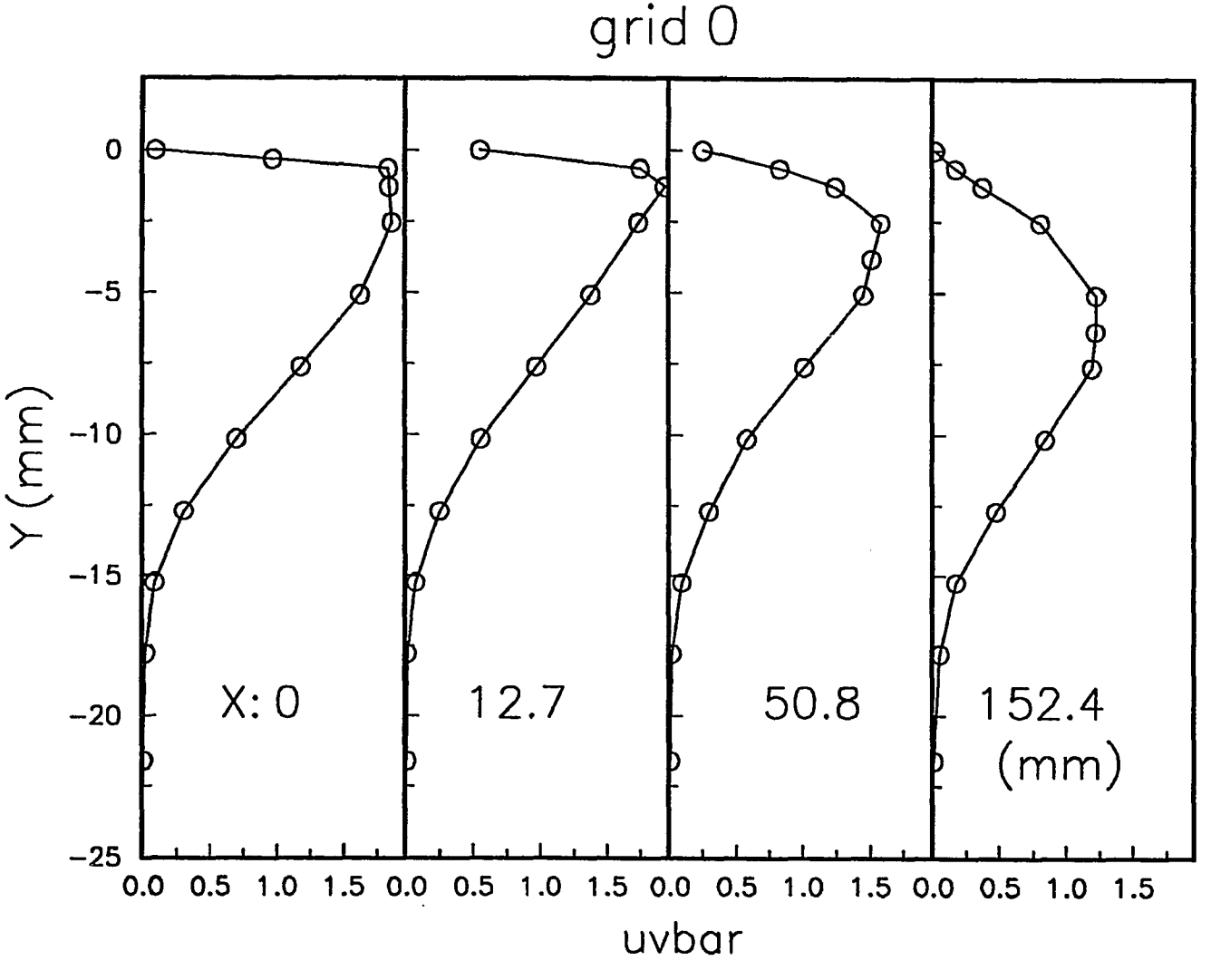

Fig. 6.11c Distribution of $(\overline{uv}/U_\infty{}^2)*10^3$, Symmetric Wake, Under No Free Stream Turbulence

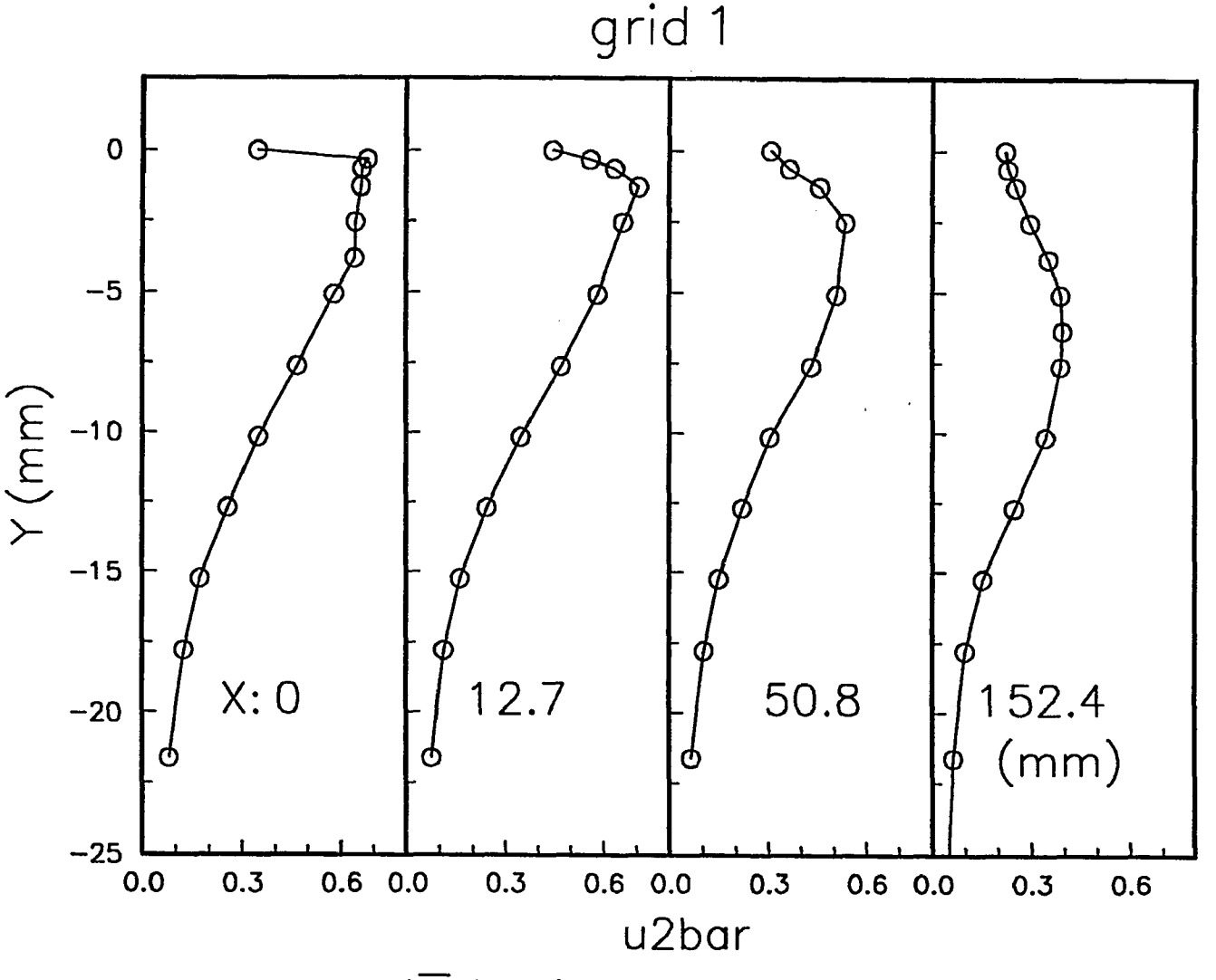

Fig. 6.12a Distribution of $(\overline{u^2}/U_\infty{}^2)*10^2$, Symmetric Wake, Under Free Stream Turbulence Generated by Grid 1

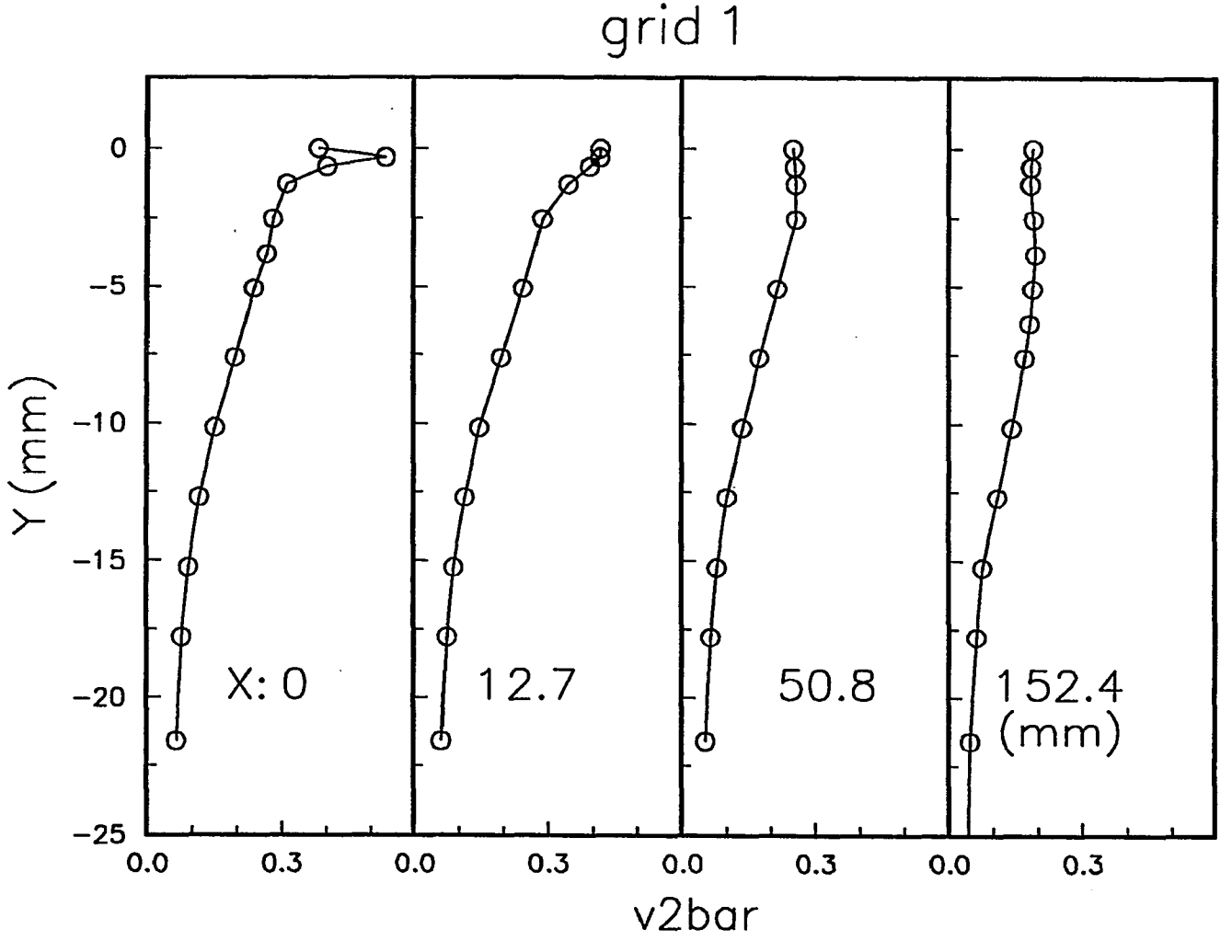

Fig. 6.12b Distribution of $(\overline{v^2}/U_\infty{}^2)*10^2$, Symmetric Wake, Under Free Stream Turbulence Generated by Grid 1

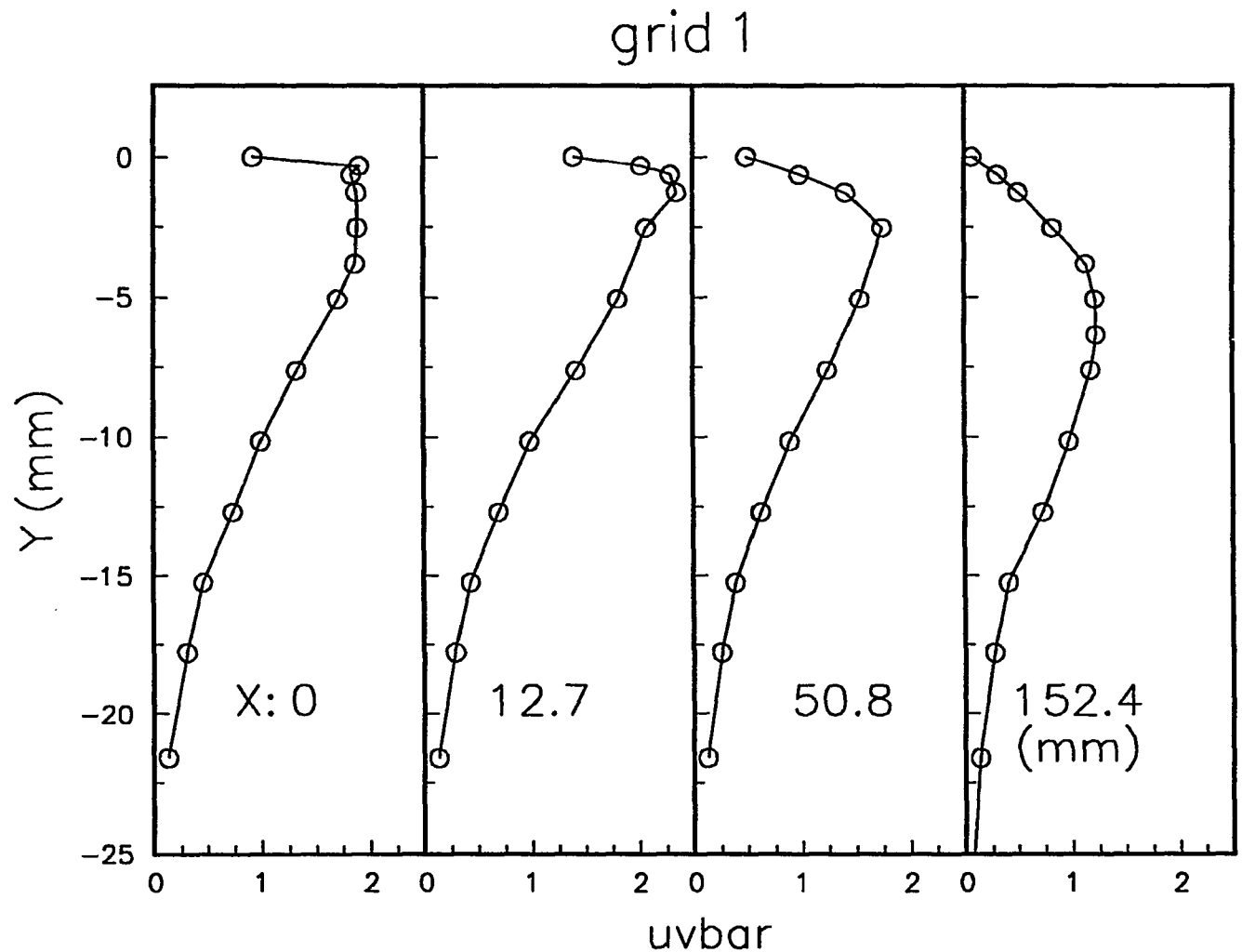

Fig. 6.12c Distribution of $(\overline{uv}/U_\infty{}^2)*10^2$, Symmetric Wake, Under Free Stream Turbulence Generated by Grid 1

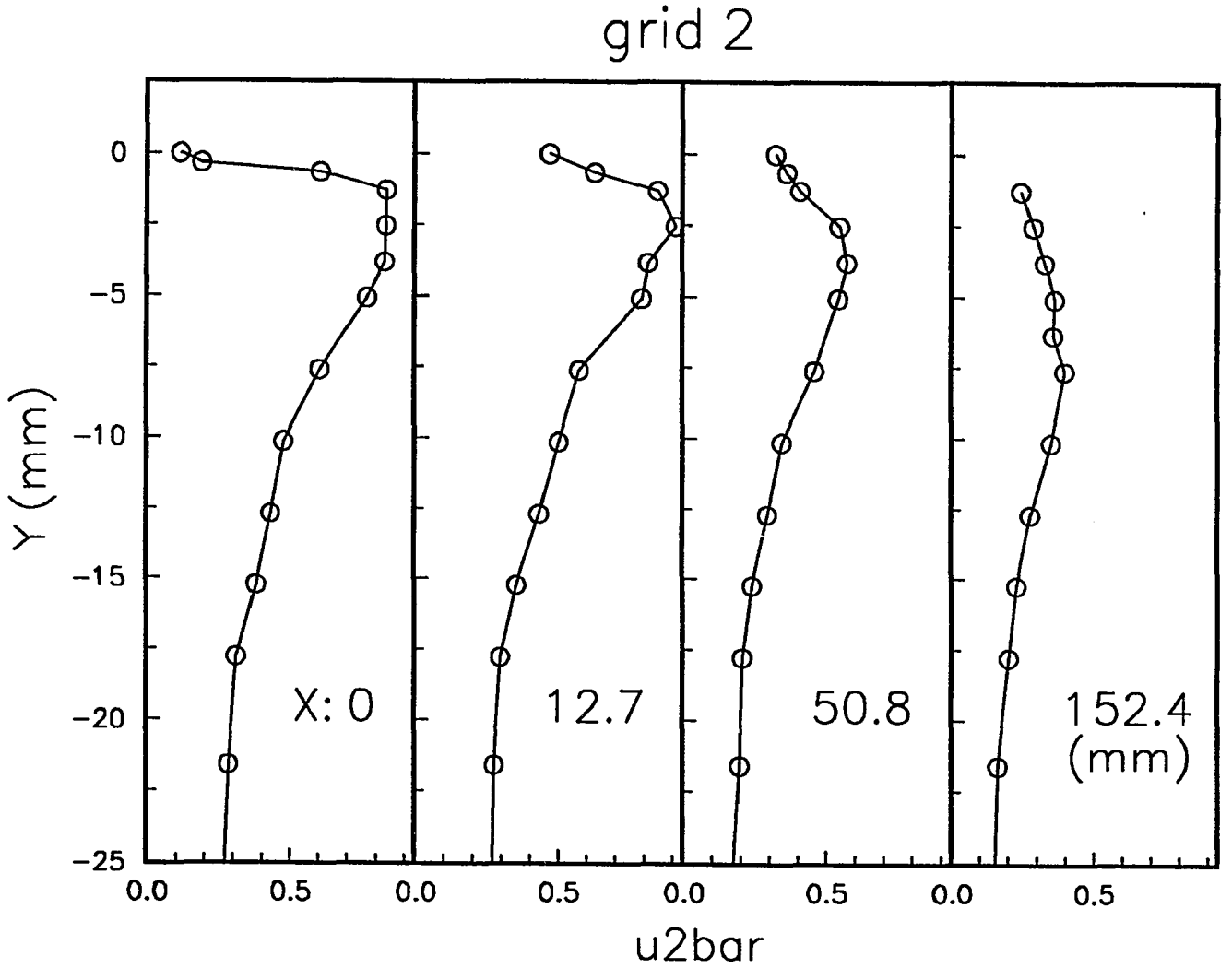

Fig. 6.13a Distribution of $(\overline{u^2}/U_\infty{}^2)*10^2$, Symmetric Wake, Under Free Stream Turbulence Generated by Grid 2

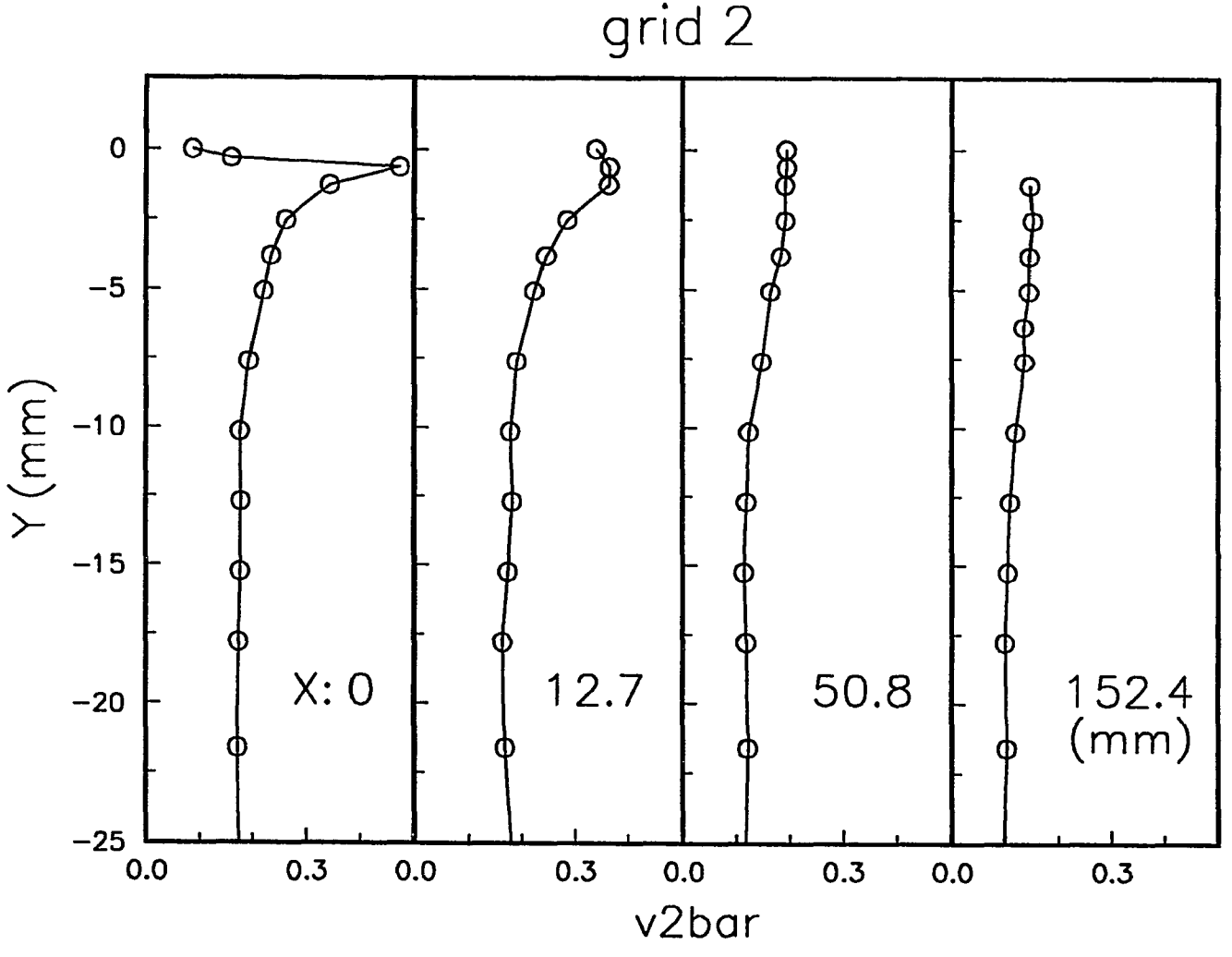

Fig. 6.13b Distribution of $(\overline{v^2}/U_\infty{}^2)*10^2$, Symmetric Wake, Under Free Stream Turbulence Generated by Grid 2

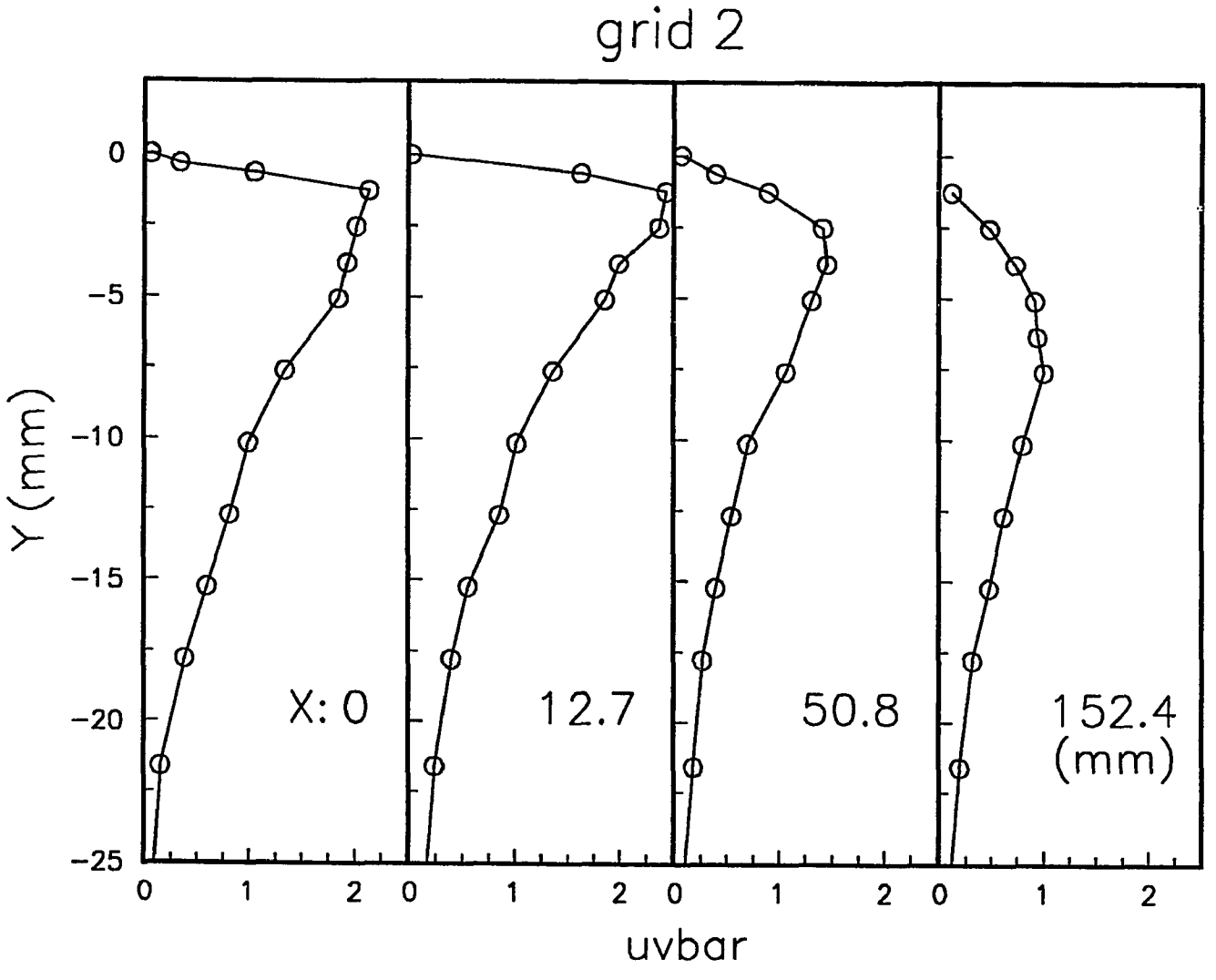

Fig. 6.13c Distribution of $(\overline{uv}/U_\infty{}^2)*10^2$, Symmetric Wake, Under Free Stream Turbulence Generated by Grid 2

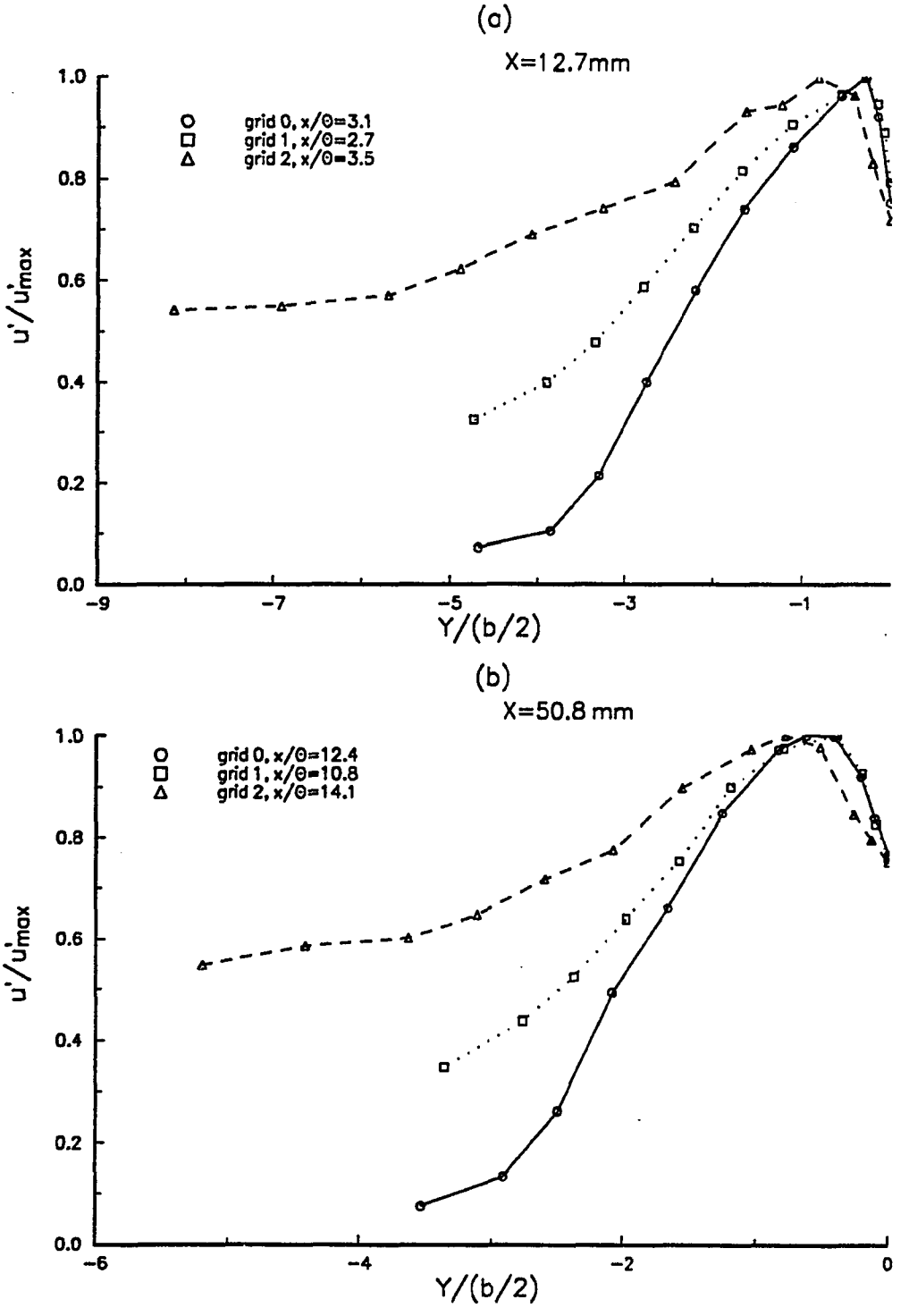

Fig. 6.14a Comparision of Turbulent Streamwise Intensity, Symmetric Wake

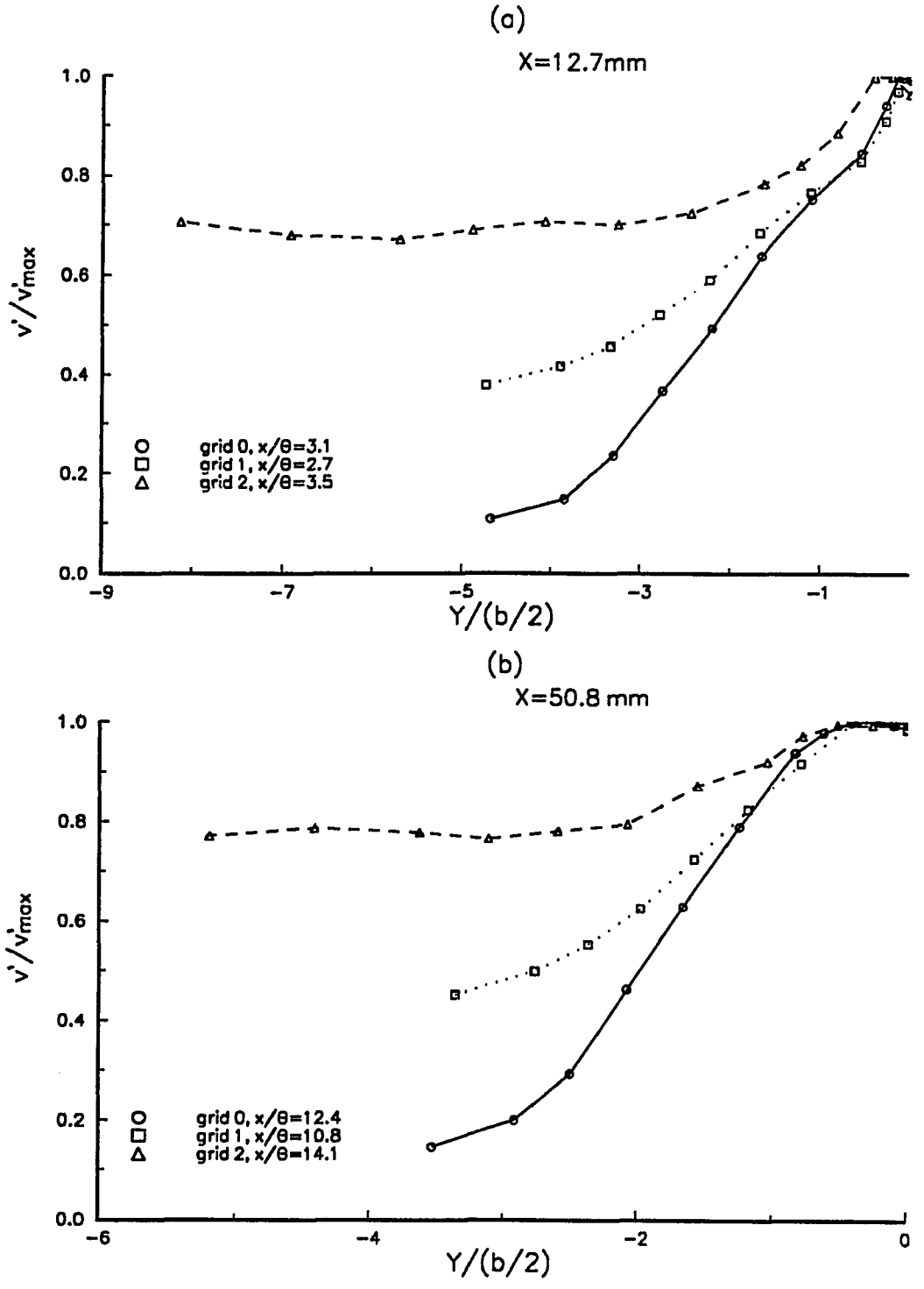

Fig. 6.14b Comparision of Turbulent Normal Intensity, Symmetric Wake

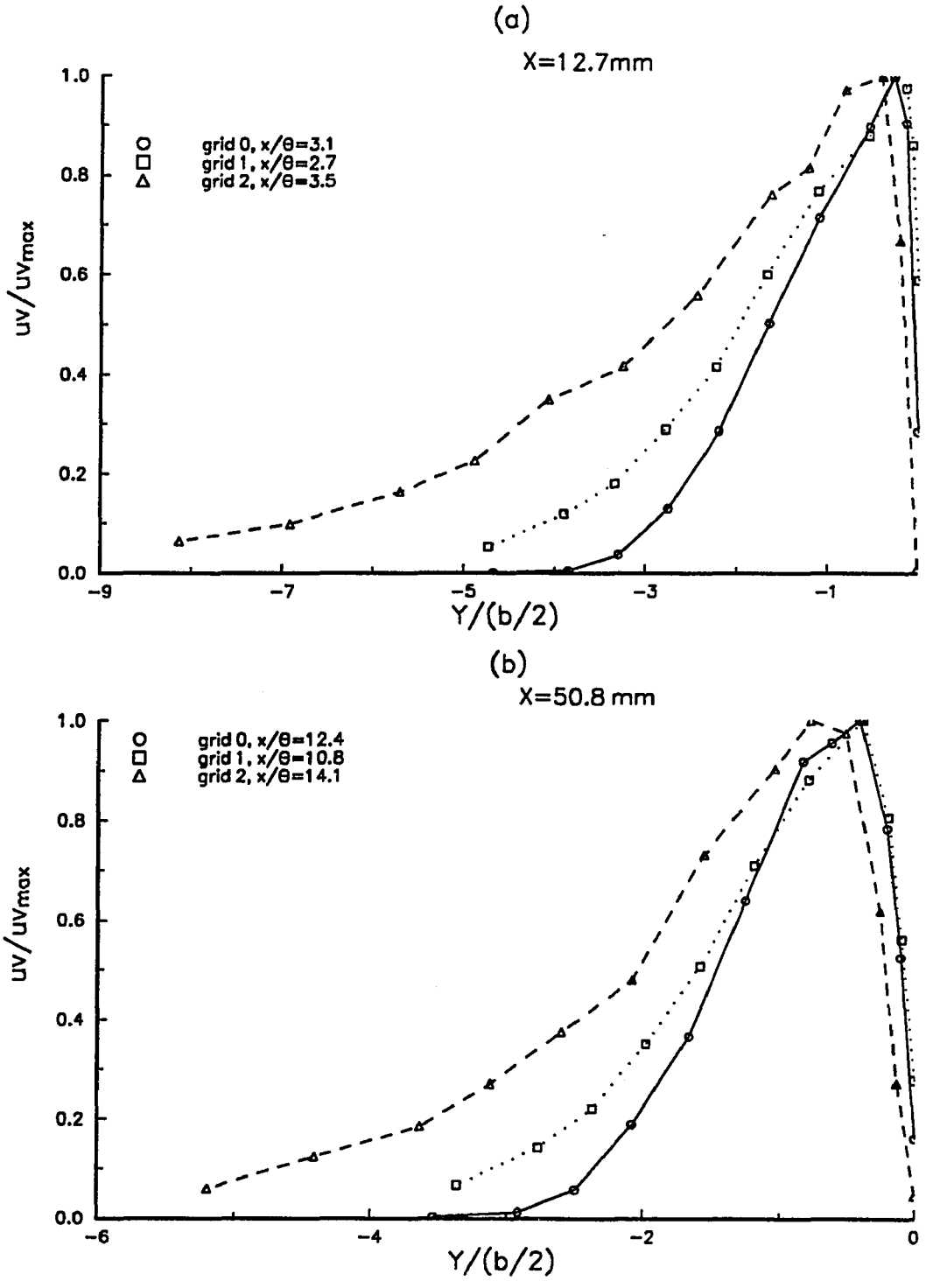

Fig. 6.14c Comparision of Turbulent Shear Stress, Symmetric Wake

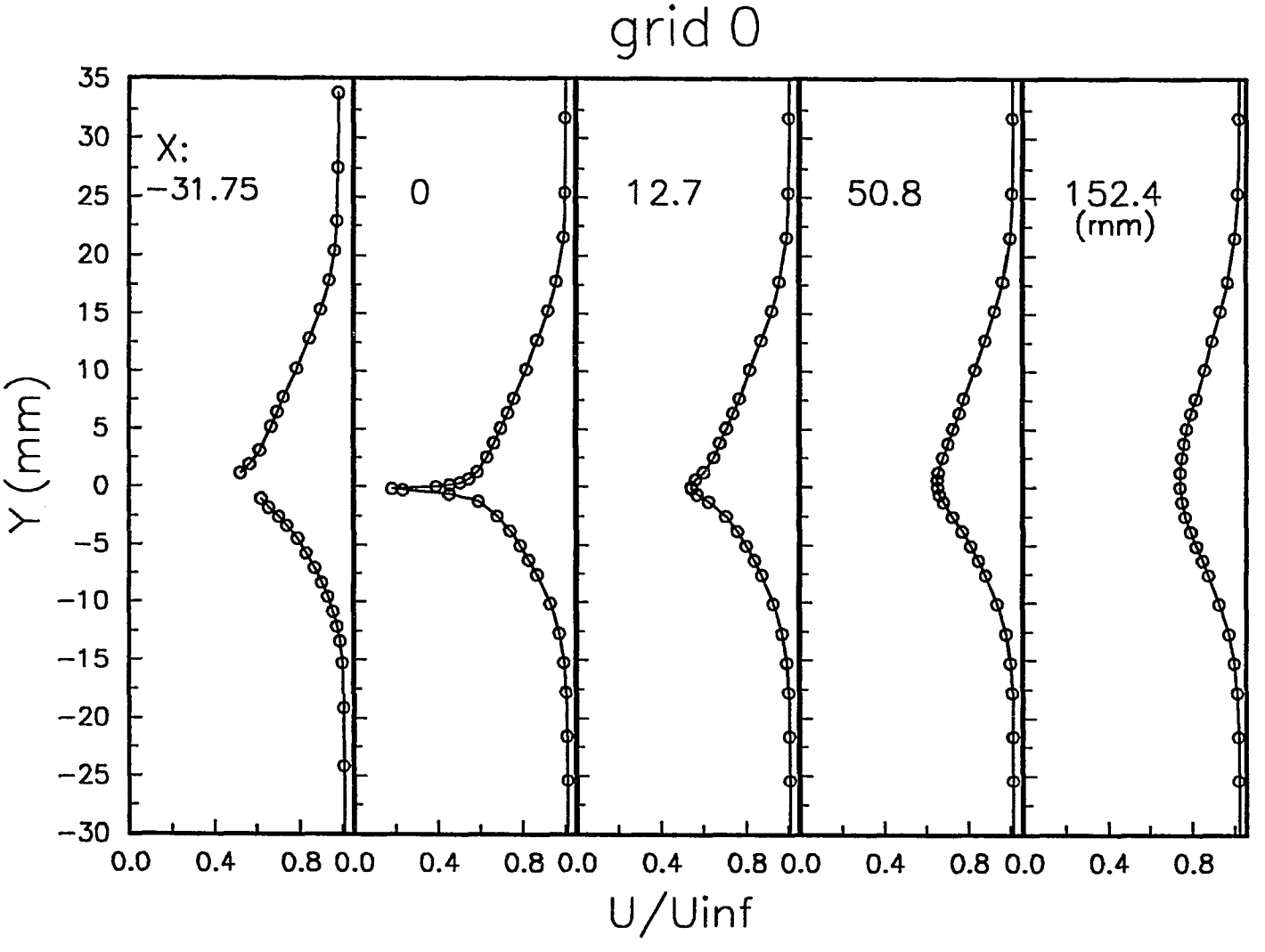

Fig. 6.15 Mean Velocity, Asymmetric Wake Under No Free Stream Turbulence

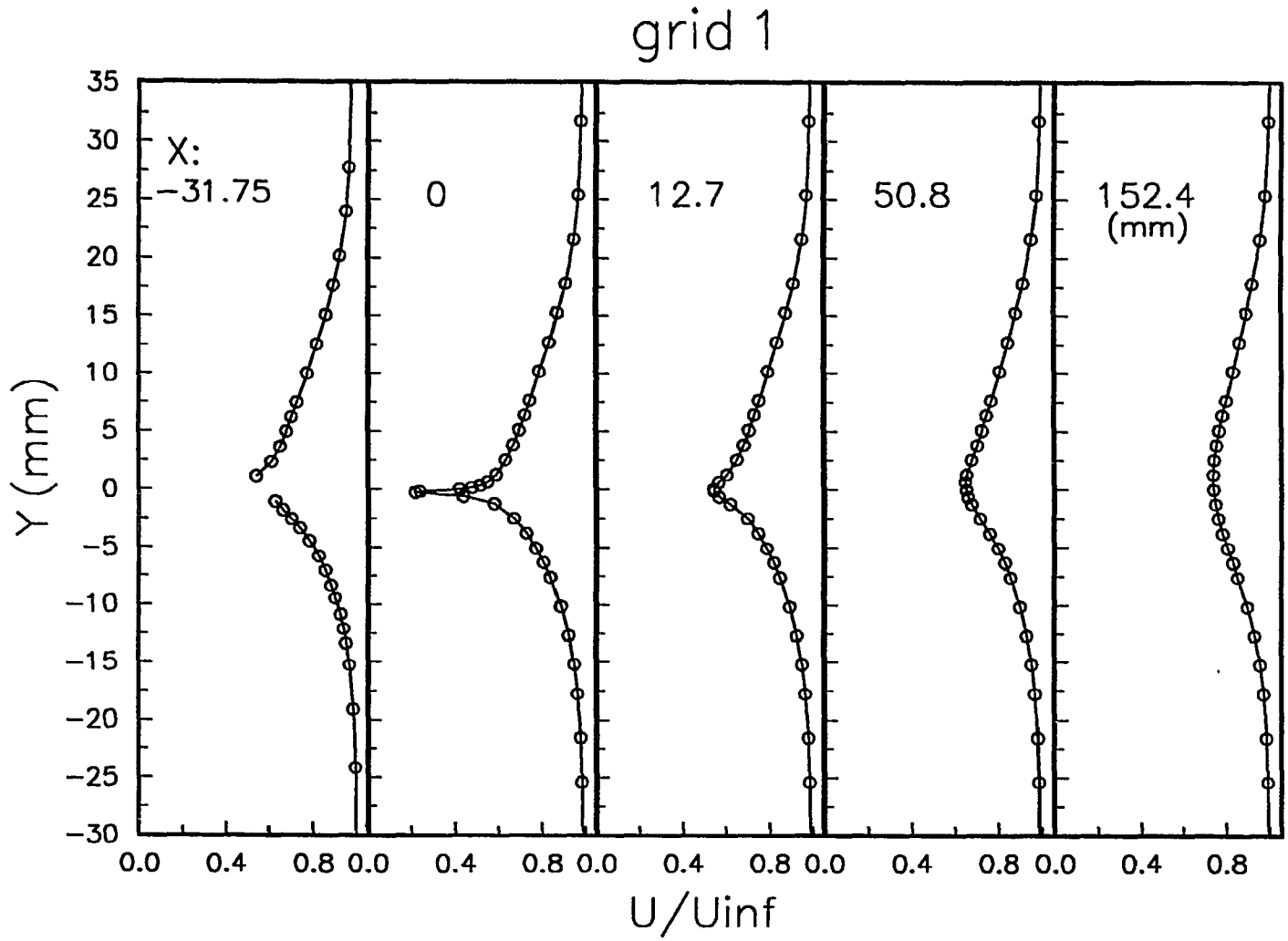

Fig. 6.16 Mean Velocity, Asymmetric Wake Under Free Stream Turbulence Generated by Grid 1

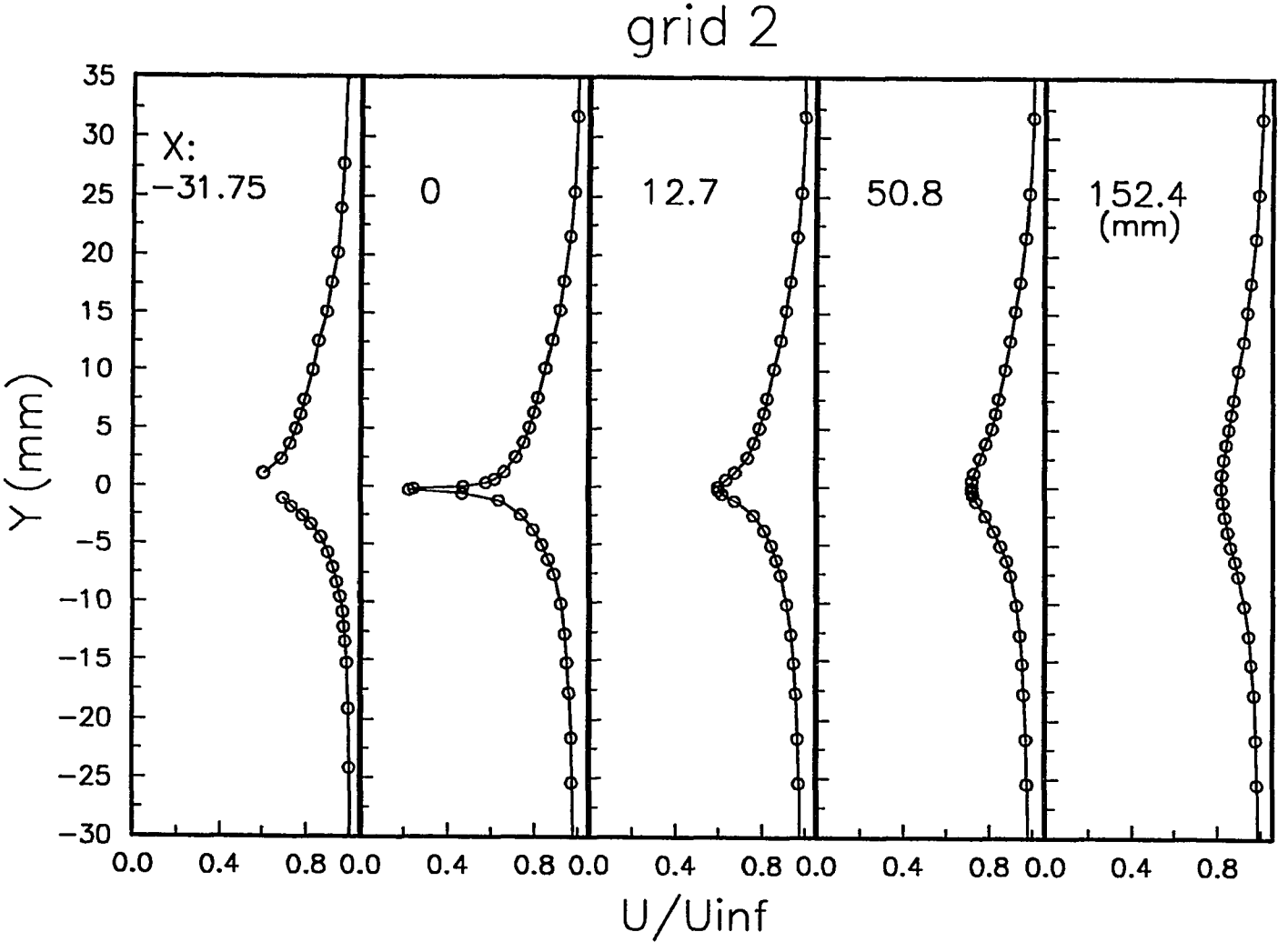

Fig. 6.17 Mean Velocity, Asymmetric Wake Under Free Stream Turbulence Generated by Grid 2

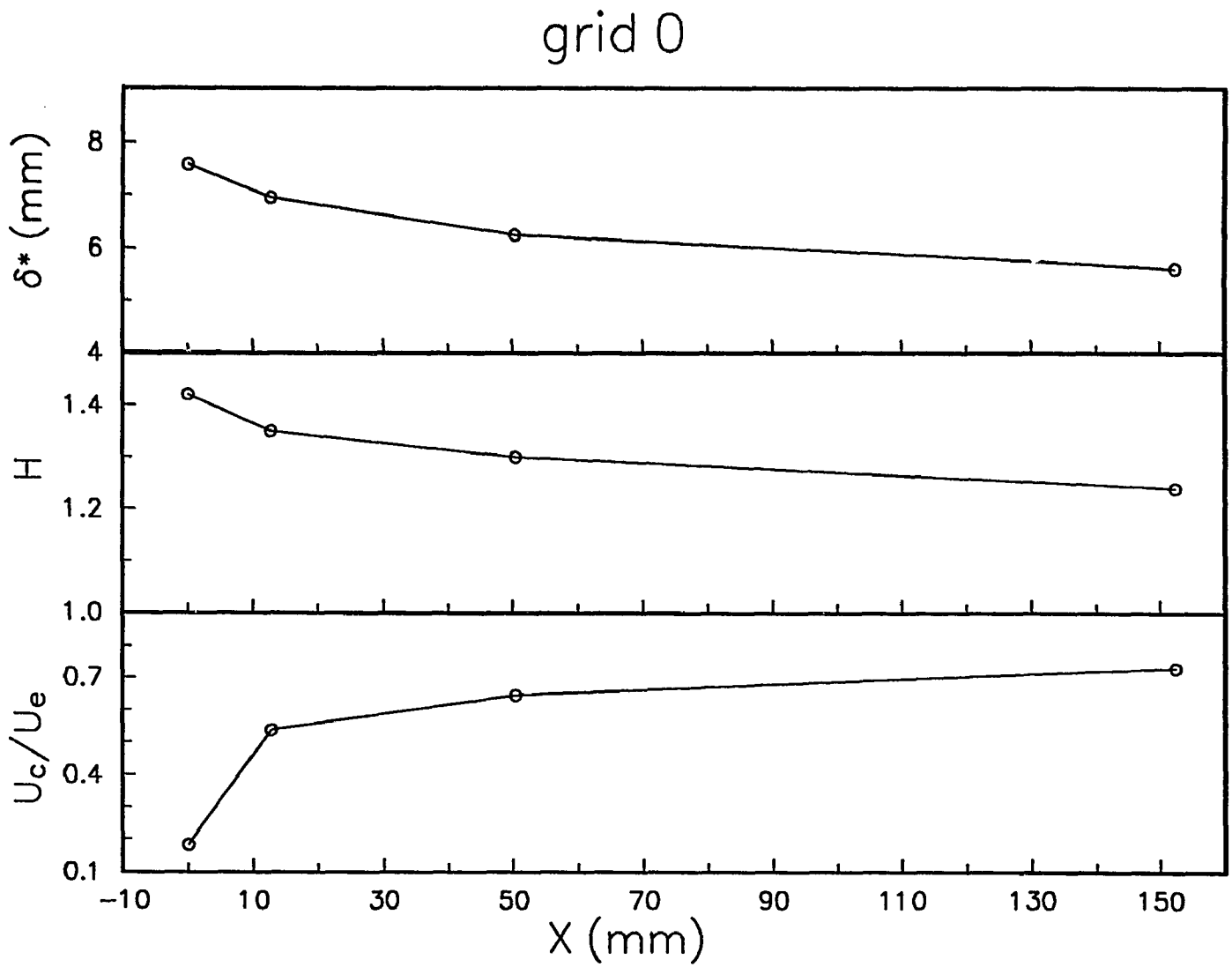

Fig.6.18 Wake Recovery and Integral Properties of Asymmetric Wake Under No Free Stream Turbulence

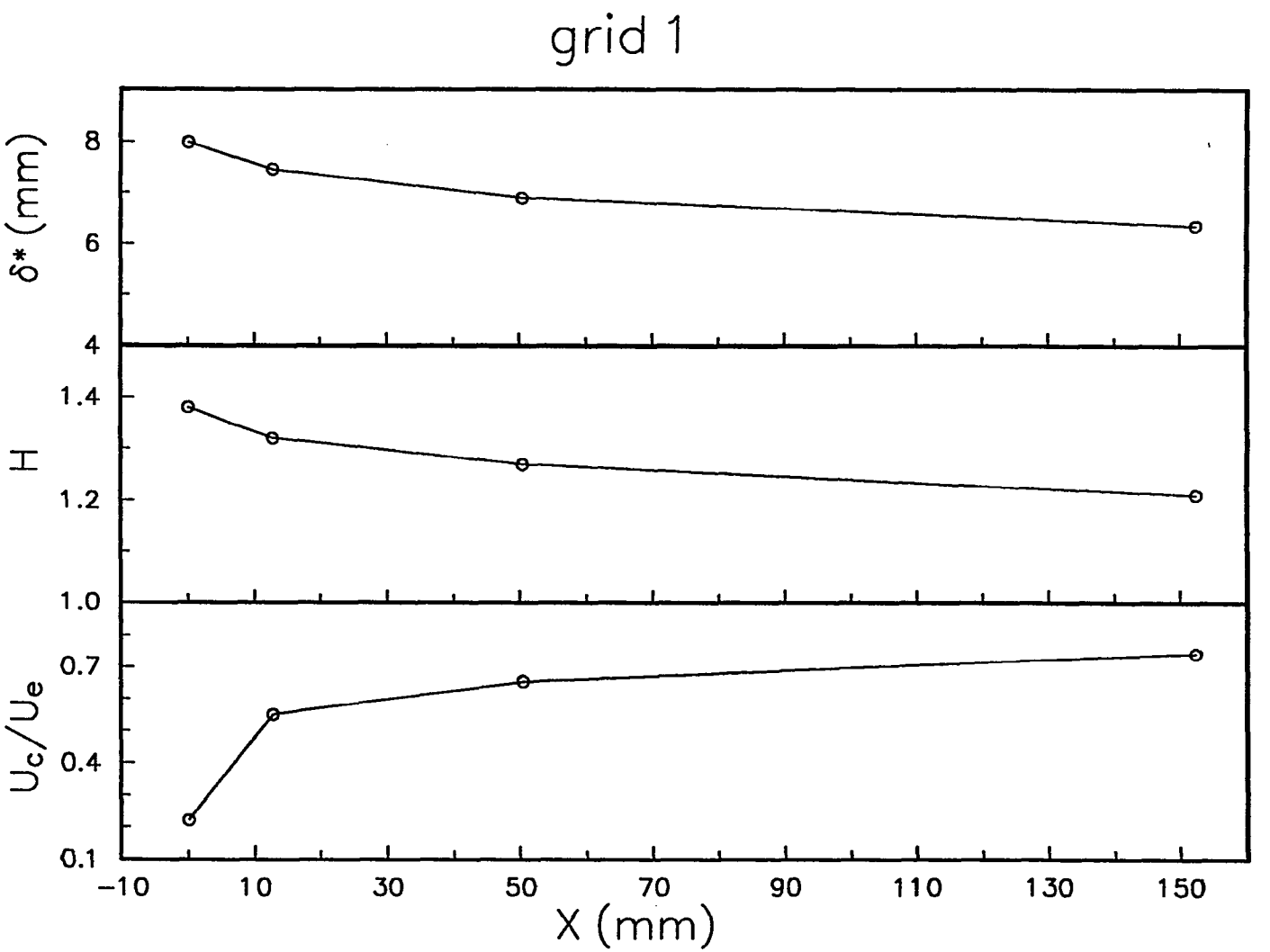

Fig.6.19 Wake Recovery and Integral Properties of Asymmetric Wake Under Free Stream Turbulence Generated by Grid 1

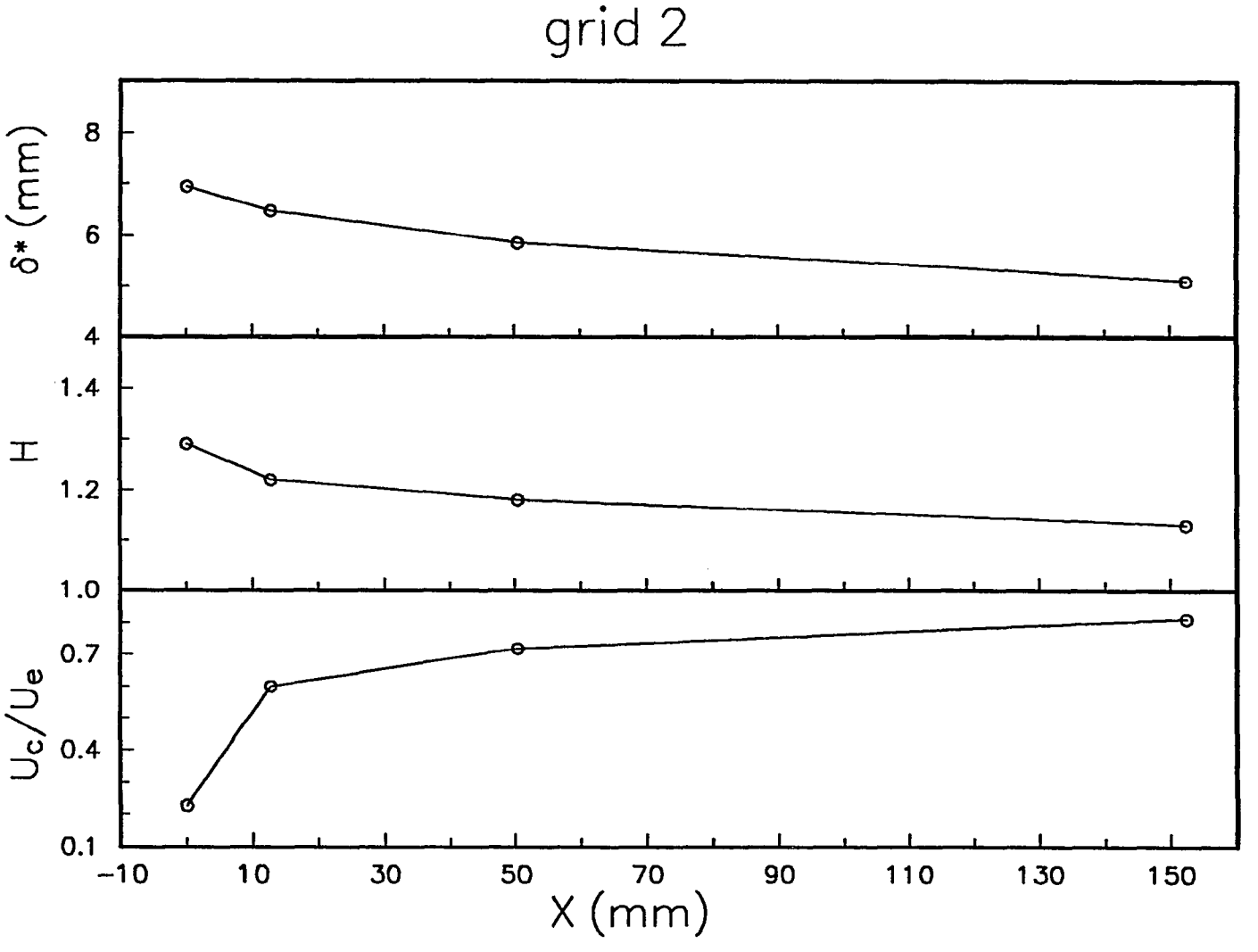

Fig.6.20 Wake Recovery and Integral Properties of Asymmetric Wake Under Free Stream Turbulence Generated by Grid 2

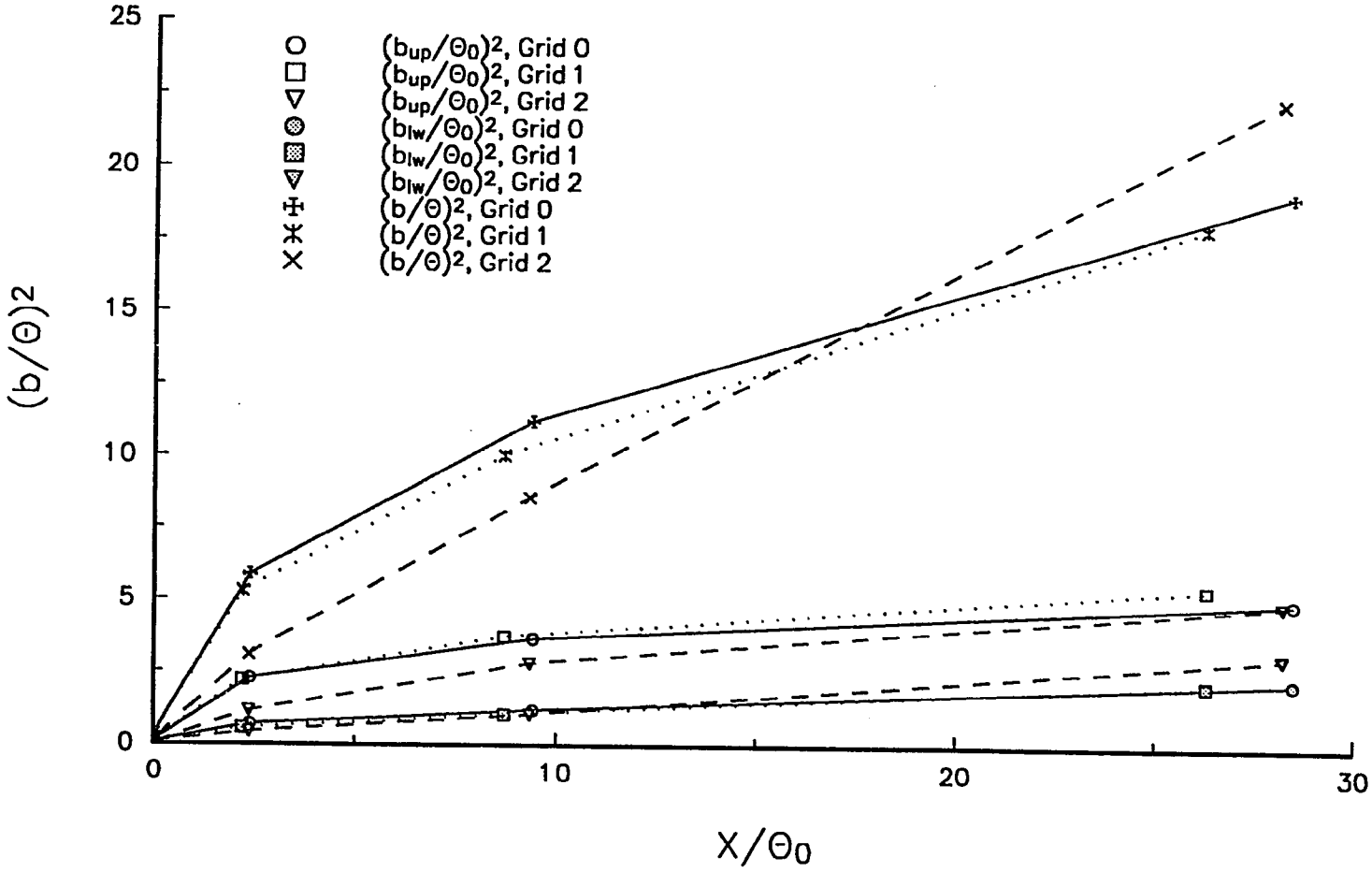

Fig. 6.21 Variation of Half Wake Width With Axial Distance, Asymmetric Wake

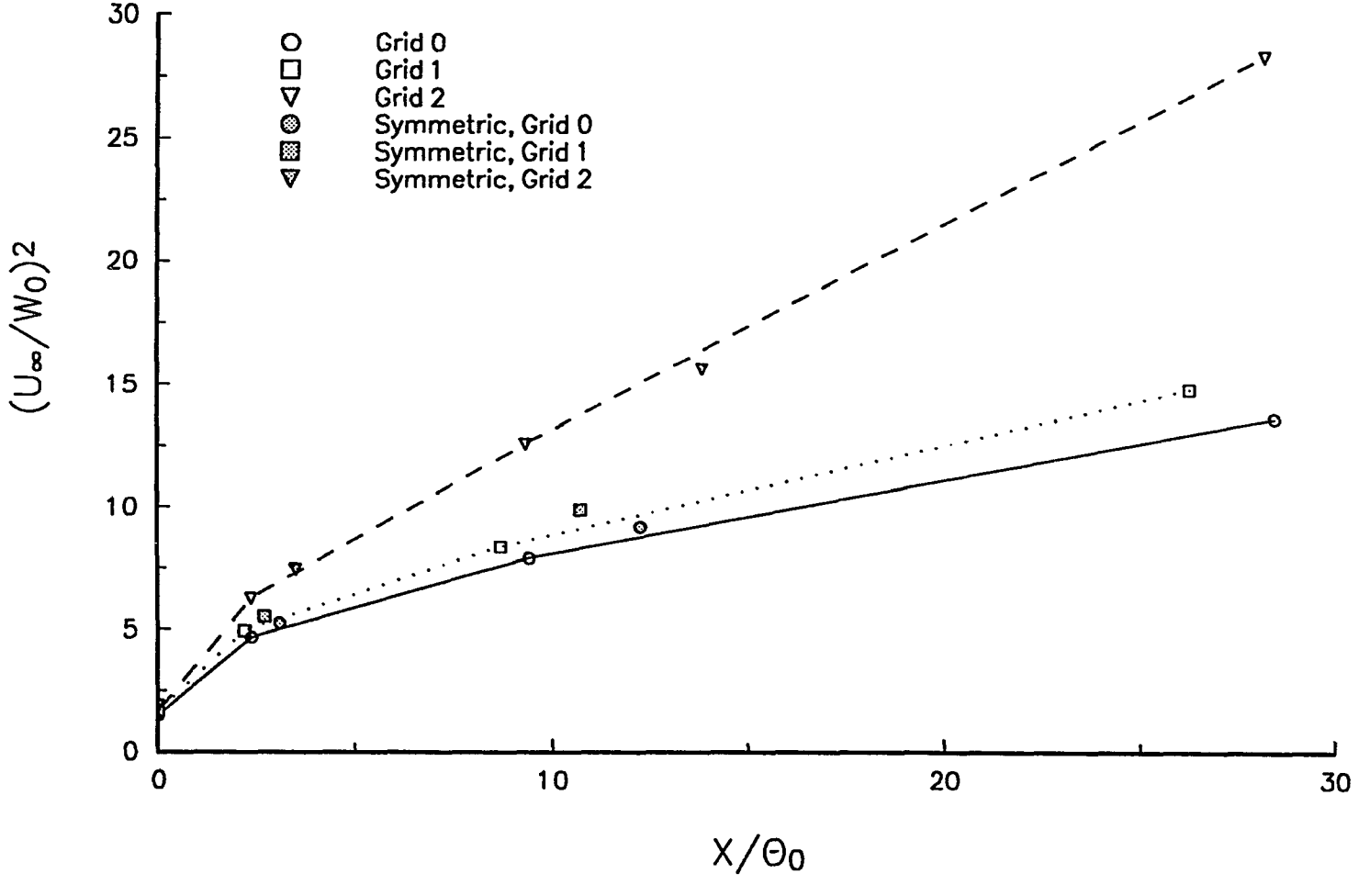

Fig. 6.22 Variation of Centerline Recovery Rate With Axial Distance, Asymmetric Wake

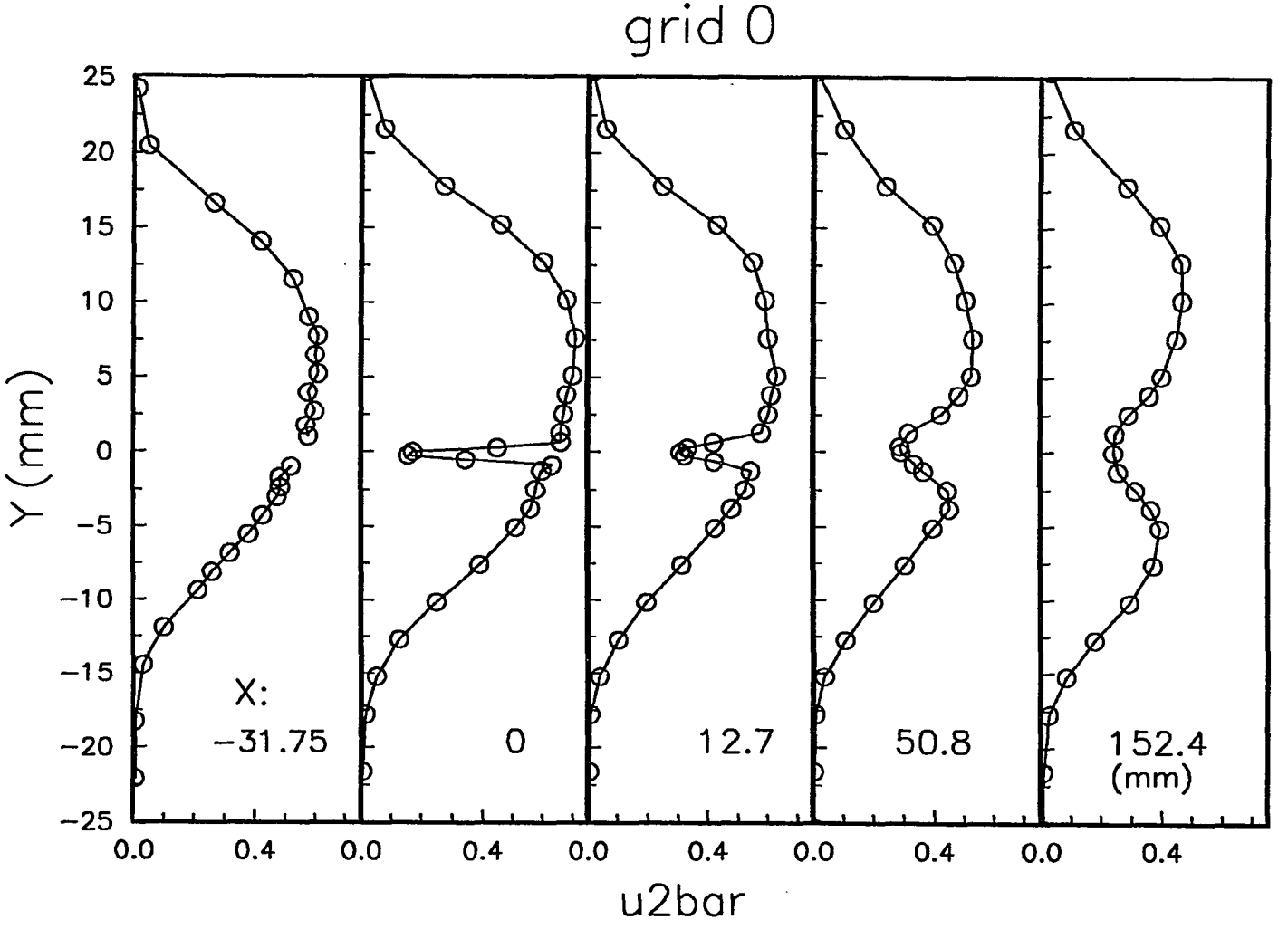

Fig.6.23a Distribution of $(\overline{u^2}/U_\infty{}^2)*10^2$, Asymmetric Wake, Under No Free Stream Turbulence

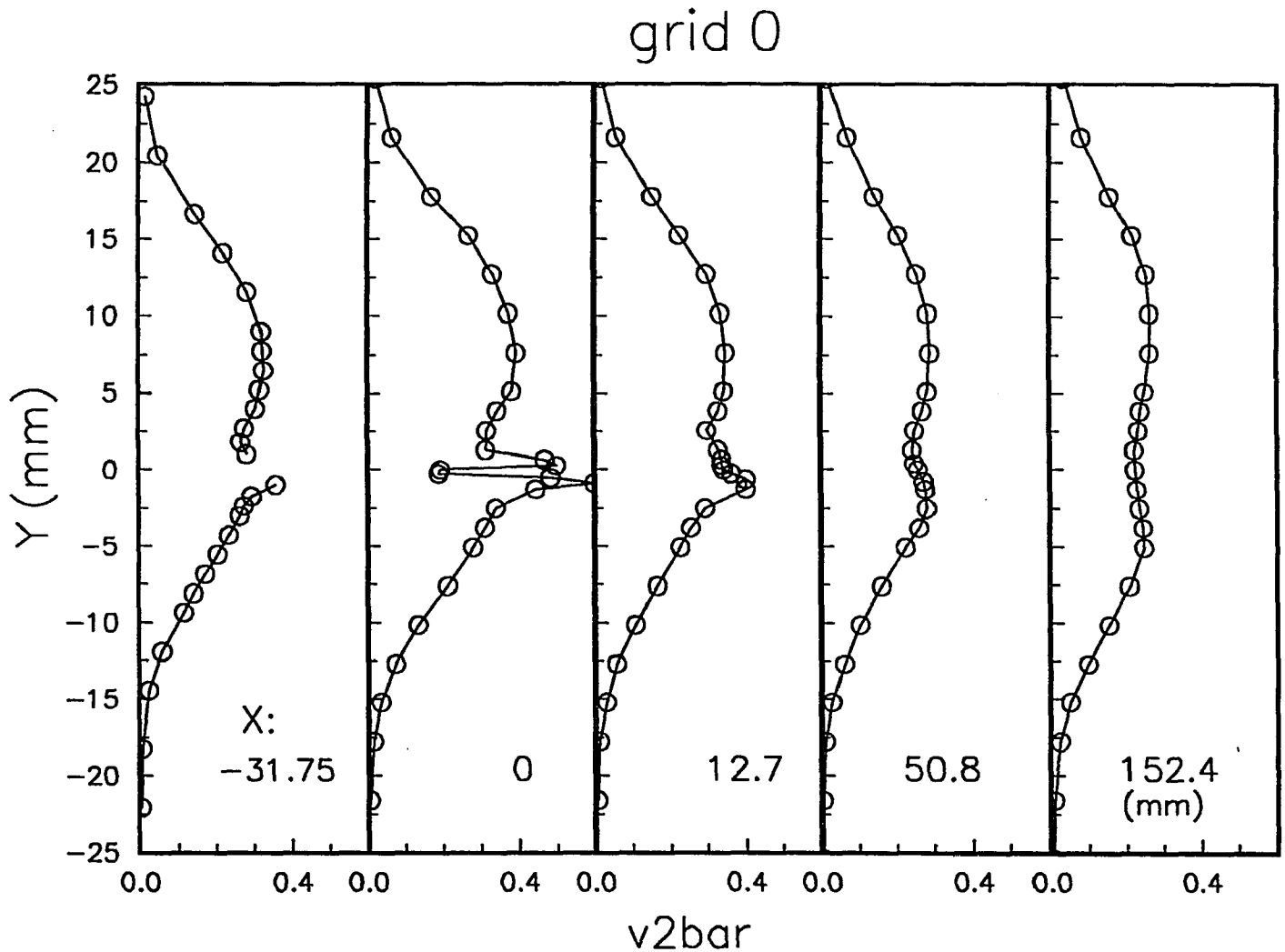

Fig.6.23b Distribution of $(\overline{v^2}/U_\infty{}^2)*10^2$, Asymmetric Wake, Under No Free Stream Turbulence

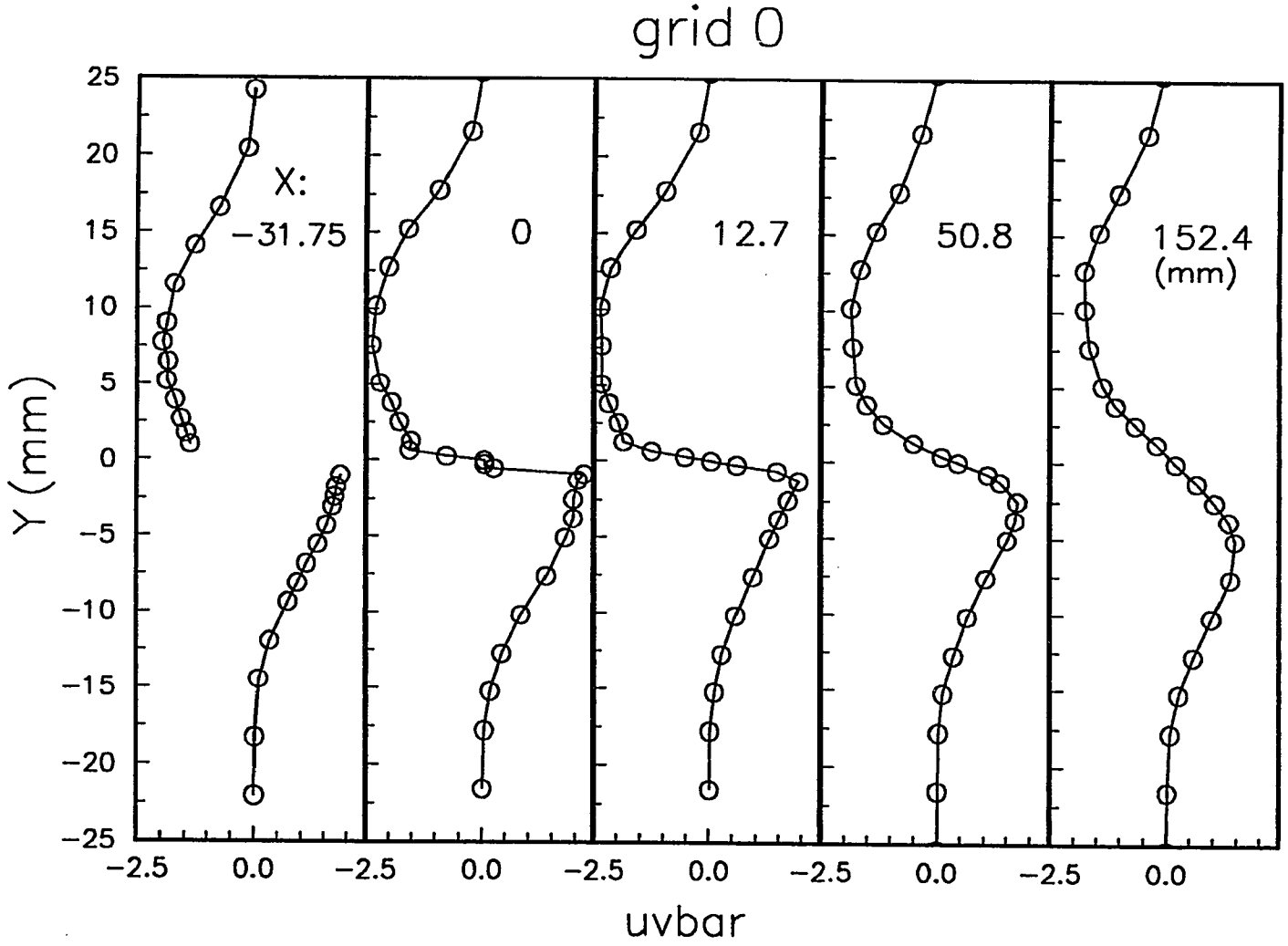

Fig.6.23c Distribution of $(\overline{uv}/U_\infty{}^2)*10^2$, Asymmetric Wake, Under No Free Stream Turbulence

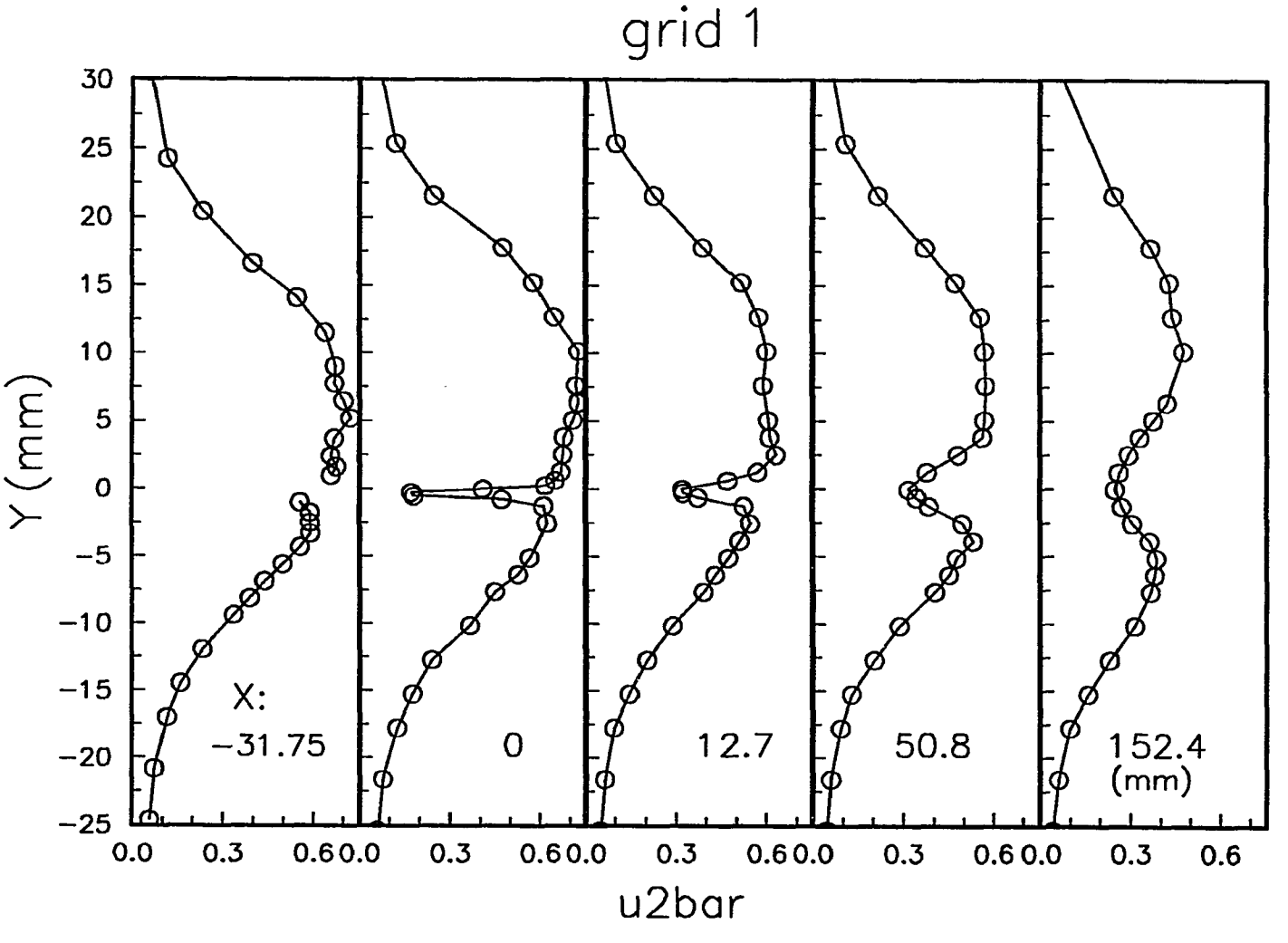

Fig.6.24a Distribution of $(\overline{u^2}/U_\infty{}^2)*10^2$, Asymmetric Wake, Under Free Stream Turbulence Generated by Grid 1

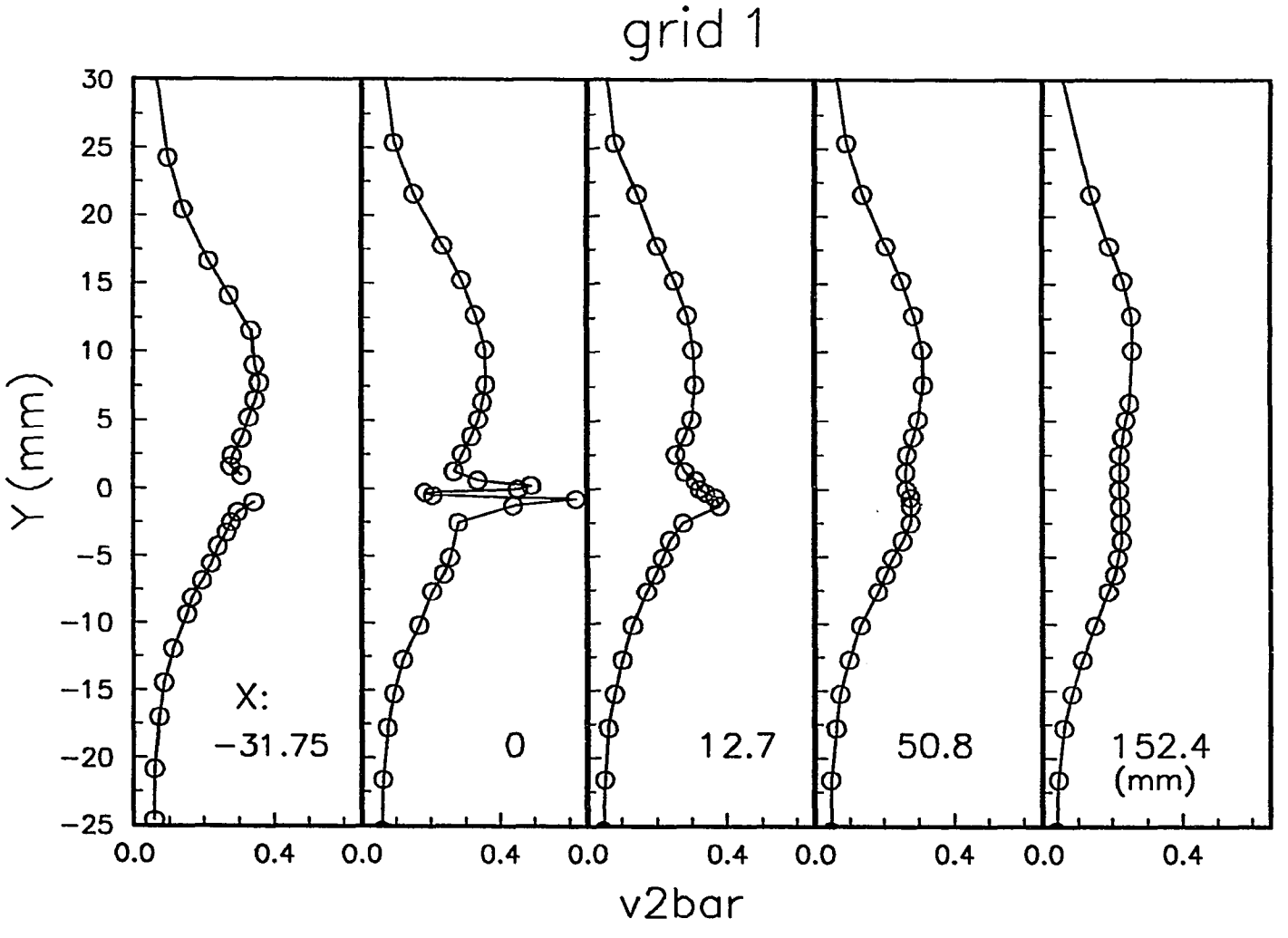

Fig.6.24b Distribution of $(\overline{v^2}/U_\infty{}^2)*10^2$, Asymmetric Wake, Under Free Stream Turbulence Generated by Grid 1

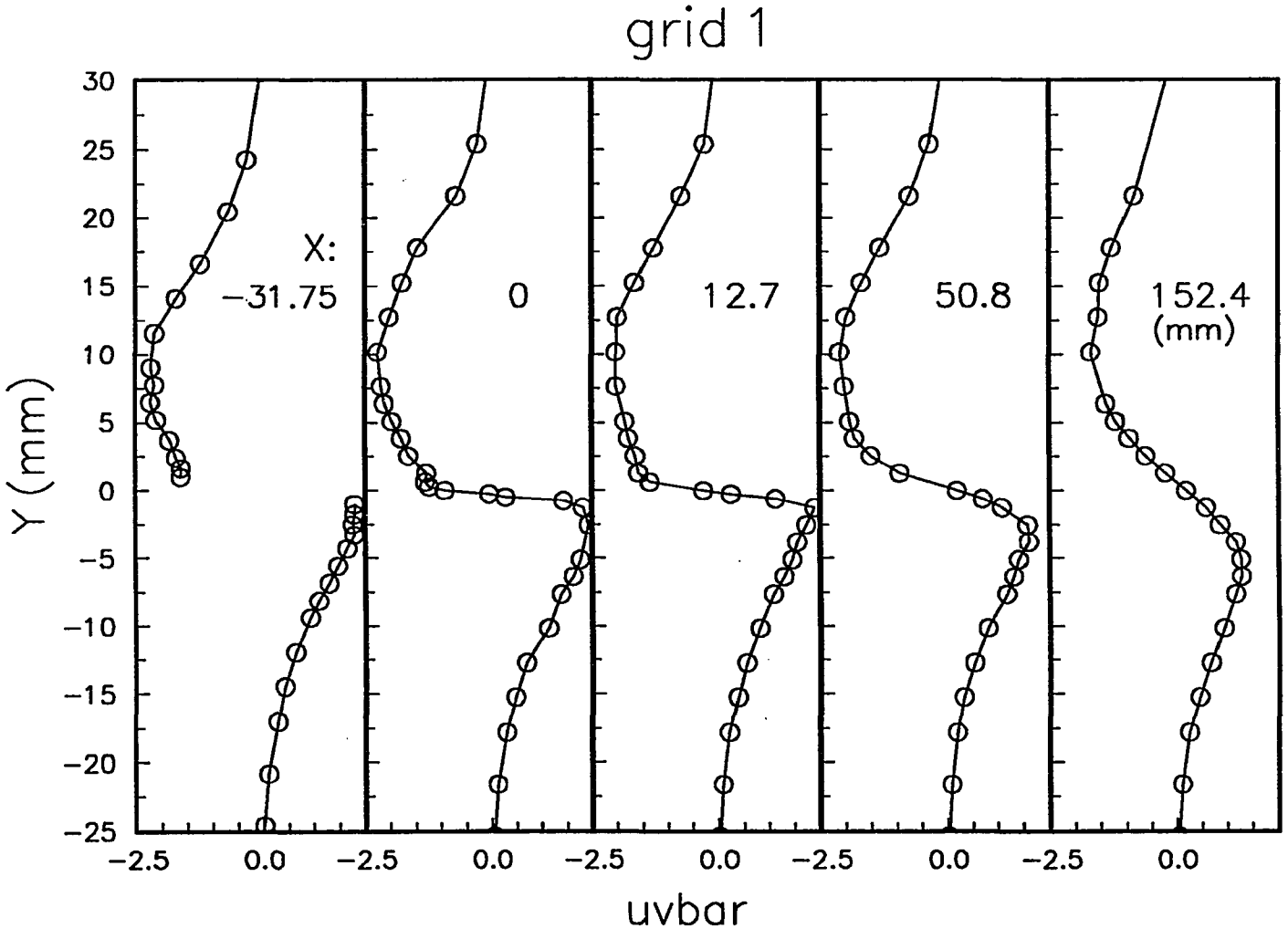

Fig.6.24c Distribution of $(\overline{uv}/U_\infty{}^2)*10^2$, Asymmetric Wake, Under Free Stream Turbulence Generated by Grid 1

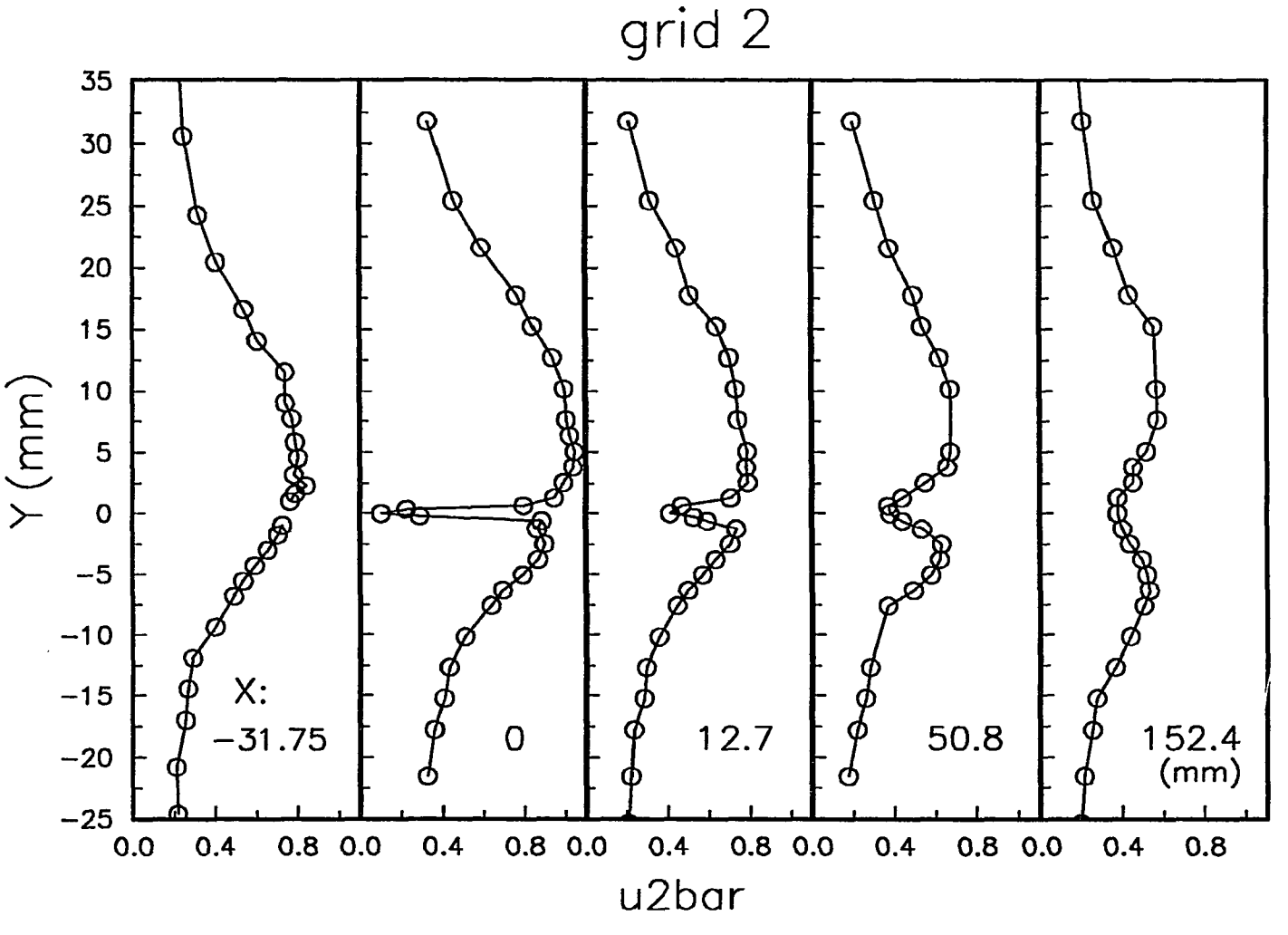

Fig.6.25a Distribution of $(\overline{u^2}/U_\infty{}^2)*10^2$, Asymmetric Wake, Under Free Stream Turbulence Generated by Grid 2

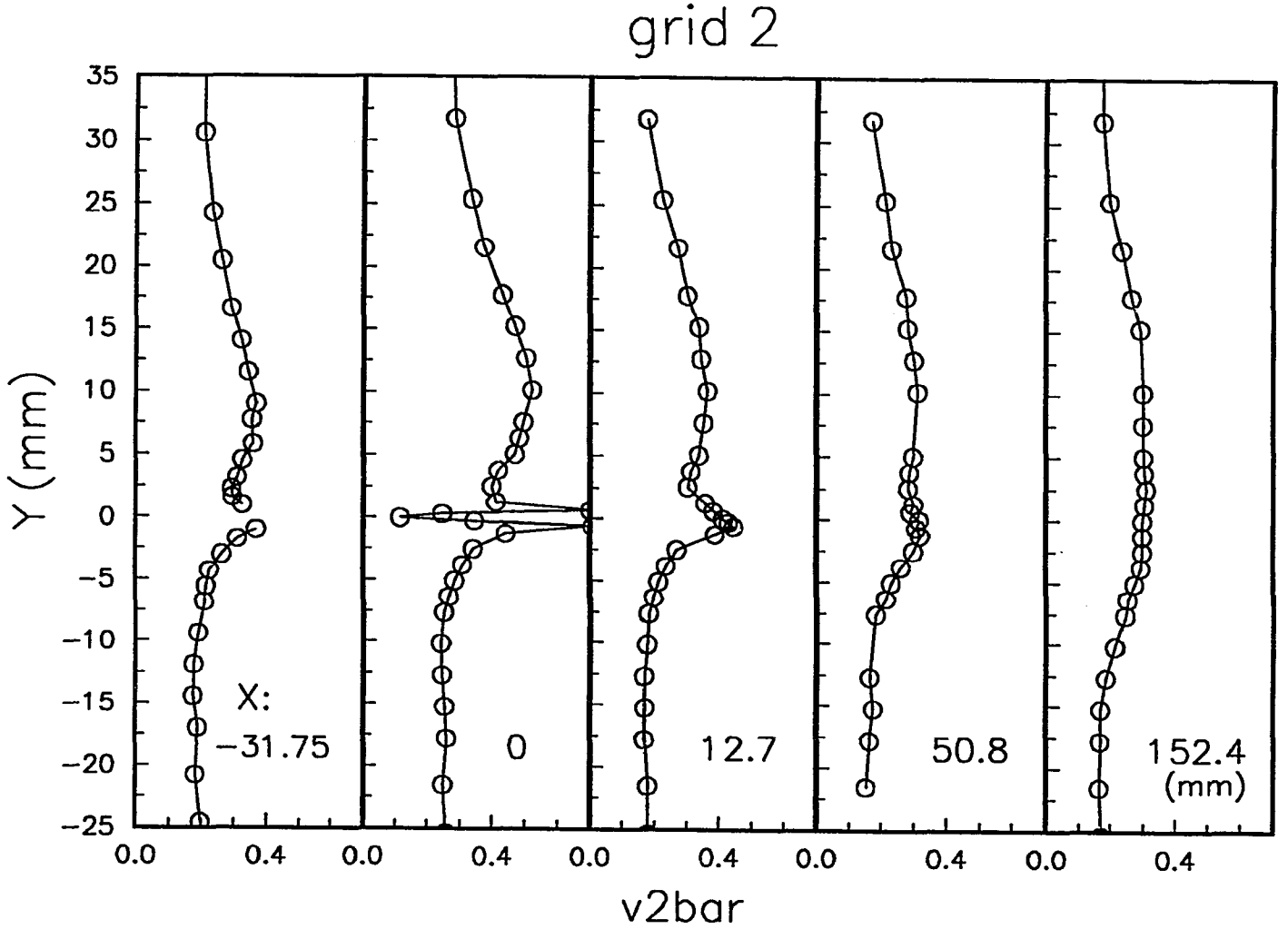

Fig.6.25a Distribution of $(\overline{v^2}/U_\infty{}^2)*10^2$, Asymmetric Wake, Under Free Stream Turbulence Generated by Grid 2

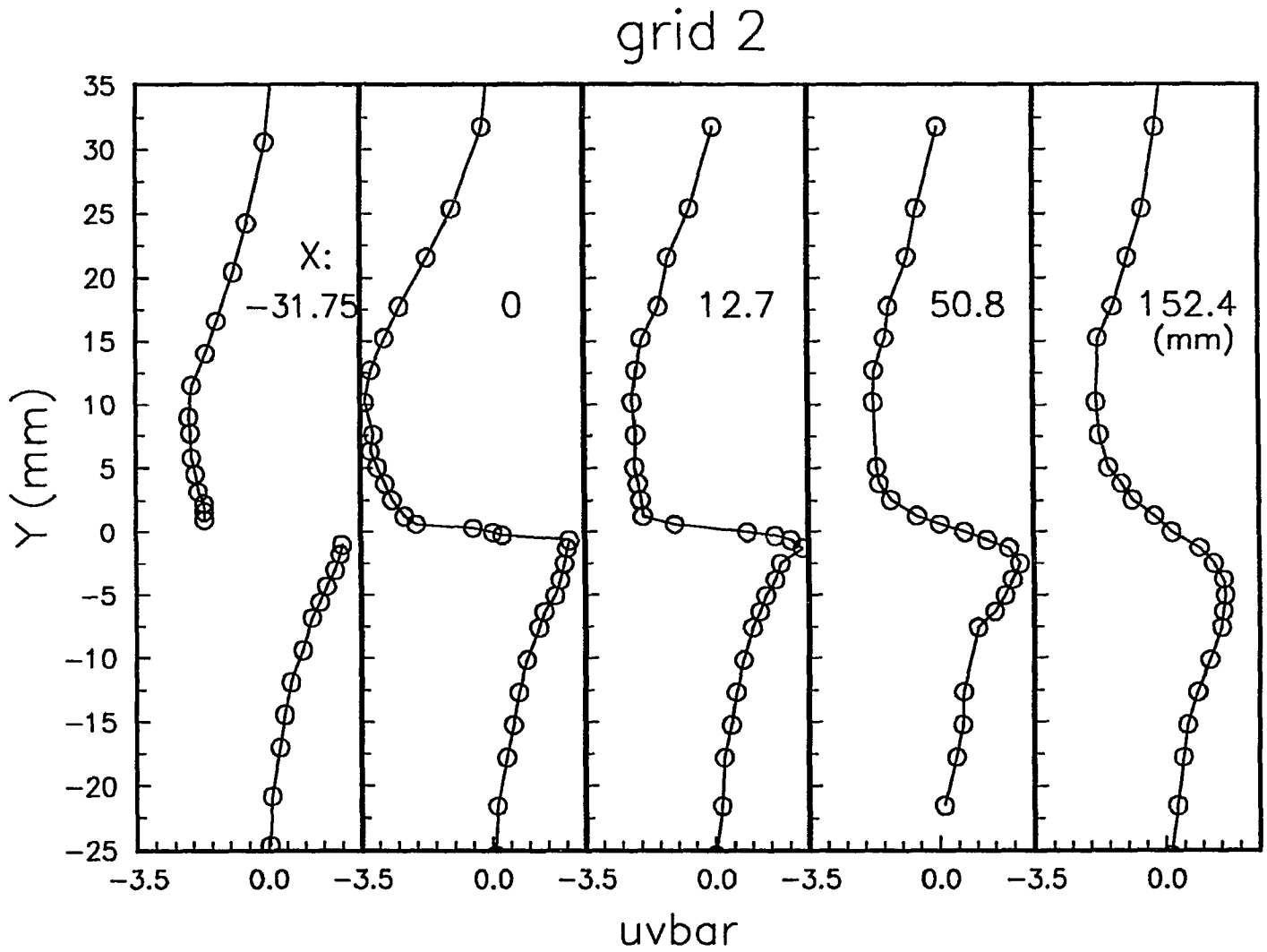

Fig.6.25c Distribution of $(\overline{uv}/U_\infty{}^2)*10^2$, Asymmetric Wake, Under Free Stream Turbulence Generated by Grid 2

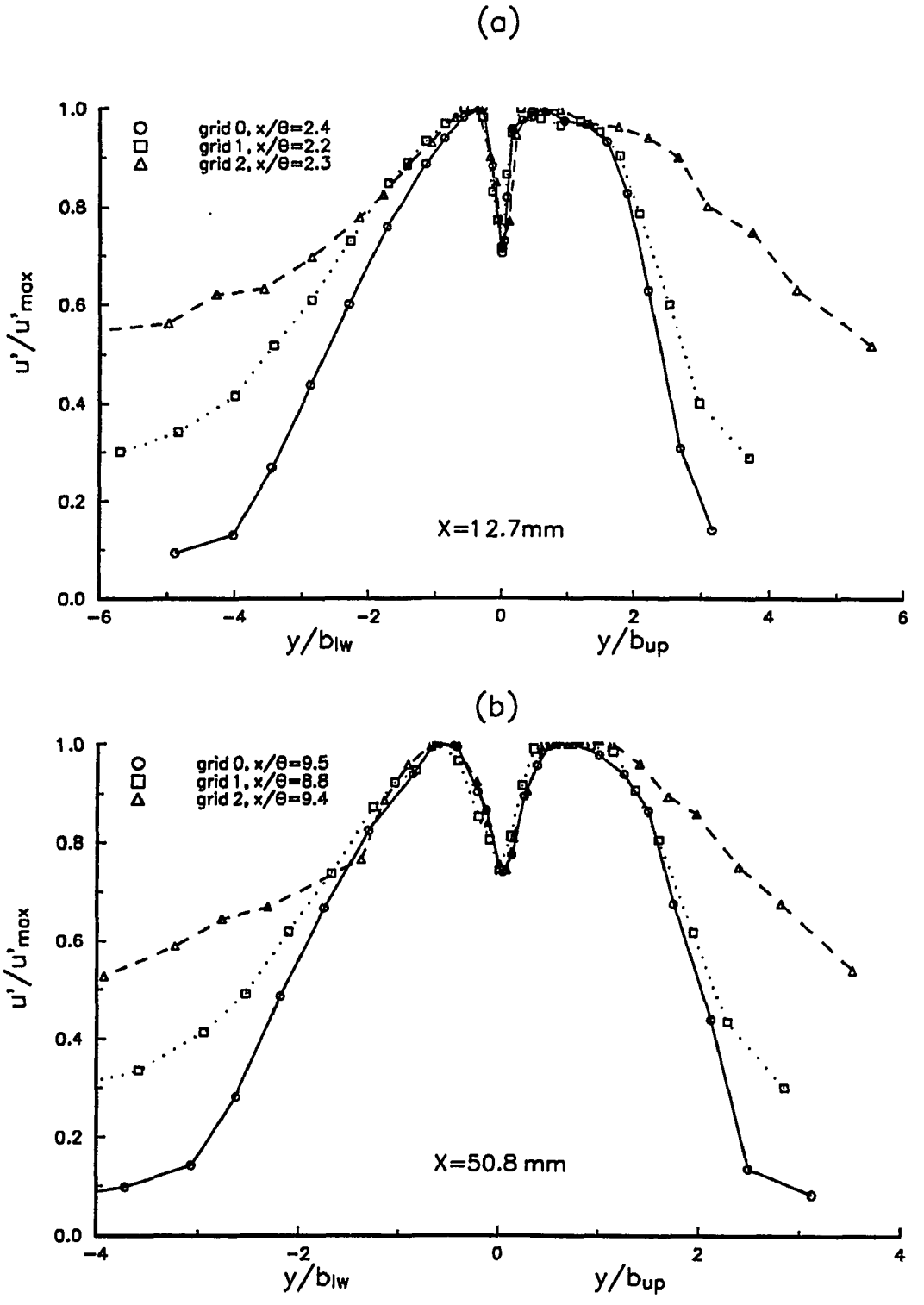

Fig. 6.26a Comparision of Turbulent Streamwise Intensity, Asymmetric Wake

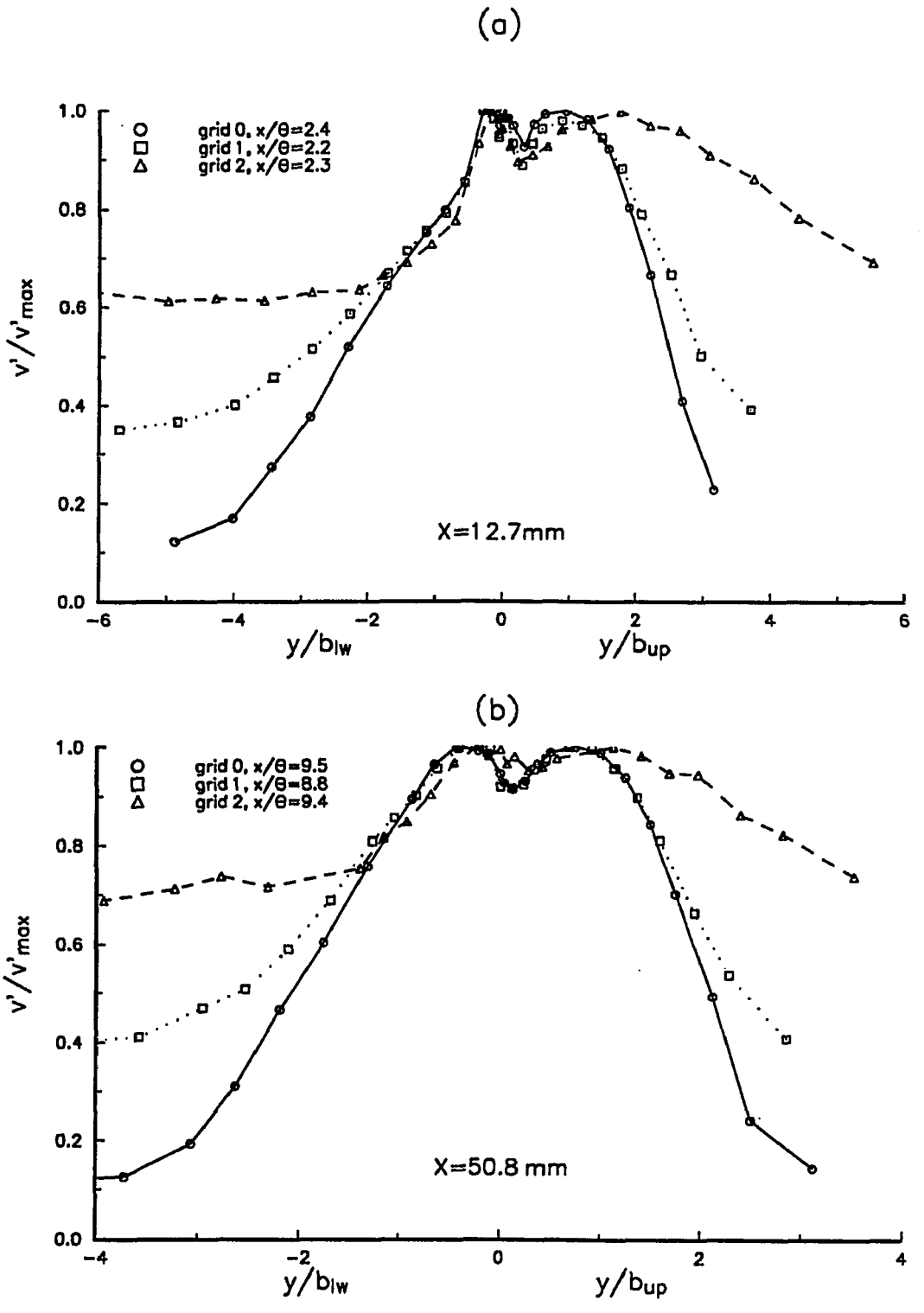

Fig. 6.26b Comparision of Turbulent Normal Intensity, Asymmetric Wake

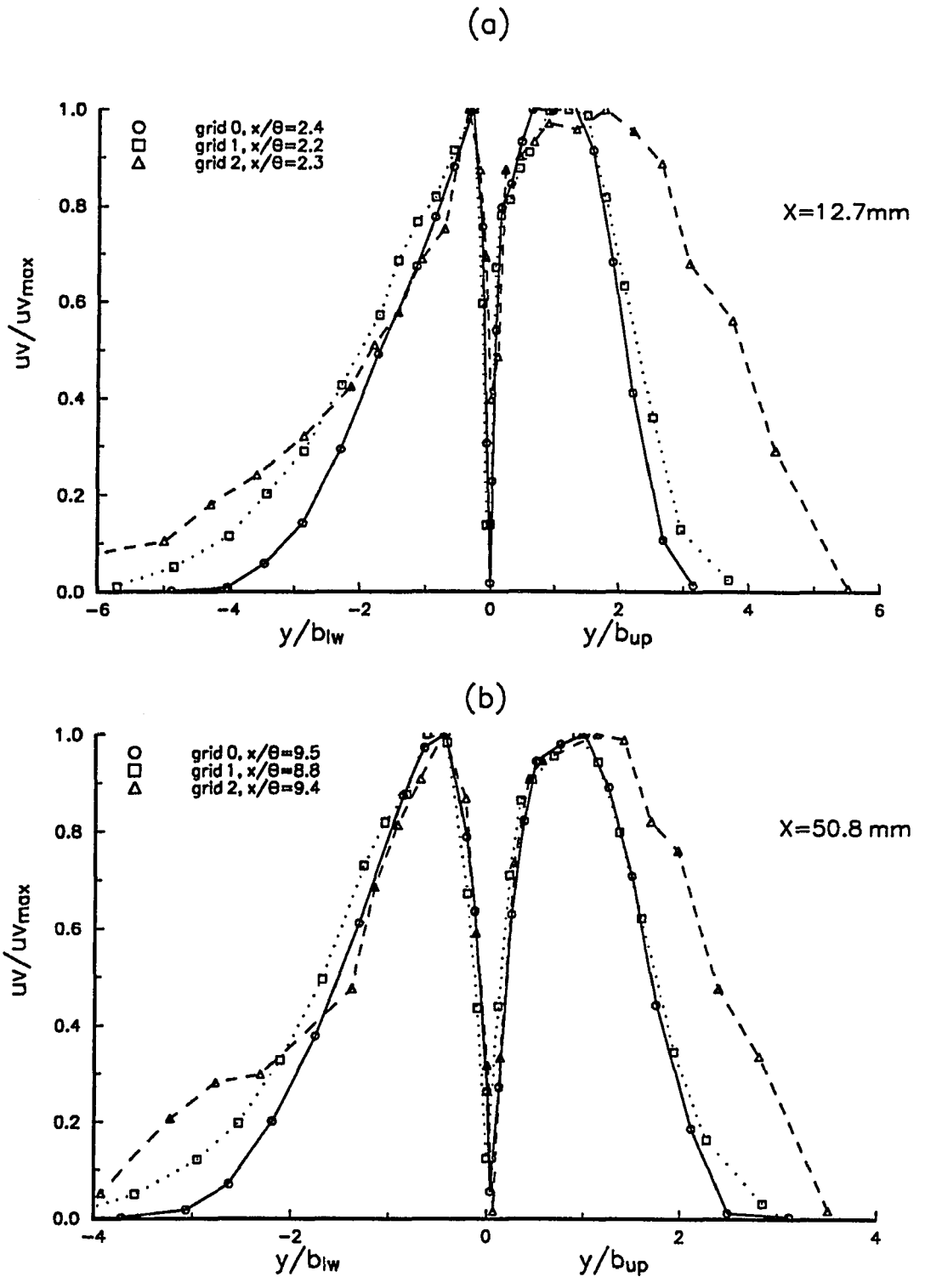

Fig. 6.26c Comparision of Turbulent Shear Stress, Asymmetric Wake

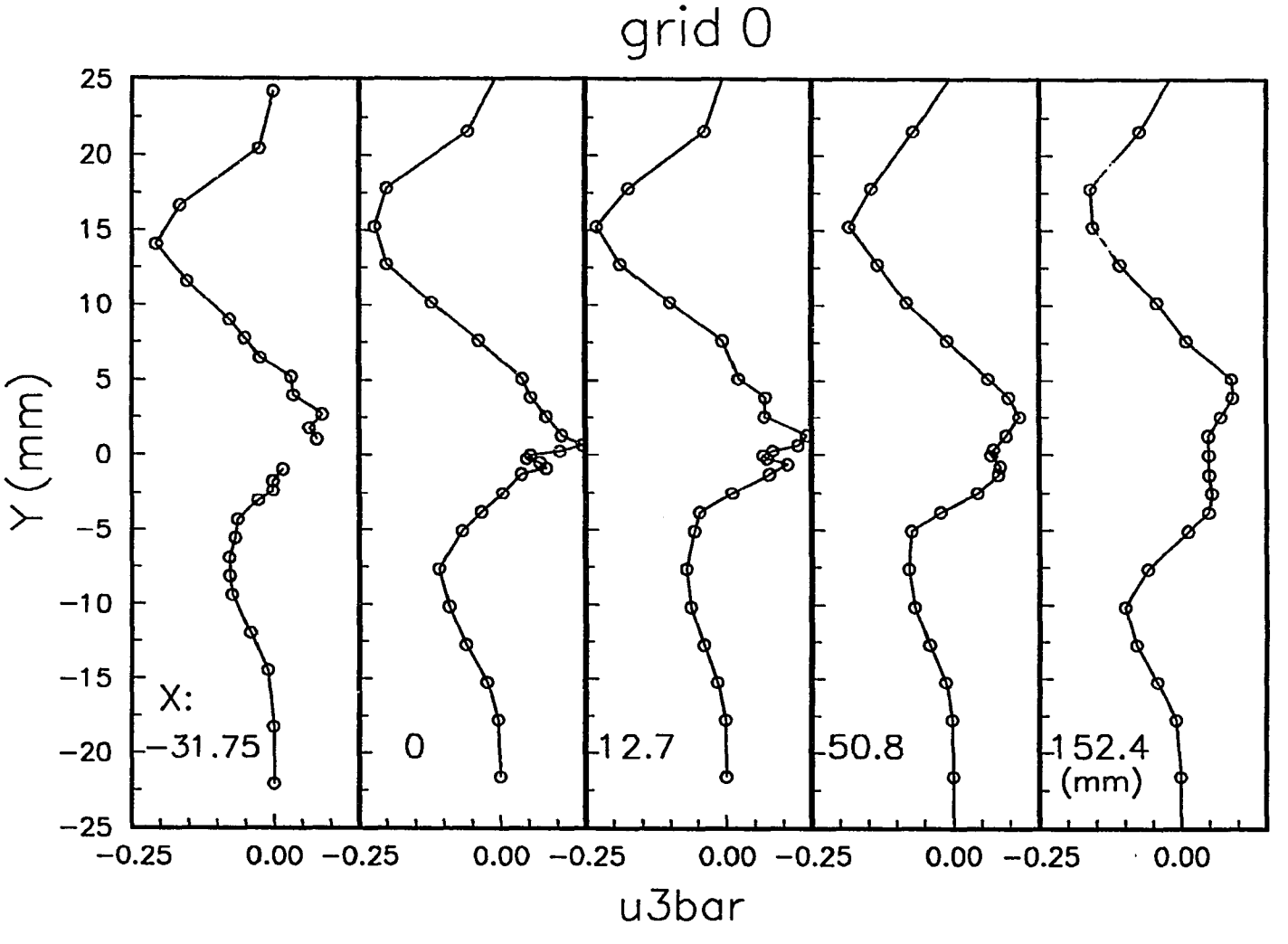

Fig.6.27a Distribution of $(\overline{u^3}/U_\infty{}^3)*10^3$, Asymmetric Wake, Under No Free Stream Turbulence

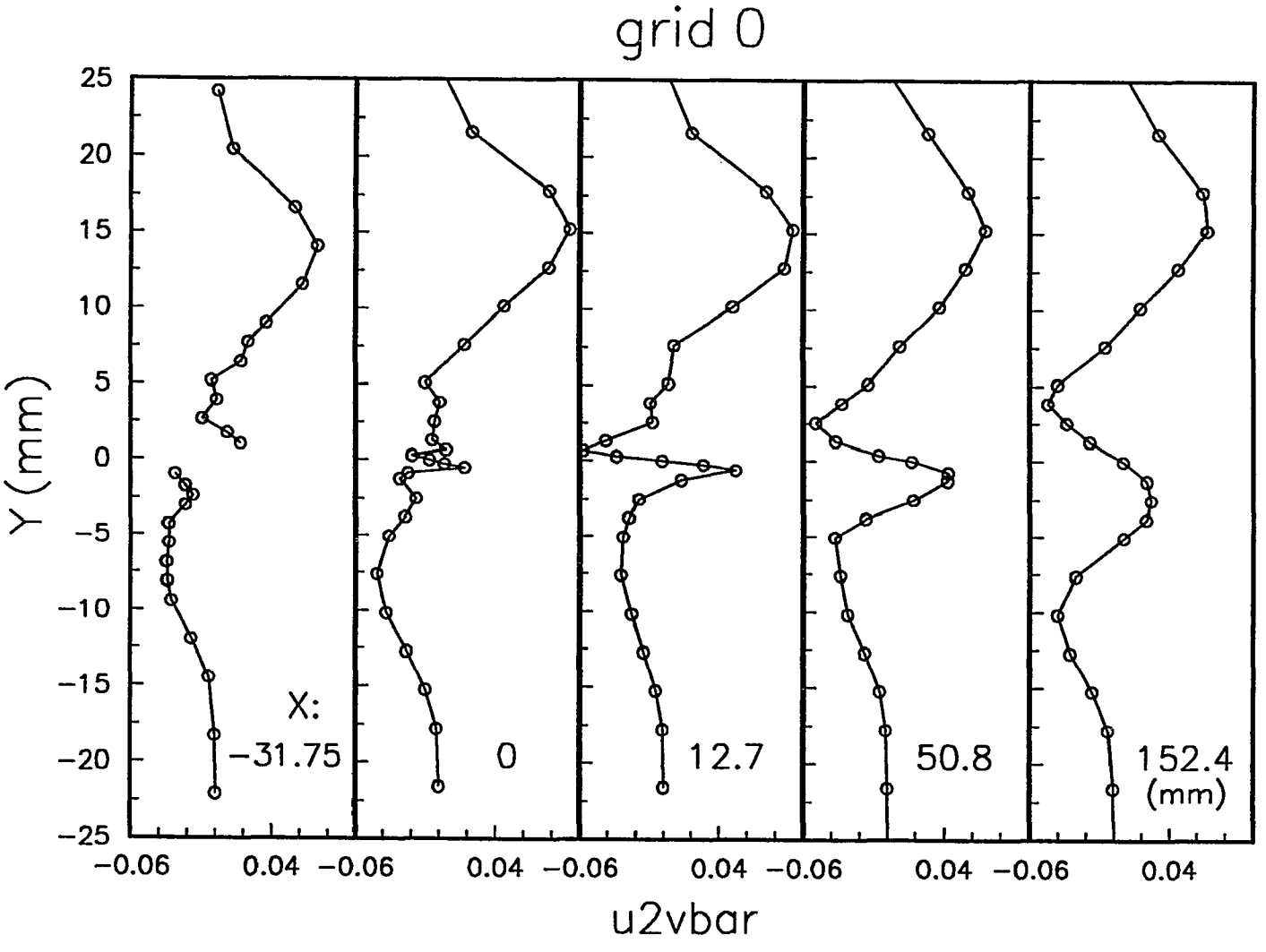

Fig.6.27b Distribution of $(\overline{u^2v}/U_\infty{}^3)*10^3$, Asymmetric Wake, Under No Free Stream Turbulence

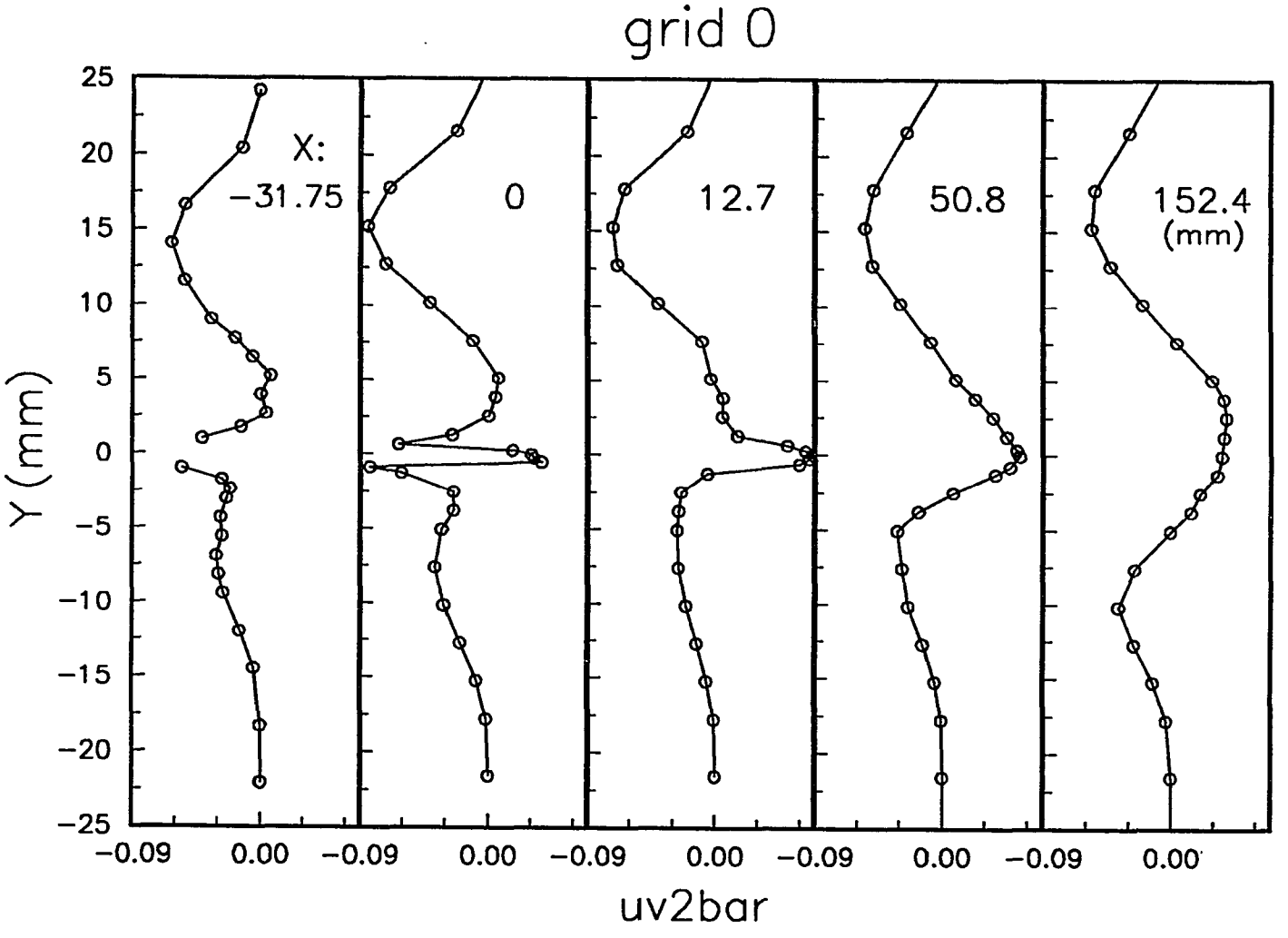

Fig.6.27c Distribution of $(\overline{uv^2}/U_\infty{}^3)*10^3$, Asymmetric Wake, Under No Free Stream Turbulence

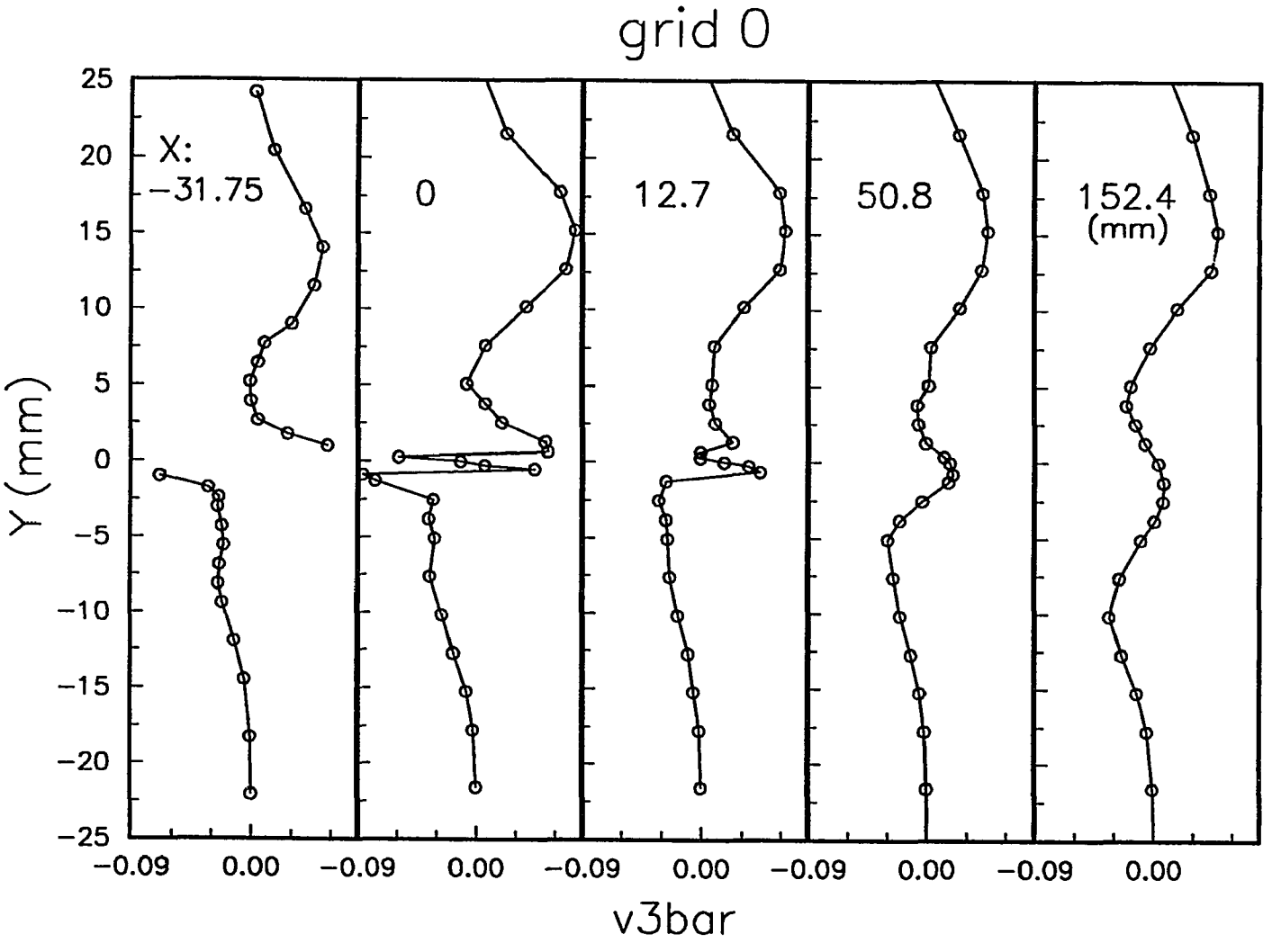

Fig.6.27d Distribution of $(\overline{v^3}/U_\infty{}^3)*10^3$, Asymmetric Wake, Under No Free Stream Turbulence

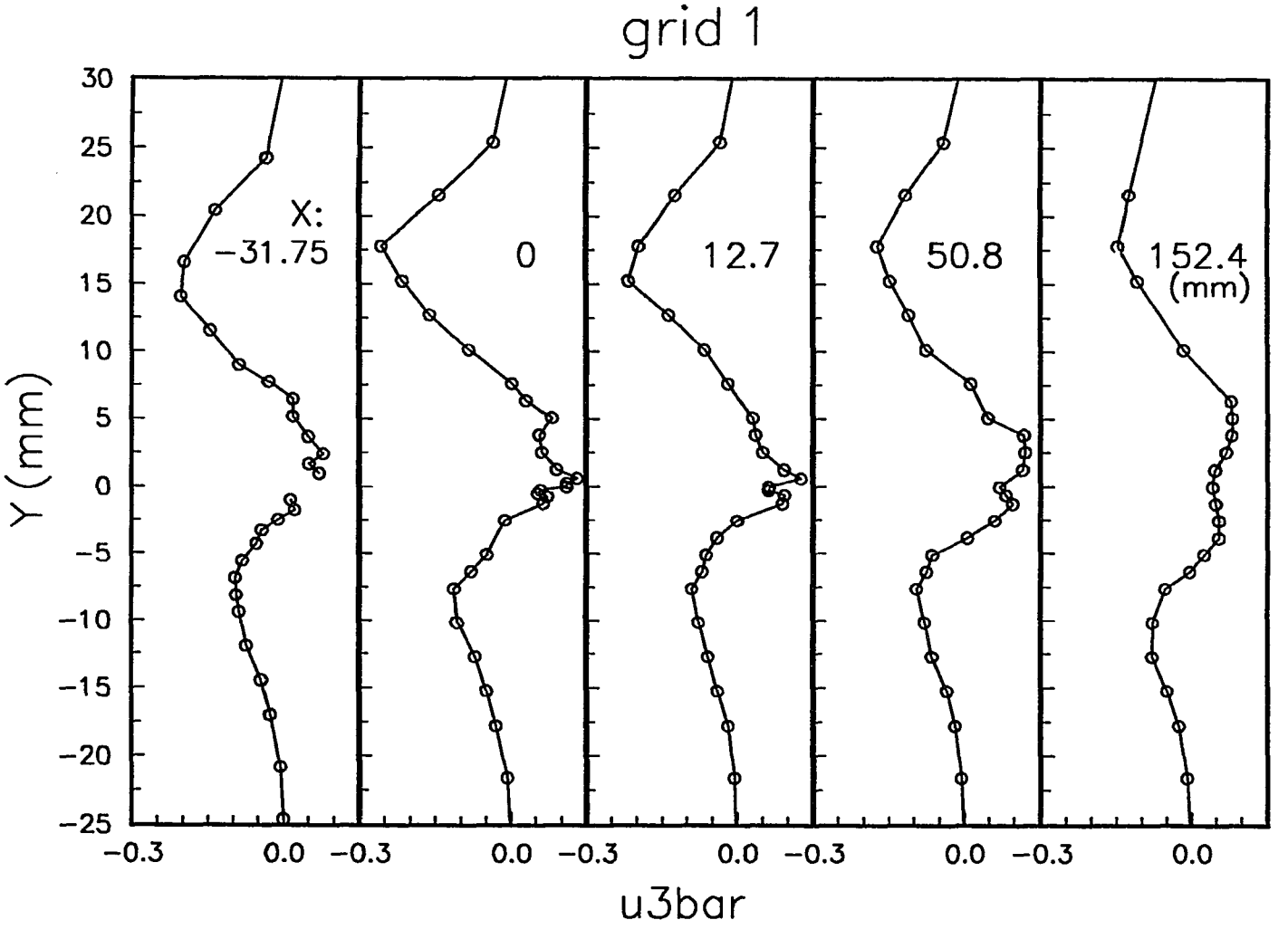

Fig.6.28a Distribution of $(\overline{u^3}/U_\infty{}^3)*10^3$, Asymmetric Wake, Under Free Stream Turbulence Generated by Grid 1

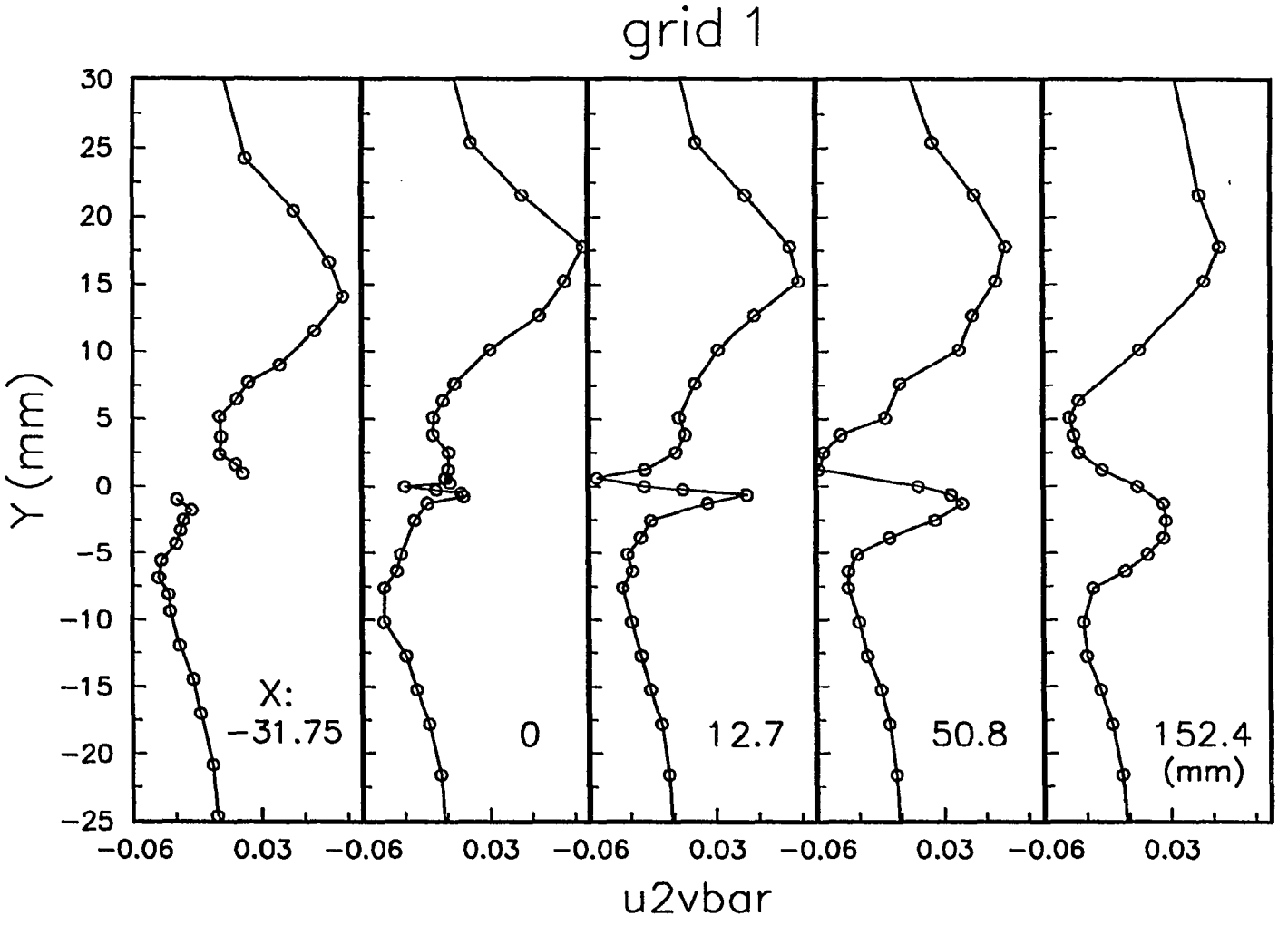

Fig.6.28b Distribution of $(\overline{u^2v}/U_\infty{}^3)*10^3$, Asymmetric Wake, Under Free Stream Turbulence Generated by Grid 1

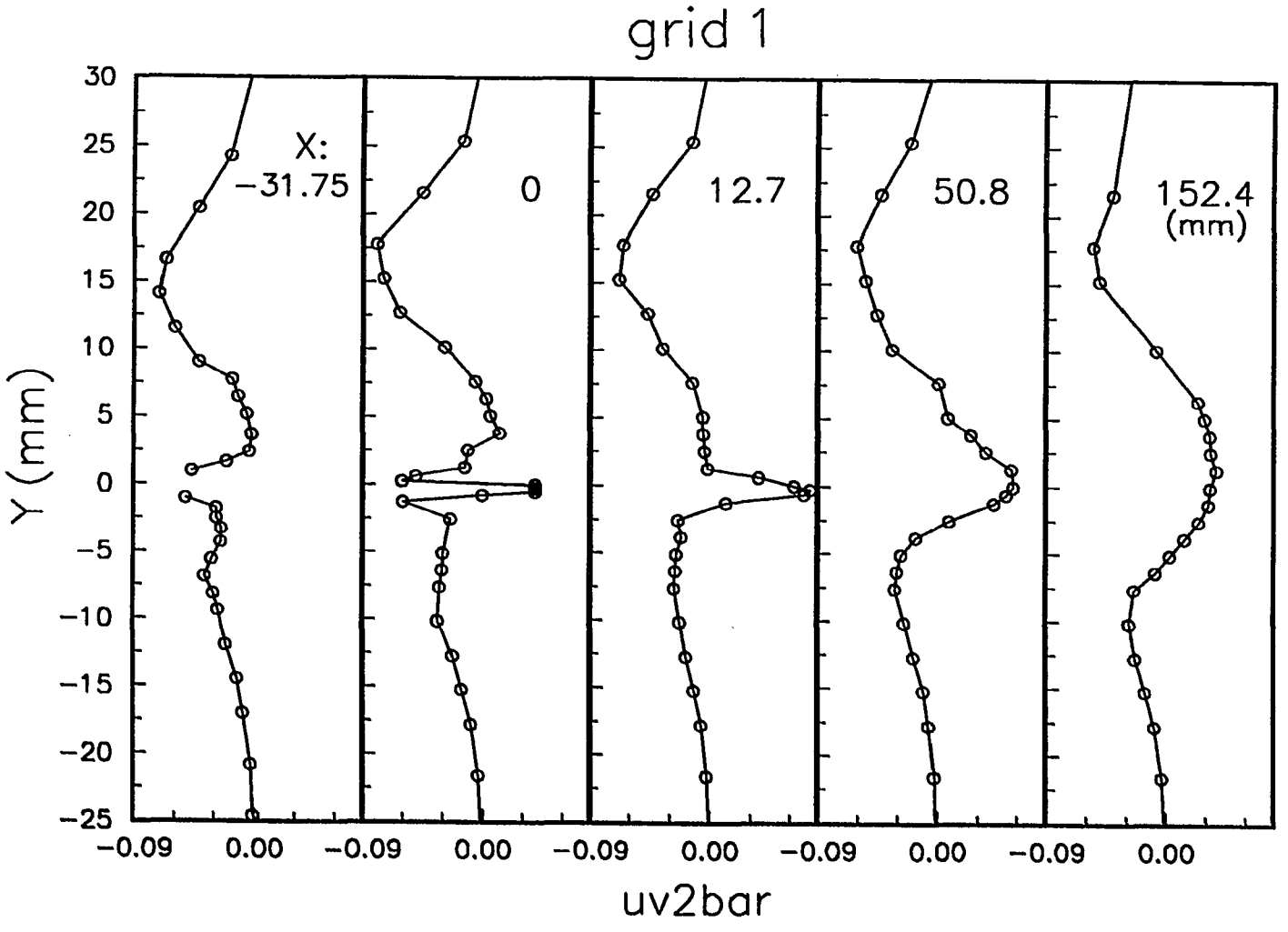

Fig.6.28c Distribution of $(\overline{uv^2}/U_\infty{}^3)*10^3$, Asymmetric Wake, Under Free Stream Turbulence Generated by Grid 1

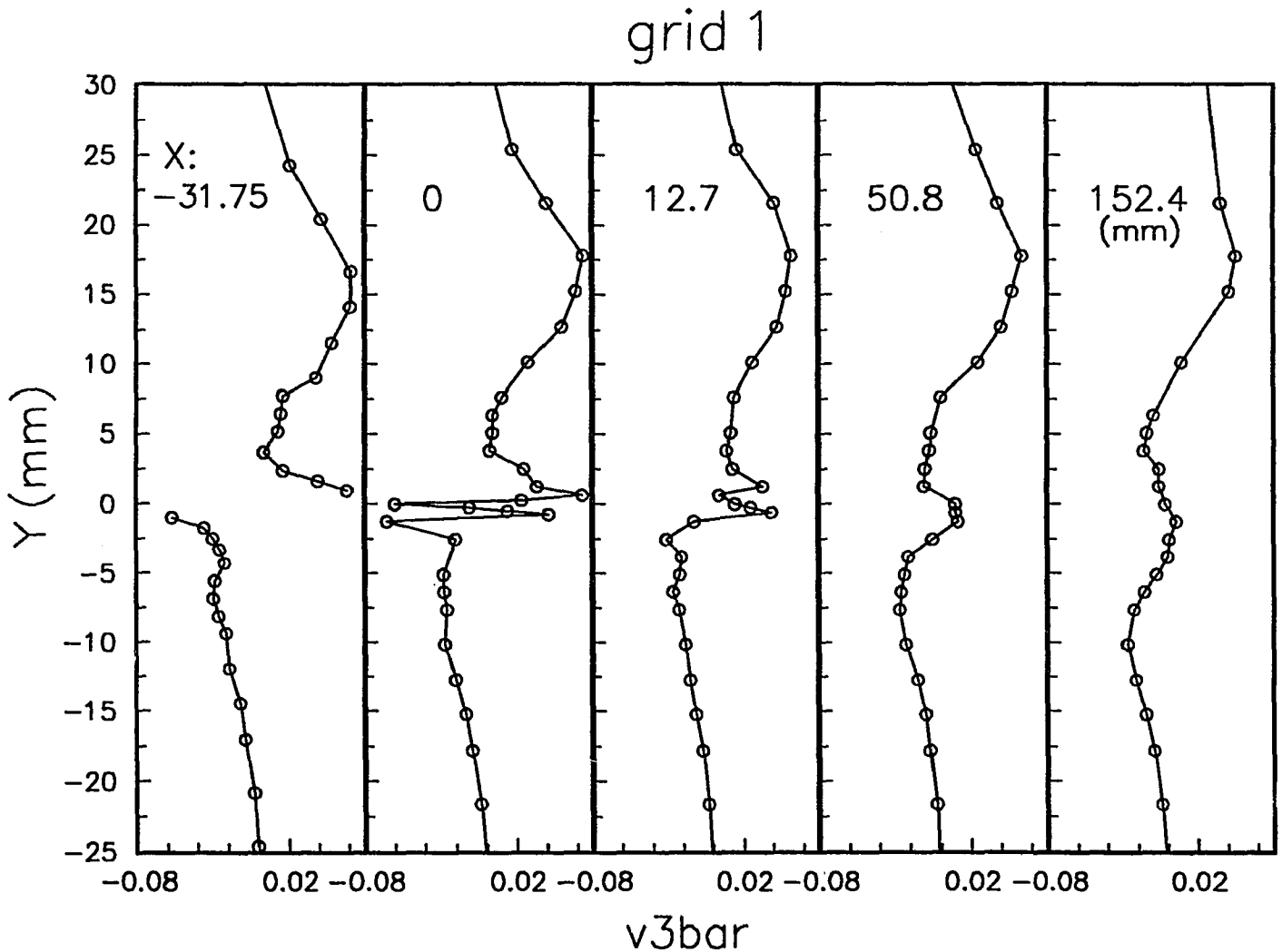

Fig.6.28d Distribution of $(\overline{v^3}/U_\infty{}^3)*10^3$, Asymmetric Wake, Under Free Stream Turbulence Generated by Grid 1

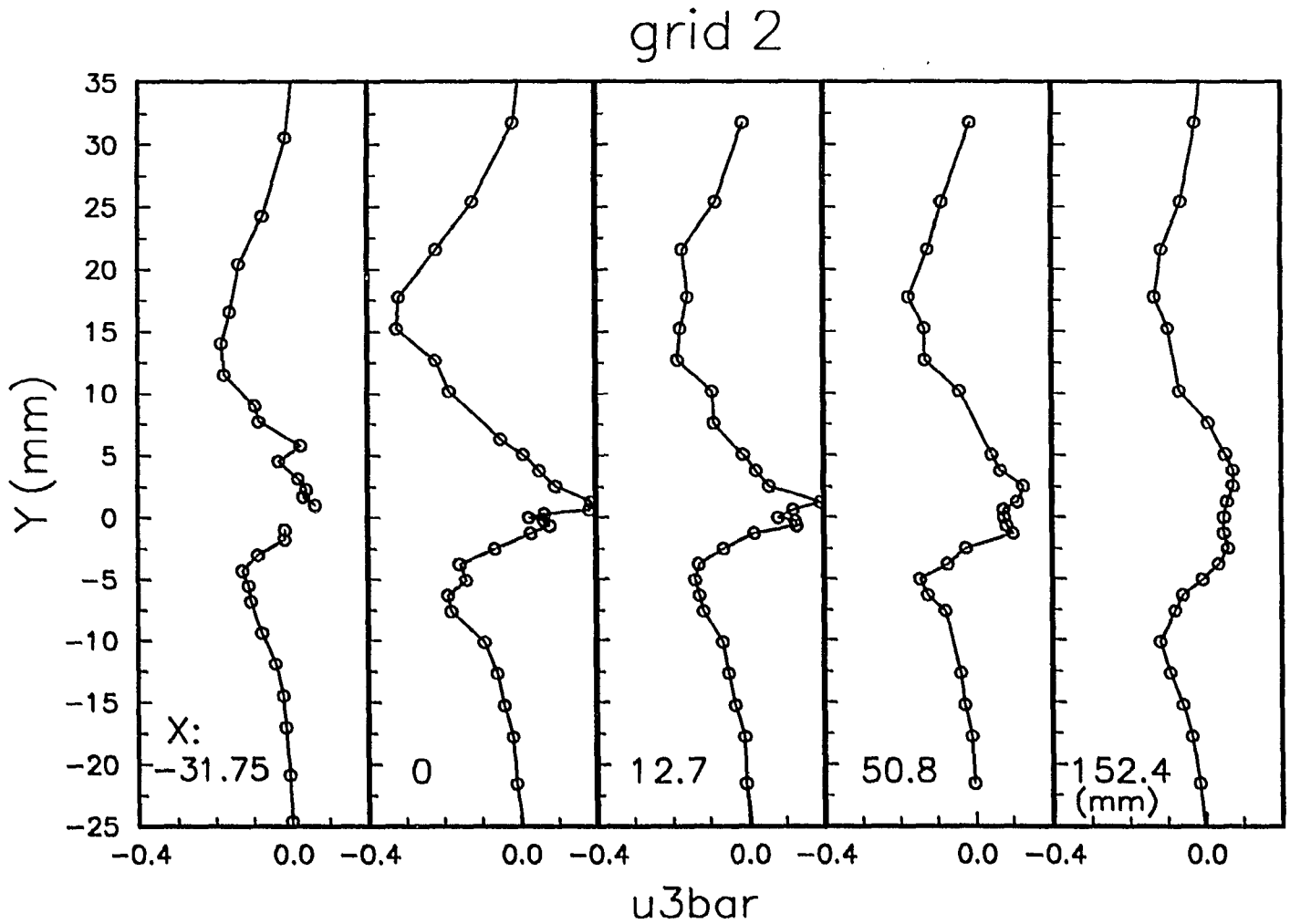

Fig.6.29a Distribution of $(\overline{u^3}/U_\infty{}^3)*10^3$, Asymmetric Wake, Under Free Stream Turbulence Generated by Grid 2

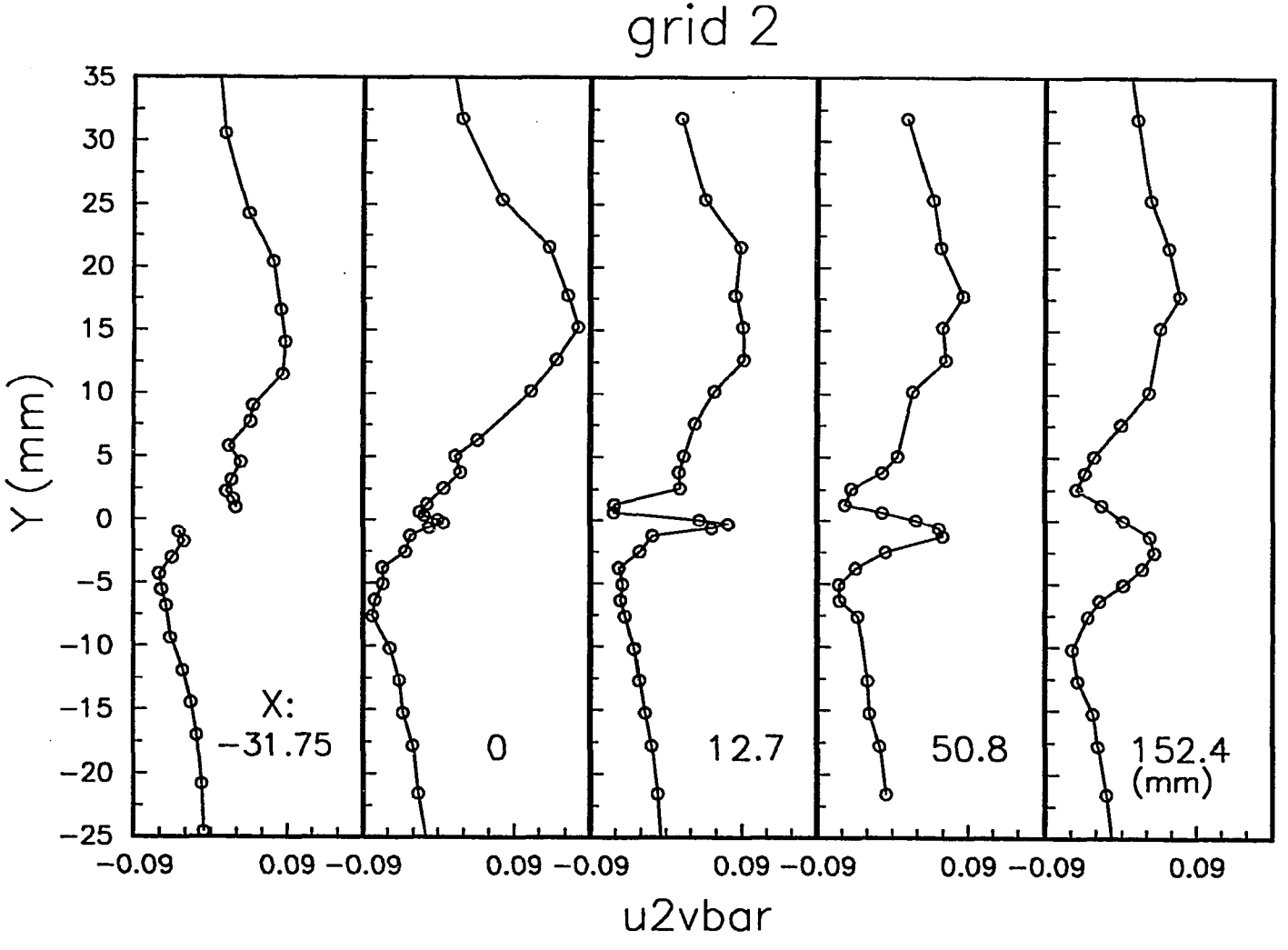

Fig.6.29b Distribution of $(\overline{u^2v}/U_\infty{}^3)*10^3$, Asymmetric Wake, Under Free Stream Turbulence Generated by Grid 2

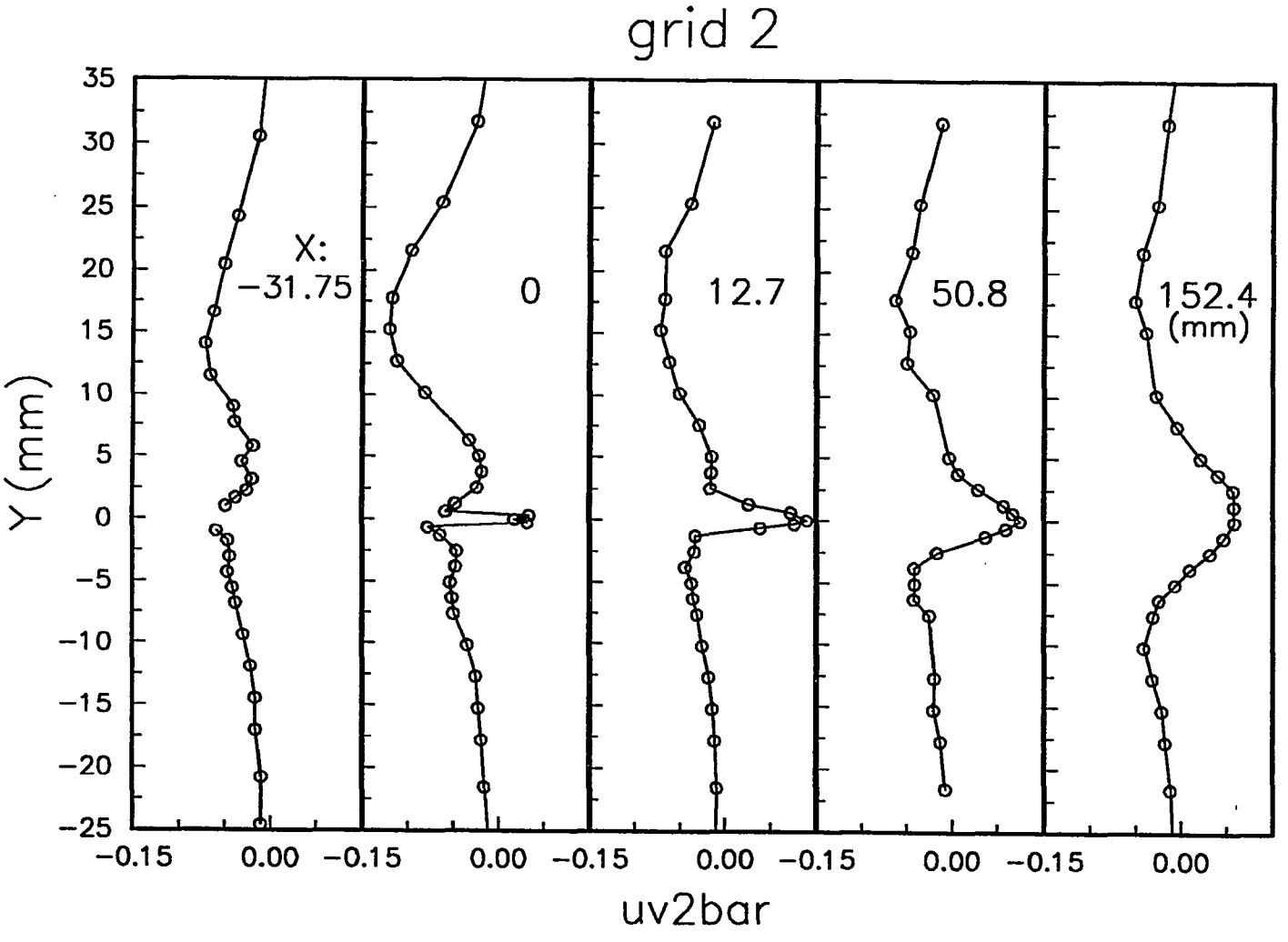

Fig.6.29c Distribution of $(\overline{uv^2}/U_\infty{}^3)*10^3$, Asymmetric Wake, Under Free Stream Turbulence Generated by Grid 2

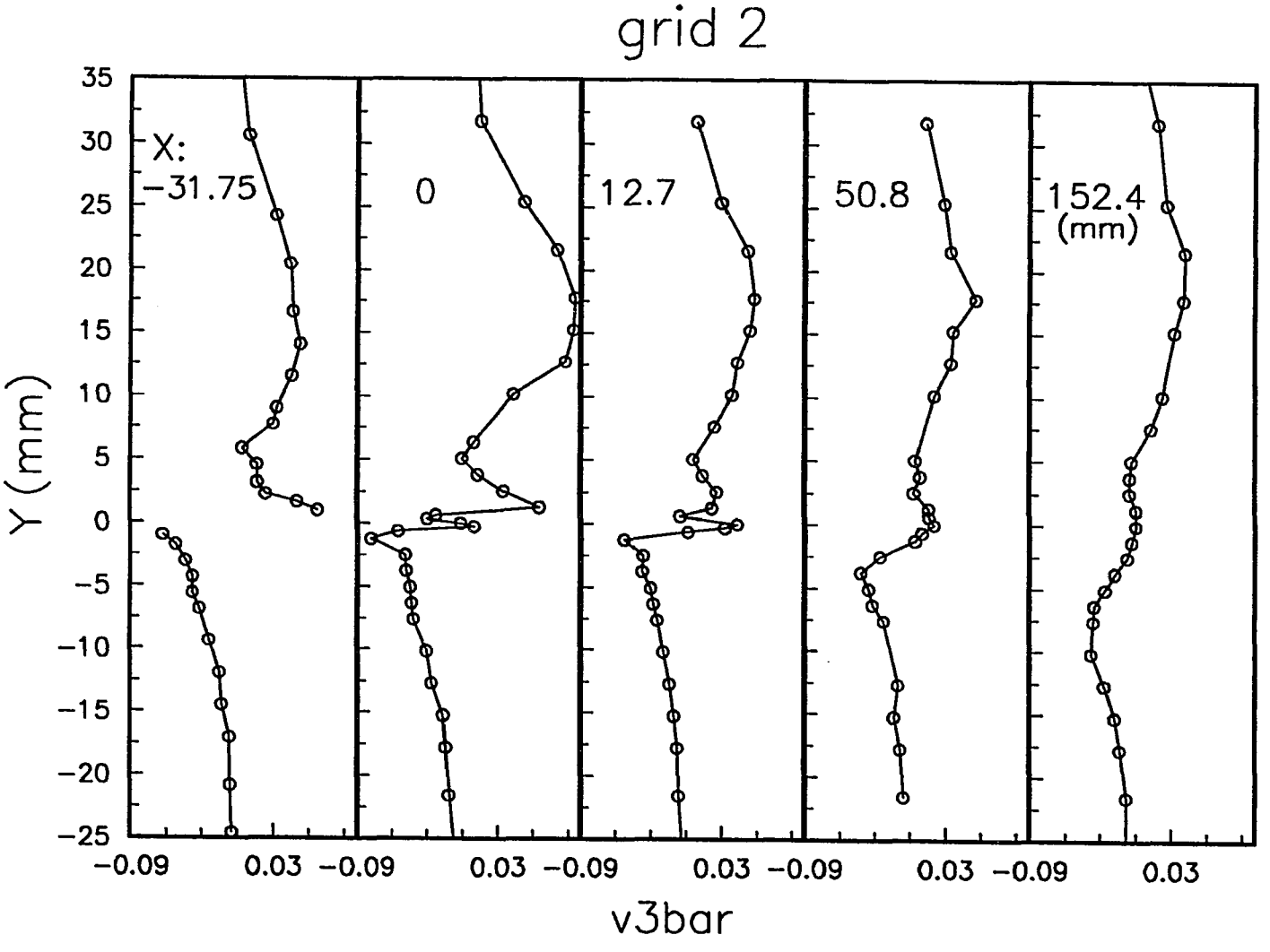

Fig.6.29d Distribution of $(\overline{v^3}/U_\infty{}^3)*10^3$, Asymmetric Wake, Under Free Stream Turbulence Generated by Grid 2

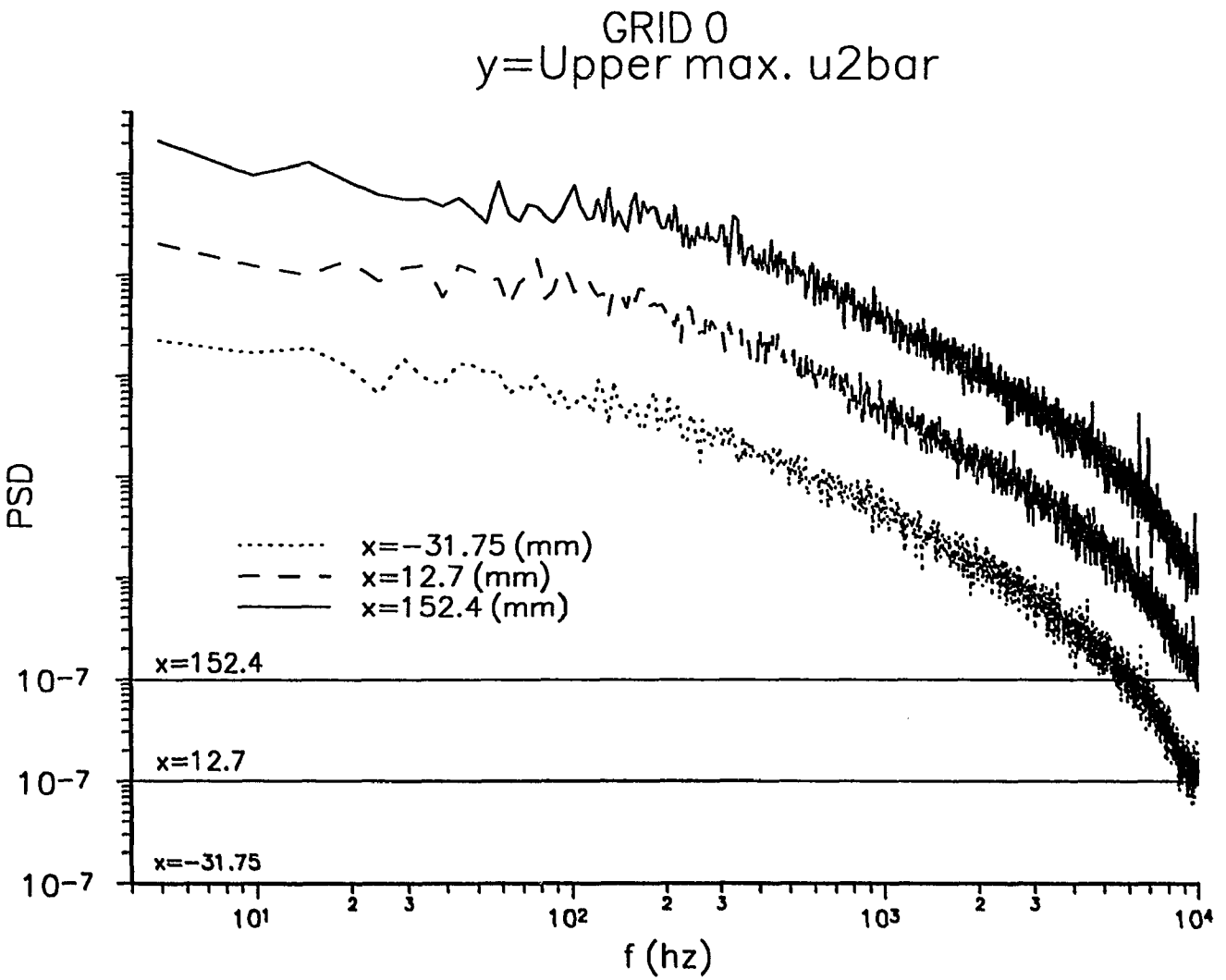

Fig. 6.30 Power Spectral Density vs. Frequency, Asymmetric Wake, Under No Free Stream Turbulence, y: Location of Max. $\overline{u^2}$

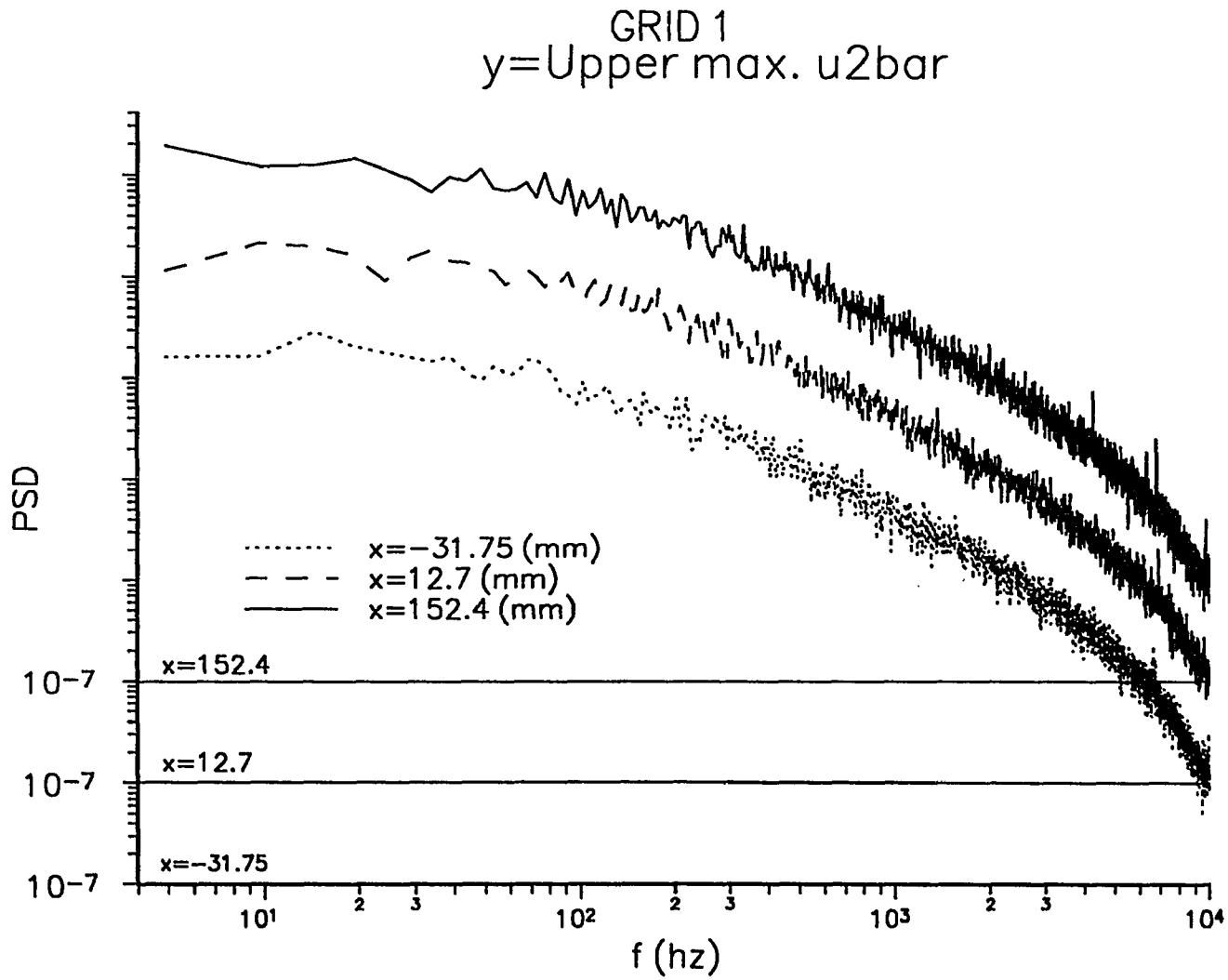

Fig. 6.31 Power Spectral Density vs. Frequency, Asymmetric Wake, Under Free Stream Turbulence due to Grid 1, y: Location of Max. $\overline{u^2}$

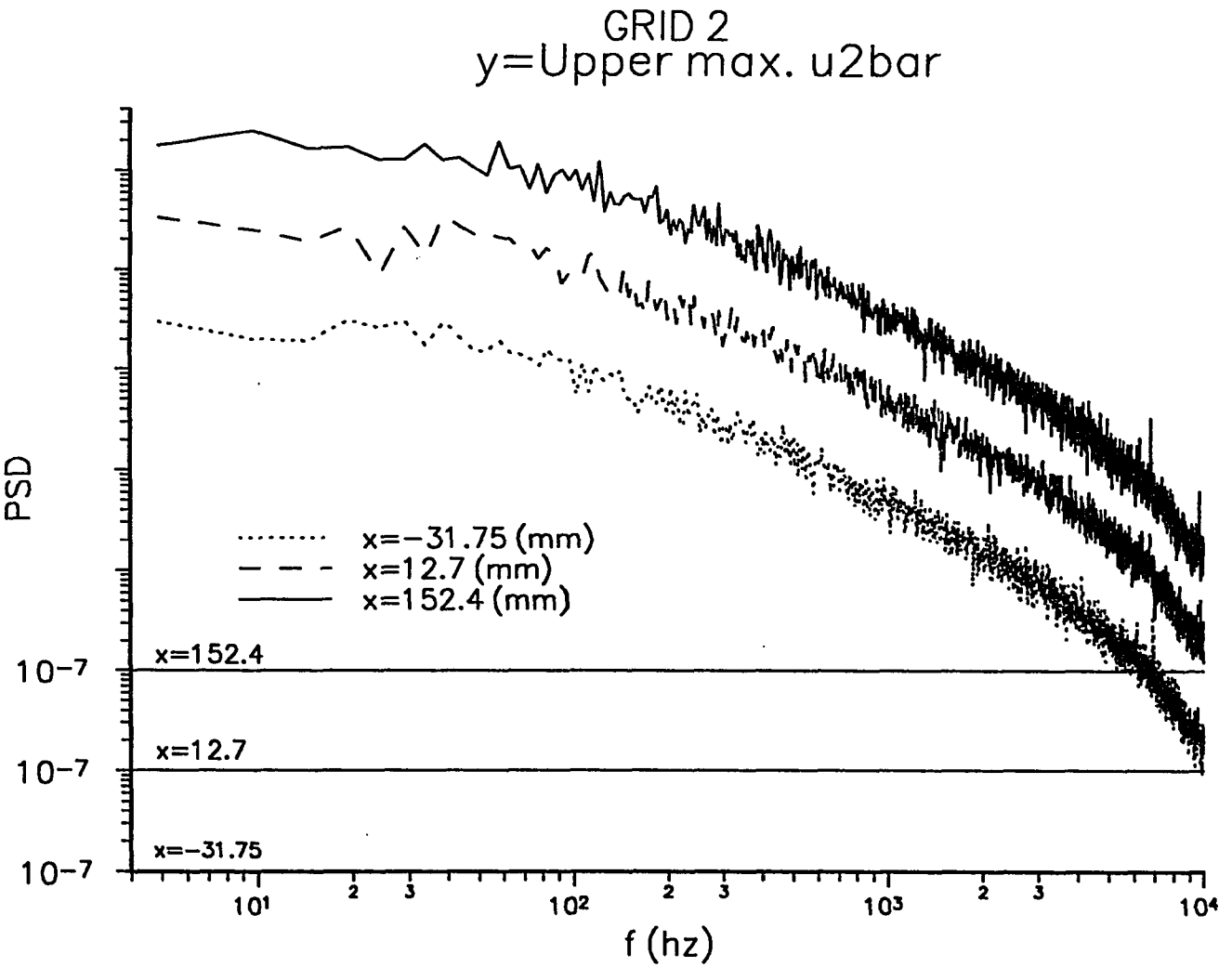

Fig. 6.32 Power Spectral Density vs. Frequency, Asymmetric Wake, Under Free Stream Turbulence due to Grid 2, y: Location of Max. $\overline{u^2}$

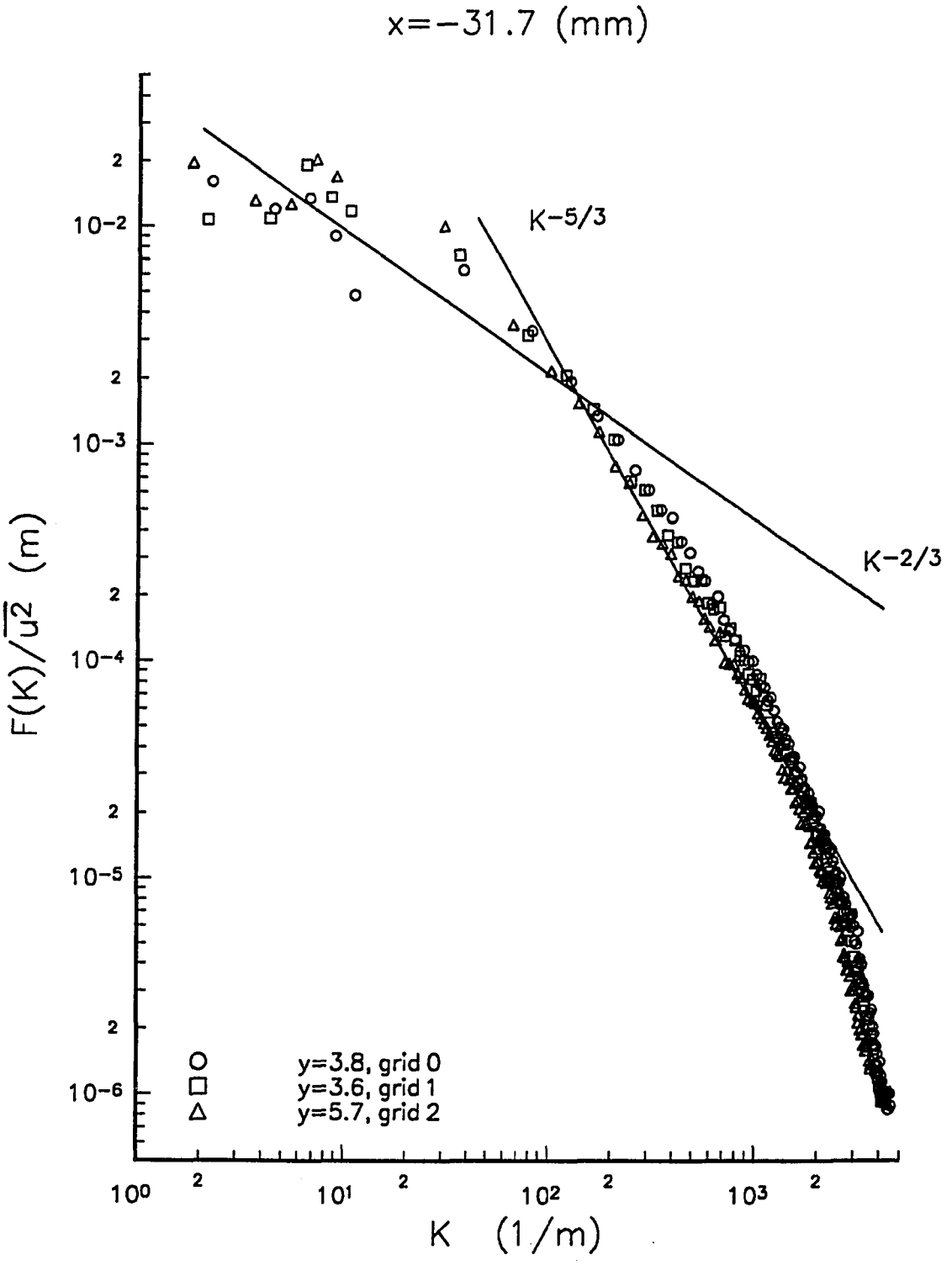

Fig. 6.33a Comparision of Spectral Function in Wave Number Domain, at Upstream Boundary Layer, X=−31.7 mm

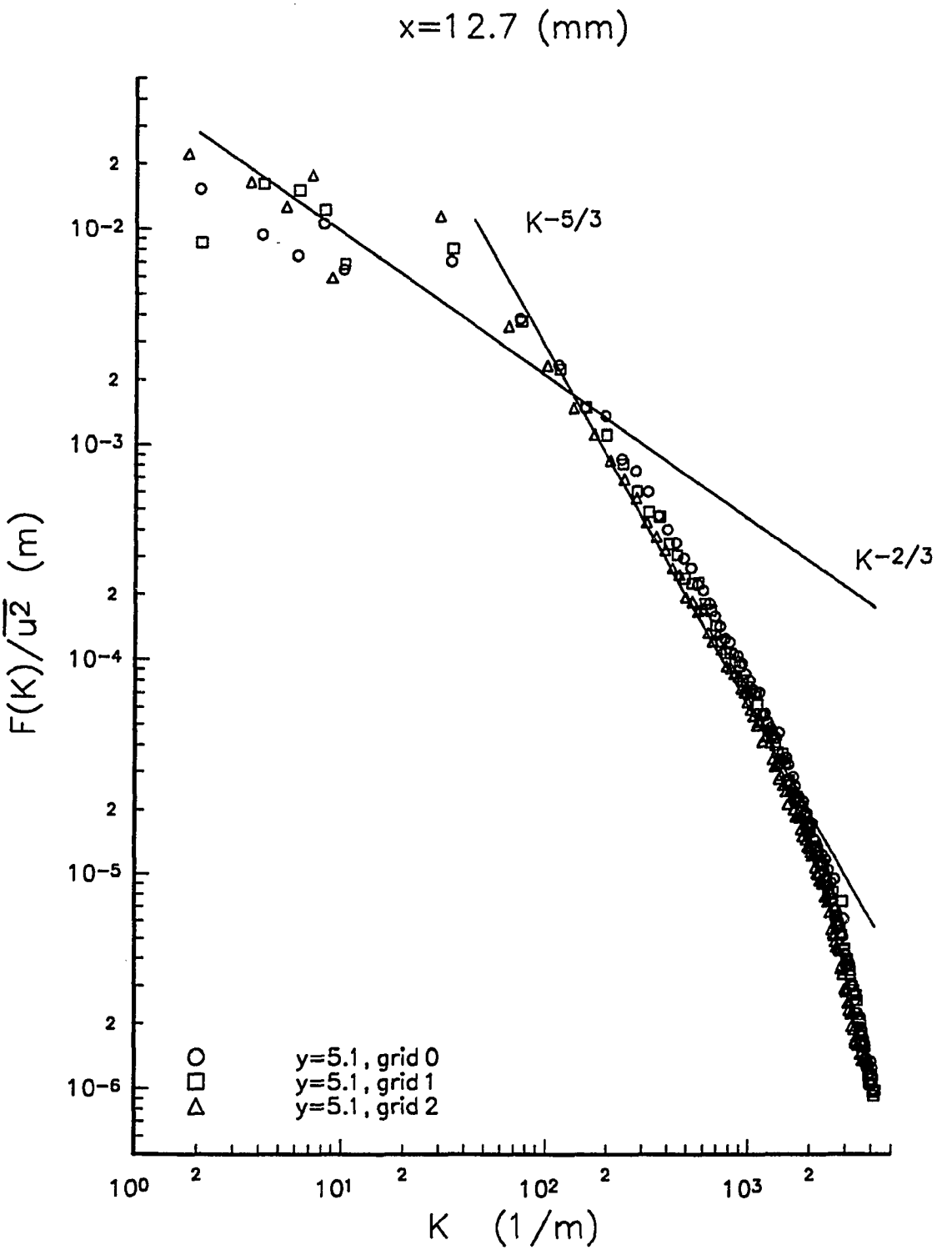

Fig. 6.33b Comparision of Spectral Function in Wave Number Domain, at X=12.7 mm

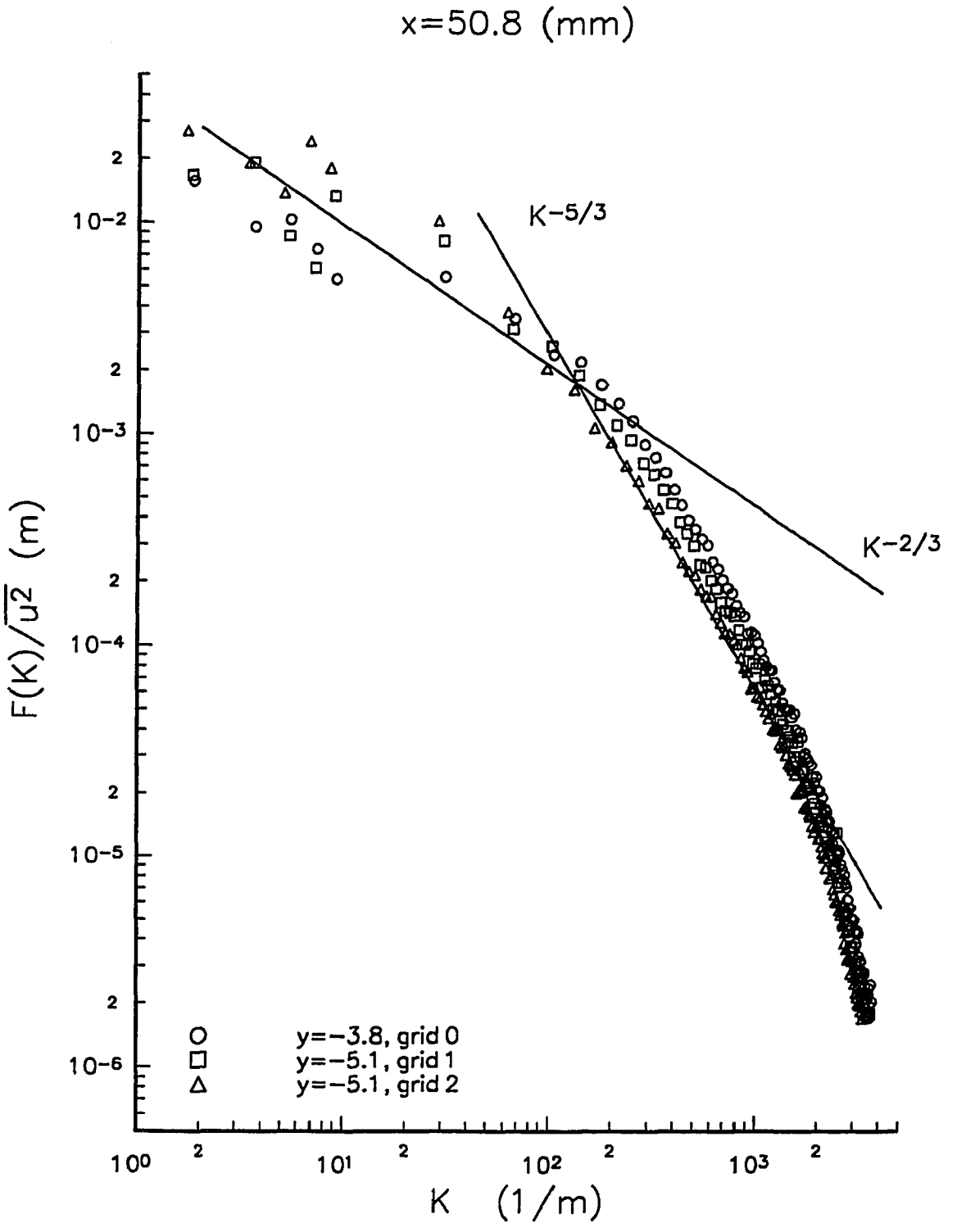

Fig. 6.33c Comparision of Spectral Function in Wave Number Domain, at X=50.8 mm

CHAPTER 7

COMPUTATIONAL RESULTS

To test the turbulence models and the calculation procedure, computations were performed for asymmetric and symmetric wakes. The results were compared with experimental data. The results of computation of far wake of a circular cylinder in presence and absence of free stream turbulence are also presented. Computations were performed for the case of asymmetric wake subjected to various levels and length scale of free steam turbulence. The numerical values of the empirical constants of the closure models used in these calculations are given in Table 7.1. These constants are selected from the standard values reported in the literature. An attempt was made to optimize these constants in the case of asymmetric wake.

7.1 Prediction of Symmetric Wake

The wake generating object is a flat plate at zero angle of attack. Figure 7.1 presents the schematic arrangement. Due to symmetry of the flow, the calculation domain consists of positive Y-axis and X-axis downstream of the plate. Sixty three non-equidistant grid nodes on the Y-axis were used. The steps in the axial direction varied from half the local momentum thickness in the near wake region to twice the local momentum thickness in the far wake region. The computation did not start at the

trailing edge, rather it started at a short distance downstream (X=12.7 mm) to reduce the effect of finite trailing edge of the object and the subsequent recirculation region. The initial conditions for the wake were obtained from experimental data. They were interpolated according to the grid geometry. The dissipation rate was estimated from the available experimental data. The experimental data set chosen for comparison of this case was that of Sastry [16].

The calculated profiles of U/Ue are presented in Fig. 7.2. Figure 7.3 shows the recovery rate of the wake as well as the variations of the shape factor, H. These figures show the results of calculation obtained with the Reynolds stress and k-ε models. The experimental data are also presented in these as well as other figures -where possible- for comparison purposes. It can be seen from Figs. 7.2 and 7.3 that the two models, k-ε and Reynolds stress - here after referred to as RS- predict the mean velocity distribution without much difference, and the predicted mean velocities are in very close agreement with the experimental data. The calculation appears to reproduce rapid initial recovery of the near wake, and its gradual recovery in the far wake. There seems to be no distinctive differences between the ability of the two models to predict the recovery of the wake.

Calculated profiles of correlation $(\overline{uv}/U_e^2)x10^4$ obtained by using the two models and experimental data are shown in Fig. 7.4. It can be seen that the two models underpredict $\overline{uv}$ in near wake. In the far wake region k-ε model seems to predict $\overline{uv}$ more accurately than the RS model. The

overprediction by RS model is due to the interpolation of experimental data at the initial station. Due to lack of measurements at Y=0, the data were actually extrapolated to obtain the initial conditions at centerline. This resulted in a nonzero uv at Y=0 (uvbar=-1.2). Furthermore, for integration of the RS model transport equations, the boundary condition imposed on $\overline{uv}$ transport equation at Y=0 is $\delta(\overline{uv})_0=0$, which results in a constant value of $\overline{uv}$ along the centerline. The nonzero value of $\overline{uv}$ at centerline seems to cause high levels of $\overline{uv}$ predicted by RS model. In an attempt to remedy this effect, $\overline{uv}$ was artificially set to zero at Y=0. However, this manipulation results in negative production of turbulence kinetic energy in the far wake region, which is physically impossible for the present wake configuration and was dismissed.

Typical profiles of r.m.s. values of normal intensities of the Reynolds stress tensor ($\sqrt{u_i^2}/U_e^2 \times 10^2$), obtained by RS model at X=381 mm, is presented in Fig. 7.5. The calculated profiles of $\sqrt{v^2}$ and $\sqrt{w^2}$ are essentially the same, and are in good agreement with experimental data. This was the case throughout the wake. However, $\sqrt{u^2}$ was close to experimental values in the outer region of the wake, and diverges from the experimental data near the central core of the wake. This again seems to be related to the initial conditions and the magnitude of $\overline{uv}$ near the centerline of the wake.

Overall, for symmetric wake, it was observed that k-ε model predicts the wake behavior more adequately with less computation time than the RS model. However, the built in assumption of isotropic turbulence structure

leads to erroneous results in normal intensities. It is further observed that RS model requires very accurate and consistent initial conditions to perform accurately.

7.2 Prediction of Asymmetric Wake

Figure 7.1 gives the schematic of asymmetric wake generation. In the present case, one of the surfaces of the plate is covered with sandpaper. The added roughness causes the boundary layer to be characteristically different from the smooth side. The wake evolves from merging of these two different boundary layers, under no pressure gradient. The experimental data selected for this computation is that of Andreopoulos and Bradshaw [13]. In this case, author's calculation started at X=25 mm. which was the first available experimental station after X=0. 125 non-equally distant nodes were chosen along the Y-axis to cover both sides of the wake. Experimental data were interpolated according to the grid geometry along Y-axis. The dissipation rate of turbulent kinetic energy was estimated form the experimental data. The values of streamline function at these nodes were calculated, and the governing equations were numerically integrated along these streamlines in (X,Ψ) space as explained in chapter IV. The steps in axial direction varied from half local momentum thickness to about one local momentum thickness. After convergence was achieved for a given computational station, the transverse position of grid nodes were computed by numerically integrating Eqn. 4.19.

Calculated profiles of mean velocity U/Ue are shown in Fig. 7.6.

Figure 7.7 presents the shape factor H and the wake recovery rate Uc/Ue. The mean velocity distribution is predicted with fair accuracy by both models. The shape factor and the wake recovery are also in good agreement with the experimental data. It is observed that the k-ε model, in the central core of wake, predicts the mean velocity closer to the measured profile than RS model. However, as far wake is approached, RS model results in more reasonable predictions.

Figure 7.8 gives the calculated profiles of non-dimensionlized Reynolds shear stress ($\overline{uv}/U_e^2$ x10^3) at a few axial positions. It is most interesting to note the peak in the $\overline{uv}$ on the smooth-wall side of the wake (negative Y) predicted in the initial stages of development of the wake. This was also present to some extent in the calculation of symmetric wake. This peak was also seen in the experimental data at the initial stages of the wake, and it gradually disappears. However, it is still distinguishable at X=100 mm in the present data. Andreopoulos and Bradshaw[13] attribute this to high levels of production of shear stress near the centerline due to transport of high momentum fluids by vertical fluctuation component of Reynolds stress tensor, and high normal gradient of mean velocity. It is surprising that k-ε model without any mechanism built into it to account for the production of Reynolds shear stress explicitly, indeed shows these peaks. However, it is believed by the author, that the presence of the peak in the initial conditions used in k-ε model, (in the computation of effective viscosity), is reflected by a decaying process in the calculation output. As far wake is reached, it seems that the k-ε model predicts the $\overline{uv}$ in closer

agreement with experimental data than RS model.

Computed profiles of non-dimensionlized turbulent kinetic energy ($K/U_e^2 \times 10^2$) are shown in Fig. 7.9, while a few profiles of ($\overline{u^2}/U_e^2 \times 10^2$) are presented in Fig. 7.10. It is observed from these figures that k-ε model calculates the level of kinetic energy much closer to experimental data than RS model. It appears that the RS model overpredicts kbar and $\overline{u^2}$ as far wake is approached. To explain this fact, kinetic energy budget were computed for both models at a typical station of X=100 mm. They are shown in Fig. 7.11. Both models predict advection, production and dissipation essentially the same. However, the diffusion of k is predicted at a much higher level by RS model than k-ε model. This seems to cause the overprediction of k and $\overline{u^2}$. These results seem to confirm the previous suggestion that k-ε model seems to be a better model, and RS model needs to be refined to perform more accurately.

In an effort to improve the RS model and investigate the modeling of pressure-strain correlation term in Reynolds stress equation, the empirical constants associated with that term were varied and asymmetric wake was predicted with those constant varied. Table 7.2 presents the values used for those constants. The output of these computations in far wake were compared with experimental data of Andreopoulos and Bradshaw [13] and those of Sastry [16]. The far wake was chosen for these comparisons because the RS model does not perform as well in the far wake as in the near wake.

Figure 7.12 presents the mean velocity profiles, uvbar and u2bar of

these computations at last axial station X=400 mm along with the data of Andreopoulos et al. [13] at the same station. There does not appear to be any particular case that makes the predicted values closer to experimental case in all the graphs. Cases 7 and 4 enhance the predicted mean velocity. While cases 6 and 8 seem to make the prediction of u2bar and uvbar closer to the experimental data. There seem to be too much discrepancy between these cases that no particular case could be selected as the best possible values.

Figure 7.13 presents the outcome of the prediction of asymmetric wake of Sastry [16], with the variation of these constants. The station presented is at X=609.6 mm which is well into the far wake region. These computations started at axial station of X=12.7 mm and various step sizes ranging from a fourth of momentum thickness in near wake to half momentum thickness in far wake were used. Standard case was not computed and case 6 did not converge.

It is most interesting to note that cases 2 and 5 improve the accuracy of mean velocity and u2bar predicted by the computation. while uvbar is predicted closer to experimental value in cases 5 and 8. There does not seem to be a specific case that improves all the quantities predicted.

It is most noteworthy to observe that these computations result in overprediction of mean velocity and uvbar in the far wake as compared to the measurement of Andreopoulos et al. [13], while they are underpredicted as compared to the measurement of Sastry [16]. This pattern is consistent for all the different values of constants used in the model. Therefore, one

can not reach values for these constants that improve the Reynolds Stress model, and the standard values was used for computation wake under free stream turbulence.

7.3 Prediction of Far Wake of a Cylinder With, and Without Free Stream Turbulence

Figure 7.14 presents the schematic arrangement of experimental set up of Komoda [20]. The data from this setup was used as initial conditions. The wake generating object was a 1 mm diameter cylinder. The grid generating turbulence was placed 305 mm upstream of the cylinder. In the case of no free stream turbulence the grid was removed. Due to symmetry of the wake 30 nodes were selected in the positive Y-axis. The experimental data at X=60 mm were interpolated to obtain the initial conditions. During the integration of equations, because of growth of the wake, the number of grid points in the Y direction were increased to ensure the wake is fully covered. The axial step used was 10 mm which is relatively large, but is justified on the bases that the wake development is very slow in the far wake region. Due to lack of data on all three normal components of Reynolds stress tensor computations were carried out with k-ε model only.

Equations 3.15 and 3.16 were integrated to give the imposed free stream conditions. Level and length scale of the free stream turbulence are presented in Fig. 7.15. The decay of grid generated turbulence is seen to be properly predicted by these equations. They constitute the boundary conditions of the closure equations at the edge of the wake for the free stream turbulence case. For the simple wake, however, these boundary

conditions were set equal to zero.

Figures 7.16 and 7.17 give a few calculated profiles of mean velocity and the development of the cylinder wakes. Figure 7.18 shows a few calculated shear stress profiles for both of the modeling cases. Predicted profiles of the turbulent kinetic energy are shown in Fig. 7.19. It is most interesting to observe that the model does indeed predict increase in mean velocity and faster recovery of the wake due to presence of free stream turbulence. As stated earlier the disturbance in the free stream reduces the shape factor, and the calculation does confirm that.

It was mentioned [25] that introduction of free stream turbulence increases the shear stress in the wake. The present computation seems to confirm it . Figure 7.18 shows that near the core of the wake, the predicted shear stress for both cases are essentially the same, this is because $\overline{uv}$ must change sign at Y=0. However, toward the edge of the wake, the free stream turbulence increases the calculated shear stress. Experimental observations point out that free stream disturbance gives rise to additional level of turbulence in the wake, specifically it increases the kinetic energy. Computed profiles of turbulence energy of the wake for both the situations shown in Fig. 7.19 indeed indicate the rise in the level of K due to free stream disturbance. The kinetic energy budget computed for both cases are given in Fig. 7.20. It is seen that the free stream disturbance increases the advection of energy due to higher mean velocity relative to the simple wake. As expected, the energy balance indicates higher rate of energy loss in the form of dissipation for the free stream case than that of simple wake. The

magnitude of the peak of production term is higher for the simple wake relative to the disturbed free stream case. However, the total energy production -the area under the curve- is greater for free stream turbulence case than the simple case. This is related to the fact that mixing in the wake is spread over much larger distance in transverse direction for disturbed free stream case than the simple wake. The diffusion of energy is essentially the same for both cases except near the centerline of the wake where in the simple wake, it seems to approach zero, and in the disturbed case, it peaks. This is contrary to the expectation of losses of energy in wake due to transport of energy from the central core to outer layer of the wake. This seems to be related to numerical error in computation of gradient of the mean velocity in the core of the wake. Overall the performance of the k-ε model under effect of free stream turbulence seems very positive.

7.4 Prediction of Asymmetric Wake under various levels of Free Stream Turbulence

Asymmetric wake under influence of free stream turbulence studied in the present work were simulated with the Reynolds stress model. There are two different levels and length scales of free stream turbulence generated by the two grids. The development of the wake under these two external stream conditions are predicted, and the results are compared to experimental data obtained earlier. The initial conditions for the computation are obtained from the experimental data at axial station

X=12.7 mm. The boundary conditions imposed on the wake are the simulated turbulence generated by these grids.

Equations 3.15 and 3.16 are integrated to simulate the turbulence generated due to the two different grids. The initial condition used for integration of these equations were the experimental data at X=0. Figures 7.21a and 7.21b present the predicted level and length scale of the turbulence due to these grids along with the experimental data. It can be seen that the decay of turbulence and growth of the dissipative length scale are predicted much closer to experimental data for grid 1 than grid 2. This is related to anisotropy of turbulence generated by grid 2, while this simulation is based upon k-ε model which does not distinguish the anisotropy of the turbulence.

For computation of wake evolution under the free stream turbulence, 96 non-equally distant nodes were chosen along the Y-axis to cover both sides of the wake. Experimental data at X=12.7 mm were interpolated according to the grid geometry along Y-axis. The dissipation rate of turbulence kinetic energy was estimated form the experimental data. The values of streamline function at these nodes were calculated, and the governing equations were numerically integrated along these streamlines in (X,Ψ) space as explained earlier. The steps in axial direction varied from half local momentum thickness to about one local momentum thickness. The boundary conditions were obtained by numerically integrating Eqns. 3.25 (a,b,c) and (3.26). The integration of these equations also started at X=12.7 mm, and the initial conditions were the experimental free stream

turbulence data at X=12.7mm. The outcome of integration of Eqns. 3.25 and 3.26 were used as a boundary condition for the transport equations of normal stresses and dissipation rate in the RS closure model. These boundary conditions are set at the edge of the wake.

Figure 7.22 presents mean velocity profile U/U_e, at two axial stations. Figure 7.22a presents the results for the lower level of free stream turbulence conditions, while Fig. 7.22b presents the outcome of computation for the higher level of free stream turbulence conditions. It can be seen from these graphs that the mean velocity predicted is closer to experimental data for the lower free stream turbulence level, and the predicted mean velocity becomes less accurate with higher free stream turbulence level. However, the maximum average deviation from the experimental data is about 2% which is still quite reasonable considering the added complexity due to the additional free stream disturbance.

Figure 7.23 presents the predicted uvbar at two axial stations under the different free stream turbulence conditions. It can be seen that higher level and larger dissipative length scale of free stream turbulence result in wider gap between the experimental and predicted uvbar. It is noteworthy to observe that computed uvbar on the smooth-wall side of the wake (negative Y) is overpredicted under lower free stream turbulence level, while it is underpredicted on the same side with higher free stream turbulence level. However, uvbar on the rough-wall side of wake (positive Y) is overpredicted under all free stream conditions. These results indicate that the RS model does not properly account for higher transport of high

momentum fluid by normal stresses and the production of shear stress due to mean velocity gradient. It was seen that the mean velocity was predicted less accurately under higher free stream conditions, and this attributes to the inaccuracy of $\overline{uv}$.

The $\overline{u^2}$ and $\overline{v^2}$ components of Reynolds stress tensor as predicted by the computation, along with experimental data are presented in Figs. 7.25 and 7.26. u2bar is seen to be predicted less accurately under higher free stream turbulence level than the lower free stream turbulence level. Specifically, the decay of the u2bar peak on the smooth-wall side of the wake seems to be much higher than the measured data under higher free stream turbulence level. This discrepancy in this peak is related to the uncertainty in the dissipation rate used as initial condition. ε was estimated from the experimental data at the initial axial station. It is apparent that the estimated dissipation rate does not reflect the actual value of dissipation rate. The initial dissipation rate was lowered by 12% to see its effect on the Reynolds stress tensor. The computed values of the Reynold stress tensor were much more inaccurate than the experimental data relative to present computation. Therefore, the initial dissipation rate was used for computation.

Overall the mean velocity and the Reynold stress tensor are predicted relatively accurately in presence of free stream turbulence. The inaccuracy is attributed to the uncertainty in the dissipation rate. This is reflected in the computed uvbar, u2bar and v2bar under higher free stream turbulence conditions.

Model	Empirical Constants Used					
K-ε	C_μ	σ_k	σ_ε	$C_{\varepsilon 1}$	$C_{\varepsilon 2}$	
	0.09	1.0	1.3	1.4	1.9	
RS	C_s	$C_{\phi 1}$	$C_{\phi 2}$	C_ε	$C_{\varepsilon 1}$	$C_{\varepsilon 2}$
	0.25	2.5	0.4	0.15	1.45	1.9

Table 7.1 Numerical Values of Empirical Constants Employed in Turbulence Closure Models

CASE	C_s	$C_{\phi 1}$	$C_{\phi 2}$	C_ε	$C_{\varepsilon 1}$	$C_{\varepsilon 2}$
1	0.25	2.5	0.4	0.15	1.45	1.9
2	0.25	3.0	0.4	0.15	1.45	1.9
3	0.25	2.0	0.4	0.15	1.45	1.9
4	0.25	2.5	0.3	0.15	1.45	1.9
5	0.25	2.5	0.5	0.15	1.45	1.9
6	0.25	3.0	0.5	0.15	1.45	1.9
7	0.25	2.0	0.3	0.15	1.45	1.9
8	0.25	1.5	0.2	0.15	1.45	1.9

Table 7.2 Variation of Constants in Reynolds Stress Model

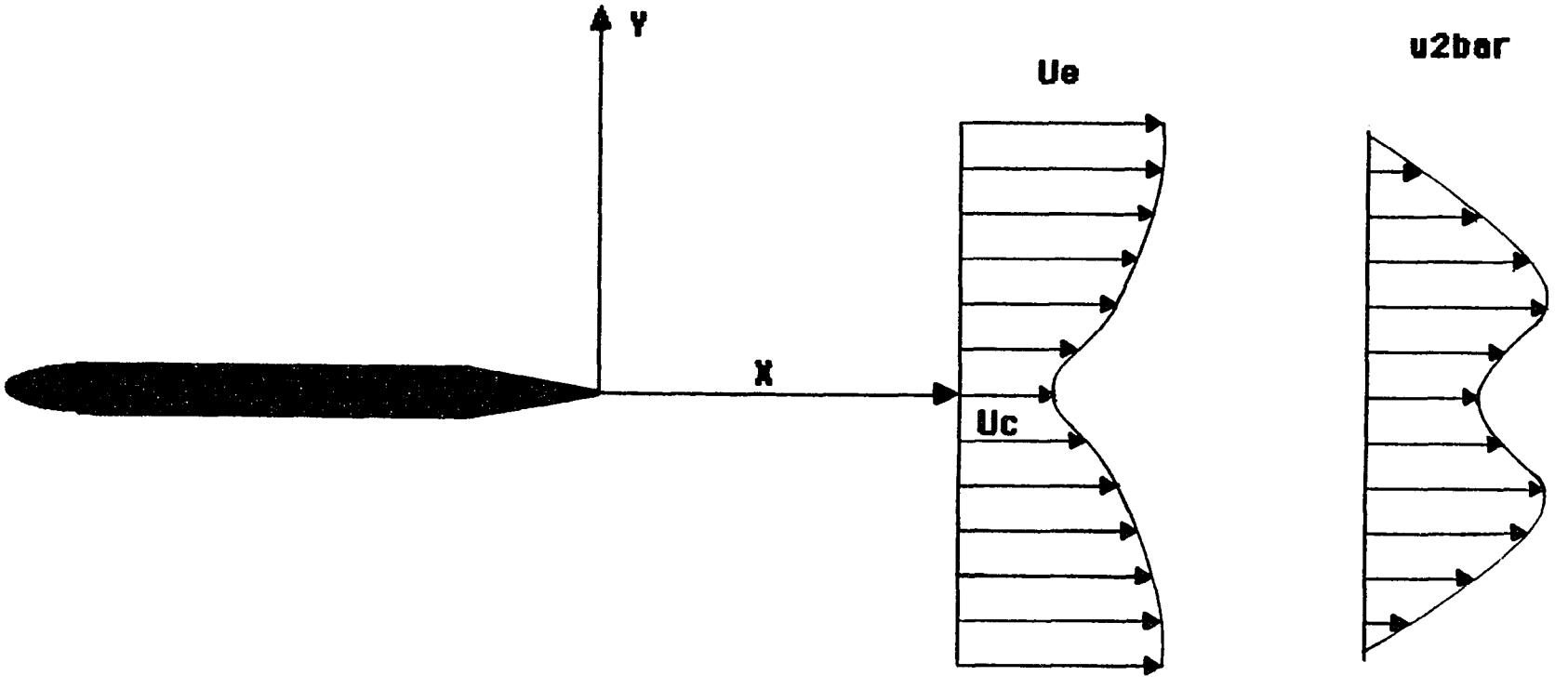

Fig. 7.1 Schematic of Symmetric and Asymmetric Wakes

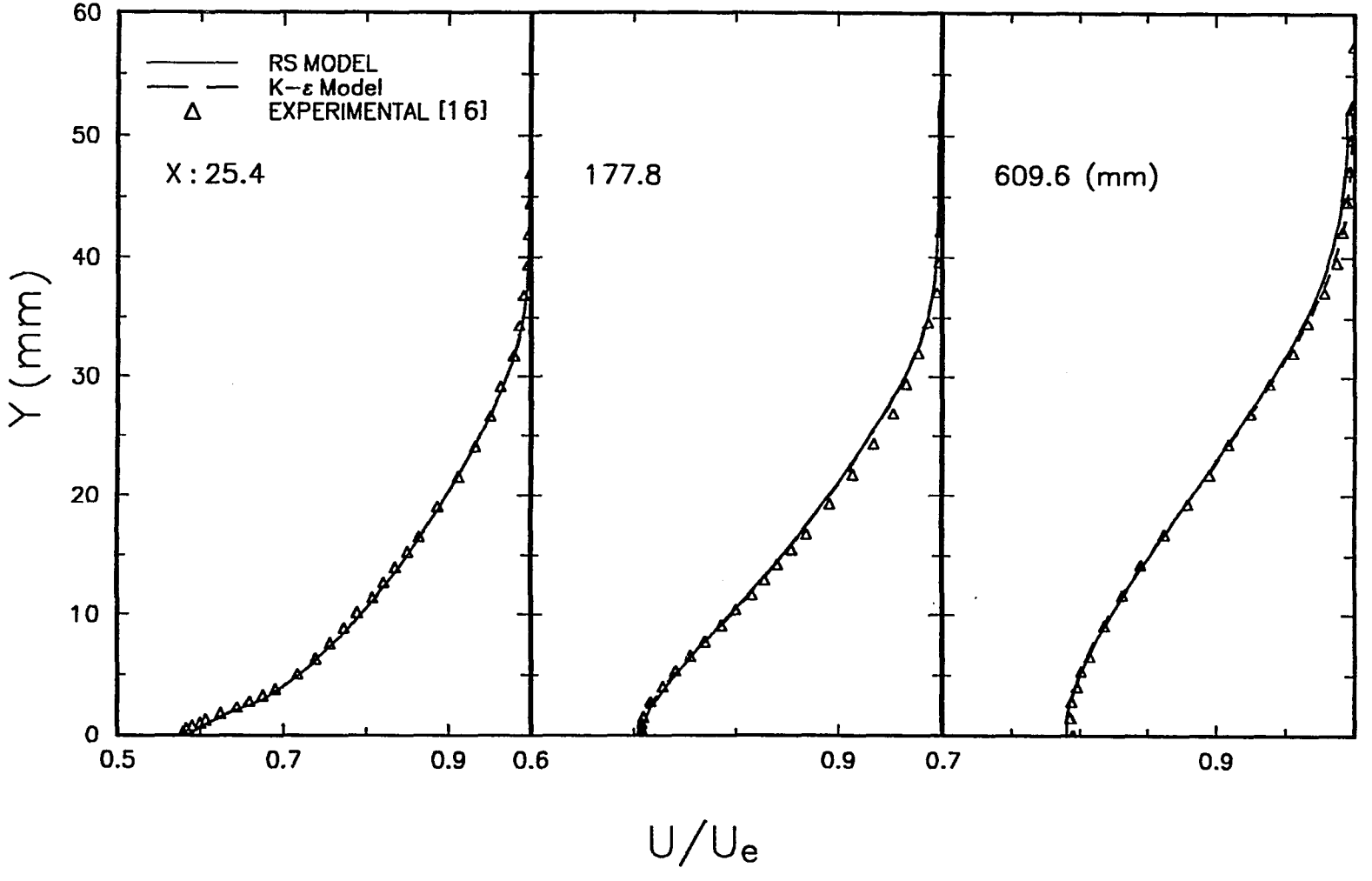

Fig. 7.2 Mean Velocity, Prediction of Symmetric Wake

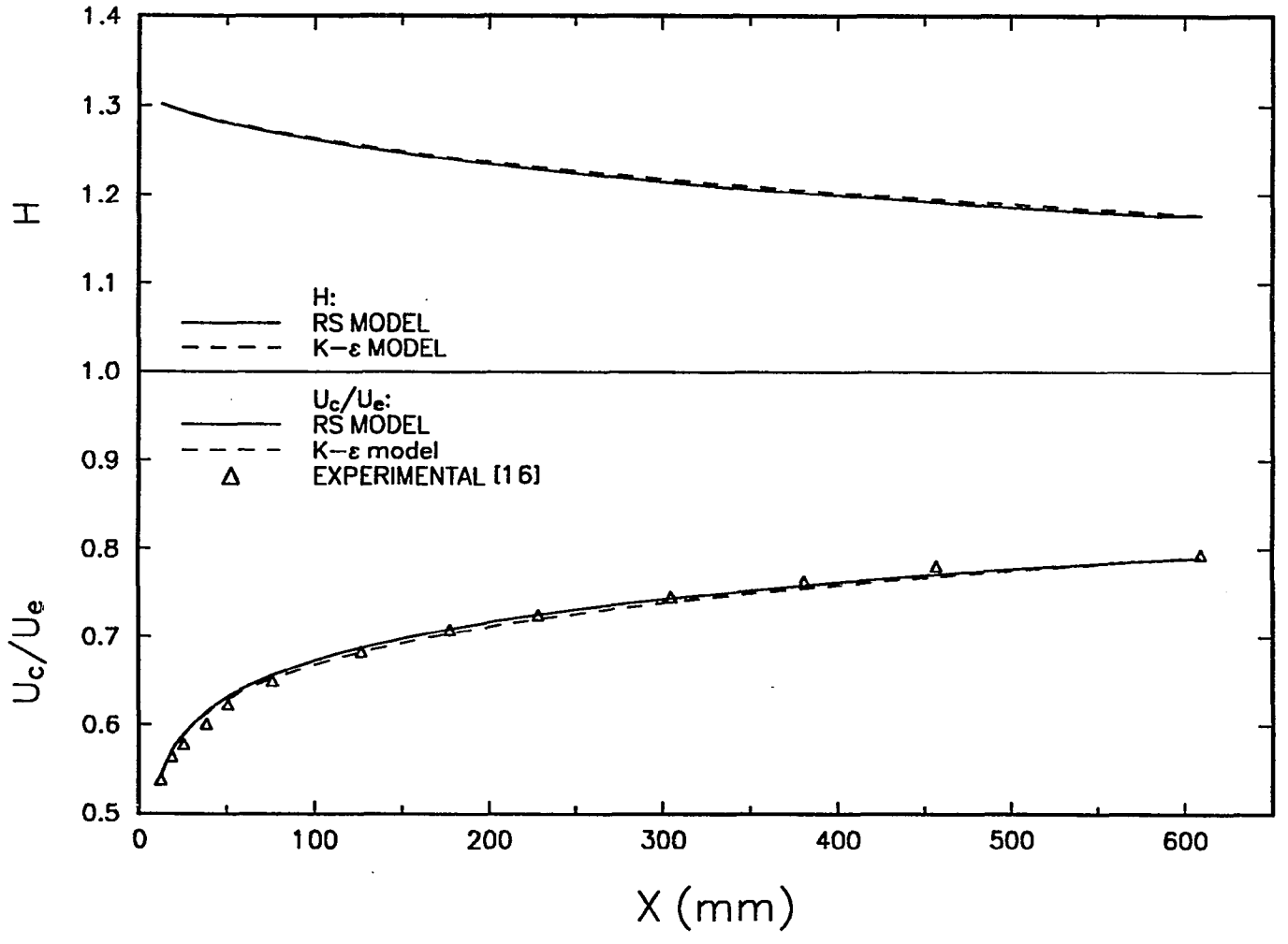

Fig. 7.3 Development of Shape Factor and Centerline Velocity, Prediction of Symmetric Wake

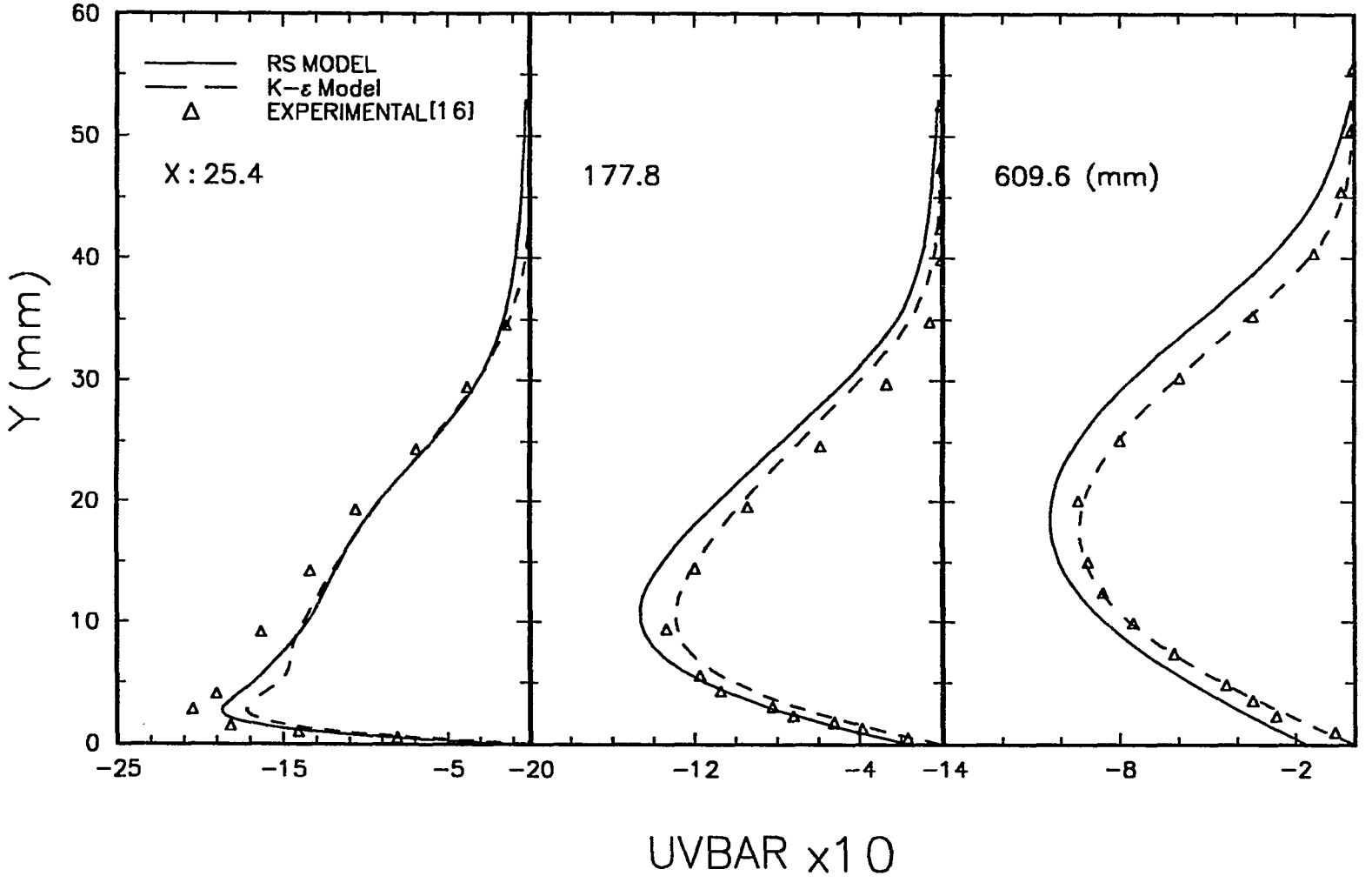

Fig. 7.4 Shear Stress Profile, Prediction of Symmetric Wake

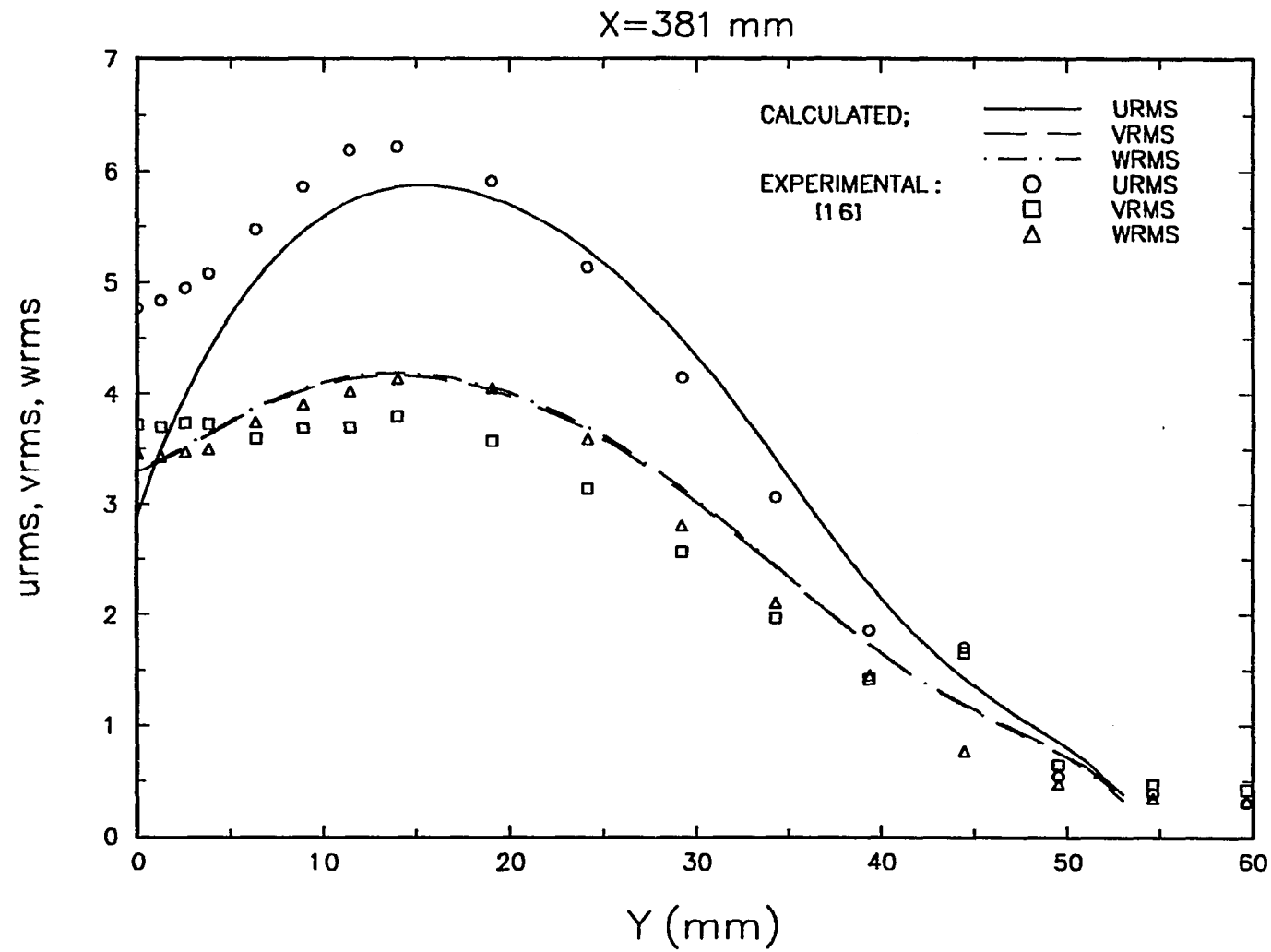

Fig. 7.5 Normal Stresses Profile, Prediction of Symmetric Wake

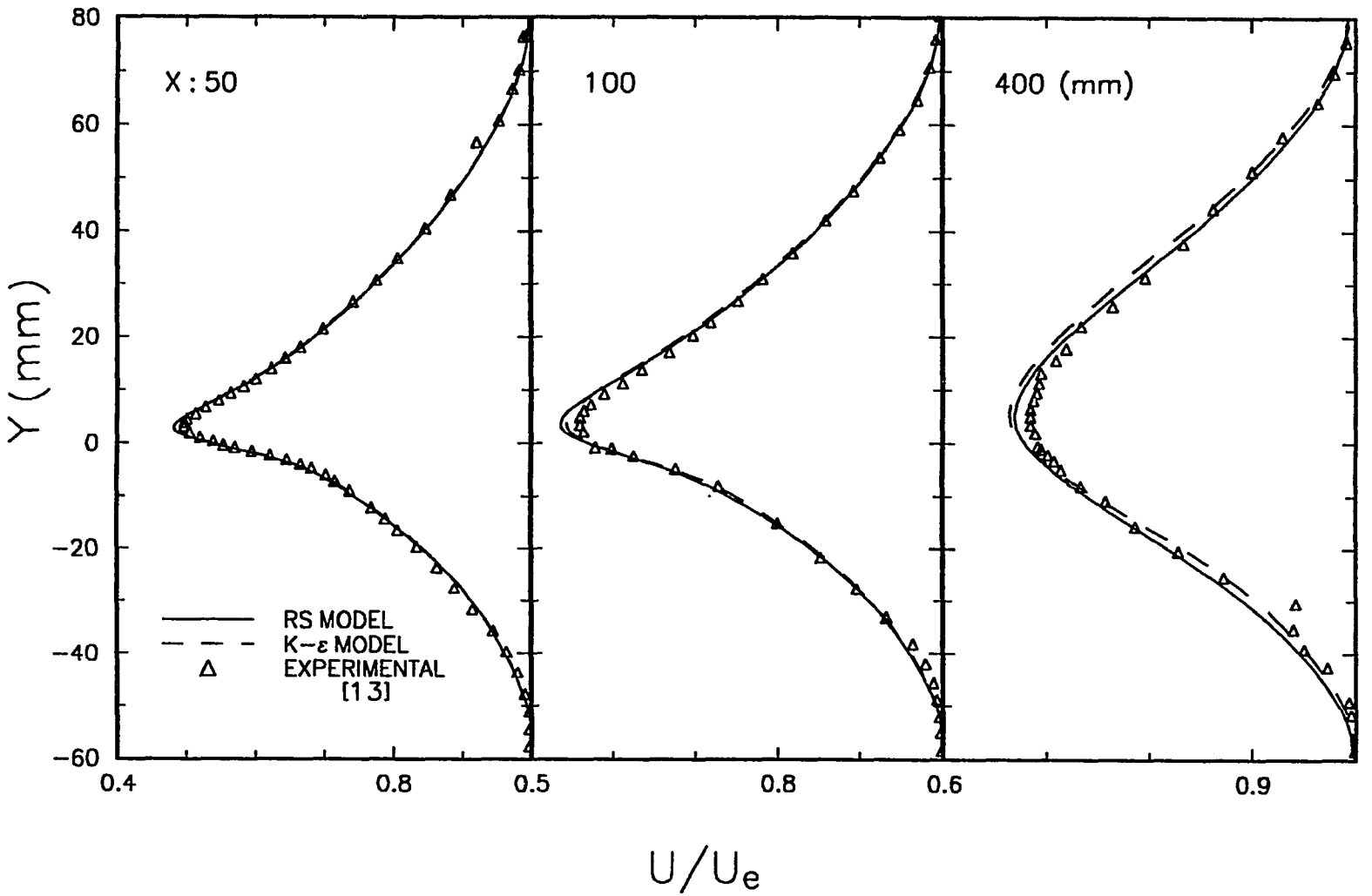

Fig. 7.6 Mean Velocity Profile, Prediction of Asymmetric Wake

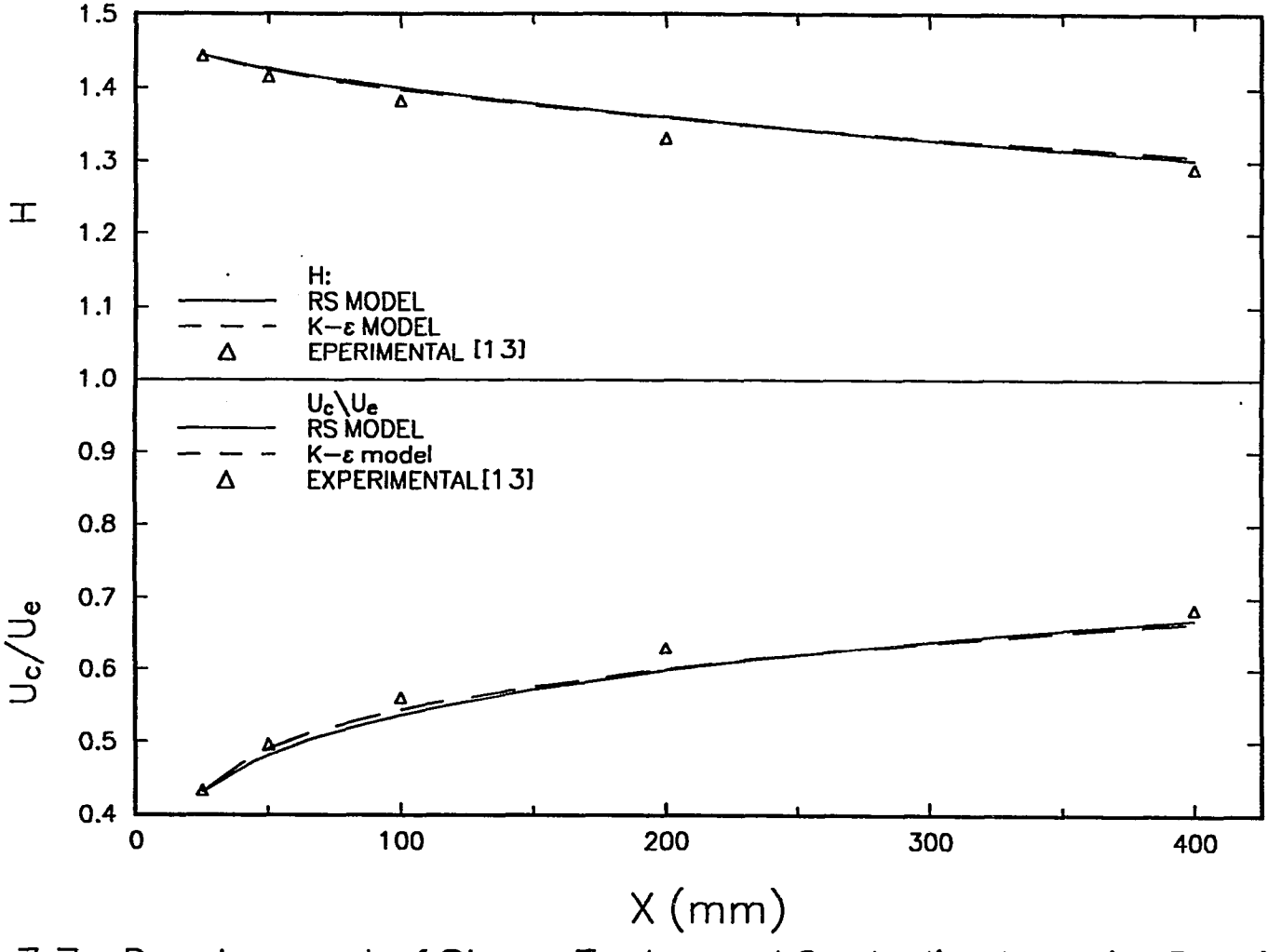

Fig. 7.7 Development of Shape Factor and Centerline Velocity, Prediction of Asymmetric Wake

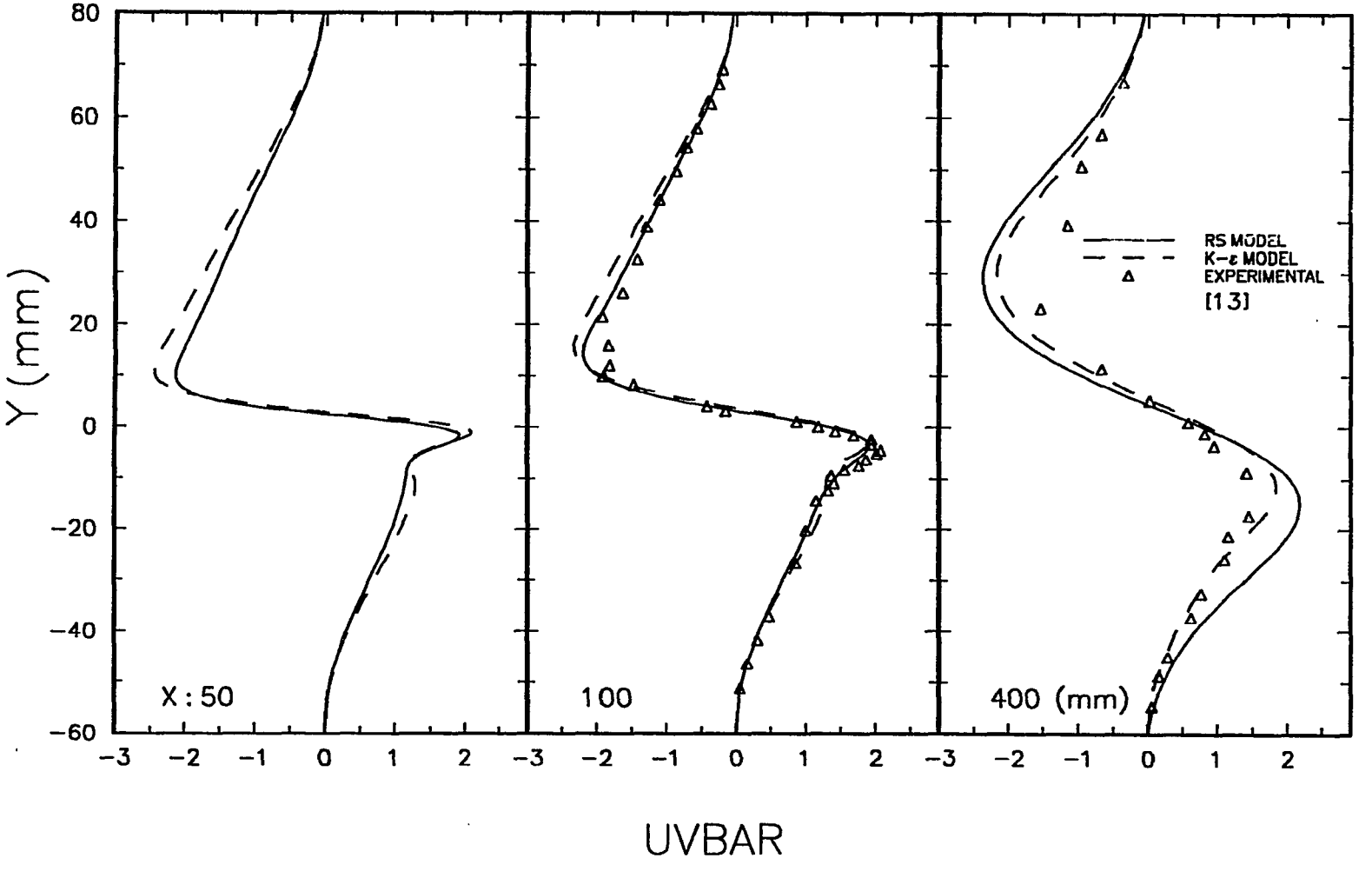

Fig. 7.8 Shear Stress Profile, Prediction of Asymmetric Wake

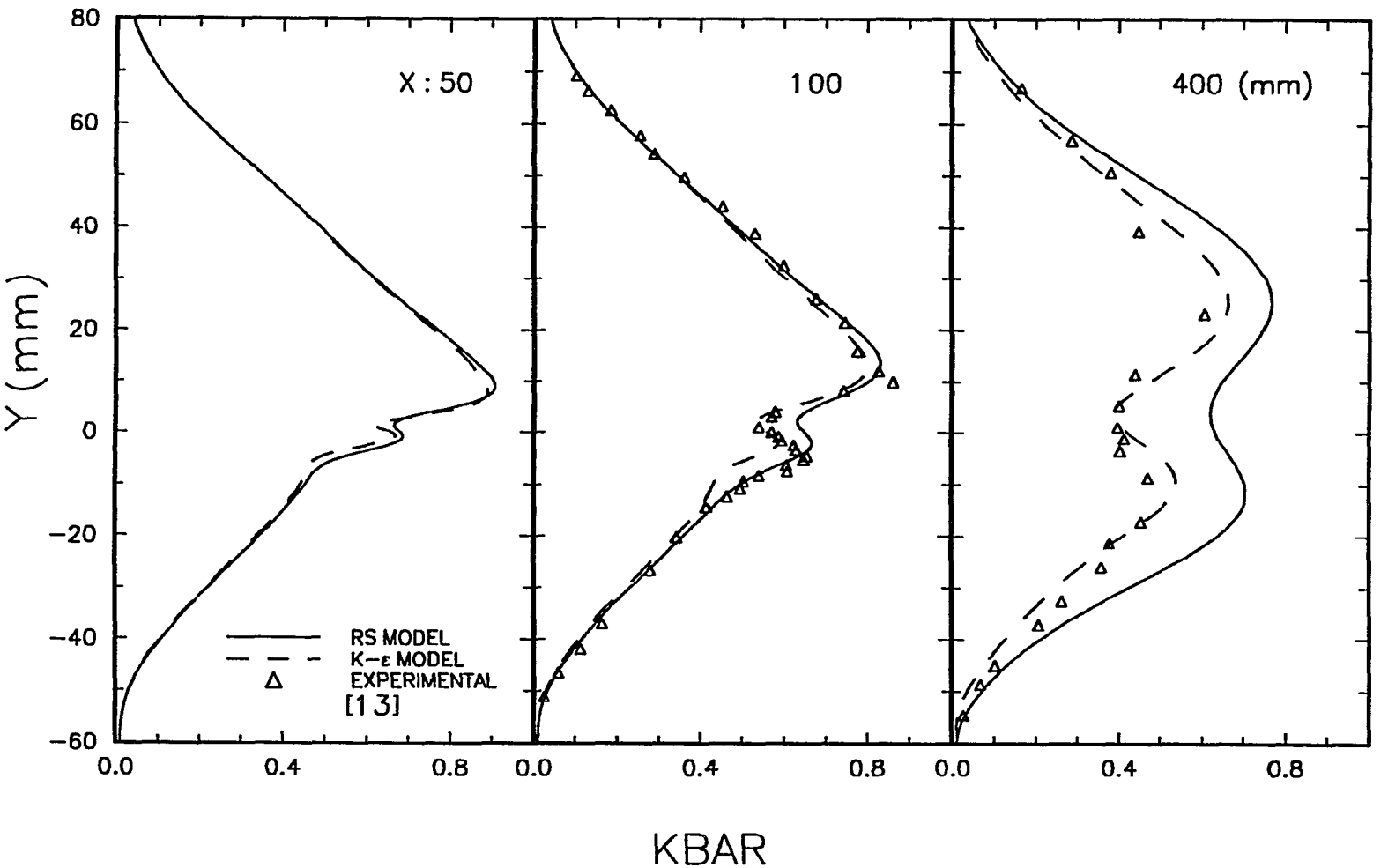

Fig. 7.9 Turbulence Kinetic Energy Profile, Prediction of Asymmetric Wake

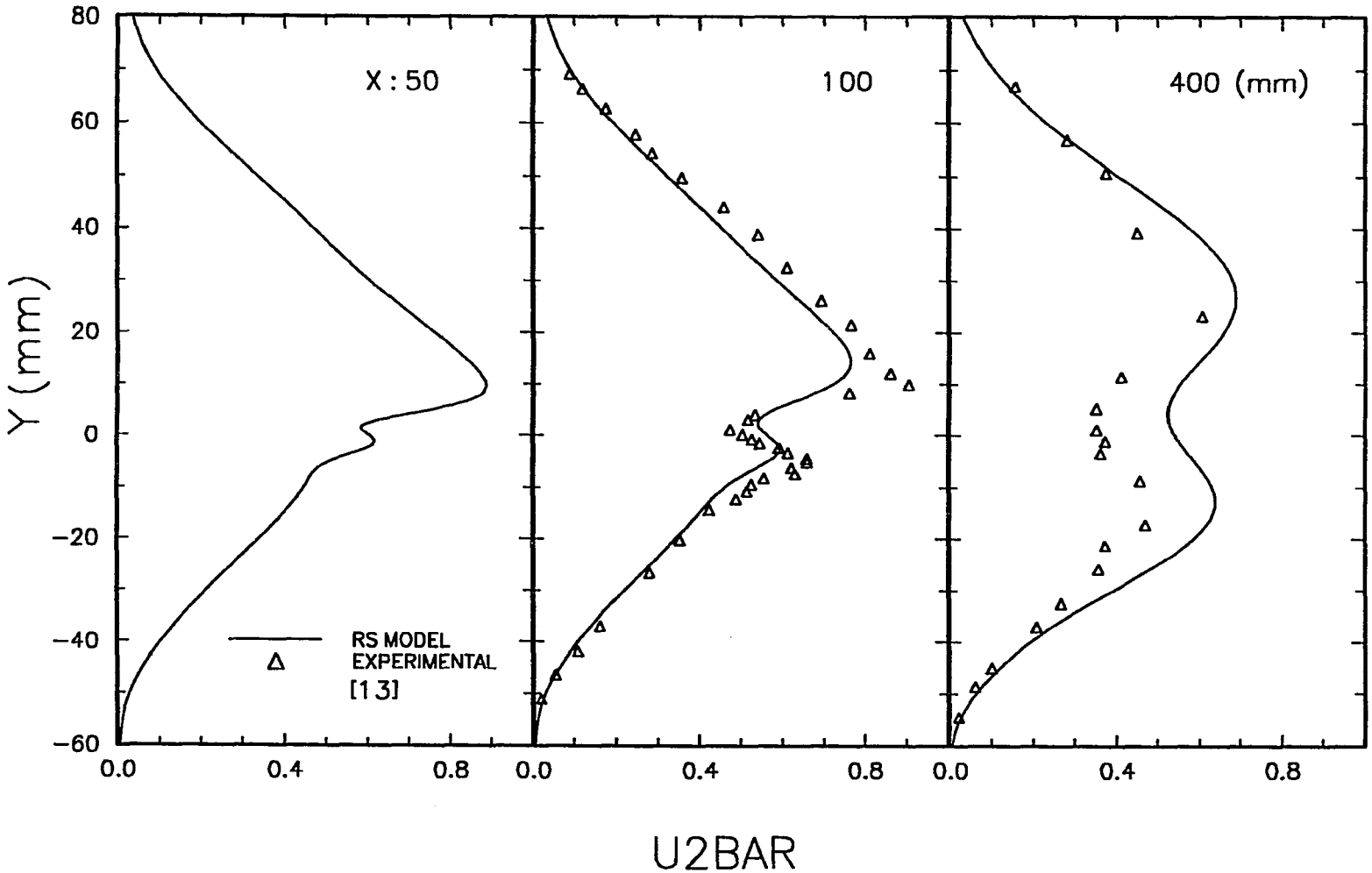

Fig. 7.10 Normal Stress Profile, Prediction of Asymmetric Wake

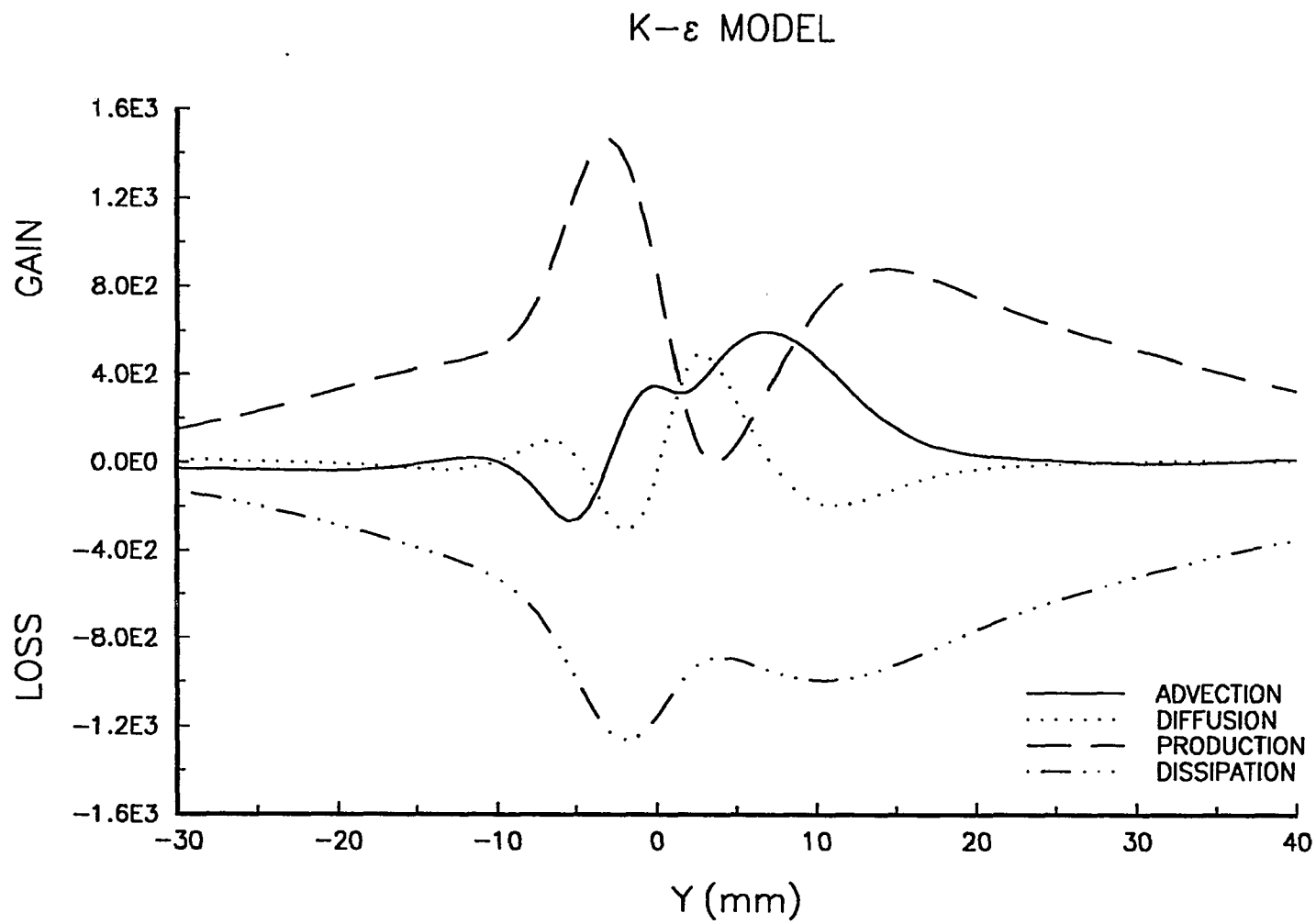

Fig. 7.11a Turbulence Kinetic Energy Budget at X=100 mm, Prediction of Asymmetric Wake, K−ε Model

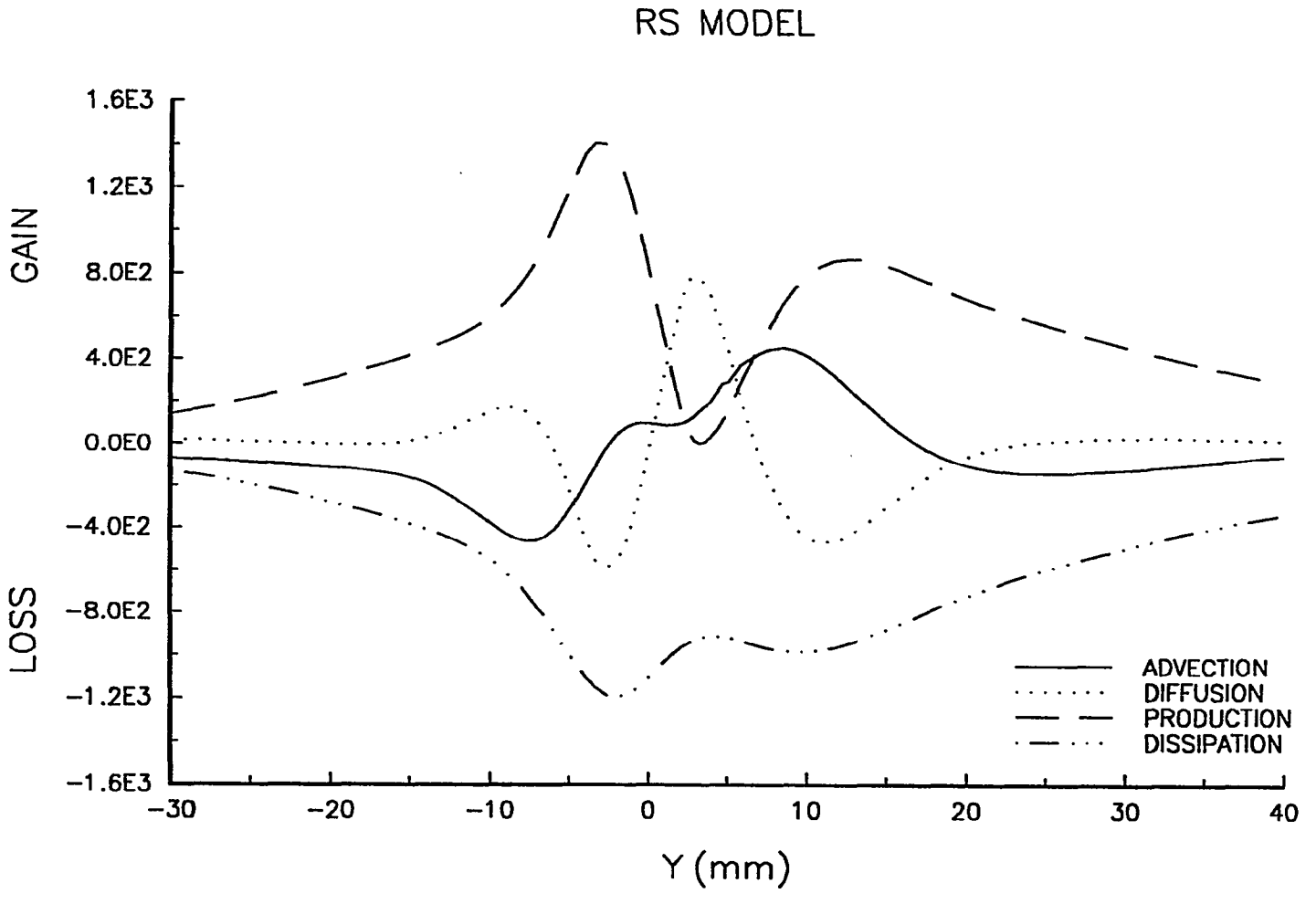

Fig. 7.11b Turbulence Kinetic Energy Budget at X=100 mm, Prediction of Asymmetric Wake, RS Model

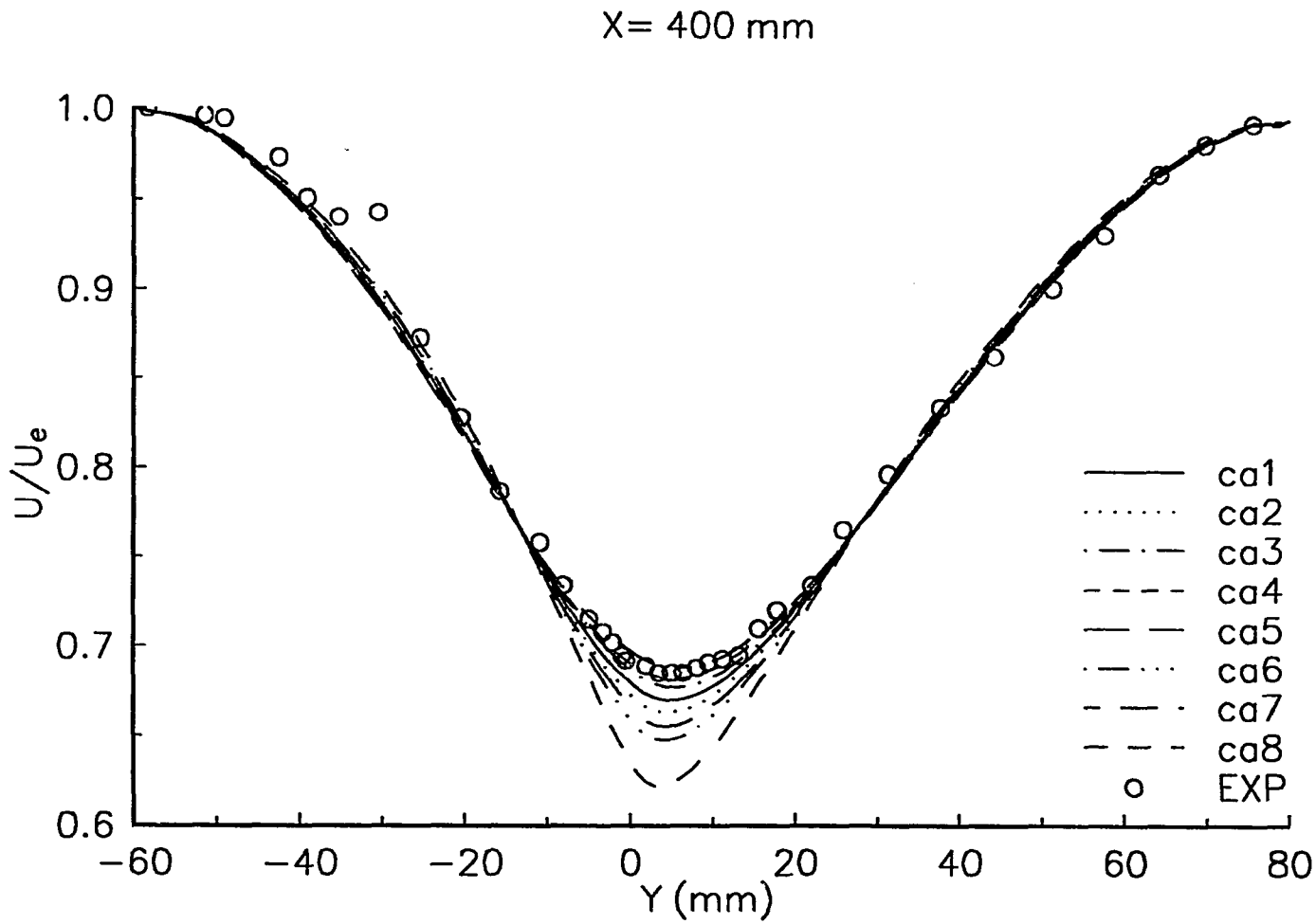

Fig. 7.12a Distribution of U/U_e due to Variation of Empirical Constants in RS Model, Asymm. Wake of Andreopoulos et al. [13]

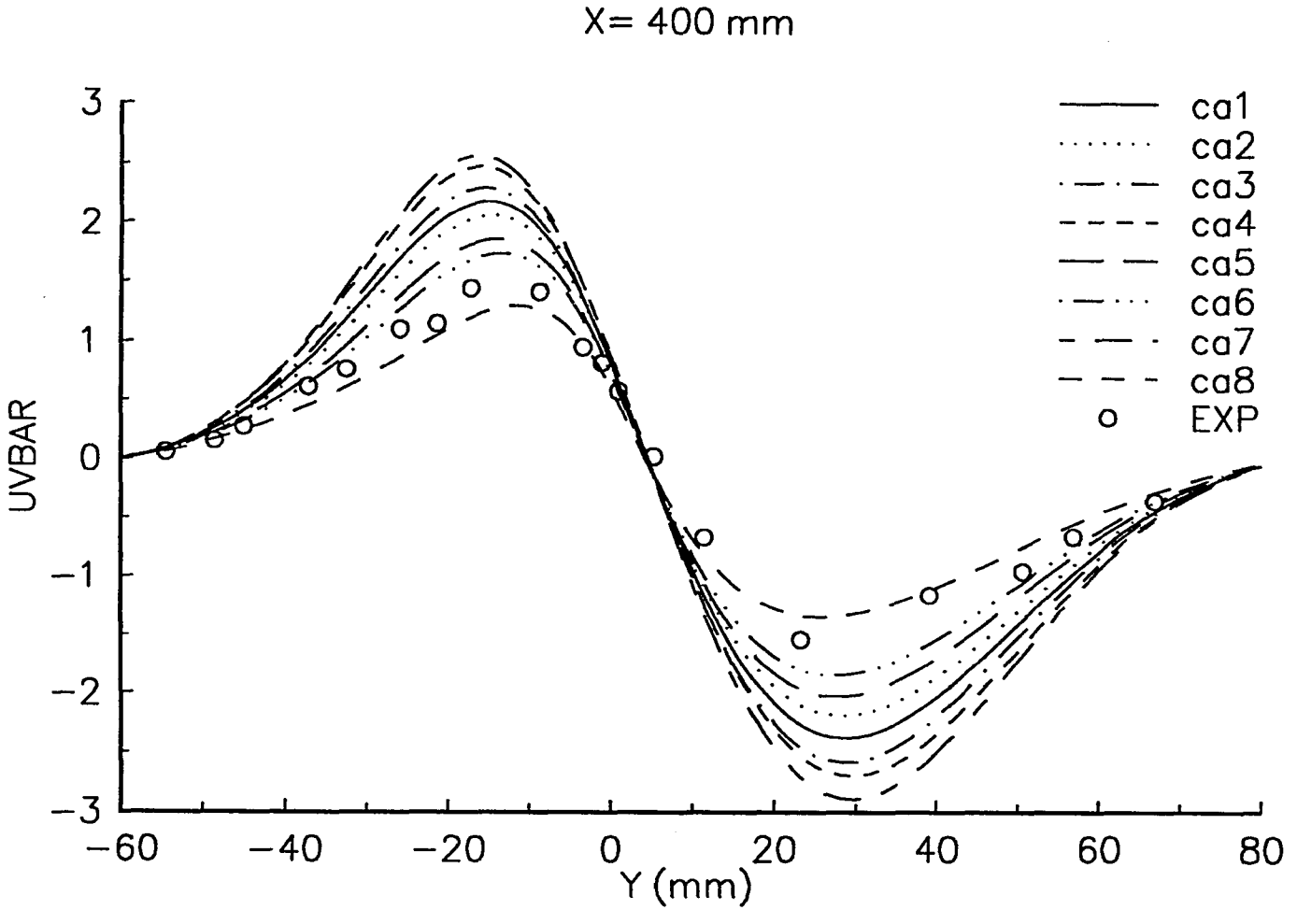

Fig. 7.12b Distribution of $(\overline{uv}/U_\infty{}^2)*10^3$ due to Variation of Empirical Constants in RS Model, Asymm. Wake of Andreopoulos et al. [13]

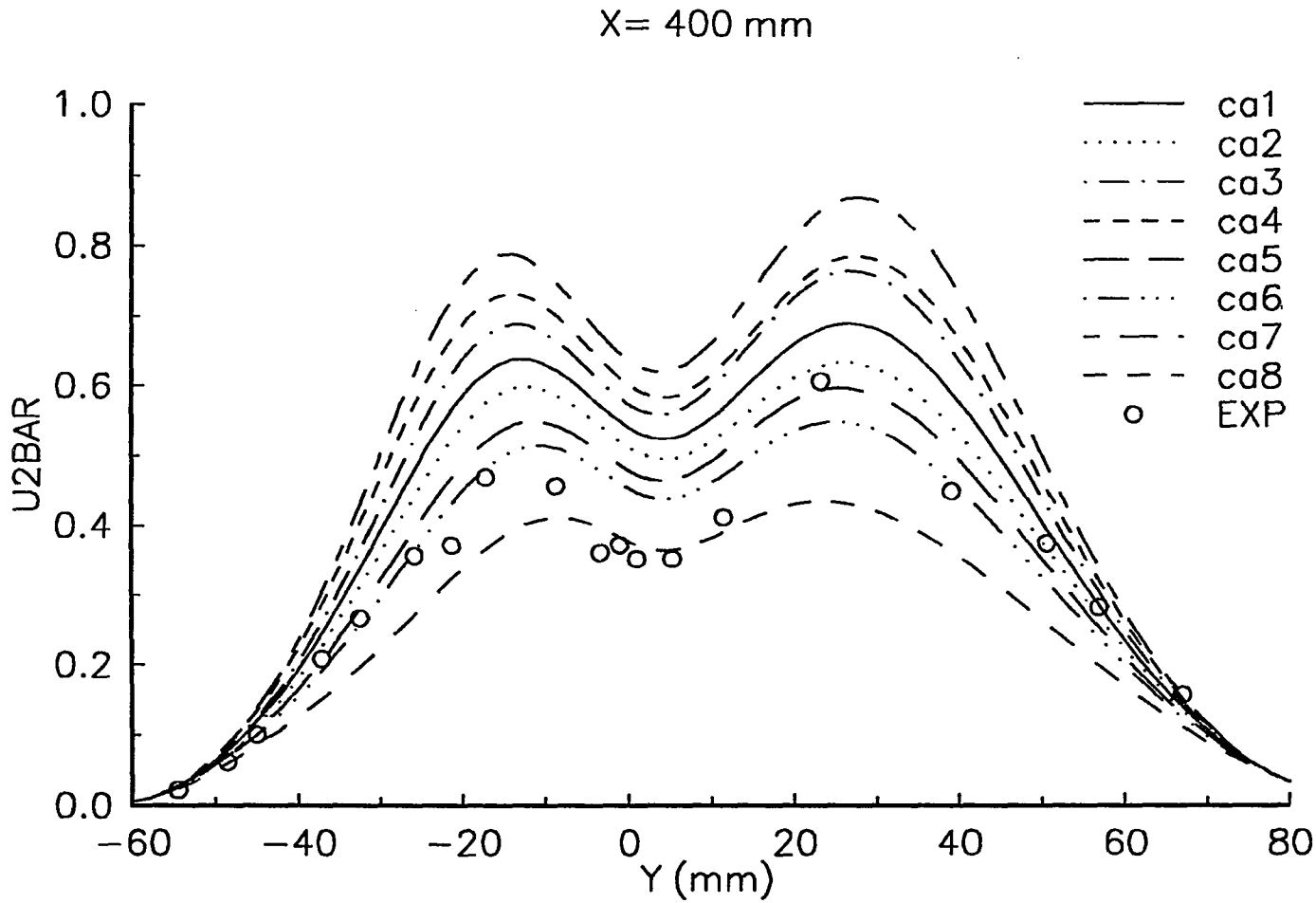

Fig. 7.12c Distribution of $(\overline{u^2}/U_\infty{}^2)*10^2$ due to Variation of Empirical Constants in RS Model, Asymm. Wake of Andreopoulos et al.[13]

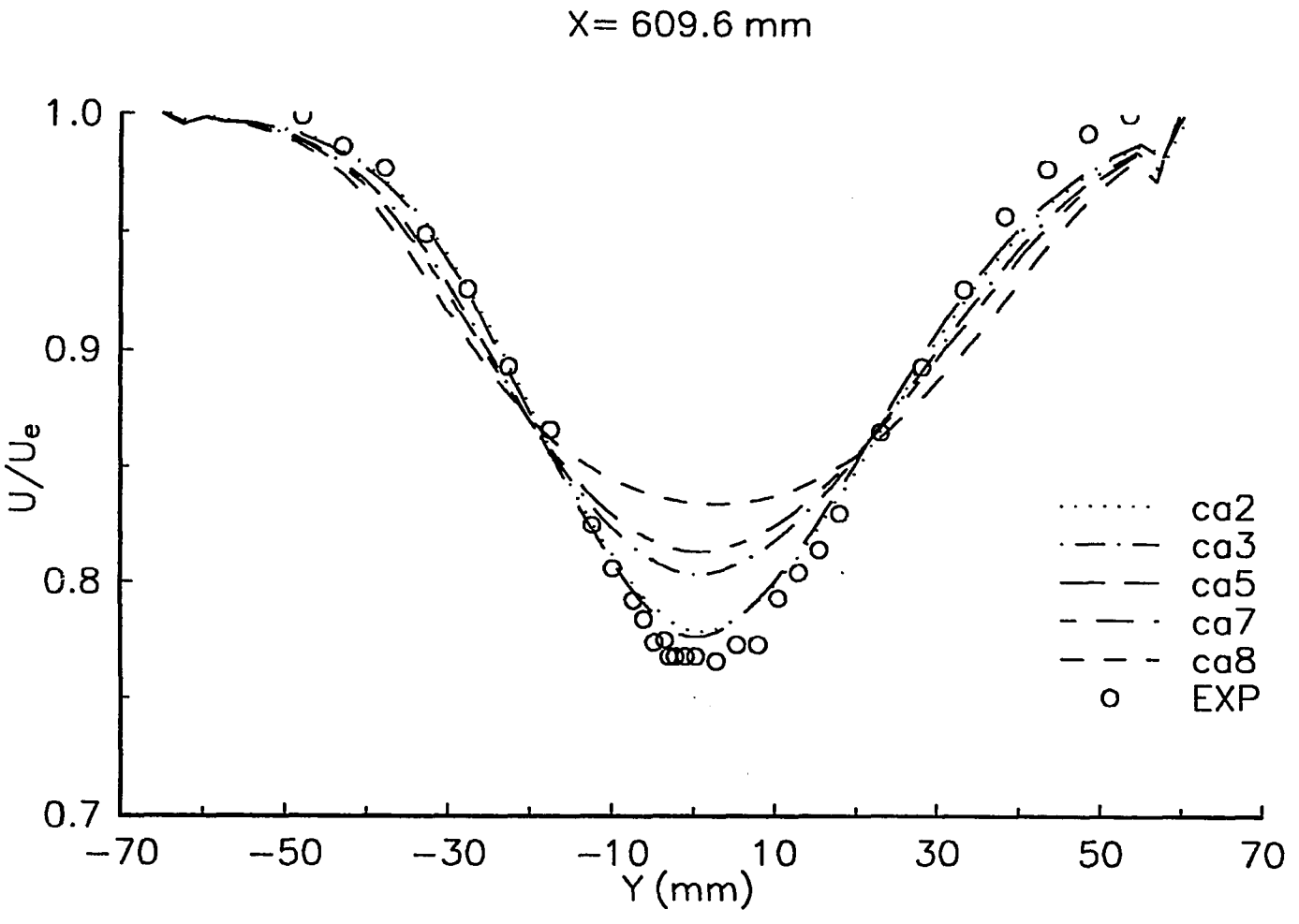

Fig. 7.13a Distribution of U/U_e due to Variation of Empirical Constants in RS Model, Asymmetric Wake of Sastry [16]

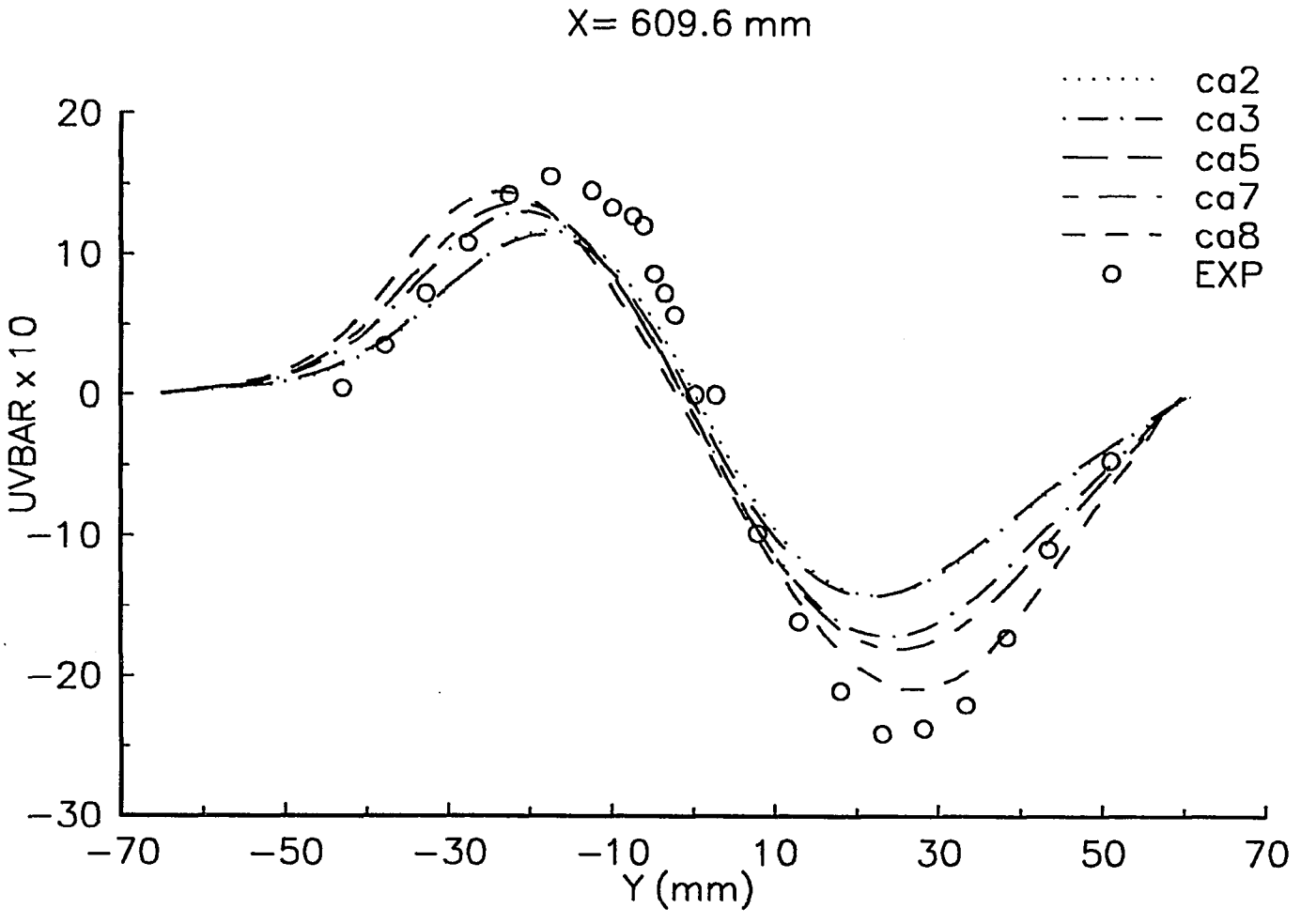

Fig. 7.13b Distribution of $(\overline{uv}/U_\infty{}^2)*10^4$ due to Variation of Empirical Constants in RS Model, Asymmetric Wake of Sastry [16]

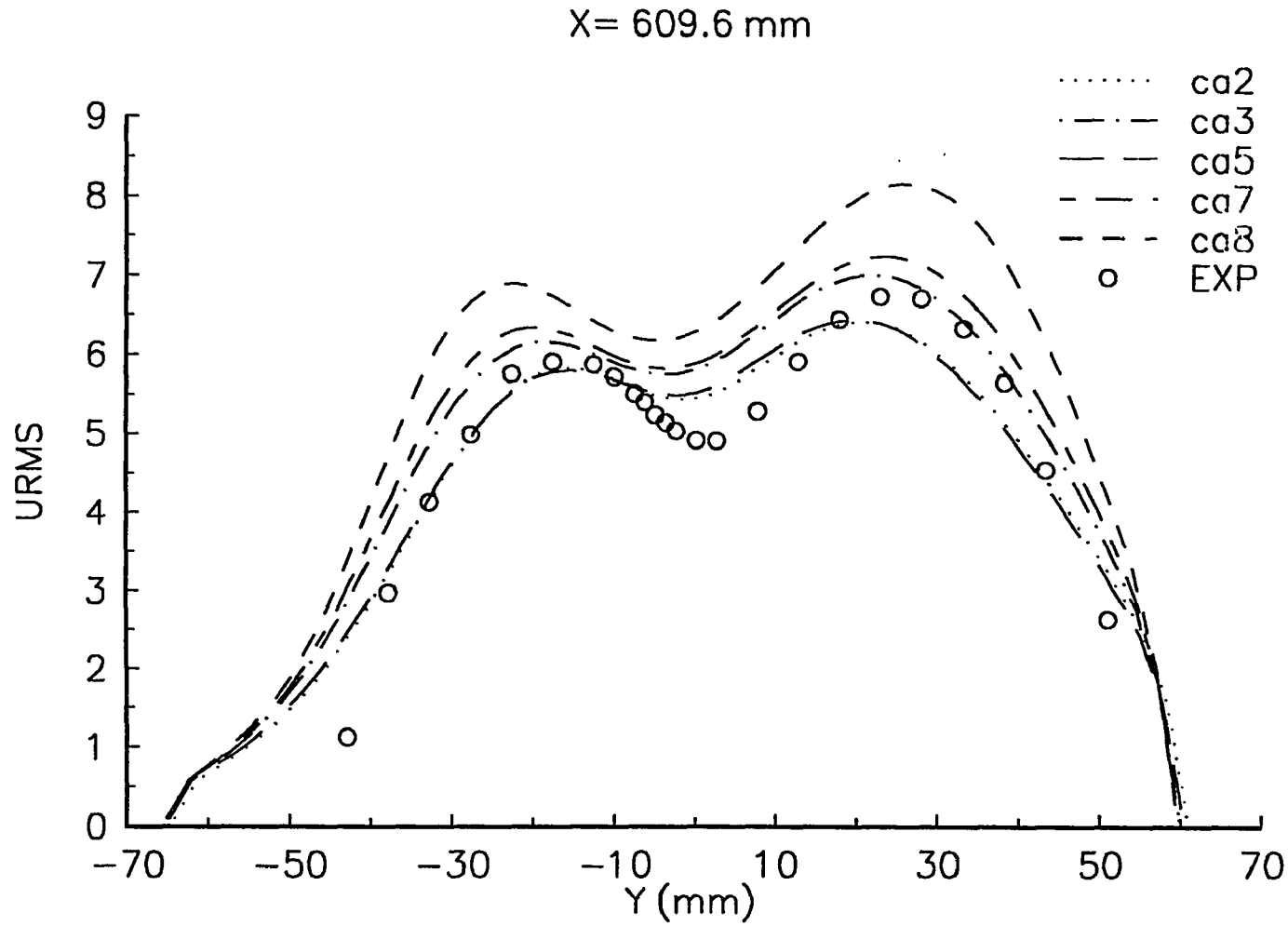

Fig. 7.13c Distribution of $(\sqrt{u^2}/U_\infty)*10^2$ due to Variation of Empirical Constants in RS Model, Asymmetric Wake of Sastry [16]

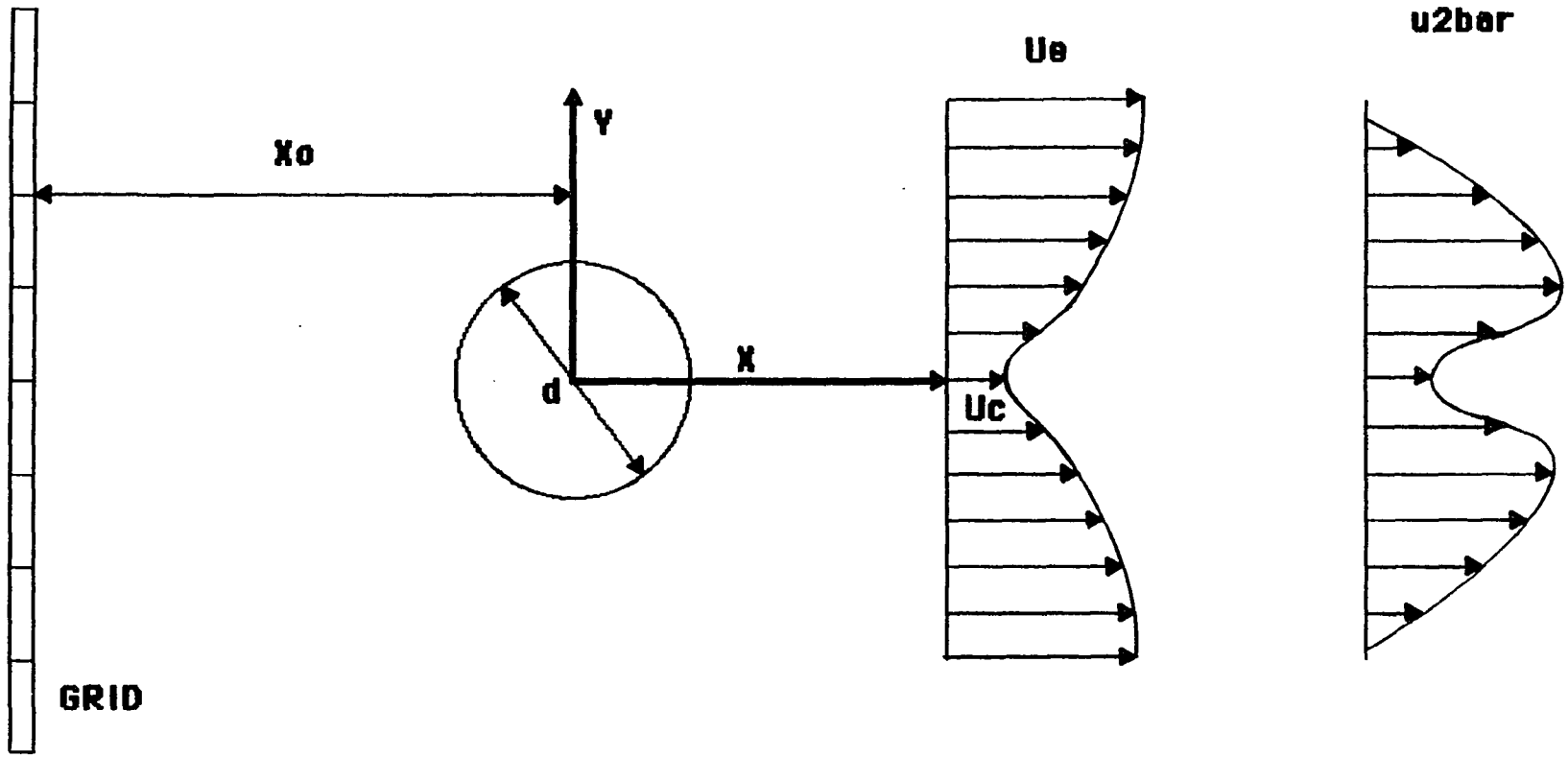

Fig. 7.14 Schematic of Cylinder Wake With and Without Free Stream Turbulence

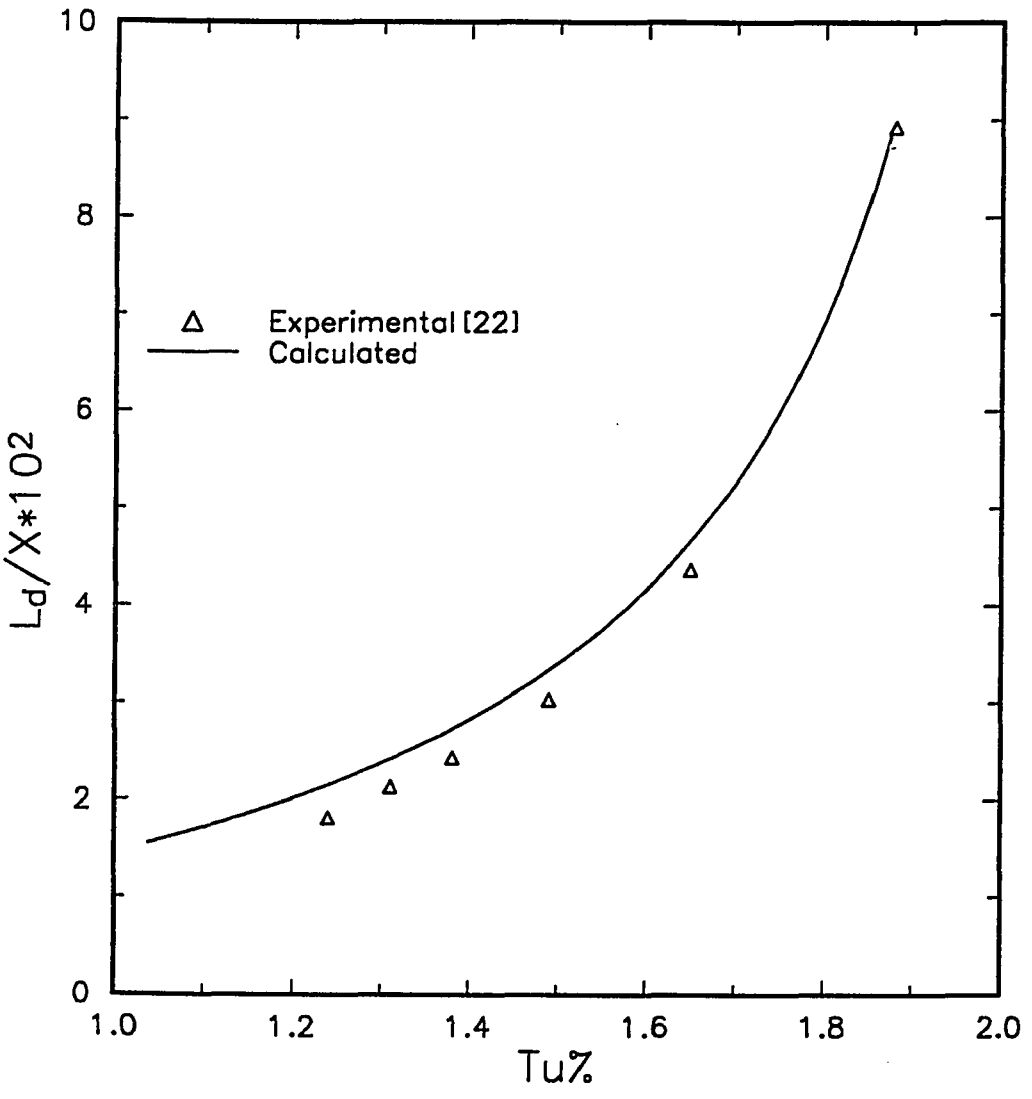

Fig. 7.15 Level and Length Scale of Free Stream Turbulence Imposed on Cylinder Wake

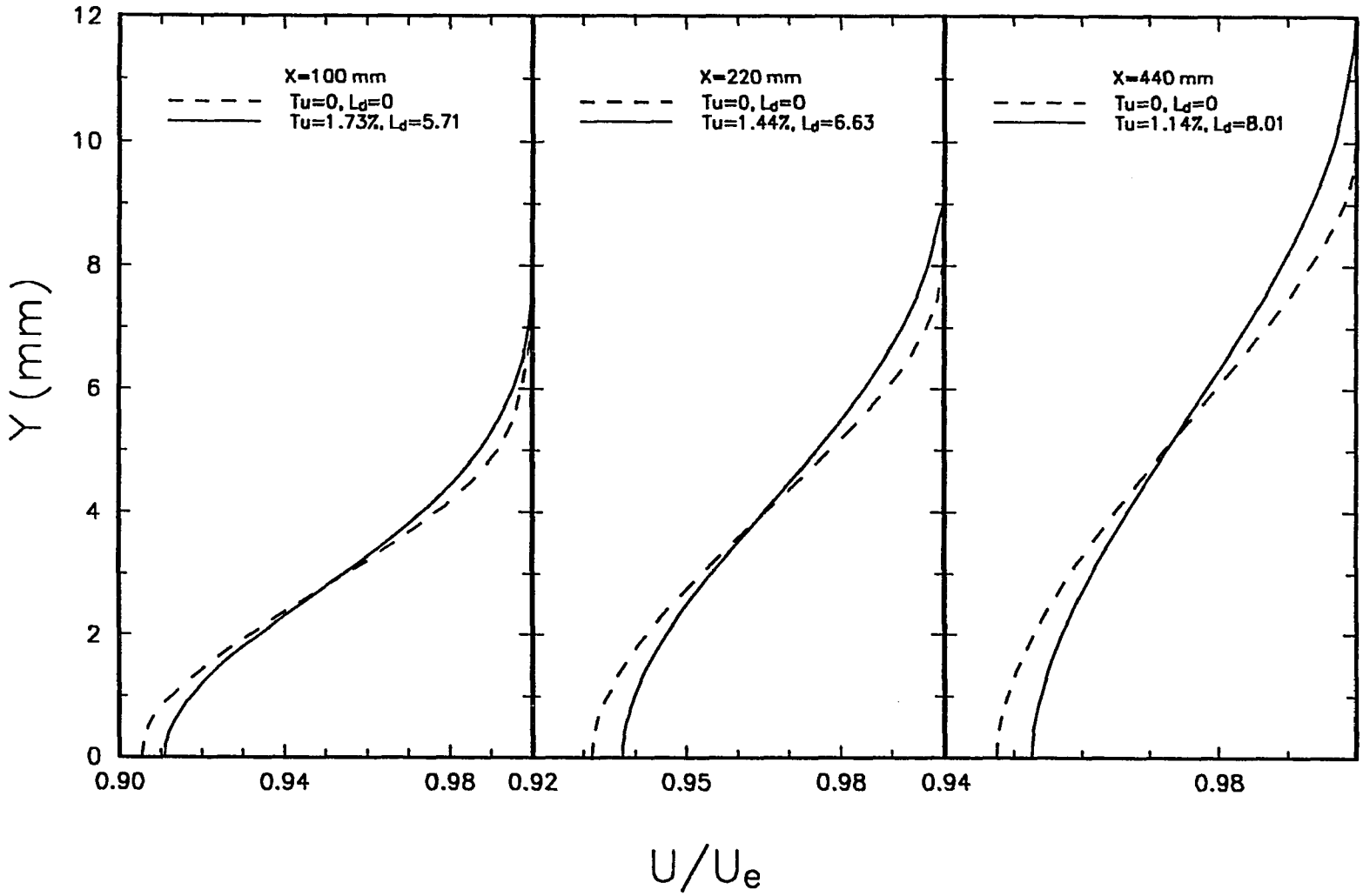

Fig. 7.16 Mean Velocity Profile, Prediction of Cylinder Wake by K−ε Model

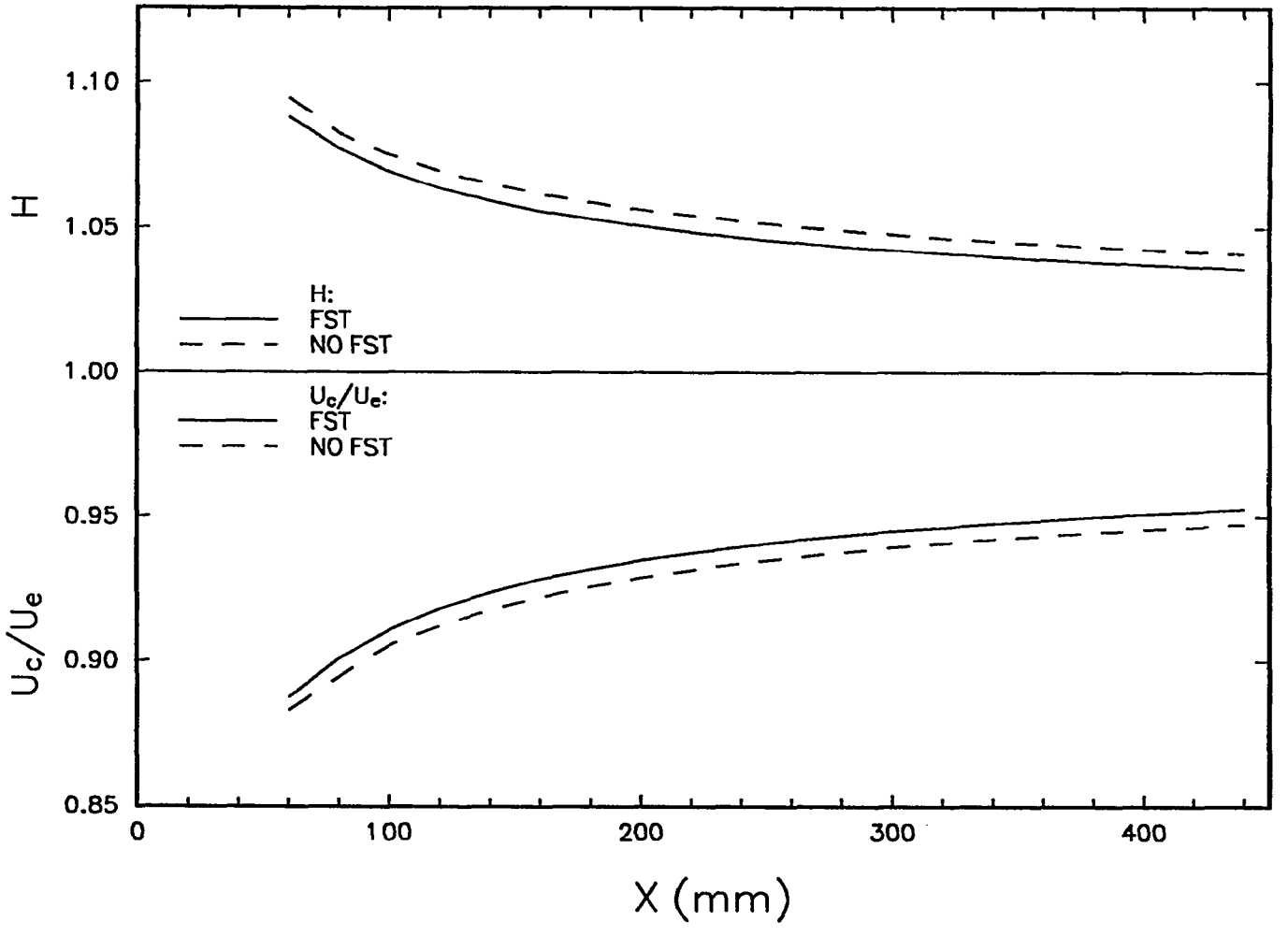

Fig. 7.17 Development of Shape Factor and Centerline Velocity, Prediction of Cylinder Wake by K−ε Model

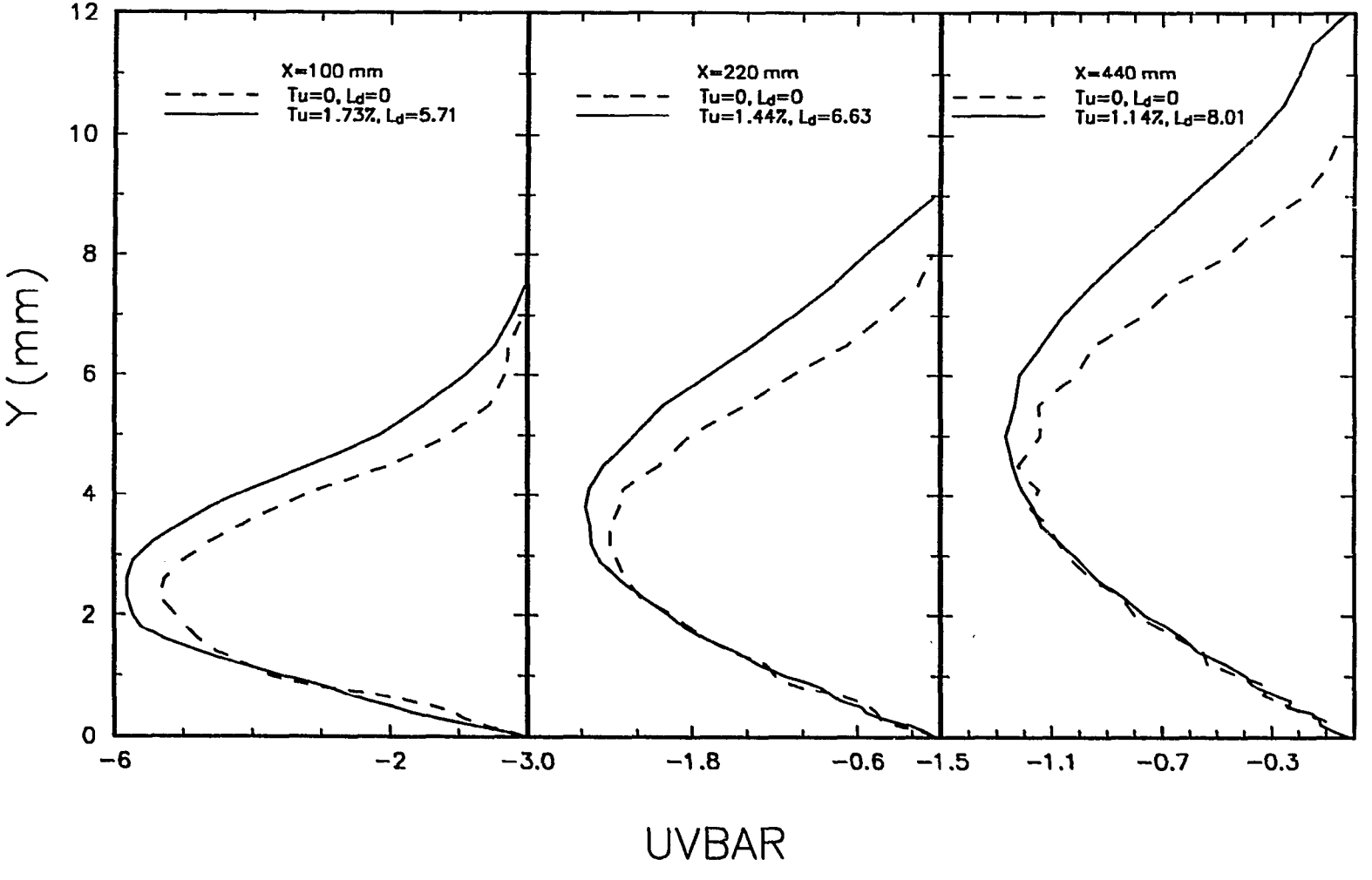

Fig. 7.18 Shear Stress Profile, Prediction of Cylinder Wake by K−ε Model

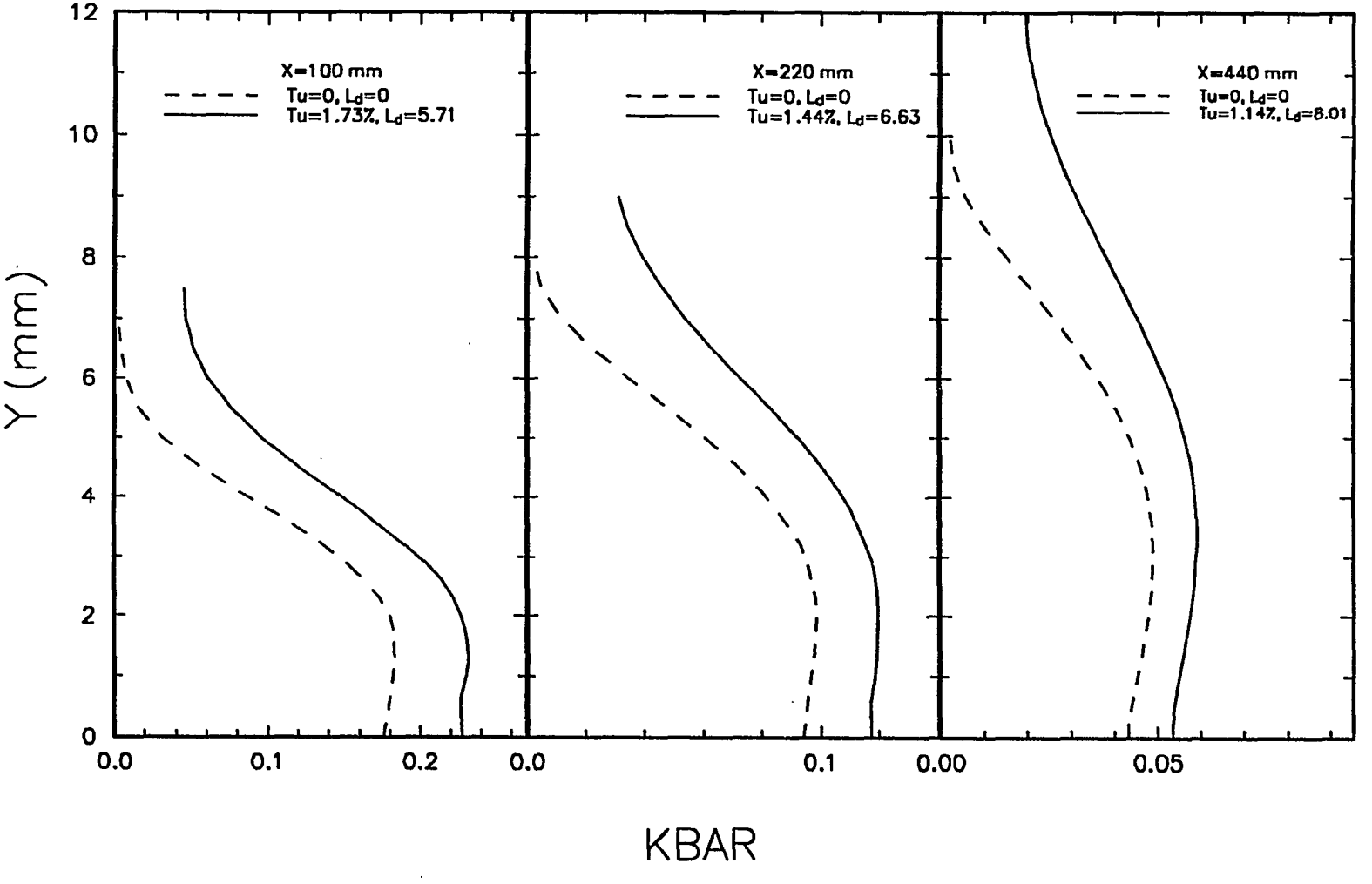

Fig. 7.19 Turbulence Kinetic Energy Profile, Prediction of Cylinder Wake by K−ε Model

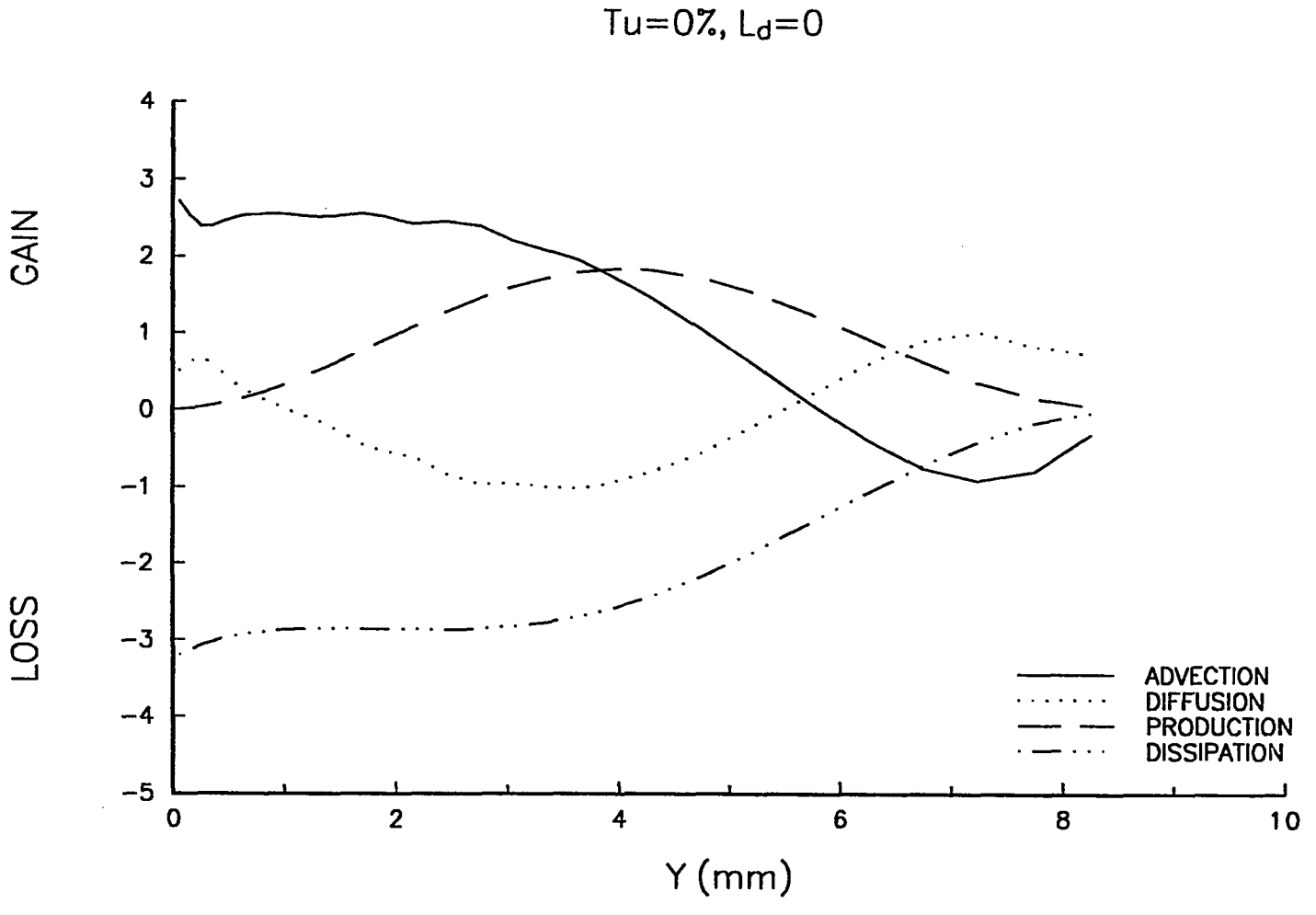

Fig. 7.20a Turbulence Kinetic Energy Budget at X=290 mm, Prediction of Cylinder Wake by K−ε Model

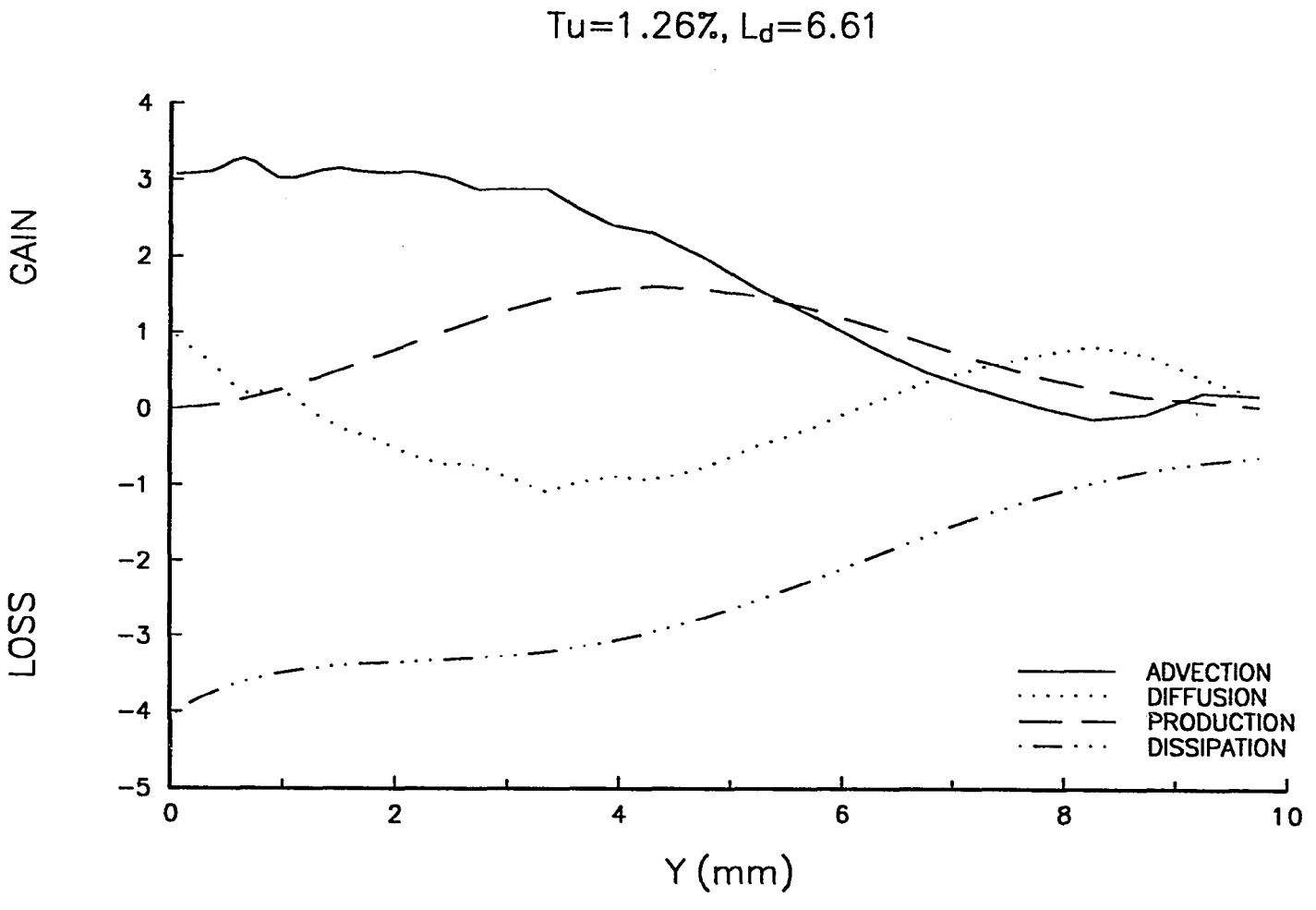

Fig. 7.20b Turbulence Kinetic Energy Budget at X=290 mm, Prediction of Cylinder Wake by K−ε Model

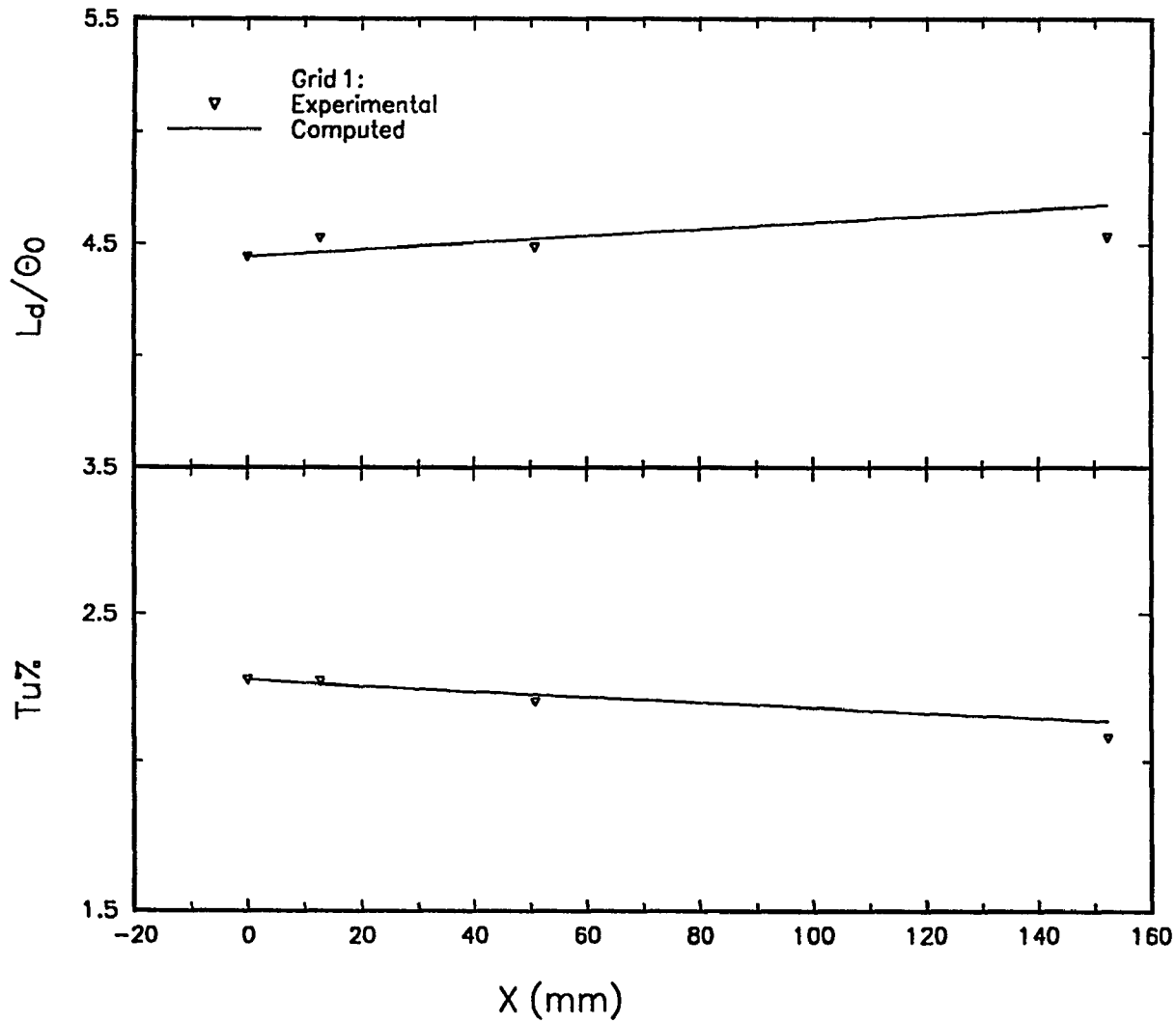

Fig. 7.21 a Prediction of Level and Length Scale of Free Stream Turbulence Generated by Grid 1

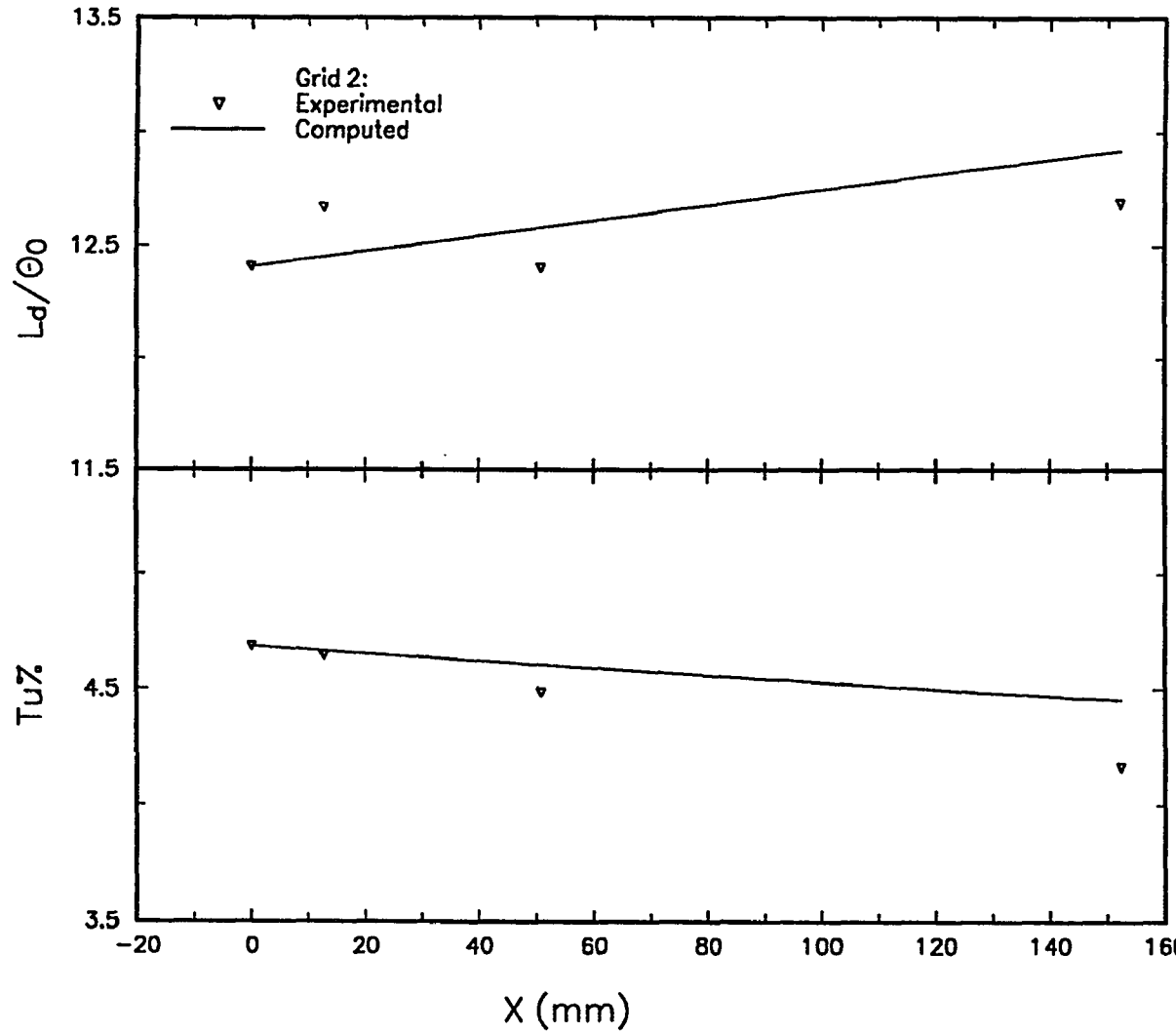

Fig. 7.21 b Prediction of Level and Length Scale of Free Stream Turbulence Generated by Grid 2

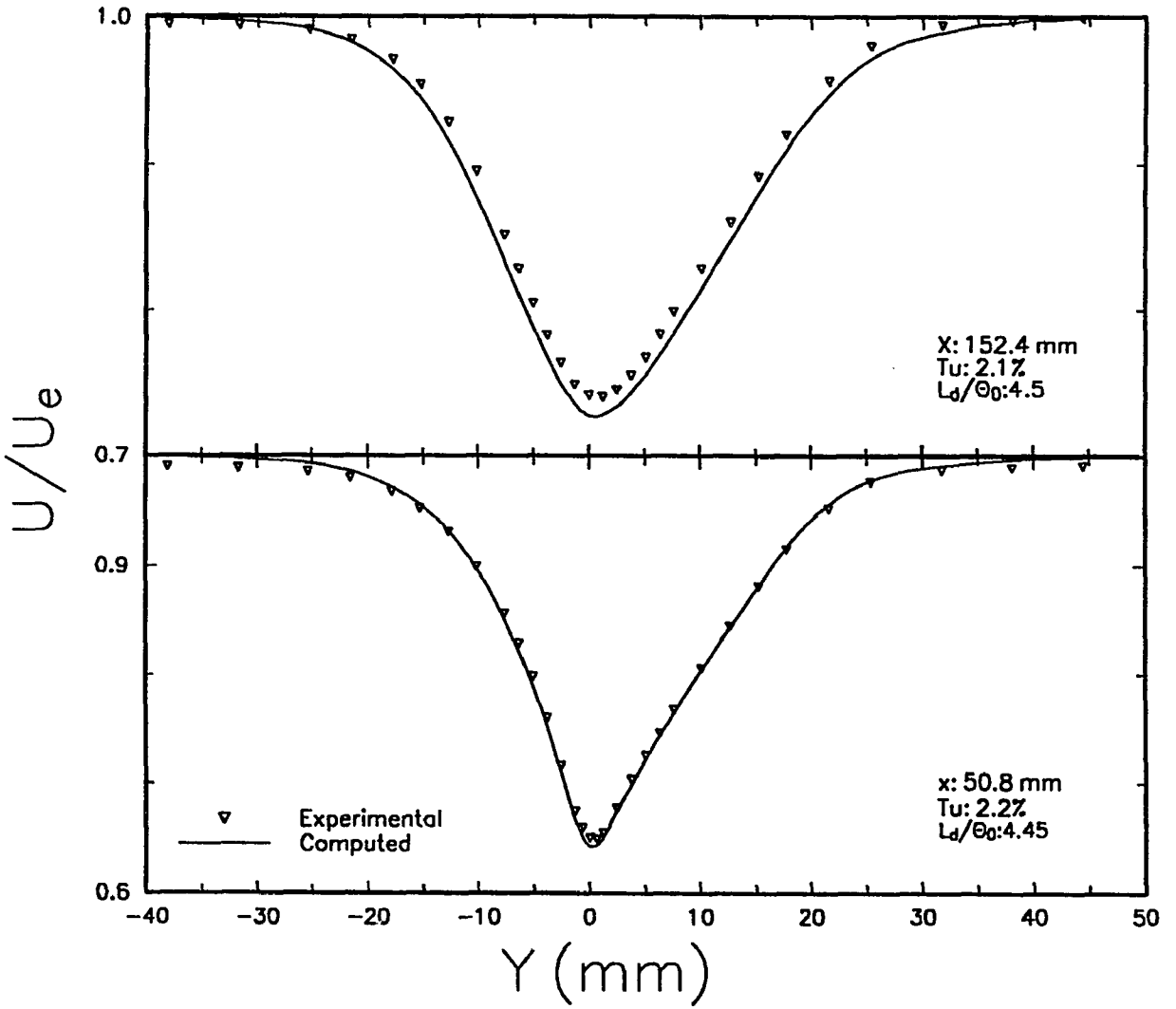

Fig. 7.22a Predicted Mean Velocity Profile Under Free Stream Turbulence by RS Model

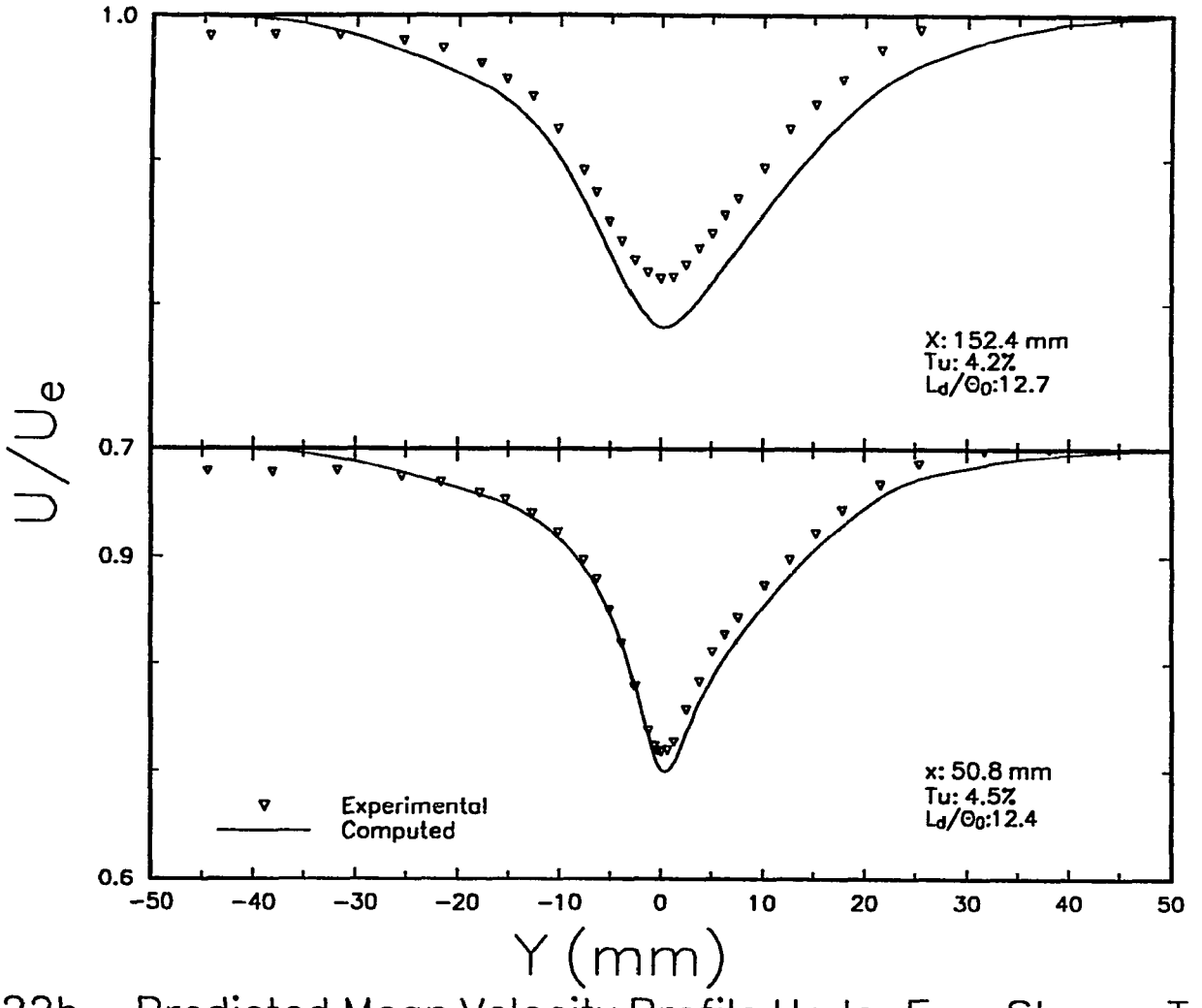

Fig. 7.22b Predicted Mean Velocity Profile Under Free Stream Turbulence by RS Model

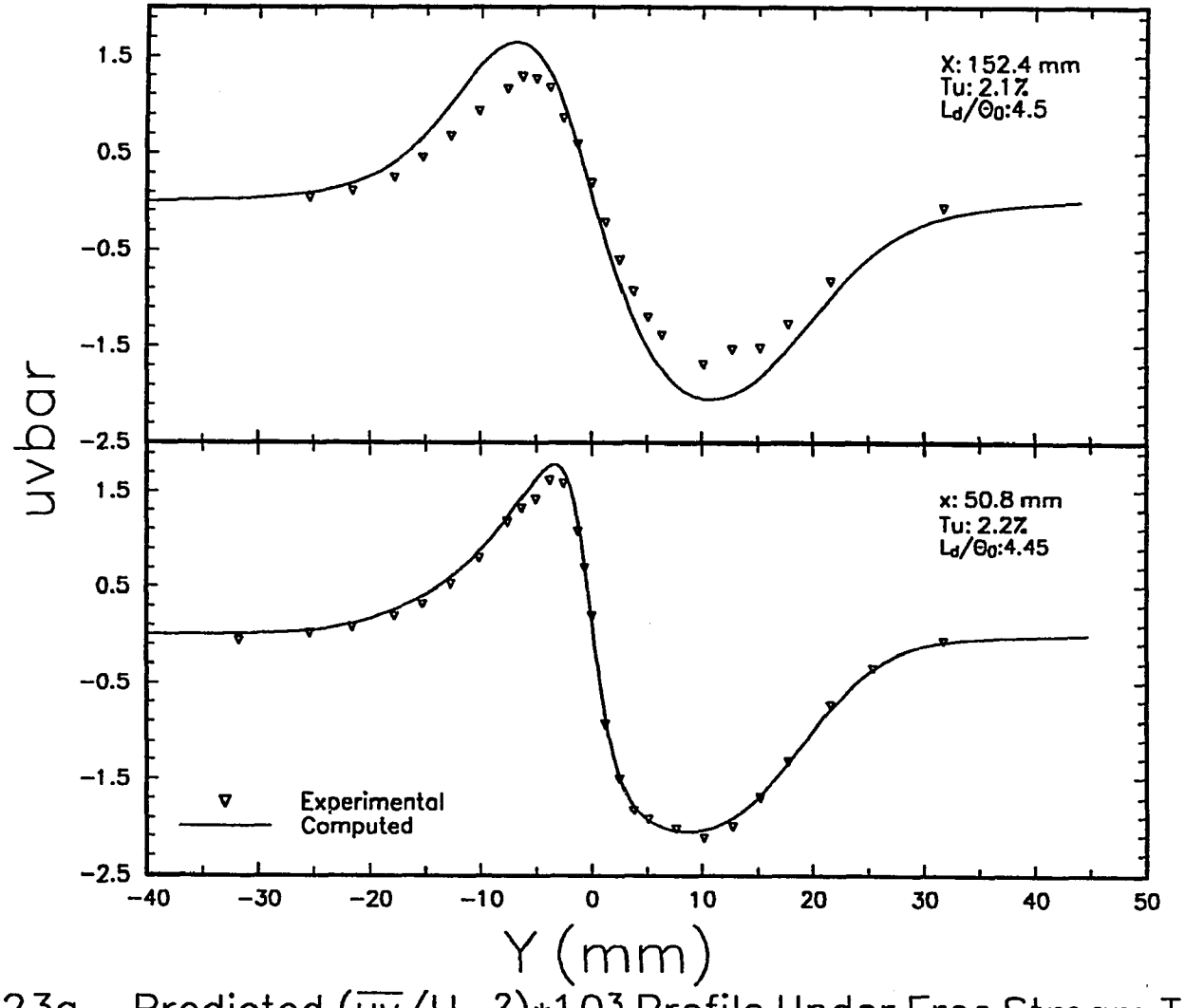

Fig. 7.23a Predicted $(\overline{uv}/U_\infty{}^2)*10^3$ Profile Under Free Stream Turbulence by RS Model

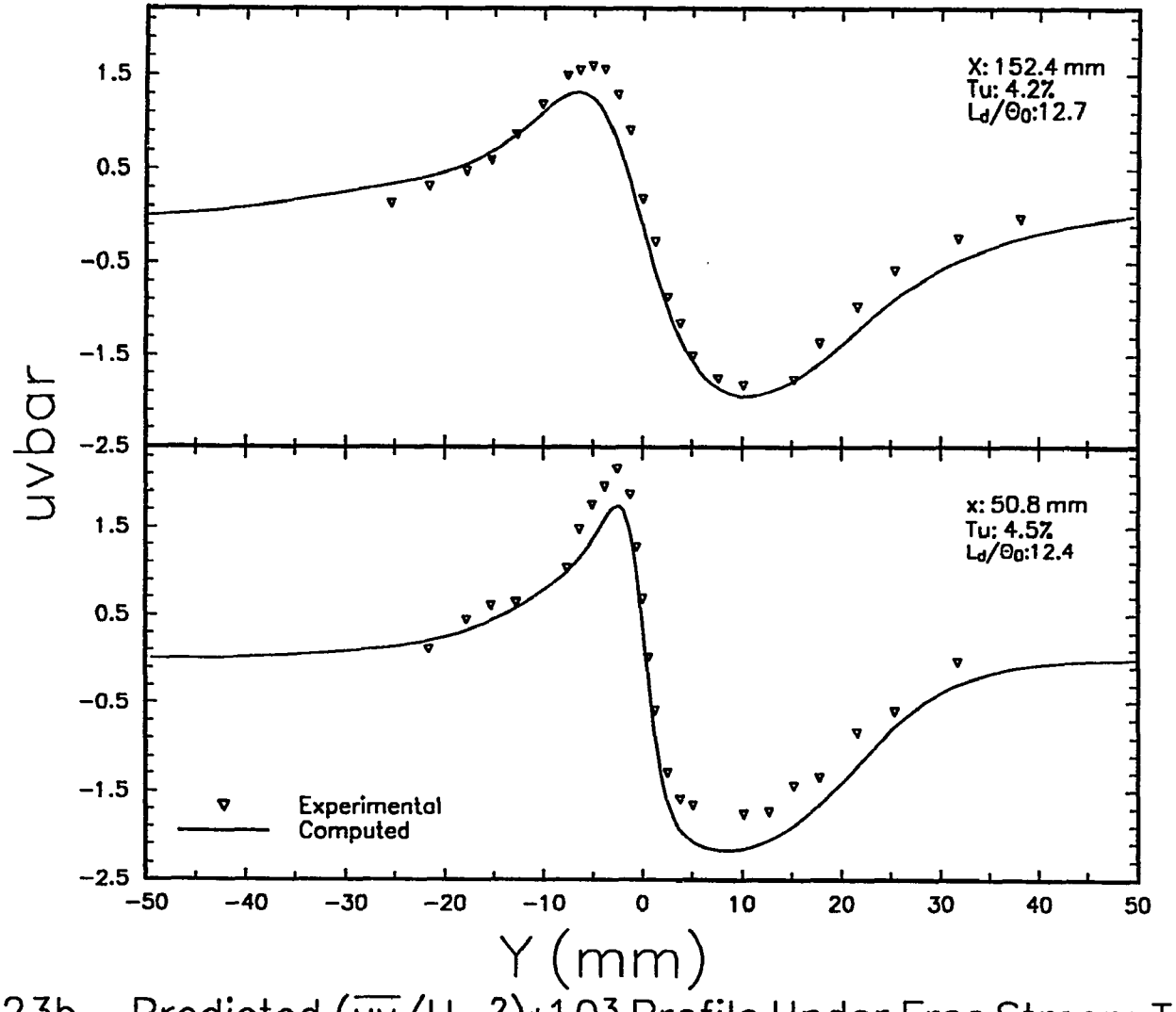

Fig. 7.23b Predicted $(\overline{uv}/U_\infty{}^2)*10^3$ Profile Under Free Stream Turbulence by RS Model

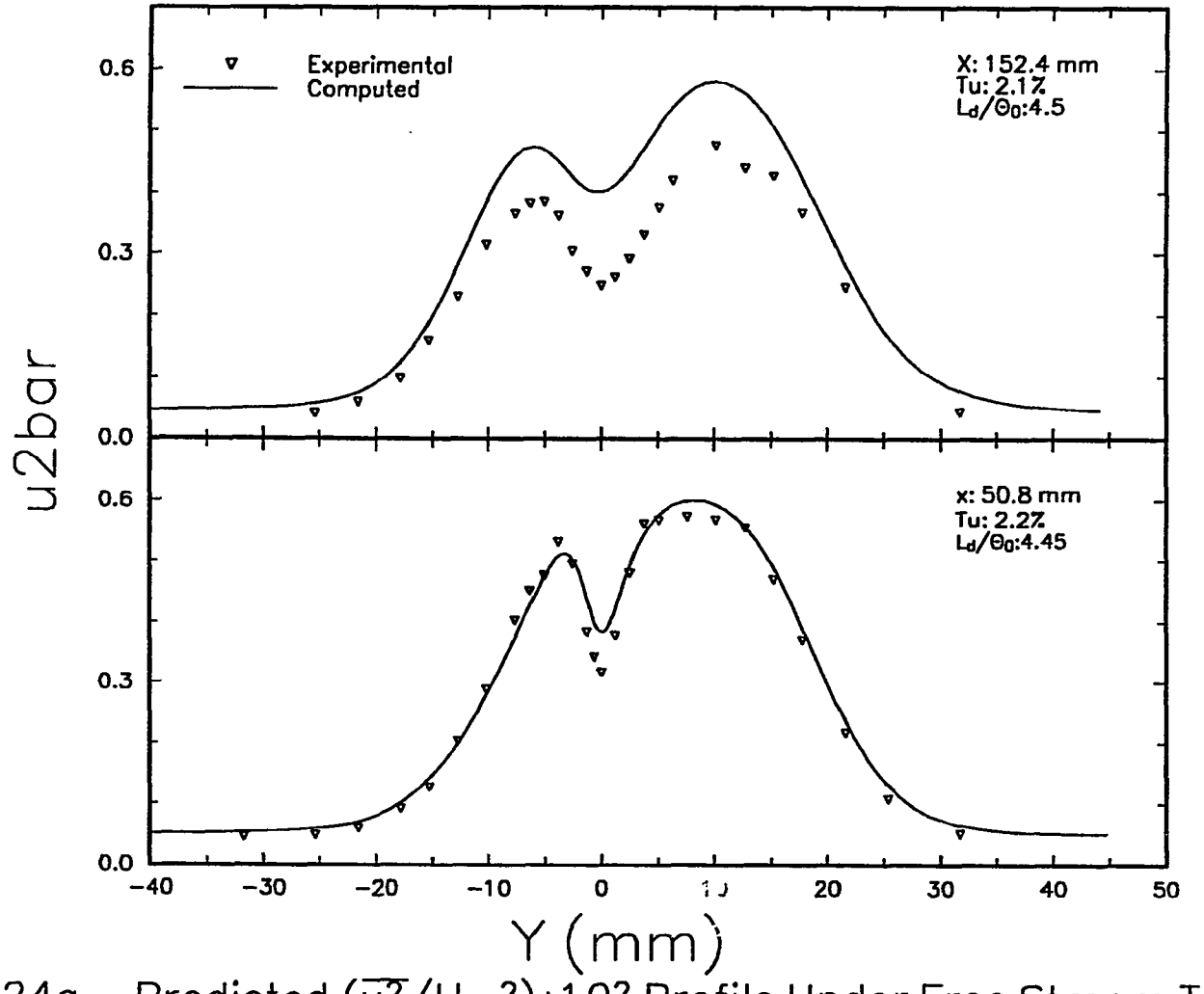

Fig. 7.24a Predicted $(\overline{u^2}/U_\infty{}^2)*10^2$ Profile Under Free Stream Turbulence by RS Model

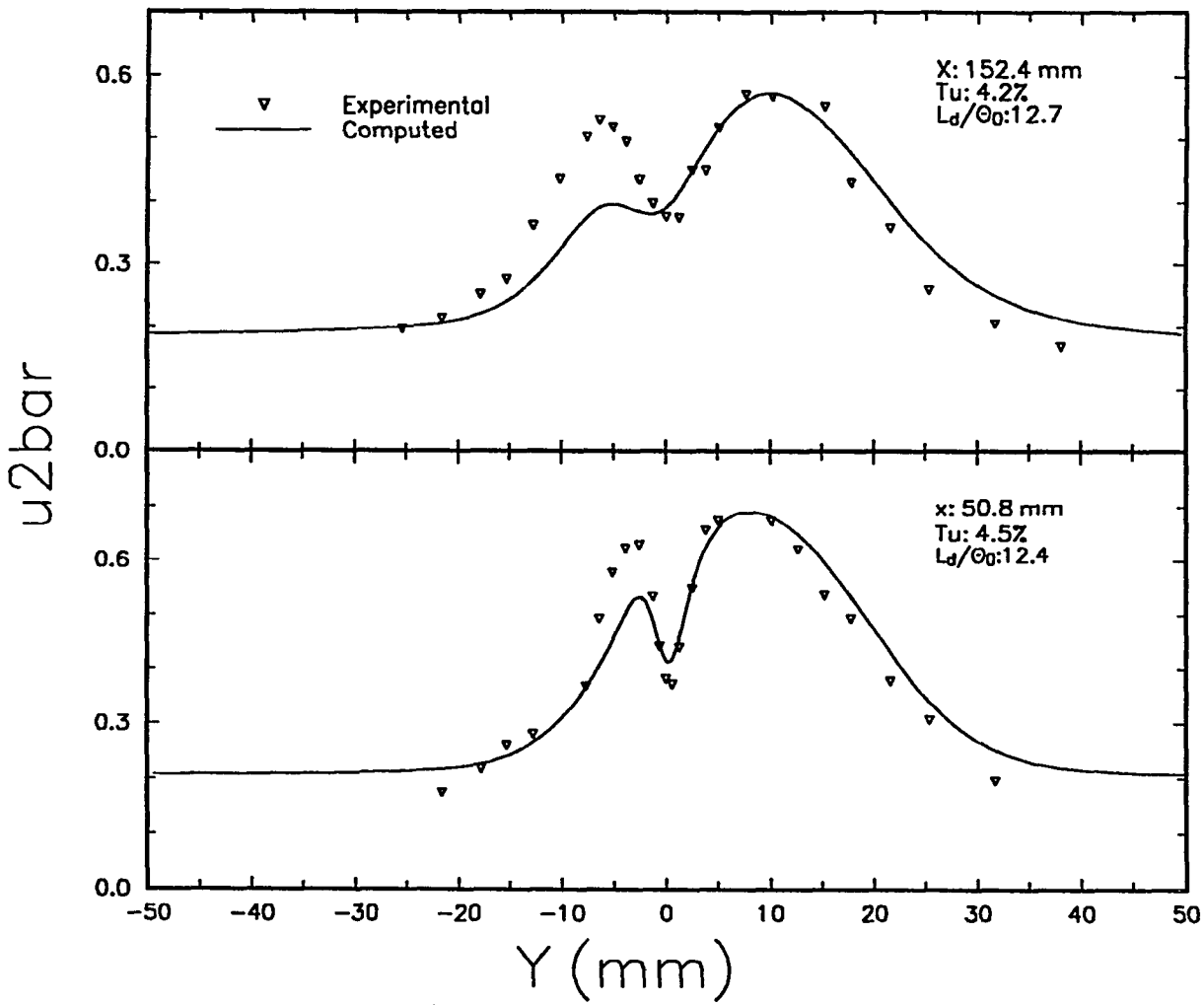

Fig. 7.24b Predicted $(\overline{u^2}/U_\infty{}^2)*10^2$ Profile Under Free Stream Turbulence by RS Model

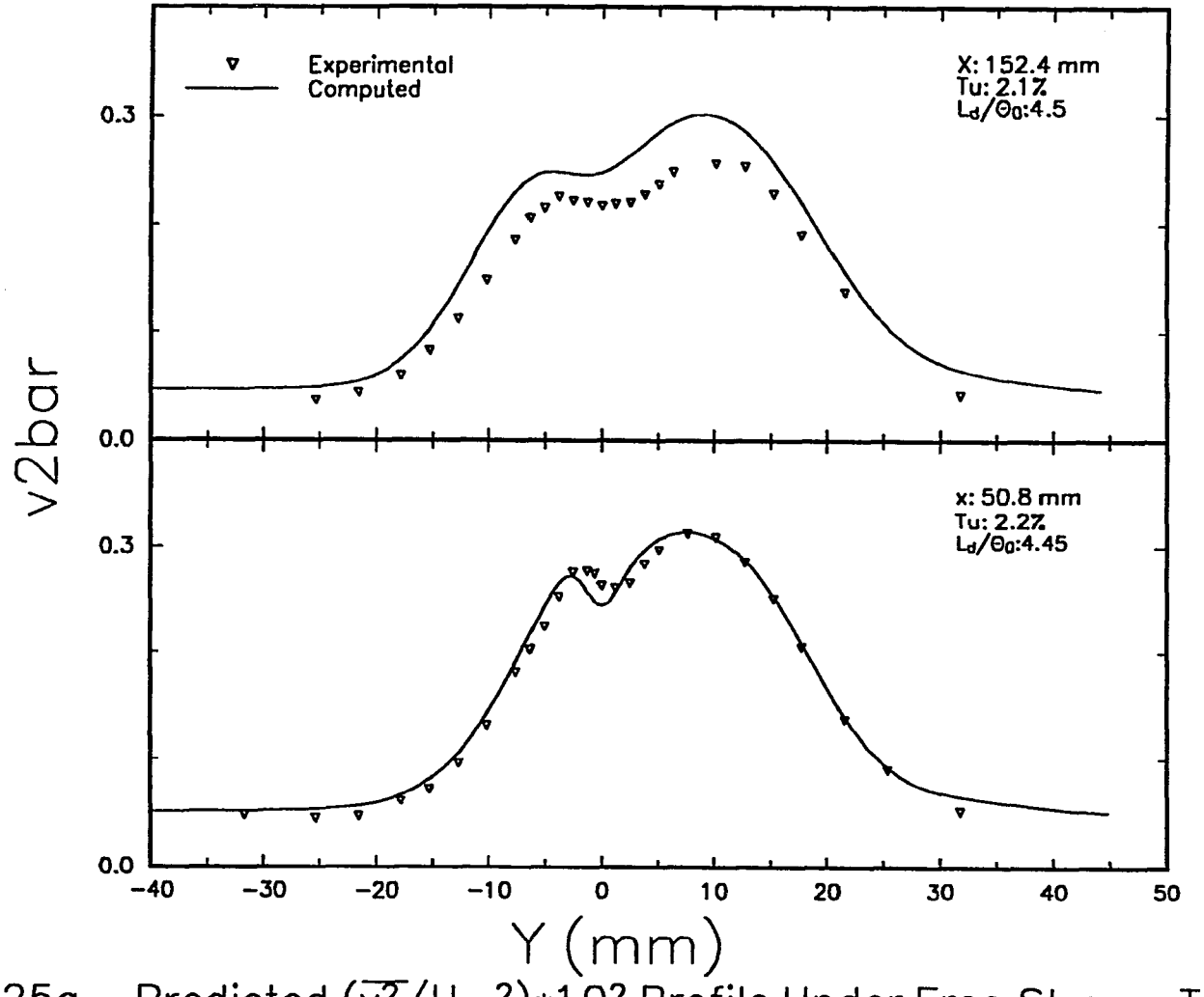

Fig. 7.25a Predicted $(\overline{v^2}/U_\infty{}^2)*10^2$ Profile Under Free Stream Turbulence by RS Model

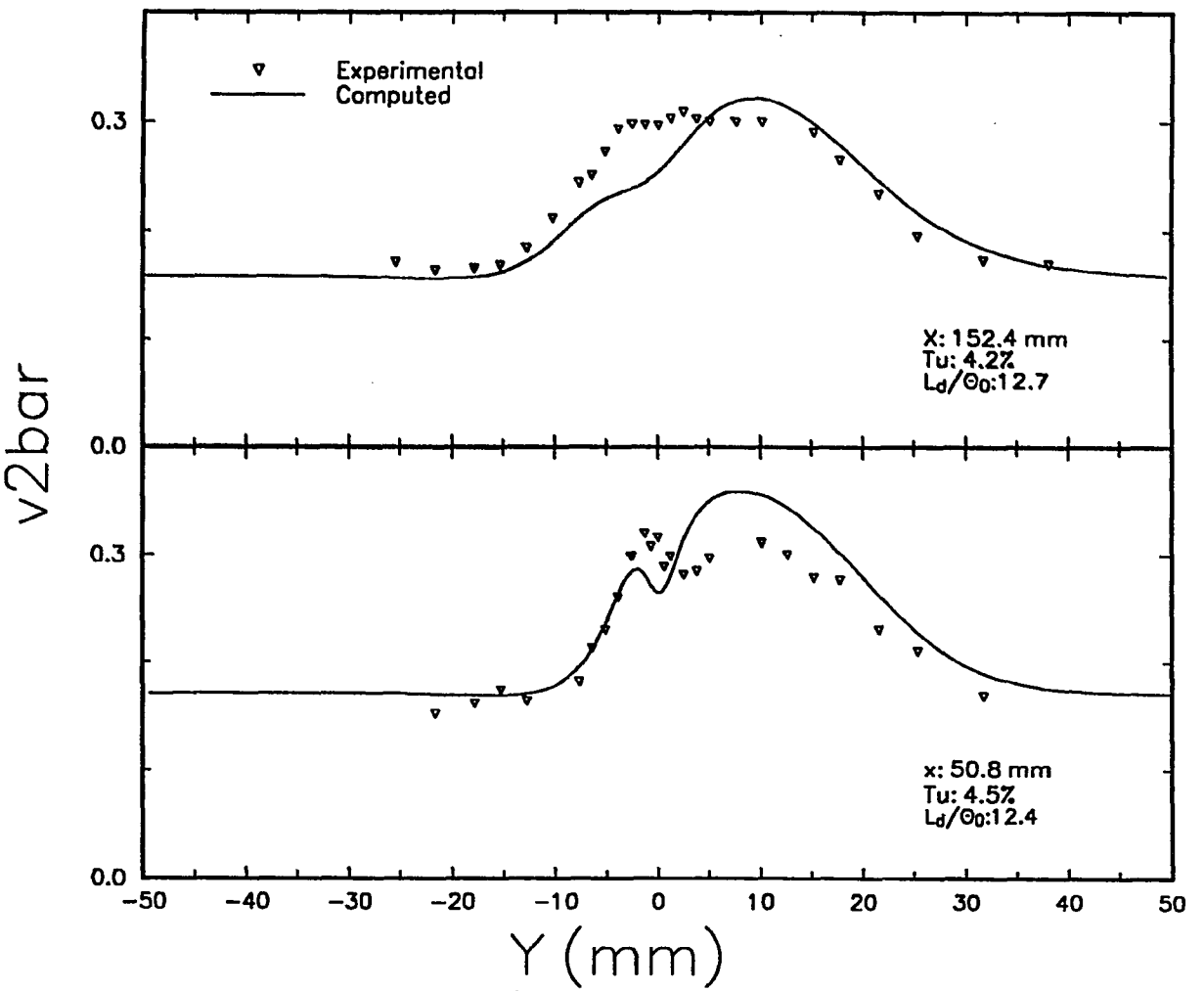

Fig. 7.25b Predicted $(\overline{v^2}/U_\infty{}^2)*10^2$ Profile Under Free Stream Turbulence by RS Model

CHAPTER 8

CONCLUSION

Investigation was undertaken to study the flow properties of symmetric and asymmetric wakes subjected to free stream turbulence. The investigation was performed by measuring the wake of a modified airfoil under the presence of free stream turbulence in the external layer. The wake flow governing equation along with K-ε and Reynolds stress turbulence closure models were numerically solved. Solutions were compared with experimental data. Based upon the measurement and the computation the following main observations are made:

1. The mean velocity and its related properties like recovery rate, H, δ^*, half-wake width of symmetric as well as asymmetric wakes are greatly affected by the presence of free stream turbulence. Recovery rate increases while shape factor decreases with higher level and larger length scale of the free stream turbulence. Displacement thickness and half-wake width become larger with moderate increase in free stream turbulence, and then decrease with higher level of free stream turbulence.

2. Presence of free stream turbulence affects the turbulence quantities

like the Reynolds stress tensor and the triple correlation greatly. The experimental data indicates that increases in the level and length scale of free stream turbulence increase the level of these quantities. It is also seen that the free stream turbulence affects these quantities in outer layer of wake, while the inner core of the wake is essentially unaffected by the free stream turbulence in the near wake.

3. Turbulence spectral functions indicate that the mechanism of transfer of energy from the larger energy containing eddies to smaller energy dissipating eddies are not affected by the presence of free stream turbulence. However, larger eddies contain higher levels of energy in the presence of free stream turbulence.

4. Presence of free stream turbulence affects asymmetric wake and symmetric wake in the same manner.

5. Computations of simple symmetric and asymmetric wakes indicate that the K-ε model and Reynolds stress model of turbulence closure result in acceptable prediction of mean velocity. However, turbulent kinetic energy and shear stress predicted with the K-ε model are closer to experimental data than those made with Reynolds stress model. The K-ε model seems to be better able to predict near wake to far wake evolution, but it is still not accurate enough in the far wake.

6. Maximum average deviation of predicted quantities from experimental data of simple wake using RS model is 23% for uvbar and 15% for u2bar in asymmetric wake, while uvbar and u2bar are predicted with maximum average deviation of 24% and 8% respectively, in symmetric wake. The computation of wake with K-ε model resulted in lower maximum average deviation consistently.

7. The far wake with and without the presence of free stream turbulence is successfully predicted by K-ε model.

8. The prediction of evolution of asymmetric near to far wake under varying free stream turbulence condition is relatively accurate with Reynolds stress model. The mean velocity is predicted quite successfully with maximum average deviation from experimental data of 2%, while the prediction of turbulent shear and normal stresses degenerates with increases in the free stream turbulence. The maximum average deviation of uvbar and u2bar from the experimental data are 18% and 10% respectively.

9. There is too much uncertainty in the estimate of dissipation rate in the wakes for the turbulence closure models to be tested with good degree of accuracy.

APPENDIX A

Computer Program for Calculation of Turbulence Quantities from the Cross-Wire Probe

A computer program was written for the computation of turbulence quantities and triple correlation incorporating the steps outlined in section 5.3.3. The output voltages of the anemometers connected to cross-wire probe were sampled by the A/D board and stored in a binary form. Each sample is 12 bits long, and is stored in 2 bytes or 16 bits length. The first 4 bits of the first byte are A/D board channel number tag which does not contribute to the value of sample.

The program reads the binary file, and converts the samples to voltages by filtering out the channel tags, and converting the binary digits to decimal integer, then converting the integer to voltages, afterward using the calibration of the hot-wire probe and Eqns. 5.5, 5.6, 5.7,and 5.8 computes the instantaneous X and Y velocities. Statistical averaging determines the appropriate turbulence quantities.

A C language listing of the program is included here.

```
#include <stdio.h>
#include <stdlib.h>
#include <io.h>
#include <fcntl.h>
#include <math.h>
#define BUFFSIZE 24576
/* program to process x-h.w. data
   ch : ref. press (dynamic head)
   ch2: x-hw WIRE #1
   ch3: x-hw WIRE #2
   program to process xhw data file in batch mode, 2 k's
   used   */
main(argc,argv)
int argc;
char *argv[];
{
     static unsigned char bigbuff[BUFFSIZE];
     char calfl[80];
     unsigned int bytes_read,i,j;
     long total=0;
     double sux,svy,suxvy,sux2,svy2,sux2vy,suxvy2,sux3,svy3,
          sbeta,sbeta2,k1,k2,e1,a1,b1,n1,u_eff_1,e2,
          a2,b2,n2,u_eff_2,ut,beta,beta_rms,cos_beta,
          sin_beta,cos_2_beta,gamma,sin_gamma,cos_gamma,
          ux,vy,ub,vb,u2b,v2b,uvb,u2vb,uv2b,u3b,v3b,
          pref,sp,dnum1,dnum2,dnum3,tempv;
     float cnum1,cnum2,cnum3;
     int fhandel,num1,num2,num3;
     FILE *outfl,*incalfl,*instfl;
       if( argc < 2 )
     {
     printf("wrong\n");
     printf("The usage format is: %s data_file \n",argv[0]);
     exit(1);
     }
     if( (fhandel= open(argv[1], O_RDONLY | O_BINARY))== -1)
       {
          printf("ERROR:can't open input file %s",argv[1]);
          exit(1);
       }
      printf("The calibration constants: \n \
     if input from a file, type <f>, otherwise hit any
          key:");
     if( ( j=getche() ) =='f' || j == 'F')
          {
           fflush(stdin);
           printf("\n \n Enter the calibration constants
                        file name:");
           scanf("%s",calfl);
           if( (incalfl=fopen(calfl,"r"))==NULL)
               {
               printf("ERROR:can't open the cal.data file
                     \n");
```

```
            exit(1);
            }
        fscanf(incalfl,"%f,%f,%f",&cnum1,&cnum2,&cnum3);
        a1=cnum1; b1=cnum2; n1=1.0/cnum3;
        printf("a=%f,b=%f,1/n=%f\n",a1,b1,n1);
        fscanf(incalfl,"%f,%f,%f",&cnum1,&cnum2,&cnum3);
        a2=cnum1; b2=cnum2; n2=1.0/cnum3;
        printf("a=%f,b=%f,1/n=%f\n",a2,b2,n2);
        fclose(incalfl);
        }
else
        {
        printf("\n");
        fflush(stdin);
        printf("Enter the constants for first wire
                (A,B,n):");
        scanf("%f,%f,%f",&cnum1,&cnum2,&cnum3);
        a1=cnum1; b1=cnum2; n1=1.0/cnum3;
        printf("a=%f,b=%f,1/n=%f\n",a1,b1,n1);
        fflush(stdin);
        printf("Enter the constants for second wire
                (A,B,n):");
        scanf("%f,%f,%f",&cnum1,&cnum2,&cnum3);
        a2=cnum1; b2=cnum2; n2=1.0/cnum3;
        printf("a=%f,b=%f,1/n=%f\n",a2,b2,n2);
        }
k1=0.340;
k2=0.290;
gamma=(45.0/180.0)*6.283185307179586/2.0;
sin_gamma=sin(gamma);
cos_gamma=cos(gamma);
c=0.0;
sp=0.0;
sux=svy=suxvy=sux2=svy2=0.0;
sux2vy=suxvy2=sux3=svy3=0.0;
sbeta=sbeta2=0.0;
total=0.0;
while( !eof(fhandel) )
 {
  if((bytes_read=read(fhandel,bigbuff,BUFFSIZE))==-1)
     {
      printf("read error\n");
      continue;
     }
 for (i=0; i< bytes_read; i+=6)
    {
    /* ----- REMOVE THE CHANNAL TAGS and COMPUTE VOLT.
            (unipolar) */
    num1=bigbuff[i+1]*16 + (bigbuff[i]-(bigbuff[i]
         & 0x0f ) ) / 16;
    dnum1=num1;
    dnum1=10*dnum1/4096;
    num2=bigbuff[i+3]*16+(bigbuff[i+2]-(bigbuff[i+2]
```

```
    & 0x0f ) ) / 16;
dnum2=num2;
e1=dnum2*10/4096;
num3=bigbuff[i+5]*16+(bigbuff[i+4]-(bigbuff[i+4]
     & 0x0f ) ) / 16;
dnum3=num3;
e2=dnum3*10/4096;
/* ------ THE FIRST WIRE SAMPLED ----- */
tempv=(e1*e1-a1)/b1;
u_eff_1=pow(tempv,n1);
/* ----- THE SECOND WIRE SAMPLED ----- */
tempv=(e2*e2-a2)/b2;
u_eff_2=pow(tempv,n2);
/* ----- BETA: ANGLE BET. UT AND NORMAL TO WIRE
    (at 90+gamma cw with x_axis, here, first wire
    sampled)----- */
cos_2_beta=(u_eff_1*u_eff_1*(1+k2*k2)-u_eff_2*
          u_eff_2*(1+k1*k1))/(u_eff_1*u_eff_1*
          (1-k2*k2)+u_eff_2*u_eff_2*(1-k1*k1));
if ( cos_2_beta < -1 || cos_2_beta > 1 )
  {
  printf("%dth scan,cos_2_beta=%f,continue\n"
         ,(i/6+total/6),cos_2_beta);
  continue;
  }
tempv=(cos_2_beta+1.0)/2.0;
cos_beta=sqrt(tempv);
beta = acos(cos_beta);
tempv=(1-cos_2_beta)/2.0;
sin_beta=sqrt(tempv);
/* ----- ALPH: ANGLE BET. UT AND NORMAL TO WIRE
     (at gamma cw with x_axis, here, second
     wire sampled) -- */
/* ------- NO NEED to compute it since
     alph=90-beta and alph_rms is equal to
     beta_rms--------------- */
/* ----- THE INSTANTANOUS VELOCITY ---------- */
tempv=(2*u_eff_1*u_eff_1)/(cos_2_beta*
      (1-k1*k1)+(1+k1*k1));
ut=sqrt(tempv);
/* -- INSTANTANOUS VELOCITIES IN X and Y AXIS --*/
ux=ut*(cos_gamma*cos_beta + sin_gamma*sin_beta);
vy=ut*(sin_gamma*cos_beta - cos_gamma*sin_beta);
/* ----- STATISTICAL ENSAMBLES ----- */
sp += dnum1;
sbeta +=beta;
sbeta2 += beta*beta;
sux += ux;
svy += vy;
suxvy += ux*vy;
sux2 += ux*ux;
svy2 += vy*vy;
sux2vy += ux*ux*vy;
```

```
        suxvy2 += ux*vy*vy;
        svy3 += vy*vy*vy;
        sux3 += ux*ux*ux;
        c++;
      }
    total += bytes_read;
    printf("Bytes read=%ld,Number of entry=%.0f \n",
                          total,c);
    /* end of xhw_data file processing */
    }
    close(fhandel);
    pref=sp/c;
    ub=sux/c;
    vb=svy/c;
    u2b=sux2/c-ub*ub;
    v2b=svy2/c-vb*vb;
    uvb=suxvy/c-ub*vb;
    u2vb=(sux2vy-2*ub*suxvy-vb*sux2)/c+2*ub*ub*vb;
    uv2b=(suxvy2-2*vb*suxvy-ub*svy2)/c+2*ub*vb*vb;
    v3b=(svy3-3*vb*svy2+3*vb*vb*svy)/c-vb*vb*vb;
    u3b=(sux3-3*ub*sux2+3*ub*ub*sux)/c-ub*ub*ub;
    beta=sbeta/c;
    beta_rms=sbeta2/c-beta*beta;
    beta_rms=sqrt(beta_rms);
    beta = beta*180.0/(6.283185307179586/2.0);
    beta_rms = beta_rms*180.0/(6.283185307179586/2.0);
    printf("the results:\n");
    printf("Pref (Volts)=%f\n",pref);
    printf("Ub=%f,Vb=%f\n",ub,vb);
    printf("u2b=%f,v2b=%f,uvb=%f \n",u2b,v2b,uvb);
    printf("u2vb=%f,uv2b=%f,u3b=%f,v3b=%f
                        \n",u2vb,uv2b,u3b,v3b);
    printf("beta=%f,beta_rms=%f \n",beta,beta_rms);
}
```

APPENDIX B

Computer Program for Calculation of Turbulence Power Spectral Density Function From Cross-Wire Probe

A computer program was written for the computation of power spectral density function of fluctuating streamwise velocity. Cross-wire measurements were used for this purpose. Binary data file containing digitized outputs of anemometers connected to cross-wire probe was processed to produce the instantaneous streamwise velocity, as explained in Appendix A. The power spectral density function was then obtained from the Fourier components of transformed instantaneous streamwise velocity. The Fourier components were obtained by using a radix 2 FFT algorithm.

A C language listing of the program is included here.

```
#include <stdio.h>
#include <stdlib.h>
#include <io.h>
#include <fcntl.h>
#include <math.h>
#define CLEAR "\x1b[2J"
double x[4096],y[4096];
/* program to process x-h.w. data, and compute the fft of ux
   ch1: ref. press (dynamic head)
   ch2: x-hw WIRE #1
   ch3: x-hw WIRE #2    */
main(argc,argv)
int argc;
char *argv[];
{    static unsigned char bigbuff[32768];
     static double psd[4096];
     char flnm[81],calfl[80];
     unsigned int bytes_read,i,j,buffsize,kblks,cntr;
     double e1,a1,b1,n1,u_eff_1,e2,a2,b2,n2,u_eff_2,ux,vy,
            tempv,k1,k2,ut,sux,sux_blk,cos_beta,sin_beta,
            cos_2_beta,sin_gamma,cos_gamma,gamma,dnum1,
            dnum2,dnum3;
     FILE *outfl,*incalfl;
     int fhandel,num1,num2,num3,nblks,n,m;
     long dtfllng,total=0;
     float cnum1,cnum2,cnum3,frq,rsmpl,nfft,c;
     if( argc < 2 )
     {
     printf("wrong\n");
     printf("The usage format is: %s data_file \n",argv[0]);
     exit(1);
     }
     if((fhandel=open(argv[1], O_RDONLY | O_BINARY) ) == -1)
       {
          printf("ERROR:can't open input file %s",argv[1]);
          exit(1);
       }
     dtfllng=filelength(fhandel);
     printf("The calibration constants: \n \ if input from a
             file, type < f >, otherwise hit any key:");
     if( ( j=getche() ) =='f' || j == 'F')
          {
           fflush(stdin);
           printf("\n \n Enter the calibration constants
                          file name:");
           scanf("%s",calfl);
           if( (incalfl=fopen(calfl,"r"))==NULL)
               {
                printf("ERROR:can't open the cal. data file
                             \n");
                exit(1);
                }
           fscanf(incalfl,"%f,%f,%f",&cnum1,&cnum2,&cnum3);
```

```
        a1=cnum1; b1=cnum2; n1=1.0/cnum3;
        printf("a=%f,b=%f,1/n=%f\n",a1,b1,n1);
        fscanf(incalfl,"%f,%f,%f",&cnum1,&cnum2,&cnum3);
        a2=cnum1; b2=cnum2; n2=1.0/cnum3;
        printf("a=%f,b=%f,1/n=%f\n",a2,b2,n2);
        fclose(incalfl);
        }
else
        {
        printf("\n");
        fflush(stdin);
        printf("Enter the constants for first wire
                (A,B,n):");
        scanf("%f,%f,%f",&cnum1,&cnum2,&cnum3);
        a1=cnum1; b1=cnum2; n1=1.0/cnum3;
        printf("a=%f,b=%f,1/n=%f\n",a1,b1,n1);
        fflush(stdin);
        printf("Enter the constants for second wire
                (A,B,n):");
        scanf("%f,%f,%f",&cnum1,&cnum2,&cnum3);
        a2=cnum1; b2=cnum2; n2=1.0/cnum3;
        printf("a=%f,b=%f,1/n=%f\n",a2,b2,n2);
        }
fflush(stdin);
printf("enter m (fft exponent < 12 ):");
scanf("%d",&m);
fflush(stdin);
while ( m > 12 )
        {
        printf("m too large, reduce it:");
        scanf("%d",&m);
        fflush(stdin);
        }
cnum1=m;
x[0]=pow(2.0,cnum1);
n=x[0];
buffsize=6*n;
printf("fft for %d discrete frequencies will be
        computed\n",n);
kblks=dtfllng/buffsize;
printf("the maximum number of blocks to average
        fft:%d \n enter the number of blocks to
        average fft:",kblks);
scanf("%d",&nblks);
fflush(stdin);
while ( nblks>kblks)
        {
        printf ( " too many blocks, reduce it:");
        scanf("%d",&nblks);
        fflush(stdin);
        }
printf("enter the output file name:");
gets(flnm);
```

```
fflush(stdin);
if( ( outfl=fopen(flnm,"w") ) == NULL )
   {
   printf("ERROR:can't open the output file:%s\n"
            ,flnm);
   exit(1);
   }
rsmpl=20000.0;
k1=0.340;
k2=0.290;
gamma=(45.0/180.0)*6.283185307179586/2.0;
sin_gamma=sin(gamma);
cos_gamma=cos(gamma);
c=nfft=0.0;
total=sux=0.0;
for (i=0; i<n; i++);
    psd[i]=0.0;
for (kblks=0;kblks<nblks;kblks++)
 {
 if((bytes_read=read(fhandel,bigbuff,buffsize))== -1)
    {
    printf("read error\n");
    continue;
    }
 total += bytes_read;
 cntr=0;
 sux_blk=0.0;
 for (i=0; i< bytes_read; i+=6)
   {
   /* ----- REMOVE THE CHANNAL TAGS and COMPUTE VOLT.
        (unipolar) */
     num1=bigbuff[i+1]*16 + (bigbuff[i] - (bigbuff[i]
          & 0x0f) )/16;
     dnum1=num1;
     dnum1=10*dnum1/4096;
     num2=bigbuff[i+3]*16 + (bigbuff[i+2]- (
          bigbuff[i+2] & 0x0f) )/16;
     dnum2=num2;
     e1=dnum2*10/4096;
     num3=bigbuff[i+5]*16 + (bigbuff[i+4] -
          (bigbuff[i+4] & 0x0f) )/16 ;
     dnum3=num3;
     e2=dnum3*10/4096;
     /* ------ THE FIRST WIRE SAMPLED ----- */
     tempv=(e1*e1-a1)/b1;
     u_eff_1=pow(tempv,n1);
     /* ----- THE SECOND WIRE SAMPLED ----- */
     tempv=(e2*e2-a2)/b2;
     u_eff_2=pow(tempv,n2);
     /* ----- BETA: ANGLE BET. UT AND NORMAL TO WIRE
          (at 90+gamma cw with x_axis, here, first
          wire sampled)  ----- */
     cos_2_beta=(u_eff_1*u_eff_1*(1+k2*k2)- u_eff_2*
```

```
                    u_eff_2*(1+k1*k1))/(u_eff_1*u_eff_1*
                    (1-k2*k2)+u_eff_2*u_eff_2*(1-k1*k1));
        if( cos_2_beta < -1 || cos_2_beta > 1 )
        {
          printf("%dth scan,cos_2_beta=%f ,continue\n"
                 ,(i/6+total/6),cos_2_beta);
          continue;
         }
       tempv=(cos_2_beta+1.0)/2.0;
       cos_beta=sqrt(tempv);
       tempv=(1-cos_2_beta)/2.0;
       sin_beta=sqrt(tempv);
       /* ----- ALPH: ANGLE BET. UT AND NORMAL TO WIRE
            (at gamma cw with x_axis, here, second
           wire sampled) ----- */
       /* ------- NO NEED to compute it since alph = 90
       -beta and alph_rms is equal to beta_rms------ */
       /* ----- THE INSTANTANOUS VELOCITY ---------- */
       tempv=(2*u_eff_1*u_eff_1)/(cos_2_beta*(1-k1*k1)
             +(1+k1*k1));
       ut=sqrt(tempv);
       /* -- INSTANTANOUS VELOCITIES IN X and Y AXIS --*/
       ux=ut*(cos_gamma*cos_beta + sin_gamma*sin_beta);
       /* ----- STATISTICAL ENSAMBLES ----- */
       sux += ux;
       sux_blk += ux;
       c++;
       x[i/6]=ux;
       y[i/6]=0.0;
       cntr++;
    }
    ut=sux_blk/cntr;
    for(i=0; i<cntr;i++)
        x[i] -= ut;
    if(n > cntr+1)
     {
        for(i=cntr+1;i<n;i++)
         x[i]=y[i]=0.0;
     }
    printf("the %.0f th fft block starts \n",nfft+1);
    fft(n,m);
    for (i=0;i<n;i++)
        psd[i]+=2.0*(x[i]*x[i]+y[i]*y[i])/(n*rsmpl);
    nfft++;
}
close(fhandel);
if (nfft==0)
  {
   printf("ERROR:no fft blocks computed \n");
   exit(1);
   }
for (j=1; j<=n/2; j++)
   {
```

```
          psd[j] /= nfft;
          frq=j*(rsmpl/n);
          fprintf(outfl,"%f,%.7f\n",frq,psd[j]);
          }
        fclose(outfl);
    }
/* fft routine */
fft(n,m)
int n,m;
{
double e,dn1,c1,s1,c,s,xt,yt,t;
int n2,n1,j,i,l,k;
n2=n;
for (k=0;k<m;k++)
    {
     n1=n2;
     n2 /=2;
     dn1=n1;
     e=6.283185307179586/dn1;
     c=1.0;
     s=0.0;
     c1=cos(e);
     s1=sin(e);
     for (j=0; j<n2; j++ )
        {
            for(i=j; i<n; i+=n1)
              {
                   l=i+n2;
                   xt=x[i] - x[l];
                   x[i]=x[i] + x[l];
                   yt=y[i] - y[l];
                   y[i]=y[i] + y[l];
                   x[l]=c*xt + s*yt;
                   y[l]=c*yt - s*xt;
               }
            t=c;
            c= c*c1 - s*s1;
            s= t*s1 + s*c1;
        }
    }
 /*-----unscramble-------*/
  for ( k=0; k<n; k++)
    {
      i=ibitr(k,m);
      if ( i > k)
          {
            xt=x[k];
            yt=y[k];
            x[k]=x[i];
            y[k]=y[i];
            x[i]=xt;
            y[i]=yt;
          }
```

```
    }
 }
/* ------ binary digit reverser function --------*/
ibitr(j,m)
int j,m;
{
int i,ibtr,j1,j2 ;
j1=j ;
ibtr=0;
for (i=0;i<m;i++)
    {
    j2=j1/2;
    ibtr=ibtr*2+(j1-2*j2);
    j1=j2;
    }
return(ibtr);
}
```

APPENDIX C

A FORTRAN listing of the computer program used for prediction of asymmetric wake with Reynolds stress model under presence of free stream turbulence is presented. The programs for other wake computation done in this investigation are similar to this program with some differences. They are not presented because of space limitations.

```
      IMPLICIT REAL*8(A-H,O-Z)
      COMMON /BLKMN/ U1(150),U(150),G1(150),G(150)
      COMMON /BLKY/ PSI(150),Y(150),YH(150),X,DX,X1,YP0,L
      COMMON /BLKKE/ TK1(150),TK(150)
      COMMON /BLKUP/ UP1(150),DUP1(150),UP(150),DUP(150)
      COMMON /BLKVP/ VP1(150),DVP1(150),VP(150),DVP(150)
      COMMON /BLKUVP/ UVP1(150),DUVP1(150),UVP(150),DUVP(150)
      COMMON /BLKDS/ TES1(150),TES(150),TGM1(150),TGM(150)
      COMMON /BLKCST/ ROW,VIC,CS,CPH1,CPH2,CES,CES1,CES2
      DIMENSION UERR(150),TERR1(150),TERR2(150),TERR3(150)
     1 ,TERR4(150),TERR5(150),VTM(150)
C **IN THIS PROGRAM, ASY. WAKE UNDER FST IS SOLVED IN X,PSI SPACE
      CS=0.25D0
      CPH1=1.5D0
      CPH2=0.2D0
      CES=0.15D0
      CES1=1.45D0
      CES2=1.9D0
      EPS=0.00001D0
      EPS1=0.001D0
C **** INPUT TO BE USED IN WAKE CALCUALTIONS
      VIC= 0.6078D0*2.5806D0*0.00001D0
C <*   READ THE  INPUT (THE OUTPUT OF IC CALCULATION )
C     NOTE  FILE "5"         *>
C******* ******** ******** ********
      READ(5,745) YP0
745   FORMAT(D17.10)
      READ(5,748)UE
748   FORMAT(F10.4)
      READ(5,749)X1,L
      X1=X1/1000.0D0
749   FORMAT(D17.10,I4)
752   FORMAT(I2)
755   FORMAT(4D17.10)
      DO 701 I=1,L
      READ(5,755)Y(I),PSI(I),U1(I),G1(I)
      G1(I)=G1(I)/U1(I)
701   CONTINUE
      READ(5,752)LBRK
      DO 703 I=1,L
      READ(5,755)UP1(I),DUP1(I),VP1(I),DVP1(I)
      DUP1(I)=DUP1(I)/U1(I)
      DVP1(I)=DVP1(I)/U1(I)
703   CONTINUE
      READ(5,752)LBRK
      DO 705 I=1,L
      READ(5,755)UVP1(I),DUVP1(I),TES1(I),TGM1(I)
      DUVP1(I)=DUVP1(I)/U1(I)
      TES1(I)=(0.08D0/0.07D0)*TES1(I)
      TGM1(I)=(0.08D0/0.07D0)*(TGM1(I)/U1(I))
705   CONTINUE
      WRITE(6,1000) X1
      WRITE(6,1005)
      WRITE(6,2006)
      WRITE(6,1006) (Y(I),PSI(I),U1(I),G1(I),I=1,L)
      WRITE(6,1010)
      WRITE(6,2011)
      WRITE(6,1011)(Y(I),UP1(I),DUP1(I),VP1(I),DVP1(I),I=1,L)
```

```
      WRITE(6,2911)
      WRITE(6,1911)(Y(I),UVP1(I),DUVP1(I),TES1(I),TGM1(I),I=1,L)
1000  FORMAT(// '******** INITIAL CONDITION AT X= ',F12.6)
1005  FORMAT(//,5X,'THE INTRPLD MEAN QUNTITS ACCORDING TO GRID'
     1 ,'SYSTEM'/,5X,'GRADIENT;"G"'/,5X,'INTEGRAL CLCULTN;"PSI"'/)
2006  FORMAT(8X,'Y',11X,'PSI',13X,'U',14X,'G')
1006  FORMAT(4(2X,F13.7))
1010  FORMAT(5X,'INITINAL CONDITION ; REYNOLDS STRESS TENSOR :')
2011  FORMAT(8X,'Y',14X,'UP',14X,'DUP',14X,'VP',14X,'DVP')
1011  FORMAT(5(2X,F14.7))
2911  FORMAT(8X,'Y',13X,'UVP',14X,'DUVP',18X,'TES',17X,'DTES')
1911  FORMAT(3(2X,F14.7),2X,F20.6,2X,F20.6)
C ***  H'J  SPACING ****
180   DO 19 I=2,L
19    YH(I)=PSI(I)-PSI(I-1)
C ***  T.K.E IC ***
      DO 20 I=1,L
20    TK1(I)=(UP1(I)+VP1(I))*0.75D0
C ***  SET INITIAL GUESS FOR FIRST STATION   ***
      DO 25  I=1,L
      U(I)=U1(I)
      G(I)=G1(I)
      TK(I)=TK1(I)
      TES(I)=TES1(I)
      TGM(I)=TGM1(I)
      UP(I)=UP1(I)
      DUP(I)=DUP1(I)
      VP(I)=VP1(I)
      DVP(I)=DVP1(I)
      UVP(I)=UVP1(I)
      DUVP(I)=DUVP1(I)
      UERR(I)=U(I)
      TERR1(I)=UP(I)
      TERR2(I)=VP(I)
      TERR4(I)=UVP(I)
      TERR5(I)=TES(I)
 25   CONTINUE
      CALL PRPTY (UE,DELS,TETA)
      YP0=YP0+DELS/2
      CALL YTRNS (UE,DELS)
      WRITE (6,1025)
      WRITE (7,1025)
1025  FORMAT(2X,'<<<<<<< START MARCHING FORWARD >>>>>>>          ')
C ***  INITIALIZE IFLG TO 0 ; TURN MATRIX COEF. ON.
      IFLG= 0
      NISO=4
C ***  SET THE AXIAL DISTANCE INCREMENT
      DX=0.0047625D0
      DX1=DX
      X=X1
      WRITE(9,8609)
8609  FORMAT('"-----INITIAL CONDITONS----"')
      CALL PLOT (UE,TETA)
      WRITE(9,8608)
8608  FORMAT('"--------SLOUTIN----------"')
      IPR=8
C***  OUTER LOOP, PREFORM FOR  NO. OF AXIAL STATIONS ****
      DO 777 IAX=1,24
```

```
      X1=X
      IF(IAX.GT.8) IPR=24
      IF(IAX.GT.8) DX=0.00635D0
      X=X+DX
C ***  SET THE FREE STREAM TURBULENCE  (LOWER EDGE
      FU2=UP1(1)
      FV2=VP1(1)
      FEPS=TES1(1)
      CALL FSTCAL(X1,X,FU2,FV2,FEPS)
      UP(1)=FU2
      VP(1)=FV2
      TES(1)=FEPS
C ***  SET THE FREE STREAM TURBULENCE  (UPPER EDGE
      FU2=UP1(L)
      FV2=VP1(L)
      FEPS=TES1(L)
      CALL FSTCAL(X1,X,FU2,FV2,FEPS)
      UP(L)=FU2
      VP(L)=FV2
      TES(L)=FEPS
C ***  INNER LOOP, DO FOR  NO. OF ITERATION OR CONVERGENCE ***
      DO 30 ITRQ=1,15
      CALL MNEQ(UE,IFLG)
      CALL TUEQ (IFLG)
C ***  TURN MATRIX FORMATION OFF
      IFLG=1
C ***  CHECK FOR CONVERGENCE ***
      DO 27  I=1,L
      IF(DABS(UERR(I)-U(I)).GT.EPS)GO TO 288
      IF(DABS(TERR1(I)-UP(I)).GT.EPS1)GO TO 288
      IF(DABS(TERR2(I)-VP(I)).GT.EPS1)GO TO 288
      IF(DABS(TERR4(I)-UVP(I)).GT.EPS1)GO TO 288
      IF(DABS(TERR5(I)-TES(I)).GT.EPS1 )GO TO 288
 27   CONTINUE
      GO TO 31
C ***  UPDATE THE ERRORS ***
 288  DO 29 I=1,L
      UERR(I)=U(I)
      TERR1(I)=UP(I)
      TERR2(I)=VP(I)
      TERR4(I)=UVP(I)
 29   TERR5(I)=TES(I)
      IF(MOD(ITRQ,40).NE.0) GO TO 30
      WRITE(6,2006)
      WRITE(6,9006)  (PSI(I),U(I),G(I),I=1,L)
      WRITE(6,2011)
      WRITE(6,9011)(PSI(I),UP(I),DUP(I),VP(I),DVP(I),I=1,L)
      WRITE(6,2911)
      WRITE(6,9911)(PSI(I),UVP(I),DUVP(I),TES(I),TGM(I),I=1,L)
9006  FORMAT(3(2X,F14.7))
9011  FORMAT(5(2X,F14.7))
9911  FORMAT(3(2X,F14.7),2X,F20.6,2X,F20.6)
 30   CONTINUE
      WRITE(6,1015) X ,X1
      WRITE(6,2006)
      WRITE(6,1006)  (Y(I),PSI(I),U1(I),G1(I),I=1,L)
      WRITE(6,2011)
      WRITE(6,1011)(PSI(I),UP1(I),DUP1(I),VP1(I),DVP1(I),I=1,L)
```

```
      WRITE(6,2911)
      WRITE(6,1911)(PSI(I),UVP1(I),DUVP1(I),TES1(I),TGM1(I),I=1,L)
      STOP
1015  FORMAT(5X,'******* SLNT FOR SYSTEM OF EQU. NOT CONVERGED'/
     1 5X,'STATION....X= ',F10.5/12X,'LAST STAT.  X1=  ',F10.5)
 31   XM=X*1000.0D0
      WRITE(6,1016) IAX,XM,ITRQ
      WRITE(7,1016) IAX,XM,ITRQ
 1016 FORMAT(1X,'----SLNT FOR SYS OF EQ CNVRGD;',I3,
     1 'TH STATION..X=',F10.4,'  ...ITRQ= ',I5)
      IF(MOD(IAX,IPR).NE.0) GO TO  40
      WRITE(7,3349)
      WRITE(6,3349)
      CALL PRPTY (UE,DELS,TETA)
      CALL YTRNS (UE,DELS)
3349  FORMAT(3X,'PROFILES AND PRPTY AT THIS STATION ARE PRINTED')
3006  FORMAT(4(2X,F13.7))
      WRITE(6,2006)
      WRITE(6,3006) (PSI(I),Y(I),U(I),G(I),I=1,L)
      WRITE(6,2011)
      WRITE(6,1011)(Y(I),UP(I),DUP(I),VP(I),DVP(I),I=1,L)
      WRITE(6,2911)
      WRITE(6,1911)(Y(I),UVP(I),DUVP(I),TES(I),TGM(I),I=1,L)
      CALL PLOT (UE,TETA)
      GO TO 401
 40   IF(MOD(IAX,NISO).NE.0) GO TO 401
      CALL PRPTY (UE,DELS,TETA)
      CALL YTRNS (UE,DELS)
C ***  SET INITIAL GUESS FOR NEXT  STATTION   ***
C401  IF(IAX.EQ.15) CALL TKEBL
401   DO 41 I=1,L
      U1(I)=U(I)
      G1(I)=G(I)
      TK1(I)=TK(I)
      TES1(I)=TES(I)
      TGM1(I)=TGM(I)
      UP1(I)=UP(I)
      DUP1(I)=DUP(I)
      VP1(I)=VP(I)
      DVP1(I)=DVP(I)
      UVP1(I)=UVP(I)
 41   DUVP1(I)=DUVP(I)
 777  CONTINUE
      STOP
      END
C************* SUBRT TO COMPUTE THE INTEGRAL PROPERTIES *********
      SUBROUTINE PRPTY (UE,DELS,TETA)
      IMPLICIT REAL*8(A-H,O-Z)
      COMMON /BLKMN/ U1(150),U(150),G1(150),G(150)
      COMMON /BLKY/ PSI(150),Y(150),YH(150),X,DX,X1,YP0,L
      DIMENSION CSCOF(4,200),BREAK(200),UTEM(200)
      ILEFT=1
      DLEFT=0.0D0
      IRIGHT=1
      DRIGHT=0.0D0
C3129 FORMAT(5X,'HALF WAKE LENGTH.............B=',F10.5)
      DO 21 I=1,L
21    UTEM(I)=(1-(U(I)/UE))/U(I)
```

```
      CALL DCSDEC(L,PSI,UTEM,ILEFT,DLEFT,IRIGHT,DRIGHT,BREAK,CSCOF)
      Y1=PSI(1)
      YL=PSI(L)
      LM1=L-1
      DELS=DCSITG(Y1,YL,LM1,BREAK,CSCOF)
      DO 2 I=1,L
2     UTEM(I)=(1.0/UE)*(1-(U(I)/UE))
      CALL DCSDEC(L,PSI,UTEM,ILEFT,DLEFT,IRIGHT,DRIGHT,BREAK,CSCOF)
      Y1=PSI(1)
      YL=PSI(L)
      LM1=L-1
      TETA=DCSITG(Y1,YL,LM1,BREAK,CSCOF)
      DELM=DELS*1000.0D0
      WRITE(6,10) DELM
      TETM=TETA*1000.0D0
      WRITE(6,20) TETM
      H=DELS/TETA
      WRITE(6,30)H
10    FORMAT(5X,'DSPLCMNT THCKNSS ..... DEL* =',F16.6,'(MM)')
20    FORMAT(5X,'MOMNTUM THCKNSS ..... TETA =',F16.6,'(MM)')
30    FORMAT(5X,'SHAPE FACTOR .....    H =',F16.6)
      RETURN
      END
C*************  PSI TO Y TRANSFORMATION ********************
      SUBROUTINE YTRNS (UE,DELS)
      IMPLICIT REAL*8(A-H,O-Z)
      COMMON /BLKMN/ U1(150),U(150),G1(150),G(150)
      COMMON /BLKY/ PSI(150),Y(150),YH(150),X,DX,X1,YP0,L
      DIMENSION CSCOF(4,200),BREAK(200),UTEM(200),PSTM(200)
      ILEFT=1
      DLEFT=0.0D0
      IRIGHT=1
      DRIGHT=0.0D0
      YA=YP0-DELS/2.0
      LP1=L+1
      UTEM(1)=1.0/UE
      PSTM(1)=0.0D0
      DO 3 I=1,L
      UTEM(I+1)= 1.0/U(I)
      PSTM(I+1)=PSI(I)
3     CONTINUE
      CALL DCSDEC(LP1,PSTM,UTEM,ILEFT,DLEFT,IRIGHT,
     1            DRIGHT,BREAK,CSCOF)
      Y1=PSTM(1)
      DO 4 I=1,L
      YL=PSTM(I+1)
 4    Y(I)=DCSITG(Y1,YL,L,BREAK,CSCOF)+YA
      YCL=Y(1)
      UCL=U(1)
      DO 100 I=2,L
      IF(U(I).GT.UCL)  GO TO 100
      UCL=U(I)
      YCL=Y(I)
100   CONTINUE
      UCL=UCL/UE
      WRITE(6,3119) YCL,UCL
3119  FORMAT(5X,'CNTRLIN POSITION .....YCL =',F16.6/
     1 5X,'CNTRLIN VELOCITY .....UC/UE =',F16.6)
```

```
      RETURN
      END
C||||||||||||||||||        *MNEQ*        ||||||||||||||||||||||||
      SUBROUTINE MNEQ (UE,IFLG)
      IMPLICIT REAL*8(A-H,O-Z)
      COMMON /BLKMN/ U1(150),U(150),G1(150),G(150)
      COMMON /BLKY/ PSI(150),Y(150),YH(150),X,DX,X1,YP0,L
      COMMON /BLKUVP/ UVP1(150),DUVP1(150),UVP(150),DUVP(150)
      COMMON /BLKCST/ ROW,VIC,CS,CPH1,CPH2,CES1,CES2
      DIMENSION A(3,3,150),B(3,3,150),C(3,3,150),D(3,150),R(3,150)
      N=2
C ***  TEST(IFLG); MATRIX ALREADY FORMED.
      IF(IFLG.EQ.1) GO TO 100
C ***  SET UP THE COEFICINT MATRIX ***
C ***  C-1,C-2,......C-LM1 ***
      LM1=L-1
      DO 1  J=1,LM1
      DO 11 JJ=1,2
11    C(1,JJ,J)=0.0D0
      C(2,1,J)=-2/YH(J+1)
 1    C(2,2,J)= 1.0D0
C ***  FIXED PART OF A-1, B-I, R-I  ***
      A(1,1,1)=1.0D0
      A(1,2,1)=0.0D0
      A(2,1,1)=2.0D0/YH(2)
      A(2,2,1)=1.0D0
      DO 2 J=2,L
      IF(J.EQ.L) GO TO 21
      A(2,1,J)=2.0D0/YH(J+1)
      A(2,2,J)=1.0D0
      GO TO 211
 21   A(2,1,L)=1.0D0
      A(2,2,L)=0.0D0
 211  B(2,1,J)=0.0D0
      B(2,2,J)=0.0D0
 2    CONTINUE
C ***  BOUNDARY CONDITION FOR PRESENT STATION ***
C      U(1)=UE
C      U(L)=UE
100   R(1,1)=0.0D0
      R(2,L)=0.0D0
C ***  CALCULATE THE VARYING PART OF MN EQ AND SOLVE THE EQUTIONS
     DO 101 J=2,L
      R(2,J-1)=-(G(J)+G(J-1))+(U(J)-U(J-1))*2.0D0/YH(J)
      U2D=U(J)*U(J)+U(J-1)*U(J-1)-U1(J)*U1(J)-U1(J-1)*U1(J-1)
      UM=U(J)+U(J-1)+U1(J)+U1(J-1)
      U2M=U(J)*U(J)+U(J-1)*U(J-1)+U1(J)*U1(J)+U1(J-1)*U1(J-1)
      BGD=VIC*(G(J)-G(J-1)+G1(J)-G1(J-1))
     1 -(UVP(J)/U(J))+(UVP(J-1)/U(J-1))
     1 -(UVP1(J)/U1(J))+(UVP1(J-1)/U1(J-1))
      BG2M=VIC*(G(J)*G(J)+G(J-1)*G(J-1)+G1(J)*G1(J)+G1(J-1)
     1 *G1(J-1))-((UVP(J)/U(J))*G(J)+(UVP(J-1)/U(J-1))*G(J-1)
     1 +(UVP1(J)/U1(J))*G1(J)+(UVP1(J-1)/U1(J-1))*G1(J-1))
      R(1,J)=-U2D/DX+U2M*BGD/2.0/YH(J)+UM*BG2M/4.0
      B(1,1,J)=2.0D0*U(J-1)/DX-U(J-1)*BGD/YH(J)-BG2M/4.0
      B(1,2,J)=VIC*U2M/2.0/YH(J)-(2.0*VIC*G(J-1)
     1 -(UVP(J-1)/U(J-1)))*UM/4.
      A(1,1,J)=2.0*U(J)/DX-U(J)*BGD/YH(J)-BG2M/4.0
```

```
      A(1,2,J)=-VIC*U2M/2.0/YH(J)-(2.0*VIC*G(J)
     1 -(UVP(J)/U(J)))*UM/4.0
101   CONTINUE
      CALL SOLV(A,B,C,D,R,N,L)
      DO 106 J=1,L
      G(J)=G(J)+D(2,J)
106   U(J)=U(J)+D(1,J)
      RETURN
      END
C||||||||||||||||||    *TUEQ*    ||||||||||||||||||||||||
      SUBROUTINE TUEQ (IFLG)
      IMPLICIT REAL*8(A-H,O-Z)
      COMMON /BLKMN/ U1(150),U(150),G1(150),G(150)
      COMMON /BLKY/ PSI(150),Y(150),YH(150),X,DX,X1,YP0,L
      COMMON /BLKKE/ TK1(150),TK(150)
      COMMON /BLKUP/ UP1(150),DUP1(150),UP(150),DUP(150)
      COMMON /BLKVP/ VP1(150),DVP1(150),VP(150),DVP(150)
      COMMON /BLKUVP/ UVP1(150),DUVP1(150),UVP(150),DUVP(150)
      COMMON /BLKDS/ TES1(150),TES(150),TGM1(150),TGM(150)
      COMMON /BLKCST/ ROW,VIC,CS,CPH1,CPH2,CES,CES1,CES2
      DIMENSION A(3,3,150),B(3,3,150),C(3,3,150),D(3,150),R(3,150)
     1 ,  S1(150),S2(150),S3(150),S4(150),R1(150),R2(150)
      N=2
C ***  TEST(IFLG); MATRIX ALREADY FORMED.
      IF(IFLG.EQ.1) GO TO 100
C *****  FIXED PART OF CLOUSER-EQ'S UP,VP,WP,TES  ***********
C ***   C-1,C-2,.....C-LM1 ***
      LM1=L-1
      DO 1 IL=1,LM1
      C(1,1,IL)=0.0D0
      C(1,2,IL)=0.0D0
      C(2,1,IL)=1.0D0
1     C(2,2,IL)=-YH(IL+1)/2.0D0
C ***  FIXED PART OF A-I, B-I  ***
      A(1,1,1)=1.0D0
      A(1,2,1)=0.0D0
      DO 2 IL=1,L
      IF (IL.EQ.1) GO TO  21
      B(2,1,IL)=0.0D0
      B(2,2,IL)=0.0D0
21    IF (IL.EQ.L) GO TO 2
      A(2,1,IL)=-1.0D0
      A(2,2,IL)=-YH(IL+1)/2.0D0
   2  CONTINUE
      A(2,1,L)=1.0D0
      A(2,2,L)=0.0D0
C *30* CALCULATE THE VARYING PART OF UP/EQ.  ***
100   CALL UPEQ (S1,S2,S3,S4,R1,R2)
      DO 3 I=1,L
      IF(I.EQ.1) GO TO 31
      B(1,1,I)=S2(I)
      B(1,2,I)=S1(I)
      A(1,1,I)=S4(I)
      A(1,2,I)=S3(I)
31    R(1,I)=R1(I)
      R(2,I)=R2(I)
3     CONTINUE
      CALL SOLV (A,B,C,D,R,N,L)
```

```
      DO 32 I=1,L
      UP(I)=UP(I)+D(1,I)
32    DUP(I)=DUP(I)+D(2,I)
C *40* CALCULATE THE VARYING PART OF VP/EQ.  ***
      CALL VPEQ (S1,S2,S3,S4,R1,R2)
      DO 4 I=1,L
      IF(I.EQ.1) GO TO 41
      B(1,1,I)=S2(I)
      B(1,2,I)=S1(I)
      A(1,1,I)=S4(I)
      A(1,2,I)=S3(I)
41    R(1,I)=R1(I)
      R(2,I)=R2(I)
4     CONTINUE
      CALL SOLV (A,B,C,D,R,N,L)
      DO 42 I=1,L
      VP(I)=VP(I)+D(1,I)
2     DVP(I)=DVP(I)+D(2,I)
C *50* CALCULATE THE VARYING PART OF WP/EQ.  ***
C ***  UPDATE THE T.K.E ***
      DO 59 I=1,L
 59   TK(I)=(UP(I)+VP(I))*0.75D0
C *60 * CALCULATE THE VARYING PART OF UVP/EQ.  ***
      CALL UVPEQ (S1,S2,S3,S4,R1,R2)
      DO 6 I=1,L
      IF(I.EQ.1) GO TO 61
      B(1,1,I)=S2(I)
      B(1,2,I)=S1(I)
      A(1,1,I)=S4(I)
      A(1,2,I)=S3(I)
61    R(1,I)=R1(I)
      R(2,I)=R2(I)
6     CONTINUE
      CALL SOLV (A,B,C,D,R,N,L)
      DO 62 I=1,L
      UVP(I)=UVP(I)+D(1,I)
62    DUVP(I)=DUVP(I)+D(2,I)
C *70*  CALCULATE THE VARYING PART OF TES/EQ.  ***
      CALL DEQ(S1,S2,S3,S4,R1,R2)
      DO 7 I=1,L
      IF(I.EQ.1)GO TO 71
      B(1,1,I)=S2(I)
      B(1,2,I)=S1(I)
      A(1,1,I)=S4(I)
      A(1,2,I)=S3(I)
71    R(1,I)=R1(I)
      R(2,I)=R2(I)
7     CONTINUE
      CALL SOLV (A,B,C,D,R,N,L)
      DO 72  I=1,L
      TES(I)=TES(I)+D(1,I)
72    TGM(I)=TGM(I)+D(2,I)
      RETURN
      END
C |||||||||||||||     *UP EQ*     ||||||||||||||||||||||||||
      SUBROUTINE UPEQ(S1,S2,S3,S4,R1,R2)
      IMPLICIT  REAL*8(A-H,O-Z)
C******      ALL THE COMMON STATMENTS     ***********
```

```
      COMMON /BLKMN/ U1(150),U(150),G1(150),G(150)
      COMMON /BLKY/ PSI(150),Y(150),YH(150),X,DX,X1,YP0,L
      COMMON /BLKKE/ TK1(150),TK(150)
      COMMON /BLKUP/ UP1(150),DUP1(150),UP(150),DUP(150)
      COMMON /BLKVP/ VP1(150),DVP1(150),VP(150),DVP(150)
      COMMON /BLKUVP/ UVP1(150),DUVP1(150),UVP(150),DUVP(150)
      COMMON /BLKDS/ TES1(150),TES(150),TGM1(150),TGM(150)
      COMMON /BLKCST/ ROW,VIC,CS,CPH1,CPH2,CES,CES1,CES2
      DIMENSION S1(150),S2(150),S3(150),S4(150),R1(150),R2(150)
C******         BOUNDARY CONDITIONS          *************
      R1(1)=0.0D0
      R2(L)=0.0D0
C********     CALCULATION OF VARIABLES     *************
      DO 1 J=2,L
      UM=(U(J)+U(J-1)+U1(J)+U1(J-1))/4.0
      U2M=(U(J)*U(J)+U(J-1)*U(J-1)+U1(J)*U1(J)+U1(J-1)
     1     *U1(J-1))/4.0
      GM=(G(J)+G(J-1)+G1(J)+G1(J-1))/4.0D0
      UMGM=UM*GM
      R1(J)=-(UM/2.0/DX)*(UP(J)+UP(J-1)-UP1(J)-UP1(J-1))
     1 +U2M*((CS*TK(J)*VP(J)/TES(J))*DUP(J)-(CS*TK(J-1)*VP(J-1)
     2 /TES(J-1))*DUP(J-1)
     3 +(CS*TK1(J)*VP1(J)/TES1(J))*DUP1(J)-(CS*TK1(J-1)*VP1(J-1)
     4 /TES1(J-1))*DUP1(J-1))/2.0/YH(J)
     5 +UMGM*((CS*TK(J)*VP(J)/TES(J))*DUP(J)+(CS*TK(J-1)*VP(J-1)
     6 /TES(J-1))*DUP(J-1)
     7 +(CS*TK1(J)*VP1(J)/TES1(J))*DUP1(J)+(CS*TK1(J-1)*VP1(J-1)
     8 /TES1(J-1))*DUP1(J-1))/4.0
     9 +((2./3.)*(CPH1-1)*TES(J)+(4.*CPH2/3.-2.)*UVP(J)
     $ *U(J)*G(J)-(CPH1*TES(J)/TK(J))*UP(J)
     1 +(2./3.)*(CPH1-1)*TES(J-1)+(4.*CPH2/3.-2.)*UVP(J-1)
     2 *U(J-1)*G(J-1)-(CPH1*TES(J-1)/TK(J-1))*UP(J-1)
     3 +(2./3.)*(CPH1-1)*TES1(J)+(4.*CPH2/3.-2.)*UVP1(J)
     4 *U1(J)*G1(J)-(CPH1*TES1(J)/TK1(J))*UP1(J)
     5 +(2./3.)*(CPH1-1)*TES1(J-1)+(4.*CPH2/3.-2)*UVP1(J-1)
     6 *U1(J-1)*G1(J-1)-(CPH1*TES1(J-1)/TK1(J-1))*UP1(J-1))/4.0D0
      R2(J-1)= -UP(J)+UP(J-1)+YH(J)*(DUP(J-1)+DUP(J))/2.0D0
      S1(J)=(U2M/2.0/YH(J)-UMGM/4.0)*(CS*TK(J-1)*VP(J-1)/TES(J-1))
      S2(J)=UM/2.0/DX+CPH1*TES(J-1)/TK(J-1)/4.0
      S3(J)=-(U2M/2.0/YH(J)+UMGM/4.0)*(CS*TK(J)*VP(J)/TES(J))
      S4(J)=UM/2.0/DX+CPH1*TES(J)/TK(J)/4.0
 1    CONTINUE
      RETURN
      END
C ||||||||||||||||     *VP EQ*     ||||||||||||||||||||||||||
      SUBROUTINE VPEQ(S1,S2,S3,S4,R1,R2)
      IMPLICIT  REAL*8(A-H,O-Z)
C******      ALL THE COMMON STATMENTS     ***********
      COMMON /BLKMN/ U1(150),U(150),G1(150),G(150)
      COMMON /BLKY/ PSI(150),Y(150),YH(150),X,DX,X1,YP0,L
      COMMON /BLKKE/ TK1(150),TK(150)
      COMMON /BLKUP/ UP1(150),DUP1(150),UP(150),DUP(150)
      COMMON /BLKVP/ VP1(150),DVP1(150),VP(150),DVP(150)
      COMMON /BLKUVP/ UVP1(150),DUVP1(150),UVP(150),DUVP(150)
      COMMON /BLKDS/ TES1(150),TES(150),TGM1(150),TGM(150)
      COMMON /BLKCST/ ROW,VIC,CS,CPH1,CPH2,CES,CES1,CES2
      DIMENSION S1(150),S2(150),S3(150),S4(150),R1(150),R2(150)
C******         BOUNDARY CONDITIONS          *************
```

```
      R1(1)=0.0D0
      R2(L)=0.0D0
      DO 1 J=2,L
      UM=(U(J)+U(J-1)+U1(J)+U1(J-1))/4.0
     U2M=(U(J)*U(J)+U(J-1)*U(J-1)+U1(J)*U1(J)+U1(J-1)*U1(J-1))/4.0
      GM=(G(J)+G(J-1)+G1(J)+G1(J-1))/4.0D0
      UMGM=UM*GM
      R1(J)=-(UM/2.0/DX)*(VP(J)+VP(J-1)-VP1(J)-VP1(J-1))
     1 +U2M*((CS*TK(J)*VP(J)/TES(J))*DVP(J)-(CS*TK(J-1)*VP(J-1)
     2 /TES(J-1))*DVP(J-1)
     3 +(CS*TK1(J)*VP1(J)/TES1(J))*DVP1(J)-(CS*TK1(J-1)*VP1(J-1)
     4 /TES1(J-1))*DVP1(J-1))/2.0/YH(J)
     5 +UMGM*((CS*TK(J)*VP(J)/TES(J))*DVP(J)+(CS*TK(J-1)*VP(J-1)
     6 /TES(J-1))*DVP(J-1)
     7 +(CS*TK1(J)*VP1(J)/TES1(J))*DVP1(J)+(CS*TK1(J-1)*VP1(J-1)
     8 /TES1(J-1))*DVP1(J-1))/4.0
     9 +((2./3.)*(CPH1-1)*TES(J)-(2./3.)*CPH2*UVP(J)
     $ *U(J)*G(J)-(CPH1*TES(J)/TK(J))*VP(J)
     1 +(2./3.)*(CPH1-1)*TES(J-1)-(2./3.)*CPH2*UVP(J-1)
     2 *U(J-1)*G(J-1)-(CPH1*TES(J-1)/TK(J-1))*VP(J-1)
     3 +(2./3.)*(CPH1-1)*TES1(J)-(2./3.)*CPH2*UVP1(J)
     4 *U1(J)*G1(J)-(CPH1*TES1(J)/TK1(J))*VP1(J)
     5 +(2./3.)*(CPH1-1)*TES1(J-1)-(2./3.)*CPH2*UVP1(J-1)
     6 *U1(J-1)*G1(J-1)-(CPH1*TES1(J-1)/TK1(J-1))*VP1(J-1))/4.0D0
      R2(J-1)= -VP(J)+VP(J-1)+YH(J)*(DVP(J)+DVP(J-1))/2.0D0
      S1(J)=(U2M/2./YH(J)-UMGM/4.)*(CS*TK(J-1)*VP(J-1)/TES(J-1))
      S2(J)= UM/2.0/DX+(U2M/2./YH(J)-UMGM/4.)*(CS*TK(J-1)*DVP(J-1)
     1 /TES(J-1))+CPH1*TES(J-1)/TK(J-1)/4.0
      S3(J)=-(U2M/2./YH(J)+UMGM/4.)*(CS*TK(J)*VP(J)/TES(J))
      S4(J)= UM/2.0/DX-(U2M/2./YH(J)+UMGM/4.)*(CS*TK(J)*DVP(J)
     1 /TES(J))+CPH1*TES(J)/TK(J)/4.0
 1    CONTINUE
      RETURN
      END
C |||||||||||||||      *WP EQ*      ||||||||||||||||||||||||||
C                 WPEQ WOULD BE WRITTEN HERE
C |||||||||||||||      *UVP EQ*      ||||||||||||||||||||||||||
      SUBROUTINE UVPEQ(S1,S2,S3,S4,R1,R2)
      IMPLICIT  REAL*8(A-H,O-Z)
C******      ALL THE COMMON STATMENTS      ***********
      COMMON /BLKMN/ U1(150),U(150),G1(150),G(150)
      COMMON /BLKY/ PSI(150),Y(150),YH(150),X,DX,X1,YP0,L
      COMMON /BLKKE/ TK1(150),TK(150)
      COMMON /BLKUP/ UP1(150),DUP1(150),UP(150),DUP(150)
      COMMON /BLKVP/ VP1(150),DVP1(150),VP(150),DVP(150)
      COMMON /BLKUVP/ UVP1(150),DUVP1(150),UVP(150),DUVP(150)
      COMMON /BLKDS/ TES1(150),TES(150),TGM1(150),TGM(150)
      COMMON /BLKCST/ ROW,VIC,CS,CPH1,CPH2,CES,CES1,CES2
      DIMENSION S1(150),S2(150),S3(150),S4(150),R1(150),R2(150)
C******        BOUNDARY CONDITIONS        *************
      R1(1)=0.0D0
      R2(L)=0.0D0
C ************ CALCULATION OF VARIABLES ************************
      DO 1 J=2,L
      UM=(U(J)+U(J-1)+U1(J)+U1(J-1))/4.0
      U2M=(U(J)*U(J)+U(J-1)*U(J-1)+U1(J)*U1(J)+
     1      U1(J-1)*U1(J-1))/4.0
      GM=(G(J)+G(J-1)+G1(J)+G1(J-1))/4.0D0
```

```
      UMGM=UM*GM
      R1(J)=-(UM/2.0/DX)*(UVP(J)+UVP(J-1)-UVP1(J)-UVP1(J-1))
     1 +U2M*((CS*TK(J)*VP(J)/TES(J))*DUVP(J)-(CS*TK(J-1)*VP(J-1)
     2 /TES(J-1))*DUVP(J-1)
     3 +(CS*TK1(J)*VP1(J)/TES1(J))*DUVP1(J)-(CS*TK1(J-1)*VP1(J-1)
     4 /TES1(J-1))*DUVP1(J-1))/2.0/YH(J)
     5 +UMGM*((CS*TK(J)*VP(J)/TES(J))*DUVP(J)+(CS*TK(J-1)*VP(J-1)
     6 /TES(J-1))*DUVP(J-1)
     7 +(CS*TK1(J)*VP1(J)/TES1(J))*DUVP1(J)+(CS*TK1(J-1)*VP1(J-1)
     8 /TES1(J-1))*DUVP1(J-1))/4.0
     9 +((CPH2-1.)*VP(J)*U(J)*G(J)-(CPH1*TES(J)/TK(J))*UVP(J)
     $ +(CPH2-1.)*VP(J-1)*U(J-1)*G(J-1)-(CPH1*TES(J-1)/TK(J-1))*
     1 UVP(J-1)+(CPH2-1.)*VP1(J)*U1(J)*G1(J)-(CPH1*TES1(J)
     2 /TK1(J))*UVP1(J)+(CPH2-1.)*VP1(J-1)*U1(J-1)*G1(J-1)
     3 -(CPH1*TES1(J-1)/TK1(J-1))*UVP1(J-1))/4.0
      R2(J-1)= -UVP(J)+UVP(J-1)+YH(J)*(DUVP(J)+DUVP(J-1))/2.0D0
      S1(J)=(U2M/2./YH(J)-UMGM/4.)*(CS*TK(J-1)*VP(J-1)/TES(J-1))
      S2(J)= UM/2./DX+CPH1*TES(J-1)/TK(J-1)/4.0
      S3(J)=-(U2M/2./YH(J)+UMGM/4.)*(CS*TK(J)*VP(J)/TES(J))
      S4(J)= UM/2.0/DX+CPH1*TES(J)/TK(J)/4.0
 1    CONTINUE
      RETURN
      END
C ||||||||||||||||||||      *DEQ*  ||||||||||||||||||||||||||||
      SUBROUTINE DEQ(S1,S2,S3,S4,R1,R2)
      IMPLICIT  REAL*8(A-H,O-Z)
C*****       ALL THE COMMON STATMENTS     ***********
      COMMON /BLKMN/ U1(150),U(150),G1(150),G(150)
      COMMON /BLKY/ PSI(150),Y(150),YH(150),X,DX,X1,YP0,L
      COMMON /BLKKE/ TK1(150),TK(150)
      COMMON /BLKUP/ UP1(150),DUP1(150),UP(150),DUP(150)
      COMMON /BLKVP/ VP1(150),DVP1(150),VP(150),DVP(150)
      COMMON /BLKUVP/ UVP1(150),DUVP1(150),UVP(150),DUVP(150)
      COMMON /BLKDS/ TES1(150),TES(150),TGM1(150),TGM(150)
      COMMON /BLKCST/ ROW,VIC,CS,CPH1,CPH2,CES,CES1,CES2
      DIMENSION S1(150),S2(150),S3(150),S4(150),R1(150),R2(150)
C  *****       BOUNDARY CONDITIONS         *************
      R1(1)=0.0D0
      R2(L)=0.0D0
C********       CALCULATION OF VARIABLES      ***********
      DO 1 J=2,L
      UM=(U(J)+U(J-1)+U1(J)+U1(J-1))/4.0
      U2M=(U(J)*U(J)+U(J-1)*U(J-1)+U1(J)*U1(J)+U1(J-1)
     1     *U1(J-1))/4.0
      GM=(G(J)+G(J-1)+G1(J)+G1(J-1))/4.0D0
      UMGM=UM*GM
      R1(J)=-(UM/2.0/DX)*(TES(J)+TES(J-1)-TES1(J)-TES1(J-1))
     1 +U2M*((CES*TK(J)*VP(J)/TES(J))*TGM(J)-(CES*TK(J-1)*VP(J-1)
     2 /TES(J-1))*TGM(J-1)
     3 +(CES*TK1(J)*VP1(J)/TES1(J))*TGM1(J)-(CES*TK1(J-1)*VP1(J-1)
     4 /TES1(J-1))*TGM1(J-1))/2.0/YH(J)
     5 +UMGM*((CES*TK(J)*VP(J)/TES(J))*TGM(J)+(CES*TK(J-1)*VP(J-1)
     6 /TES(J-1))*TGM(J-1)
     7 +(CES*TK1(J)*VP1(J)/TES1(J))*TGM1(J)+(CES*TK1(J-1)*VP1(J-1)
     8 /TES1(J-1))*TGM1(J-1))/4.0
     9 +(-(CES1*UVP(J)*U(J)*G(J)/TK(J))*TES(J)
     $ -(CES2/TK(J))*TES(J)*TES(J)
     1 -(CES1*UVP(J-1)*U(J-1)*G(J-1)/TK(J-1))*TES(J-1)
```

```
     2 -(CES2/TK(J-1))*TES(J-1)*TES(J-1)
     3 -(CES1*UVP1(J)*U1(J)*G1(J)/TK1(J))*TES1(J)
     4 -(CES2/TK1(J))*TES1(J)*TES1(J)
     5 -(CES1*UVP1(J-1)*U1(J-1)*G1(J-1)/TK1(J-1))*TES1(J-1)
     6 -(CES2/TK1(J-1))*TES1(J-1)*TES1(J-1))/4.0D0
       R2(J-1)= -TES(J)+TES(J-1)+YH(J)*(TGM(J-1)+TGM(J))/2.0D0
       S1(J)=(U2M/2./YH(J)-UMGM/4.0)*(CES*TK(J-1)*VP(J-1)/TES(J-1))
       S2(J)= UM/2.0/DX+(CES1*UVP(J-1)*U(J-1)*G(J-1)/TK(J-1))/4.0
     1 +(CES2/TK(J-1))*TES(J-1)/2.0
       S3(J)=-(U2M/2./YH(J)+UMGM/4.0)*(CES*TK(J)*VP(J)/TES(J))
       S4(J)= UM/2.0/DX+(CES1*UVP(J)*U(J)*G(J)/TK(J))/4.0
     1 +(CES2/TK(J))*TES(J)/2.0
 1     CONTINUE
       RETURN
       END
C||||||||||||||||||||   *SOLVE*      ||||||||||||||||||||||||||
       SUBROUTINE SOLV(A,B,C,D,R,N,L)
       IMPLICIT REAL*8(A-H,O-Z)
       DIMENSION A(3,3,150),B(3,3,150),C(3,3,150),D(3,150)
     1 ,R(3,150),DEL(3,3,150),GAM(3,3,150),W(3,150)
     2 ,DELT(3,3),BT(3,3),T2(3),WK(25)
C-------------------------------------------------------------
C       1.  FORWARD SWEEP
C-------------------------------------------------------------
C ***  DEL 0  ***
       DO 11 I=1,N
       DO 11 J=1,N
 11    DEL(I,J,1)=A(I,J,1)
C ***  DEL'J  AND GAM'J ***
       DO 1 IL=2,L
C ***  SOLVE GAM'J BASED ON DEL'J-1 AND B'J ***
       DO 12 I=1,N
       DO 12 J=1,N
       DELT(I,J)=DEL(I,J,IL-1)
12     GAM(I,J,IL)=0.0D0
       CALL DLINRG(N,DELT,3,BT,3)
       DO 13 I=1,N
       DO 13 J=1,N
       DO 13 IJ=1,N
13     GAM(I,J,IL)=GAM(I,J,IL)+B(I,IJ,IL)*BT(IJ,J)
C ***  PREPARE FOR GAM'J*C'J-1 ***
       DO 113 I=1,N
       DO 113 J=1,N
113    BT(I,J)=0.0D0
       DO 14 I=1,N
       DO 14 J=1,N
       DO 14 IJ=1,N
 14    BT(I,J)=BT(I,J)+GAM(I,IJ,IL)*C(IJ,J,IL-1)
       DO 15 I=1,N
       DO 15 J=1,N
 15    DEL(I,J,IL)=A(I,J,IL)-BT(I,J)
 1      CONTINUE
C-------------------------------------------------------------
C            2.  CALCULATION OF W'J
C-------------------------------------------------------------
C ***    W'0=R'0  ***
        DO 21 I =1,N
21      W(I,1)=R(I,1)
```

```
C ***    W'I = R'I-GAM'I*W'I-1 ***
         DO 2 IL=2,L
C ***    PREPER FOR GAM'I * W'I-1 ***
         DO 22 I=1,N
22       T2(I)=0.0D0
         DO 23 I=1,N
         DO 23 II=1,N
23       T2(I)=GAM(I,II,IL)*W(II,IL-1)+T2(I)
C ***    W'I=R'I-GAM'I*W'I-1 ***
         DO 24 I=1,N
24       W(I,IL)=R(I,IL)-T2(I)
2        CONTINUE
C-------------------------------------------------------------
C           3.  BACKWARD STEP TO CALCULATE D'I
C-------------------------------------------------------------
C ***    DEL'L*D'L=W'L    ***
         DO 31 I=1,N
31       T2(I)=W(I,L)
         DO 32 I=1,N
         DO 32 J=1,N
 32      DELT(I,J)=DEL(I,J,L)
         CALL DLSARG(N,DELT,3,T2,1,WK)
         DO 33 I=1,N
 33      D(I,L)=WK(I)
C ***    CONTINUE BACK STEP FOR D'L-1,D'L-2,.......D'1 ***
         LM1=L-1
         DO 3 LL=1,LM1
         IL=L-LL
C  ***   DEL'I*D'I=W'I-C'I*D'I+1   ***
C  ***   PREPER FOR C'I*D'I   ***
         DO 34 I=1,N
 34      T2(I)=0.0D0
         DO 35 I=1,N
         DO 35 II=1,N
 35      T2(I)=C(I,II,IL)*D(II,IL+1)+T2(I)
         DO 37 I=1,N
         T2(I)=W(I,IL)-T2(I)
         DO 37 J=1,N
37       DELT(I,J)=DEL(I,J,IL)
         CALL DLSARG(N,DELT,3,T2,1,WK)
         DO 38 I=1,N
 38      D(I,IL)=WK(I)
 3       CONTINUE
         RETURN
         END
        SUBROUTINE PLOT(UE,TETA)
C******SUBROUTINE TO PREPER DATA FOR PLOTING
        IMPLICIT REAL*8(A-H,O-Z)
        COMMON /BLKMN/ U1(150),U(150),G1(150),G(150)
        COMMON /BLKY/ PSI(150),Y(150),YH(150),X,DX,X1,YP0,L
        COMMON /BLKKE/ TK1(150),TK(150)
        COMMON /BLKUP/ UP1(150),DUP1(150),UP(150),DUP(150)
        COMMON /BLKVP/ VP1(150),DVP1(150),VP(150),DVP(150)
        COMMON /BLKUVP/ UVP1(150),DUVP1(150),UVP(150),DUVP(150)
        COMMON /BLKDS/ TES1(150),TES(150),TGM1(150),TGM(150)
        COMMON /BLKCST/ ROW,VIC,CS,CPH1,CPH2,CES,CES1,CES2
        XMM=X*1000
        WRITE(9,30)XMM
```

```
      WRITE(9,20)
      DO 1 I=1,L
      YMM=Y(I)*1000
      UND=U(I)/UE
      UVBAR= (UVP(I)/UE/UE)*1000
      U2BAR=(UP(I)/UE/UE)*100
      V2BAR=(VP(I)/UE/UE)*100
      EPS=((TES(I)*0.005401)/(UE**3))*10000
      WRITE(9,10)YMM,UND,U2BAR,V2BAR,UVBAR,EPS
10    FORMAT(6(1X,F9.4))
1     CONTINUE
20    FORMAT(4X,'"Y MM"',4X,'"U/UE"',4X,'"U2BAR"',4X,'"V2BAR"',3X
     1 ,'"UVBAR"',3X,'"EPS"')
30    FORMAT(3X,'"X(MM) =" ',F10.4)
      RETURN
      END
      SUBROUTINE TKEBL
      IMPLICIT REAL*8(A-H,O-Z)
      COMMON /BLKMN/ U1(150),U(150),G1(150),G(150)
      COMMON /BLKY/ PSI(150),Y(150),YH(150),X,DX,X1,YP0,L
      COMMON /BLKKE/ TK1(150),TK(150)
      COMMON /BLKUP/ UP1(150),DUP1(150),UP(150),DUP(150)
      COMMON /BLKVP/ VP1(150),DVP1(150),VP(150),DVP(150)
      COMMON /BLKUVP/ UVP1(150),DUVP1(150),UVP(150),DUVP(150)
      COMMON /BLKDS/ TES1(150),TES(150),TGM1(150),TGM(150)
      COMMON /BLKCST/ ROW,VIC,CS,CPH1,CPH2,CES,CES1,CES2
      XBM=1000.0D0*(X+X1)/2.0D0
      WRITE(6,100)XBM
100   FORMAT(5X,'"TRBU. KINETIC ENERGY BALANC, AT X="',F10.5/
     1 6X,'"Y"',10X,'"ADV"',13X,'"DIF"',11X,'"PRD"',10X,'"DIS"')
      DO 1 J=2,L
      UM=(U(J)+U(J-1)+U1(J)+U1(J-1))/4.0
      U2M=(U(J)*U(J)+U(J-1)*U(J-1)+U1(J)*U1(J)+U1(J-1)
     1 *U1(J-1))/4.0
      GM=(G(J)+G(J-1)+G1(J)+G1(J-1))/4.0D0
      UMGM=UM*GM
      ADV=0.75D0*(UM/2.0/DX)*(UP(J)+UP(J-1)-UP1(J)-UP1(J-1)
     1 +VP(J)+VP(J-1)-VP1(J)-VP1(J-1))
      DIF=
     1 +U2M*((CS*TK(J)*VP(J)/TES(J))*DUP(J)-(CS*TK(J-1)*VP(J-1)
     2 /TES(J-1))*DUP(J-1)
     3 +(CS*TK1(J)*VP1(J)/TES1(J))*DUP1(J)-(CS*TK1(J-1)*VP1(J-1)
     4 /TES1(J-1))*DUP1(J-1))/2.0/YH(J)
     5 +UMGM*((CS*TK(J)*VP(J)/TES(J))*DUP(J)+(CS*TK(J-1)*VP(J-1)
     6 /TES(J-1))*DUP(J-1)
     7 +(CS*TK1(J)*VP1(J)/TES1(J))*DUP1(J)+(CS*TK1(J-1)*VP1(J-1)
     8 /TES1(J-1))*DUP1(J-1))/4.0
     1 +U2M*((CS*TK(J)*VP(J)/TES(J))*DVP(J)-(CS*TK(J-1)*VP(J-1)
     2 /TES(J-1))*DVP(J-1)
     3 +(CS*TK1(J)*VP1(J)/TES1(J))*DVP1(J)-(CS*TK1(J-1)*VP1(J-1)
     4 /TES1(J-1))*DVP1(J-1))/2.0/YH(J)
     5 +UMGM*((CS*TK(J)*VP(J)/TES(J))*DVP(J)+(CS*TK(J-1)*VP(J-1)
     6 /TES(J-1))*DVP(J-1)
     7 +(CS*TK1(J)*VP1(J)/TES1(J))*DVP1(J)+(CS*TK1(J-1)*VP1(J-1)
     8 /TES1(J-1))*DVP1(J-1))/4.0
      PRD=
     $ (-UVP(J)*U(J)*G(J)-UVP(J-1)*U(J-1)*G(J-1)
     $ -UVP1(J)*U1(J)*G1(J)-UVP1(J-1)*U1(J-1)*G1(J-1))/4.0D0
```

```
      DIS=-(TES(J)+TES(J-1)+TES1(J)+TES(J-1))/4.0D0
      YB=1000.0D0*(Y(J)+Y(J-1))/2.0D0
 1    WRITE(6,200)YB,ADV,DIF,PRD,DIS
200   FORMAT(5(1X,E14.7))
      RETURN
      END
      SUBROUTINE FSTCAL(X1,X,FU2,FV2,FEPS)
      IMPLICIT REAL*8(A-H,O-Z)
C **** THIS PROGRAM CALCULATES F S T (RS)
C     FST(1): U2B
C     FST(2): V2B
C     FST(3): EPS
C     W2B=0.5*(U2B+V2B)
C **** EK=0.5*(U2B+V2B+W2B)< WITH ABOVE ASUMPTION >=0.75*(U2B+V2B)
      EXTERNAL FCN, DIVPRK, DSET
      PARAMETER (NEQ=3)
      DIMENSION FST(5), PARM(50)
C     ERROR TOLERANCE < FOR IMSL ROUTINE >
      TOL=0.000001D0
C     SET PARAMETER TO DEFAULT < IMSL ROUTINE >
      CALL DSET(50, 0.0D0, PARM, 1)
      PARM(10)=1.0D0
      IDO=1
      XBEG=X1
      XEND=X
      FST(1)=FU2
      FST(2)=FV2
      FST(3)=FEPS
      CALL DIVPRK(IDO,NEQ,FCN,XBEG,XEND,TOL,PARM,FST)
      IDO=3
      CALL DIVPRK(IDO,NEQ,FCN,XBEG,XEND,TOL,PARM,FST)
      FU2=FST(1)
      FV2=FST(2)
      FEPS=FST(3)
      RETURN
      END
C *** SUBROUTINE FCN  ****
      SUBROUTINE FCN(NEQ, X, FST, FSTPRM)
      IMPLICIT REAL*8(A-H,O-Z)
      COMMON /BLKCST/ ROW,VIC,CS,CPH1,CPH2,CES,CES1,CES2
      DIMENSION FST(5), FSTPRM(5)
      EK= 0.75*(FST(1)+FST(2))
      U=22.5D0
      FSTPRM(1)=-(2.0*FST(3)/3.0+CPH1*(FST(3)/EK)*
     1           (FST(1)-2.*EK/3.))/U
      FSTPRM(2)=-(2.0*FST(3)/3.0+CPH1*(FST(3)/EK)*(FST(2)-2.
     1          *EK/3.))/U
      FSTPRM(3)=-(CES2*FST(3)*FST(3)/EK)/U
      RETURN
      END
```

REFERENCES

1. Hah, C. and Lakshminarayana, B., " Measurement and Prediction of Mean Velocity and Turbulence Structure in the Near Wake of an Airfoil", J.F.M., Vol. 115, 1982, pp. 251-282.

2. Raj, R. and Lakshminarayana, B., "Characteristics of the Wakes behind a Cascade of Airfoils", J.F.M. , Vol. 61, 1973, pp. 707-730.

3. Bradshaw, P., "Effect of Streamline Curvature on Turbulent Flow", AGARD, Report No. AG-169, 1973.

4. Goldstein, S., " On the Two-Dimensional Steady Flow of a Viscous Fluid Behind a Solid Body-I.", Proc. of the Royal Society of London Series A, Vol. 142, 1933, pp. 545-562.

5. Berger, S.A., Laminar Wakes, American Elsevier, New York, 1971

6. Schlichting, H., Boundary Layer Theory, McGraw-Hill , 1968.

7. Tennekes, H. and Lumley, J. L., A First Course in Turbulence, MIT Press 1980.

8. Raj, R., "On the Investigation of Cascade and Turbomachinery Rotor Wake Characteristics", Ph.D. Thesis, Dept. of Aerospace Engineering, The Pennsylvania State University, 1974.

9. Robinson, J. L., "Similarity Solution in Several Turbulent Shear Flows", NPL Report 1242, 1967.

10. Alber, I.E., "Turbulent Wake of a Thin, Flat Plate", AIAA Journal, Vol.

18, No. 9, Sep. 1980, pp. 1044-1051.

11. Bogucz, E.A. and Walker, J.D.A., "The turbulent Near Wake at a Sharp Trailing Edge", J.F.M., Vol. 196, 1988, pp. 555-584.

12. Page, R.H. and Ostowari, C., "Turbulent Near Wake of a Symmetrical Body", AIAA Journal, Vol. 26, No. 1, Jan. 1988, pp. 115-117.

13. Andreopoulos, J. and Bradshaw, P., "Measurements of Interacting Turbulent Shear Layers in the Near Wake of a Flat Plate", J.F.M., Vol. 100., 1980, pp. 639-668.

14. Ramaprian, B. R. , Patel, V. C. and Sastry, M. S. ," The Symmetric Turbulent Wake of a Flat Plate", AIAA Journal, Vol. 20, No. 8, Sep. 1982, pp. 1228-1235.

15. Nakayama, A. and Liu, B., "The Turbulent Near Wake of a Flat Plate at Low Reynolds Number", J.F.M., Vol 217, 1990, pp. 93-114.

16. Sastry, M. S., "Turbulent Wake Behind Streamlined Bodies" Ph.D. Thesis, University of Iowa, 1981.

17. Nakayama, A., "Curvature and Pressure-Gradient Effects on a Small-Defect Wake", J.F.M., Vol. 175, 1987, pp. 215-246.

18. Ramjee, V., Tulapurkara, E.G. and Rajasekar, R.," Development of Airfoil Wake in a Longitudinally Curved Stream", AIAA Journal, Vol. 26, No. 8, Aug. 1988, pp. 948-953.

19. Browne,L.W.B., Antonia, R.A. and Shah, D.A.," Turbulent Energy Dissipation in a Wake", J.F.M., Vol. 179, 1987, pp. 307-326.

20. Park, S.O., Kim, J.S. and Lee, B.I., "Hot-Wire Measurements of Near Wakes Behind an Oscillating Airfoil", AIAA Journal, Vol. 28, No. 1, Jan. 1990, pp. 22-28.

21. Engleson, P. S., Huval, C. J. and Perkins, F. E., "Turbulence in the Early Wake of a Fixed Flat Plate" , MIT Hydrodynamics Lab., TR. No. 46, Feb. 1961

22. Komoda, H., "On the Effect of Free Stream Turbulence on the Structure of Turbulent Wake", J. Japan Society, Areo. Eng., Oct. 1957, pp. 247-279.

23. Symes, C.R. and Fink, L.E., "Effects of External Turbulence Upon the Flow Past Cylinders", Lecture Notes in Physics, Structure and Mechanism of Turbulence, Edited by H. Fielder, Proceedings , Berlin 1977, Springer -Verlag, New York 1978, pp. 86-102.

24. Pal,S., "Wake-Boundary Layer Interaction in Turbomachinery", Ph.D. Thesis, Dept. of Mechanical Engineering, The City College of City University of New York , 1981.

25. Chandrsuda, C., Mehta, R.D., Wier, A.D., Bradshaw, P., "Effect of Free Stream Turbulence on Large Structure in Turbulent Mixing Layers", J.F.M., Vol. 85, 1978, pp. 693-704.

26. Cimbala, J.M. and Kerin, M.V., "Effect of Free Stream Conditions on the Far Wake of a Circular Cylinder", AIAA Journal, Vol. 28, No.8, Aug. 1990, pp. 1369-1373.

27. Pal, S. and Raj, R., " Wake Behavior in the Presence of Free Stream Turbulence ", J. of Eng. for Power, Vol. 103, No. 3, Jul. 1981, pp. 490-498.

28. Pal, S. and Raj, R., "Characteristics of Wake Turbulence Due to Free Stream Turbulence Environment", AIAA/SAE/ASME 16th Joint Propulsion Conference, Paper No. AIAA-80-1079, 1980.

29. Ardebili, M., Hazarika, B.K. and Raj. R., "The Separated and Non-Separated Airfoil Wake in the Presence of Free Stream Turbulence", AIAA Third Applied Aerodynamics Conference, AIAA Paper No. 85-5027, 1985.

30. Ahmed, Q.A., Luxton, R.E. and Antoina, R.A., "The Behavior of a Two-Dimensional Wake in a Uniformly Sheared Turbulent Flow", J. of Appl. Mech., June, 1975, pp. 283-288.

31. Kiya, M., Suzuki, Y., Arie, M. and Hagino, M., "A Contribution to the Free Stream Turbulence Effect on the Flow Past a Circular Cylinder", J.F.M., Vol. 115, 1982, pp. 151-164.

32. Gorla, R. S. R., "Effects of Unsteady Free Stream Velocity and Free Stream Turbulence at a Stagnation Point", ASME Paper No. 82-GT/69, 1982.

33. Hah, C. and Lakshminarayana, B., "Free Stream Turbulence Effects on the Development of Rotor Wake", AIAA 13th Fluid and Plasma Dynamics Conf., Paper No. AIAA-80-1431, July, 1980.

34. Evans, L.R. ,"Computation of Unsteady Laminar Boundary Layers Subject to Traveling Wave Free Stream Fluctuations", AIAA Journal, Vol. 27, No. 8, Nov. 1989, pp. 1644-1646.

35. Liu, X. and Rodi, W., " Experiments on Transitional Boundary Layers with Wake-Induced Unsteadiness", J.F.M., Vol. 231, 1991, pp. 229-256.

36. Bandyopadhyay, P. R., "Reynolds Number Dependence of the Free Stream Turbulence Effects on Turbulent Boundary Layers", AIAA Journal, Vol. 30, No. 7, Jul. 1992, pp. 1901-1912.

37. Pope, S.B. and Whitelaw, J.H., "The Calculation of Near-Wake Flows", J.F.M., Vol. 73, 1976, pp. 9-32.

38. Patel, V.C. and Scheuerer, G., "Calculation of Two-Dimensional Near and Far Wakes", AIAA Journal, Vol. 20, No. 7, July 1982, pp. 900-907.

39. Ricklefs, U., Fink, L.E., and Symes, C.R., "Prediction of the Wake Behind Circular Cylinder in Nearly Homogeneous Turbulent Streams", Proceeding of First International Conference on Numerical Methods in Laminar and Turbulent Flow, Sawnesea, 1978, pp. 301-315.

40. Launder, B.E., Morse, A., Rodi, W. and Spalding, D.B., " The Prediction of Free Shear Flows - a Comparison of the Performance of Six Turbulent Models", NASA- Langly Conference on Free Shear Flows, Hampton, Virginia, 1972.

41. Gorla, R.S.R., "Effect of Free Stream Turbulence on Flow Separation", International Journal of Turbo and Jet Engines, Vol. 2, 1985, pp. 293-298.

42. Rodi, W., Scheuerer, G., "Calculation of Turbulent Boundary Layers Under the Effects of Free Stream Turbulence", Proceeding of Fifth Turbulent Shear Flow, Cornell University, 1985, pp. 2.19-2.25.

43. Chang, K.C., Bui,M.N., Cebeci, T. and Whitelaw, J.H., "The Calculation of Turbulent Wakes.", AIAA Journal, Vol. 24, No. 2, Feb., 1986, pp. 200-201.

44. Lakshminarayana, B. and Zhang, J., " Analysis of Three-Dimensional Turbulent Wakes by a Momentum Integral Technique", AIAA Journal, Vol. 26, No. 6, Jun. 1988, pp. 661-668.

45. Horstman, C.C., "Numerical Simulation of Turbulent Trailing Edge Flows", Proceeding of Symposium on "Numerical and Physical Aspect of Aerodynamic Flows II", Edited by T. Cebeci, 1983, pp. 113-124.

46. Chen, H.C. and Patel, V.C., "Laminar Flow at the Trailing Edge of a Flat Plate", AIAA Journal, Vol. 25, No. 7, July 1987, pp. 920-928.

47. Agoropoulos, D., and Squire, L.C.," Interaction Between Turbulent Wakes and Boundary Layers", AIAA Journal, Vol. 26, No. 10, Oct. 1988, pp. 1194-1200.

48. Khodadadi, J.M. and Vlachos, N.S., "Effects of Turbulence Model Constants on Computation of Confined Swirling Flows", AIAA Journal, Vol. 28, No. 4, Apr. 1990, 750-752.

49. Bradshaw, P., Cebeci, T. and Whitelaw, J.H., Engineering Calculation Methods for Turbulent Flow, Academic Press, 1981.

50. Launder, B.E. and Spalding, D.B., Mathematical Models of Turbulence, Academic Press, 1972.

51. Hanjalic, K. and Launder, B.E., "Contribution Towards a Reynolds-Stress Closure for Low-Reynolds-Number Turbulence", J.F.M. Vol. 74, 1976, pp. 593-610.

52. Daly, B.J. and Harlow, F.H., "Transport Equations in Turbulence", The Phy. of Fluids, Vol. 13, No.11, Nov. 1970, pp. 2634-2649.

53. Hanjalic, K. and Launder, B.E., "A Reynolds Stress Model of Turbulence and Its Application to Thin Shear flow", J.F.M. Vol. 52, 1972, pp.609-638.

54. Launder, B.E., Reece, G.j. and Rodi, W., "Progress in the Development of a Reynolds-Stress Turbulence Closure", J.F.M. Vol. 68, 1975, pp. 537-566.

55. Shir, C.C., "A Preliminary Numerical Study of Atmospheric Turbulent Flows in the Idealized Planetary Boundary Layer", Journal of the Atmospheric Science Vol. 30, Oct. 1973, pp. 1327-1339.

56. Chou, P.Y., "On Velocity Correlations and the Solutions of the Equations of Turbulent Fluctuation", Quart. Appl. Math. Vol 3, 1945, pp. 38-54.

57. Patankar, R., Numerical Heat Transfer and Fluid Flow, McGraw-Hill, 1981.

58. Hah, C., "A Numerical and Experimental Study of Turbulent Wakes of Turbomachinery Rotor Blades, Isolated Airfoil, and A Cascade of Airfoils", Ph.D. Thesis, Dept. of Aerospace Engineering, The Pennsylvania State University, 1981.

59. Keller, B.H. and Cebeci, T., "Accurate Numerical Methods for Boundary-Layer Flows. II: Two-Dimensional Turbulent Flows", AIAA Journal, Vol.10, No. 9, Sep. 1972, pp. 1193-1199.

60. Cebeci, T. and Bradshaw, P., Momentum Transfer in Boundary Layers, Hemisphere Publishing Corp., 1977

61. Hazarika, B.K., "An Investigation of the Flow Characteristics in the Blade Endwall Corner Region", Ph.D. Thesis, Dept. of Mechanical Engineering, The City College of City University of New York , 1987.

62. Bendat, J.S., and Piersol, A.G., Random Data: Analysis and Measurement, Wiley Interscience, 1971.

63. Burrus, C.S. and Parks, T.W., DFT/FFT and Convolution Algorithms Theory and Implementation, John Wiley and Sons, 1985.

64. Hinze, J.O., Turbulence, McGraw-Hill, 1975.